

142

CENTRAL RESEARCH LIBRARY
DOCUMENT COLLECTION

MARTIN MARIETTA ENERGY SYSTEMS LIBRARIES

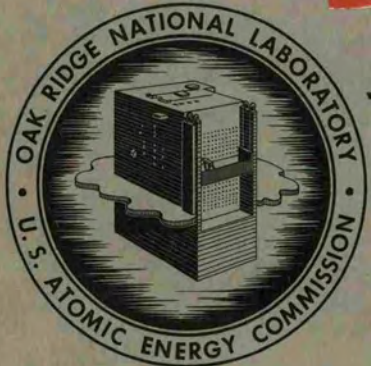


3 4456 0323325 8

ORNL-3017
 UC-34 - Physics and Mathematics
 TID-4500 (15th ed.)

SOLID STATE DIVISION
 ANNUAL PROGRESS REPORT
 FOR PERIOD ENDING AUGUST 31, 1960

CENTRAL RESEARCH LIBRARY
 DOCUMENT COLLECTION
LIBRARY LOAN COPY
 DO NOT TRANSFER TO ANOTHER
 If you wish someone else to see
 document, send in name with document
 and the library will arrange a loan.



OAK RIDGE NATIONAL LABORATORY
 operated by
 UNION CARBIDE CORPORATION
 for the
 U.S. ATOMIC ENERGY COMMISSION

Printed in USA. Price \$2.50. Available from the
Office of Technical Services
Department of Commerce
Washington 25, D. C.

LEGAL NOTICE

This report was prepared as an account of Government sponsored work. Neither the United States, nor the Commission, nor any person acting on behalf of the Commission:

- A. Makes any warranty or representation, expressed or implied, with respect to the accuracy, completeness, or usefulness of the information contained in this report, or that the use of any information, apparatus, method, or process disclosed in this report may not infringe privately owned rights; or
- B. Assumes any liabilities with respect to the use of, or for damages resulting from the use of any information, apparatus, method, or process disclosed in this report.

As used in the above, "person acting on behalf of the Commission" includes any employee or contractor of the Commission, or employee of such contractor, to the extent that such employee or contractor of the Commission, or employee of such contractor prepares, disseminates, or provides access to, any information pursuant to his employment or contract with the Commission, or his employment with such contractor.

ORNL-3017
UC-34 – Physics and Mathematics
TID-4500 (15th ed.)

Contract No. W-7405-eng-26

SOLID STATE DIVISION
ANNUAL PROGRESS REPORT
For Period Ending August 31, 1960

D. S. Billington, Director
J. H. Crawford, Jr., Associate Director

DATE ISSUED

NOV 29 1960

OAK RIDGE NATIONAL LABORATORY
Oak Ridge, Tennessee
operated by
UNION CARBIDE CORPORATION
for the
U. S. ATOMIC ENERGY COMMISSION

MARTIN MARIETTA ENERGY SYSTEMS LIBRARIES



3 4456 0323325 8



SOLID STATE DIVISION ANNUAL PROGRESS REPORT

SUMMARY

PART I. THEORY

1. Theory of Dislocations

Inertia-Free Model of Dislocation Line Motion. – The decrement and change in modulus due to dislocation line motion have been calculated, using a vibrating string model having no inertia and a damping force proportional to the velocity. The calculations have been made for both exponential and delta function distributions of loop length.

2. Theory of Radiation Damage

Energy Loss of Moving Charged Particles in a Valence or Ionic Crystal. – A theoretical expression is derived for the spatial rate of energy loss of a charged particle moving through a valence or ionic crystal and for the spatial rate of production of hole-electron pairs.

Electron Transport in a Magnetic Field. – A method has been developed for calculating electron transport properties in a strong magnetic field with a temperature gradient as the driving force. Landau wave functions for free electrons in a magnetic field have been used. Laplace transforms have been used to solve the differential equation for the density matrix in the Landau representation. The density matrix may then be used to calculate expectation values for the velocity operator.

Neutron Flux Spectra in Graphite-Moderated Reactors. – The fast-neutron flux has been computed, using a homogeneous model reactor to obtain the energy dependence and a simplified heterogeneous model to obtain the spatial variation. The results are in reasonable accord with available experiments in the ORNL Graphite Reactor.

PART II. METALS AND ALLOYS

3. Low-Temperature Irradiation Studies

Radiation Effects in Copper and Aluminum Arising from Fissile Impurities. – Detailed isochronal annealing studies of copper irradiated near 4°K by fast neutrons show no annealing

peaks below the main 35 to 45°K peak. Uranium-235 fission fragment damage in copper and aluminum shows exponential saturation plus a linear damage rate term with strong suppression of the 35 to 45°K peak at high damage concentrations. Boron-10 fission damage in copper shows annealing peaks at low temperatures combined with continuous-type annealing.

Length Change Measurements in Aluminum and Copper. – Length changes in U^{235} -doped copper and aluminum bombarded at 4.5°K have been measured. Subsequent isochronal annealing studies show identical fractional recovery of length change and resistivity in the case of aluminum. Similarities between fission and neutron damage are illustrated.

Isochronal Annealing of Neutron-Irradiated Metals. – The isochronal annealing behavior of high-purity Cu, Ag, Au, Ni, Pd, Pt, and Al have been studied following neutron bombardments near 4°K. The same annealing peak structures found after electron and deuteron irradiations are not observed here.

Helium Refrigerator Modification. – Work is in progress on modifications to the present low-temperature bombardment facility in an effort to obtain a larger sample chamber operating at 4 to 5°K. The present sample chamber is not large enough to carry out several important experiments.

Energy Release in Reactor-Irradiated Copper. Part II. The 600 to 700°K Release. – By using the gamma-ray flux of the Oak Ridge Research Reactor as a means for homogeneously heating a sample, the stored energy associated with radiation-induced defects in copper has been determined. Estimates of defect concentrations are made, assuming several defect models.

Internal Oxidation Studies of Dilute Noble Metal Alloys. – The residual resistivity of several dilute copper-base alloys was found to decrease considerably upon annealing in oxygen at small pressures. The change in resistivity of a dilute nickel-in-copper alloy was much smaller after such a treatment. These observations are discussed in terms of the preferential internal oxidation of solute atoms. A study of the effect

of internal oxidation on the resistance minimum in these alloys would indicate that greater caution is required in relating the presence of the minimum to the major alloying agent. The effect of internal oxidation on the residual resistivity of 99.995% gold has also been investigated.

Effects of Gaseous Impurities on the Magnetic Properties of Copper. – The magnetic susceptibility has been determined as a function of temperature and magnetic field for copper that has been annealed, in turn, in a reducing and an oxidizing atmosphere. In 99.999% pure copper oxidation caused a ferromagnetic contribution to appear. The amount of ferromagnetic material could be estimated to be a little less but of the same magnitude as the amount of paramagnetic impurity present in the reduced material. Doping copper with 0.1% iron causes the same effects to appear in such a magnitude as to make it impossible to use a sensitive susceptibility balance to obtain quantitative results. The effects seen in 99.999% pure copper can be explained if oxidation of copper causes iron, present as a trace impurity, to precipitate.

4. Dislocation Interactions

Temperature Dependence of the Effect of Fast-Neutron-Induced Defects on the Internal Friction and Young's Modulus of Copper. – By measuring the internal friction and modulus of a copper single crystal while it is being irradiated at constant temperature, it is possible to obtain a relative measure of the number of radiation defects mobile enough to diffuse to dislocation lines and pin them. These experiments are being continued. So far, defects have been found to become mobile in temperature intervals centered at 45, 160, 275, and 330°K. The last two of these account for over 90% of the observed defects.

Temperature Dependence of Internal Friction Following Deformation at 78°K. – Techniques have been developed which allow one to hold a sample at the boiling point of nitrogen while it is deformed and mounted in the internal friction apparatus. Preliminary measurements indicate that the method will be useful in studying the behavior of point defects produced during plastic deformation.

Effect of Fast-Neutron Irradiation on Internal Friction in Copper Single Crystals at Megacycle Frequencies. – Room-temperature measurements

of internal friction were made, during irradiation, at frequencies from 10 to 110 Mc, using the pulse echo method. The pinning of dislocation lines by radiation defects causes a transition from damping-limited dislocation motion to line-tension-limited motion; the variation of internal friction with irradiation time is as predicted for this case by the theory of Granato and Lücke. From the measured etch pit density and the parameters obtained in fitting the theory to the internal friction data, values are derived for the dislocation density, average line length, and damping constant.

5. Investigations of Metal Surfaces

The kinetics of the electrochemical dissolution of copper crystals in deaerated CuSO_4 solutions are being investigated using a galvanostatic technique. Conditions have been defined for the dissolution via a dislocation mechanism; this dissolution leaves pits at points where dislocations intersect the surface. Other conditions of potential and current cause the surface to be faceted by the dissolution, and apparently dislocations are not involved in this mechanism.

The kinetics of the dissolution of copper crystals in aerated solutions of HCl are being studied by measuring the change in conductivity of the solution. The experiments are designed to elucidate the role of dislocations and of crystal plane in the chemical reactivity of metal surfaces.

A mechanism has been suggested for the development of etch pits at dislocations, and several etch solutions have been found which will satisfactorily form pits at dislocations on the (111), (100), and (110) faces of pure copper.

Studies on the growth of more perfect copper crystals and on the surface preparation of such crystals are described.

6. Alloy Studies

The radiation-enhanced atomic rearrangement responsible for a decrease in the electrical resistivity of copper-aluminum alloys is being studied using electron and gamma irradiations. As the electron energies and fluxes are lowered, a smaller rate of decrease in resistivity is observed upon irradiation at a fixed temperature. A comparison of the flux dependence of the reaction upon electron and gamma irradiation with results previously obtained upon neutron irradiation leads to the

conclusion that the annealing of radiation-produced defects involves some amount of vacancy-interstitial pair recombination.

The annealing behavior of a deformed copper-silicon alloy suggests that enhanced atomic rearrangements may also take place following plastic deformation.

The crystallographic theory of the martensitic cubic to orthorhombic phase transformation is described in terms of a generalized lattice-invariant shear. Certain solutions for the undistorted plane are given as explicit functions of the lattice parameters of the two phases.

7. Electron Microscope Studies

The results of an electron microscope study of fission fragment tracks in thin films of UO_2 are summarized. Two different replica techniques employed by the group during the past year are described; and an explanation of the mechanism of the replica stripping behavior of Victawet, a water-soluble parting material, is presented.

8. Surface Bombardment of Solids

A beam of Ar^+ ions has been used to bombard the surface of type 304 stainless steel. The resultant sputtering was studied by measuring the loss of mass of the metal and the results expressed as a "sputtering ratio"

$$S = \frac{N_{\text{SA}}}{N_{\text{Ar}^+}},$$

where N_{SA} is the number of particles removed and N_{Ar^+} is the number of incident Ar^+ ions during the experiment. This ratio has been determined at ion energies from 1 to 5 kev. At 3 kev the value is 2.3 ± 0.1 atoms/ion. The r-f ion source-electrostatic lens combination used was studied, and it was found that 95% of the ions impinging on the target were within 100 ev of the expected energy.

9. Brittle Fracture of Metals

Further purification of zone-refined and vacuum-melted iron has been carried out. Solid-state electrolysis, solid-state zone refining (between alpha and gamma ranges), electron-beam melting, and heat treatments in high vacuum have been used. Physical property measurements have shown some success for each of these methods.

PART III. NONMETALS

10. Semiconductor Studies

Radiation-Induced Disorder in Semiconductors. – The variation of σ and μ_H of *n*-type germanium with neutron bombardment has been treated on the basis of a disordered-region model of lattice damage. It is found that the bulk of the initial change in these properties can be accounted for in terms of disordered regions ~ 100 Å in radius for the neutron spectrum employed.

Transmutation Doping and Recoil Effects in Semiconductors Exposed to Thermal Neutrons. – Nuclear reactions accompanying thermal-neutron capture in semiconductors have been employed to examine (a) recoil effects, (b) chemical impurity introduction, (c) impurity compensation, and (d) time-dependent observations of electronic properties via the fixed rate of radioactive decay.

Transmutation Doping and Recoil Effects in Isotopic Enriched Ge^{74} Exposed to Thermal Neutrons. – Recoil effects following thermal-neutron capture have been investigated in 95.8%-enriched Ge^{74} samples. Vacuum anneal subsequent to irradiation has also been employed to examine the donor action of the As^{75} introduced by transmutations. Application of the "replacement-collision" model to these results is discussed.

Annealing Studies of Irradiated Germanium. – Annealing studies of Co^{60} -irradiated antimony-doped *n*-type germanium reveal a complex annealing process in which the impurity atoms present have a major role. Measurements of mobility and carrier concentration indicate that the ionized defect first migrates to an impurity and is then released before its final removal.

Thermoelectric Power in Germanium. – The thermoelectric power in germanium has been measured with increased attention to eliminating contact effects and experimental errors. Emphasis has been placed on measurements at differential temperatures less than 1°C.

Radiation Effects in *n*-Type Tellurium-Doped Germanium. – The effect of fast-neutron irradiation, thermal-neutron irradiation and subsequent transmutation introduction of chemical impurities, and thermal annealing has been investigated for *n*-type germanium that was chemically doped with donor-type tellurium. It is shown that fast-neutron-induced disorder introduces defect states or disordered regions that remove or compensate the tellurium donor impurity upon vacuum anneal.

Exploratory Measurements to Determine the Annealing Behavior of Radiation-Induced Recombination Centers in Germanium. – An experimental survey employing minority-carrier lifetime has been made of the annealing above room temperature of recombination centers induced by 14-Mev monoenergetic neutrons, fission neutrons, and Co^{60} gamma rays. In each case three specimens were used of the following type and resistivity: 2-ohm-cm *p*-type, 2-ohm-cm *n*-type, and 15-ohm-cm *n*-type. A large difference in the annealing behavior was observed among the three types of radiation damage as well as the three types of specimens. More detailed studies are now in progress, including the effect of different impurities.

Some Fast-Neutron Effects in Germanium. – Bombardment of germanium with 3.98×10^{20} *nvt*, produces a measured volume expansion of 0.77% and a calculated x-ray volume expansion of 0.46%, indicating the production of vacancies by neutron irradiation. Unexpectedly, one test showed an increase in hardness in a sample so irradiated.

Gamma Irradiation of Silicon. – Hall coefficient measurements have been continued on *n*-type silicon containing varying amounts of oxygen. It was found that, in addition to a net acceptor level located 0.17 eV below the conduction band, a level close to 0.5 eV below the conduction band is introduced. The introduction of the deep level is highly sensitive to the oxygen content and apparently also to the original resistivity of the samples.

Electrical Conductivity and Thermoelectric Voltage of Cuprous Oxide. – The electrical conductivity of two cuprous oxide samples has been studied as a function of temperature, of pressure, and of electrical contact to the sample. The conductivity below $\sim 300^\circ\text{C}$ is sensitive to time at room and elevated temperatures and to pressure. Little difference has been noted between a silver-plated contact and a gold-foil pressure contact.

11. Alkali Halides

On the Mechanism for the Production of *F* Centers in NaCl by Irradiation with Gamma Rays. – One mechanism for the creation of defects in alkali halides by ionizing radiation requires the evaporation of vacancies from dislocation jogs. Hence, dislocation climb would be expected if this mechanism operates. No climb was detected

in Co^{60} gamma-irradiated NaCl which could account for the extent of defect production as indicated by the production of *F* centers.

Defect Interactions in Irradiated Calcium-Doped Potassium Chloride. – Studies have been made of the optical behavior of an absorption band in x-irradiated calcium-doped KCl. The center responsible for this band has been identified as a Cl_2^- molecular ion, one component of which occupies a cation vacancy. The behavior of this band under various treatments suggests that it is converted into a Cl_3^- molecular ion by ionization.

Magnetic Measurements of Alkali Halides. – Measurements of the magnetic susceptibility of alkali halides at low temperatures have been started with the hope of determining oscillator strengths and other properties of color centers. Results to date on KCl indicate that uncolored material supplied by Harshaw and Isomet contains less than 10^{16} magnetic centers per cubic centimeter. Additive coloration, producing *F* centers, causes the appearance of magnetic centers. Annealing at 120°C to produce the colloid band causes the major part of the low-temperature paramagnetism to disappear. Some preliminary results on CsBr indicate that, in this compound too, coloration produces magnetic centers.

Magnetic Susceptibility of Potassium Rhenium Bromide. – The temperature dependence of the magnetic susceptibility of K_2ReBr_6 has been measured between room temperature and 5°K . A magnetic phase change occurs at 15.5°K . Apparently, the material is antiferromagnetic at low temperatures.

12. Covalent Crystals

Hyperfine Interactions of Defects of Quartz. – Hyperfine interactions of the E'_1 center with five Si^{29} nuclei have been observed. The interactions produce hyperfine lines whose separation is 404, 8.0, 6.8, 0.6, and ~ 0.4 oersteds for [00.1] parallel to *H*, the applied magnetic field. These results show that the model that has been suggested is not a good one. Another possible model is suggested.

A Defect Structure of Silica. – An inverse ratio is established between the concentration of hydrogen, determined by the intensity of the O-H stretching mode, and the concentration of the E'_1 center, produced by a Co^{60} gamma-ray dose of $\sim 10^6$ *r*, in several silicas. In the silica with the

least hydrogen, the concentration of the E_1' center is observed to be $\sim 1.7 \times 10^{19} \text{ cm}^{-3}$ for an x-ray dose of $\sim 10^9$ rads if the irradiation and measurement are carried out at 78°K without intervening warmup. No saturation of concentration is evident. It is suggested that the E_1 center is a fundamental characteristic of the silica structure.

Electron Spin Resonance in Neutron-Irradiated TiO_2 . - Observations at room temperature on neutron-irradiated TiO_2 single crystals have shown a complex ESR spectrum. One set of lines, having $g_{\text{obs}} = 1.986$ and $g_{\text{obs}} = 1.991$, has been observed as a function of orientation of the crystal with respect to H , the applied magnetic field. An analysis of the data suggests that there may be two centers, one with spin $S = \frac{1}{2}$ and the second with spin $S = 1$.

13. Graphite and Ceramics

Stored Energy in X-10 Pile Graphite. - Pre-annealing calorimetric studies of X-10 pile graphite show (1) confirmation of previous stored-energy growth rates, (2) importance of low-temperature annealing, (3) lack of significant damage in the moderator 4 ft west of center, and (4) a slow buildup of damage near the center of the reactor moderator.

Ceramics. - The temperature for the dehydration of asbestos is lowered by reactor irradiation. The weight-loss-temperature relation is insensitive to the rate of heating at rates in the range from 50 to 500°C/hr . The effect of irradiation on the dehydration of muscovite mica was studied kinetically. Both the activation energy and the Arrhenius factor are decreased by irradiation.

14. Polymers

The relative effectiveness of reactor and gamma radiation in producing cross links in polystyrene was investigated by molecular weight measurements. The intensities of the gamma sources were measured with ceric sulfate, while the intensity of the reactor radiation was determined independently by calorimetric measurements. Apparently, reactor radiation cross-links polystyrene 3.3 times as fast as gamma radiation alone.

The infrared spectrophotometer used to measure radiation-induced changes in molecular structure was calibrated for olefinic groups by measurement of solutions of hydrocarbon standards in carbon

disulfide. Equations for the infrared absorption coefficients were calculated with the Oracle using the least-squares method of curve fitting. These equations will be formulated into a system of simultaneous equations to be solved for the concentrations of isomeric olefin groups in irradiated specimens which contain several such groups.

15. Dosimetry Studies

Neutron Flux Measurements in the ORNL Graphite Reactor. - Fast-flux measurements with threshold and resonance reactions are tabulated for Holes A, 19, 51, 52, and 1768.

Ceric Sulfate as a Pile Dosimeter. - The relative yield for the ceric-to-cerous reaction for reactor neutrons compared with that for gamma rays is 1.0 ± 0.1 for Hole 51 and 1.4 ± 0.2 for Hole 19. This compares well with the value of 1.2 ± 0.1 determined from proton irradiations.

The Variation of Atomic Displacements with Neutron Energy. - The effect of forward scattering of neutrons was calculated for copper and zinc, and the average recoil energy from neutrons in the range 2 to 5 Mev was found to be roughly constant. This helps to explain the results from monoenergetic-neutron irradiations of germanium.

PART IV. REACTOR MATERIALS

16. High-Temperature Fuel Materials

Evaluation studies on the irradiation behavior of reactor fuels were continued during the past year, with emphasis on UO_2 and the EGCR first fuel loading. Fission gas release data were obtained with varying density, temperature, stoichiometry, and burnup. Microstructural changes were observed at the higher temperatures. Dispersions of UC_2 in graphite and graphite coatings were also investigated as a part of the GCR advanced materials studies.

An in-pile experiment is being used to study the continuous evolution of fission gas under varying conditions of temperature, power density, and burnup for a variety of fuel materials. A large increase in fission gas release was observed for UO_2 which was oxidized during irradiation. During the period of irradiation ($1.2 \times 10^{20} \text{ nvt}$) the thermal conductivity of the UO_2 did not change.

17. Radiation Metallurgy

The brittle fracture program for pressure vessel steels was extended to include isothermal annealing studies. The results of impact tests showed some recovery at 400°F and 90% recovery at 850°F. In the tensile tests, slight recovery was observed between 250 and 400°F, and a very complicated behavior between 400 and 600°F. A final stage of recovery was observed above 600°F.

Stress-rupture studies have continued on Inconel and type 304 stainless steel by in-pile tube burst

tests. Studies have also been initiated for beryllium, niobium, and Zircaloy-2. Tube burst tests are presently being assembled for all three new materials. Several experiments have been run to determine the effect of internal helium generation on the physical and mechanical properties of beryllium. First tests on a high-temperature irradiation indicated that the swelling was much greater than observed from low-temperature irradiation followed by postirradiation annealing.

CONTENTS

SUMMARY	iii
PART I. THEORY	
1. THEORY OF DISLOCATIONS.....	3
Inertia-Free Model of Dislocation Line Motion	3
2. THEORY OF RADIATION DAMAGE	7
Energy Loss of Moving Charged Particles in a Valence or Ionic Crystal	7
Electron Transport in a Magnetic Field.....	8
Neutron Flux Spectra in Graphite-Moderated Reactors	11
PART II. METALS AND ALLOYS	
3. LOW TEMPERATURE IRRADIATION STUDIES	21
Radiation Effects in Copper and Aluminum Arising from Fissile Impurities	21
Length Change Measurements in Aluminum and Copper	25
Isochronal Annealing of Neutron-Irradiated Metals	28
Helium Refrigerator Modification	31
Energy Release in Reactor-Irradiated Copper. Part II. The 600 to 700°K Release.....	31
Internal Oxidation Studies of Dilute Noble Metal Alloys	32
Introduction	32
Internal Oxidation in Copper-Iron Alloys	32
Internal Oxidation in Copper-Nickel Alloys	32
Internal Oxidation in a Gold Alloy.....	34
Effects of Gaseous Impurities on the Magnetic Properties of Copper	34
4. DISLOCATION INTERACTIONS.....	36
Temperature Dependence of the Effect of Fast-Neutron-Induced Defects on the Internal Friction and Young's Modulus of Copper	36
Temperature Dependence of Internal Friction Following Deformation at 78°K	38
Effect of Fast-Neutron Irradiation on Internal Friction in Copper Single Crystals at Megacycle Frequencies.....	40
5. INVESTIGATIONS OF METAL SURFACES	42
Electrochemical Dissolution of Copper Single Crystals	42
Dissolution of Copper in Aqueous Hydrochloric Acid	44
The Role of Crystal Imperfections in the Chemical Reactivity of Metal Surfaces	44
Etch Pits at Dislocations in Copper	45
Growth of Crystals and Preparation of Surfaces	45
6. ALLOY STUDIES	46
Irradiation Effects on Copper-Aluminum (15 at. % Al) Alloys	46
Electron Irradiation	46
Gamma Irradiation.....	47
Theoretical Analysis	48

Annealing Effects on Deformed Copper-Silicon Alloys	48
The Generalized Theory of the Martensitic Cubic to Orthorhombic Phase Transformation	49
7. ELECTRON MICROSCOPE STUDIES	50
Fission Fragment Tracks in UO ₂ Films	50
Replica Studies	50
8. SURFACE BOMBARDMENT OF SOLIDS.....	52
Sputtering Ratio of Type 304 Stainless Steel	52
9. BRITTLE FRACTURE OF METALS	56
PART III. NONMETALS	
10. SEMICONDUCTOR STUDIES.....	61
Radiation-Induced Disorder in Semiconductors	61
Transmutation Doping and Recoil Effects in Semiconductors Exposed to Thermal Neutrons	63
Transmutation Doping and Recoil Effects in Isotopic Enriched Ge ⁷⁴ Exposed to Thermal Neutrons	63
Annealing Studies of Irradiated Germanium.....	66
Thermoelectric Power in Germanium	69
Radiation Effects in <i>n</i> -Type Tellurium-Doped Germanium	73
Exploratory Measurements to Determine the Annealing Behavior of Radiation-Induced Recombination Centers in Germanium	75
Some Fast-Neutron Effects in Germanium	77
Gamma Irradiation of Silicon	78
Electrical Conductivity and Thermoelectric Voltage of Cuprous Oxide	79
11. ALKALI HALIDES	82
On the Mechanism for the Production of <i>F</i> Centers in NaCl by Irradiation with Gamma Rays	82
Defect Interactions in Irradiated Calcium-Doped Potassium Chloride	82
Magnetic Measurements of Alkali Halides.....	84
Magnetic Susceptibility of Potassium Rhenium Bromide.....	87
12. COVALENT CRYSTALS	89
Hyperfine Interactions of Defects of Quartz	89
A Defect Structure of Silica.....	90
Electron Spin Resonance in Neutron-Irradiated TiO ₂	93
13. GRAPHITE AND CERAMICS.....	97
Stored Energy in X-10 Pile Graphite	97
Ceramics.....	97
The Effect of Irradiation on the Thermal Stability of Asbestos	98
The Effect of Irradiation on the Thermal Stability of Muscovite Mica	99

14. POLYMERS	101
Comparison of Effects of Reactor and Gamma Irradiation on Polystyrene	101
Infrared Studies of Plastics and Elastomers	102
Influence of Thickness and Orientation of Polymers on the Effects of Radiation	103
15. DOSIMETRY STUDIES	104
Neutron Flux Measurements in the ORNL Graphite Reactor	104
Ceric Sulfate as a Pile Dosimeter	104
The Variation of Atomic Displacements with Neutron Energy	105
PART IV. REACTOR MATERIALS	
16. HIGH-TEMPERATURE FUEL MATERIALS	109
UO ₂ Irradiation Studies – Fission Gas Release	109
UO ₂ Irradiation Studies – EGCR Prototype Fuel	112
Advanced Fuel Materials Studies	113
Instantaneous Fission Gas Release Experiment	114
Thermal Conductivity of UO ₂	114
Fission Gas Release	115
17. RADIATION METALLURGY	116
Brittle Fracture of Metals – Annealing Studies	116
Beryllium Irradiation Studies	118
Zircaloy-2 Test Program	119
Inconel Tube Burst Tests	120
Stainless Steel and INOR-8 Tube Burst Tests	122
Niobium Tube Burst Tests	123
PUBLICATIONS, PAPERS, AND SPEECHES	125

Part I
THEORY



1. THEORY OF DISLOCATIONS

INERTIA-FREE MODEL OF DISLOCATION LINE MOTION

O. S. Oen

D. K. Holmes

M. T. Robinson

It has been proposed by Koehler¹ that many aspects of mechanical damping due to the presence of dislocations can be described by a model which assumes that the dislocation line segment acts like a damped vibrating string. With this model the equation of motion for the displacement, y , of a pinned line segment in the presence of an external oscillating stress field is

$$A \frac{\partial^2 y}{\partial t^2} + B \frac{\partial y}{\partial t} - C \frac{\partial^2 y}{\partial x^2} = \sigma_0 b \cos \omega t , \quad (1)$$

$$y(-l/2, t) = y(l/2, t) = 0 .$$

Here A is the effective mass per unit length of the dislocation, B is the damping force per unit length, C is the line tension, b is the Burgers vector, and σ_0 is the resolved shear stress. An approximate solution which is valid in the kilocycle range has been discussed by Koehler for the above equation. Granato and Lücker² have found a general solution expressed as an infinite series. They discussed the consequences of their solution by retaining only the first term in the infinite series. Their analysis leads to an incorrect value for the change in modulus at high frequencies. On the other hand, Weertman³ has given the general solution in a mathematical closed form. Unfortunately, it is very difficult to assess the role of the various parameters using Weertman's solution.

Recent experimental work on copper single crystals by Thompson and Paré⁴ shows that the internal friction is inversely proportional to the frequency in the megacycle frequency range. This result can be explained by the above model if the damping constant B is large enough so that the dislocation motion is damping-limited in some frequency range. If this is the case, the inertia will not become important until a very high frequency is reached. Hence, it was decided to investigate the type of solution obtained with the inertia term absent. The equation of motion then becomes

$$B \frac{\partial y}{\partial t} - C \frac{\partial^2 y}{\partial x^2} = \sigma_0 b \cos \omega t , \quad (2)$$

$$y(-l/2, t) = y(l/2, t) = 0 .$$

¹J. S. Koehler, *Imperfections in Nearly Perfect Crystals*, p 197, Wiley, New York, 1952.

²A. Granato and K. Lücker, *J. Appl. Phys.* **27**, 583 (1956).

³J. Weertman, *J. Appl. Phys.* **26**, 202 (1955).

⁴D. O. Thompson and V. K. Paré, "Dislocation Interaction," this report.

The above equation has the steady-state solution

$$y(x,t) = \frac{\sigma_0 b}{\omega B} \left\{ \sin \omega t \left[1 - \frac{\cosh kx \cos kx \cosh (kl/2) \cos (kl/2) + \sinh kx \sin kx \sinh (kl/2) \sin (kl/2)}{\cosh^2 (kl/2) - \sin^2 (kl/2)} \right] \right. \\ \left. + \cos \omega t \frac{\cosh kx \cos kx \sinh (kl/2) \sin (kl/2) - \sinh kx \sin kx \cosh (kl/2) \cos (kl/2)}{\cosh^2 (kl/2) - \sin^2 (kl/2)} \right\}, \quad (3a)$$

where $k^2 = \omega B/2C$. Expressed as a sum of harmonics, the displacement is

$$y(x,t) = \frac{4\sigma_0 b}{\pi} \sum_{n=0}^{\infty} \frac{\sin \alpha_n [x + (l/2)]}{2n + 1} \left(\frac{\alpha_n^2 C \cos \omega t + \omega B \sin \omega t}{\alpha_n^4 C^2 + \omega^2 B^2} \right), \quad (3b)$$

where $\alpha_n = (2n + 1)\pi/l$.

The decrement, Δ , is computed as follows:

$$\Delta = \frac{\int_0^{\infty} E_1(l)N(l) dl}{\sigma_0^2/\mu}, \quad (4)$$

where μ is the shear modulus, $N(l) dl$ the number of loops per unit volume having lengths between l and $l + dl$, and $E_1(l)$ the energy loss per cycle for one loop length l , which is given by

$$E_1 = \int_{-l/2}^{l/2} dx \int_0^{2\pi/\omega} \sigma_0 b \cos \omega t \frac{dy}{dt}(x,t) dt. \quad (5)$$

The change in modulus, $\Delta\mu/\mu$, is given by

$$\frac{\Delta\mu}{\mu} = \mu b \int_0^{\infty} E_2(l)N(l) dl, \quad (6)$$

where

$$E_2(l) = \int_{-l/2}^{l/2} dx y \left(x, \frac{2n\pi}{\omega} \right). \quad (7)$$

Both the decrement and change in modulus have been calculated, using the delta function distribution,

$$N(l) = \frac{L}{l_0} \delta(l - l_0),$$

and the exponential distribution,

$$N(l) = \frac{L}{l_0^2} e^{-l/l_0}.$$

Here L is total line length per unit volume and l_0 is the average loop length.

For the delta function distribution the decrement is found to be

$$\frac{\Delta}{\pi L l_0^2} = \frac{1}{(k l_0)^3} \left(k l_0 - \frac{\sinh k l_0 + \sin k l_0}{\cosh k l_0 + \cos k l_0} \right), \quad (8a)$$

which in series representation is

$$\frac{\Delta}{\pi L l_0^2} = \frac{32}{\pi^6} \sum_{n=0}^{\infty} \frac{(k l_0)^2}{(2n+1)^6} \left[1 + \frac{4}{\pi^4} \frac{(k l_0)^4}{(2n+1)^4} \right]^{-1}. \quad (8b)$$

On the other hand, the change in modulus becomes

$$\frac{\Delta\mu}{\mu L l_0^2} = \frac{1}{(k l_0)^3} \left(\frac{\sinh k l_0 - \sin k l_0}{\cosh k l_0 + \cos k l_0} \right), \quad (9a)$$

which in series form is

$$\frac{\Delta\mu}{\mu L l_0^2} = \frac{16}{\pi^4} \sum_{n=0}^{\infty} \frac{1}{(2n+1)^4} \left[1 + \frac{4}{\pi^4} \frac{(k l_0)^4}{(2n+1)^4} \right]^{-1}. \quad (9b)$$

It has been found that the first term in the series expansion for the decrement follows the whole series very closely for all values of k . On the other hand, for the change in modulus the first term follows the series very closely for small k , but not at all for large k .

For the exponential loop length distribution the decrement is

$$\frac{\Delta}{\pi L l_0^2} = \frac{1}{(k l_0)^3} \int_0^{\infty} \left(k l_0 x - \frac{\sinh k l_0 x + \sin k l_0 x}{\cosh k l_0 x + \cos k l_0 x} \right) e^{-x} dx, \quad (10)$$

and the change in modulus is

$$\frac{\Delta\mu}{\mu} \left(\frac{1}{L l_0^2} \right) = \frac{1}{(k l_0)^3} \int_0^{\infty} \left(\frac{\sinh k l_0 x - \sin k l_0 x}{\cosh k l_0 x + \cos k l_0 x} \right) e^{-x} dx. \quad (11)$$

The above integrals have been computed on an IBM 704 computer for many values of the parameter $k l_0$, and the results, together with those for the delta distribution, are shown in Fig. 1.1. For high frequencies it is seen that both distribution functions of loop length predict a decrement which is inversely proportional to the frequency, thus agreeing with the experimental observations of Thompson and Paré.⁴ The asymptotic forms for the change in modulus and the decrement are given in Table 1.1.

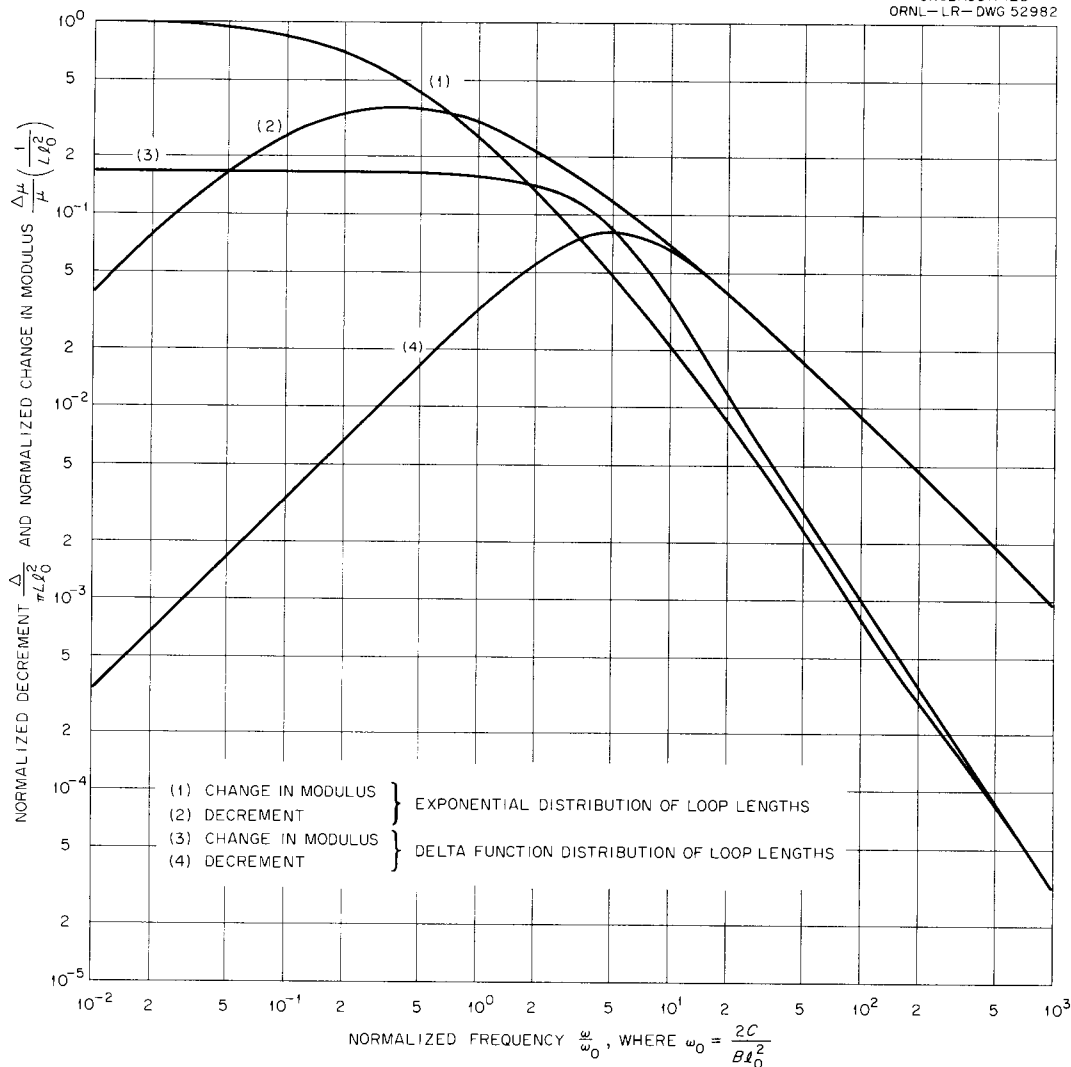


Fig. 1.1. Normalized Decrement $\frac{\Delta}{\pi L l_0^2}$ and Normalized Change in Modulus $(\Delta\mu/\mu)(1/Ll_0^2)$.

Table 1.1. Asymptotic Forms for the Change in Modulus and the Decrement

$$\omega_0 = 2C/Bl_0^2$$

Distribution of Loop Lengths	$\frac{\Delta}{\pi L l_0^2}$		$(\Delta\mu/\mu)(1/Ll_0^2)$	
	Low Frequencies	High Frequencies	Low Frequencies	High Frequencies
Exponential	$4 \frac{\omega}{\omega_0}$	$\frac{\omega_0}{\omega}$	1	$\left(\frac{\omega_0}{\omega}\right)^{3/2}$
Delta function	$\frac{4}{120} \frac{\omega}{\omega_0}$	$\frac{\omega_0}{\omega}$	$\frac{1}{6}$	$\left(\frac{\omega_0}{\omega}\right)^{3/2}$

2. THEORY OF RADIATION DAMAGE

ENERGY LOSS OF MOVING CHARGED PARTICLES IN A VALENCE OR IONIC CRYSTAL

H. C. Schweinler

The following situation is envisaged: A charged particle moves through a valence or ionic crystal. The particle is constrained to move with constant velocity. This motion constitutes a (time-dependent) perturbation upon the system of electrons in the crystal. Under the influence of this perturbation, electrons are removed from the valence band and added to the conduction band.

The problem is formulated in a general way, using time-dependent wave mechanics and antisymmetrized product (i.e., determinantal) wave functions for the electron system. Expressions are given both for dE/dx , the energy given to the electron system per unit length of path of the impinging particle, and for $d\#_p/dx$, the number of pairs (hole-electron pairs) created per unit length of path. The ratio of these last two quantities gives the energy expended in the crystal per hole-electron pair created.

In all calculations here referred to, the only mechanism of energy transfer considered is that of the excitation of electrons from valence to conduction band. Other energy-loss mechanisms, such as Rutherford scattering, will, of course, enter; but their effect is additive and is not further considered here.

The calculation has been carried out for the following situation (of great practical importance): The form of one of the two energy bands is an ellipsoid of revolution, which may be off center in momentum space; the other band is spherical and centered about the origin. The transition probability for an electron from any state of the valence band to any state of the conduction band involves a sixfold integration; five integrations have been carried out analytically, leaving one final integration to be performed numerically. Certain approximations to the latter, good over a restricted range of incident particle velocities, are also useful.

This energy-loss mechanism has a threshold, which will be described in more detail immediately. The above calculation is best for low-energy transfers, that is, energy transfers just above the threshold energy. For larger energy transfers, which arise for the most part (but not invariably) from more energetic particles, the above-described calculation is inadequate because the assumed form of the valence and conduction-band energy surfaces is inadequate. (The form described above holds only in the neighborhood of the band edges.) Expressions have been obtained for the energy loss in the general case, but these expressions involve the energy as a function of quasi-momentum of the electrons throughout both the valence and the conduction band. These are not known with any degree of confidence, and so the equations thus derived, while more general, are less specifically useful.

Several results of this investigation are of interest. First, the process has a threshold. The threshold is strikingly dependent upon energy-band structure; it is, for example, 128 eV for a proton moving in silicon, while for a proton moving in an alkali halide crystal it is over a hundred times higher. Second, the energy loss per ion pair at threshold is only slightly greater than the energy gap between valence

and conduction band; it is, for example, 1.19 ev per ion pair in silicon, for which the band gap $E_G = 1.10$ ev. Third, the energy loss per unit length of path and per ion pair is expected to depend upon the direction of motion of the charged particle with respect to the crystallographic axes (and to have a fairly strong dependence on direction near threshold). Fourth, velocity rather than energy of the moving particle is a more appropriate independent variable for describing the energy loss and the number of hole-electron pairs formed, and the latter two quantities should be divided by the square of the charge of the moving particle for uniformity of presentation of data.

It is clear from the above that this theory provides rational criteria in searching for threshold detectors for charged particles with a wide range of thresholds and with improved sensitivity. It also becomes evident upon reflection that such a search will provide much information of a fundamental nature bearing upon the energy-band structure of valence and ionic crystals. The critical velocity (velocity of the charged particle at threshold) is low for crystals one of whose energy band extrema is off center in momentum space, being approximately the ratio of the energy gap to the momentum difference between extrema, and these last two quantities are of utmost importance in the theoretical description of the energy-band structure of solids.

ELECTRON TRANSPORT IN A MAGNETIC FIELD

J. H. Barrett

Several authors¹ have calculated electron transport properties in a strong magnetic field with an electric field as the driving force. The objective of the present research is to calculate these strong-field properties with a temperature gradient as the driving force.

In calculating transport properties, a weak magnetic field can be treated as a perturbation term in the Hamiltonian operator, as done, for instance, by Jones.² Perturbation theory is only valid if the collision time is much less than $1/\omega_c$, where ω_c is the cyclotron angular frequency. For strong magnetic fields, Landau wave functions³ may be used:

$$\phi_{nkl}(x,y,z) = (\text{normalization constant}) e^{ik_x x} e^{-(a/2)(y-y_0)^2} H_n[\sqrt{a}(y-y_0)] e^{ilz} ,$$

where the magnetic field H has been assumed to be in the z direction, the vector potential \mathbf{A} has been chosen as $(-Hy, 0, 0)$, and

$$\alpha = \frac{e|H|}{\hbar c} = \frac{m}{\hbar} \omega_c ,$$

$$y_0 = \frac{\hbar c}{eH} k ,$$

¹E. N. Adams and T. D. Holstein, *Phys. and Chem. Solids* **10**, 254 (1959); P. N. Argyres, *Phys. Rev.* **117**, 315 (1960). These articles contain further references.

²H. Jones, vol 19, p 227 in *Encyclopedia of Physics*, ed. by S. Flügge, Springer-Verlag, Berlin, 1956.

³L. Landau, *Z. Physik* **64**, 629 (1930).

e = the absolute value of the electron charge ,

H_n = Hermite polynomial .

This avoids the treatment of the magnetic field as a perturbation. However, the Landau wave functions have zero diagonal matrix elements for the v_x and v_y operators. This means that the standard technique² of using the distribution function will not work for computing transverse effects. A method which will work is the use of the density matrix.

The wave function for an electron may be expanded in terms of the Landau functions (r will be used to stand for the set of quantum numbers $n k l$; spin is ignored):

$$\psi(x, y, z, t) = \sum_r a_r(t) \phi_r(x, y, z) .$$

The density matrix is defined as⁴

$$\rho_{rr'}(t) = a_r(t) a_{r'}^*(t) . \quad (1)$$

It obeys the differential equation

$$\dot{\rho}_{rr'}(t) = \frac{i}{\hbar} [(\rho b)_{rr'} - (b\rho)_{rr'}] , \quad (2)$$

where b is the Hamiltonian matrix. The expectation value for an operator q is

$$\langle q \rangle = \text{trace} (\rho q) . \quad (3)$$

For the Landau wave functions

$$(v_x)_{r'r} = -\frac{eH}{mc} \frac{1}{\sqrt{2\alpha}} (\sqrt{n+1} \delta_{r'r_+} + \sqrt{n} \delta_{r'r_-}) , \quad (4)$$

$$(v_y)_{r'r} = i \frac{e|H|}{mc} \frac{1}{\sqrt{2\alpha}} (\sqrt{n+1} \delta_{r'r_+} - \sqrt{n} \delta_{r'r_-}) ,$$

where $r_{\pm} = (n \pm 1 k l)$. Equations (3) and (4) give

$$\langle v_x \rangle = 2 \sum_r R(\rho_{rr_+}) (v_x)_{r_+r} , \quad (5)$$

$$\langle v_y \rangle = -2i \sum_r I(\rho_{rr_+}) (v_y)_{r_+r} ,$$

where $R()$ and $I()$ denote the real and imaginary parts. For a many-electron wave function the density matrix must be defined differently, but Eqs. (2)–(5) still hold⁵ as long as the many-electron operators H and Q are sums of one-electron operators: $H = \sum_i h_i$, $Q = \sum_i q_i$. The localization which the Landau wave functions possess eliminates any need to use wave packets as must be done with plane waves.

⁴For instance, see R. C. Tolman, *The Principles of Statistical Mechanics*, p 327, Oxford University Press, London, 1938.

⁵W. Kohn and J. M. Luttinger, *Phys. Rev.* **108**, 590 (1957).

The Laplace transform is a convenient way of solving Eq. (2) for the density matrix. Write the Hamiltonian as $b = b^0 + \lambda b^s$, where b^0 will be taken as the Hamiltonian for free electrons in a magnetic field, b^s will be taken as the scattering potential of randomly located point imperfections, and $0 \leq \lambda \leq 1$. Let $P_{rr'}(s)$ be the transform of $\rho_{rr'}(t)$, $(\rho_{rr'})_0 =$ initial value of $\rho_{rr'}$, and $\omega_{rr'} = (b_{rr} - b_{r'r'})/\hbar$. The matrix $b_{rr'}^0$ will be diagonal for Landau wave functions.

The transform of Eq. (2) is

$$(s + i\omega_{rr'})P_{rr'} = (\rho_{rr'})_0 + \frac{i}{\hbar} \lambda b_{rr'}^s (P_{rr} - P_{r'r'}) + \frac{i}{\hbar} \lambda \sum_{r''}' (P_{rr''} b_{r''r'}^s - b_{rr''}^s P_{r''r'}) . \quad (6)$$

The prime on the sum indicates $r'' \neq r, r'$.

Equation (6) may be solved by using an expansion in powers of λ . Let

$$P_{rr'} = \sum_{p=0}^{\infty} \lambda^p P_{rr'}^p . \quad (7)$$

Most of the terms in the series of Eq. (7) will have uncorrelated phases. Among the off-diagonal elements the lowest-order terms which have correlated phases are $P_{rr_+}^2$. The correlated part contains a factor

$$\frac{1}{b^2 s} \sum_{r''}' \left\{ \left[\frac{(\rho_{r''r''})_0 - (\rho_{rr})_0}{s + i\omega_{rr''}} + \frac{(\rho_{r''r''})_0 - (\rho_{r_+r_+})_0}{s + i\omega_{r''r_+}} \right] b_{rr''}^s b_{r''r_+}^s \right\} .$$

The higher-order terms in the expansion will contribute a level broadening $\Gamma_{rr'}$ to all terms. The effect will be to replace $(s + i\omega_{rr'})$ by $(s + i\omega_{rr'} + \Gamma_{rr'})$. The diagonal elements ρ_{rr} are not completely determined by this expansion method. However, if the Γ 's are all taken to be very much less than ω_c , the effects of the level broadening will be very small. In this case the diagonal elements may be taken to be the Fermi-Dirac distribution function. The variation of $(\rho_{r''r''})_0$ with y_0'' may be approximated by

$$(\rho_{r''r''})_0 = (\rho_{r''r''})_0 \Big|_{y_0''=y_0} + \frac{\partial(\rho_{r''r''})_0}{\partial y_0''} \Big|_{y_0''=y_0} (y_0'' - y_0) .$$

The Poisson summation formula may be used to simplify the energy density of states. After performing the sum over r'' and finding the inverse Laplace transform, an expression for ρ_{rr_+} is obtained. The correlated part, as $t \rightarrow \infty$, is

$$(\rho_{rr_+})_{\text{correlated}} = \frac{1}{2(\Gamma_{rr_+} - i\omega_c)} \left[\gamma_r \frac{\partial(\rho_{rr})_0}{\partial y_0} + \gamma_{r_+} \frac{\partial(\rho_{r_+r_+})_0}{\partial y_0} \right] \sqrt{\frac{n+1}{2\alpha}} , \quad (8)$$

where

$$\gamma_r = \frac{2\pi}{\hbar} n_s V^2 g(b_{rr}^0) \left[1 + \frac{1}{\sqrt{2}} \sqrt{\frac{\hbar\omega_c}{b_{rr}^0}} \sum_{\nu=1}^{\infty} \frac{(-1)^\nu}{\sqrt{\nu}} \cos \left(\frac{2\pi\nu b_{rr}^0}{\hbar\omega_c} - \frac{\pi}{4} \right) \right] ,$$

n_s = number of scattering centers per unit volume ,

V = integral over all space of the potential due to a scattering center ,

$$g(b_{rr}^0) = \frac{1}{2\pi^2} \left(\frac{2m}{\hbar^2} \right)^{3/2} \sqrt{b_{rr}^0} .$$

The quantity $g(b_{rr}^0)$ is just the density of states (spin degeneracy included) in the absence of a magnetic field. The bracket in the expression for γ_r represents a small fluctuation in the density of states due to the magnetic field. The expression for γ_r is valid for $\hbar\omega_c \ll b_{rr}^0$. The level broadening constant $\Gamma_{rr'}$ can be written as $\Gamma_{rr'} = \frac{1}{2} (\gamma_r + \gamma_{r'})$.

NEUTRON FLUX SPECTRA IN GRAPHITE-MODERATED REACTORS

M. T. Robinson D. K. Holmes O. S. Oen

One of the uncertainties in interpreting the results of irradiations of solids in nuclear reactors is that of the fast-neutron flux spectrum. Experimental measurements of fast flux spectra are restricted to the use of a few threshold detectors (e.g., fission of Np^{237} and U^{238}) in the important region above about 0.1 Mev. The experiments are incapable of distinguishing spectral details and must be supplemented with considerable theoretical calculation. In principle, such calculations ought to be carried out by stochastic methods, but these are not well adapted to the expeditious production of results. For this reason, the problem has been divided into two parts: in the first, the *energy dependence* of the fast flux is determined for a *homogeneous* reactor; in the second, the *spatial dependence* is found for a *heterogeneous* reactor, using Fermi age theory with certain modifications.

The neutron collision density per logarithmic energy interval in an infinite homogeneous reactor is given by the integral equation

$$K(E) \equiv E \Sigma_t(E) \phi(E) = E S(E) + E \int_E^{E/\alpha} K(E') P(E' \rightarrow E) \frac{dE'}{E'} , \quad (1)$$

where E is the neutron energy, $\Sigma_t(E)$ is the macroscopic total neutron cross section of the moderator, $\phi(E)$ is the neutron flux density per unit energy interval, $S(E)$ is the neutron source density in the reactor, $P(E' \rightarrow E)$ is the probability that a neutron of energy E' will be scattered into the range E to $E + dE$, and α is the maximum fractional change in the energy of a neutron in a single collision. The neutron source density employed in the calculations was the fission source as given by Leachman,⁶

$$S(E) = 2\pi^{-1/2} a(aE)^{1/2} e^{-aE} , \quad (2)$$

with $a = 0.7751 \text{ Mev}^{-1}$. As written, the source is normalized to one neutron per unit volume and time

⁶R. B. Leachman, *Proc. Intern. Conf. Peaceful Uses Atomic Energy, Geneva, 1955* 2, 193.

over all energies. The scattering probability may be defined in terms of the differential elastic scattering cross section:

$$P(E' \rightarrow E) = \frac{2\pi \Sigma_s(\theta, E')}{\Sigma_t(E')} \left| \frac{d \cos \theta}{dE} \right|, \quad (3)$$

where $\Sigma_s(\theta, E')$ is the macroscopic differential cross section and θ is the c.m. scattering angle. The maximum fractional energy change is

$$\alpha = \left(\frac{A-1}{A+1} \right)^2 = 0.7161 \text{ for carbon}, \quad (4)$$

where A is the mass number of the moderator.

Equation (1) has been solved numerically on an IBM 704 digital computer in three different approximations. The results are plotted in Fig. 2.1. In the first approximation (curve A of Fig. 2.1), the scattering probability was represented by an expansion in Legendre polynomials as

$$P(E' \rightarrow E) = \frac{2}{(1-\alpha)E'} \sum_{n=0}^4 A_n(E') P_n \left[\frac{2(E/E') - 1 - \alpha}{1-\alpha} \right], \quad \alpha E' \leq E \leq E', \quad (5)$$

$$= 0 \quad \text{otherwise},$$

where the $P_n(x)$ are the Legendre polynomials. The coefficients $A_n(E')$ were derived from an approximation based on experimental data⁷ on the scattering of neutrons by C¹². The coefficients are shown in Fig. 2.2. The insets in Fig. 2.1 show the scattering probabilities as functions of the c.m. scattering angle for three energies. The second approximation also utilized Eq. (5), but with all the $A_n(E')$ for $n \geq 1$ set to zero; that is, the scattering was assumed to be spherically symmetrical in the c.m. system. These results are shown in curve B of Fig. 2.1. The final approximation, shown in curve C, assumed that the collision density resulting from a *monoenergetic* neutron source could be represented everywhere by its asymptotic value $1/\xi_s$, where

$$\xi_s = 1 - \frac{\alpha}{1-\alpha} \ln \alpha. \quad (6)$$

Examination of the three curves of Fig. 2.1 shows that the three approximations lie very close to one another, especially in the lower energy region. The second and third approximations predict too high a collision density below about 3.5 Mev and too high a result thereafter. The peculiar wiggles in curve A and in the 2-to-4-Mev region result from the great changes in the differential scattering cross section in this region.

⁷J. E. Wills *et al.*, *Phys. Rev.* **109**, 891 (1958); N. A. Bostrom *et al.*, WADC-TN-59-107 (February 1959); J. R. Beyster, M. Walt, and E. W. Salini, *Phys. Rev.* **104**, 1319 (1956).

UNCLASSIFIED
ORNL-LR-DWG 52772

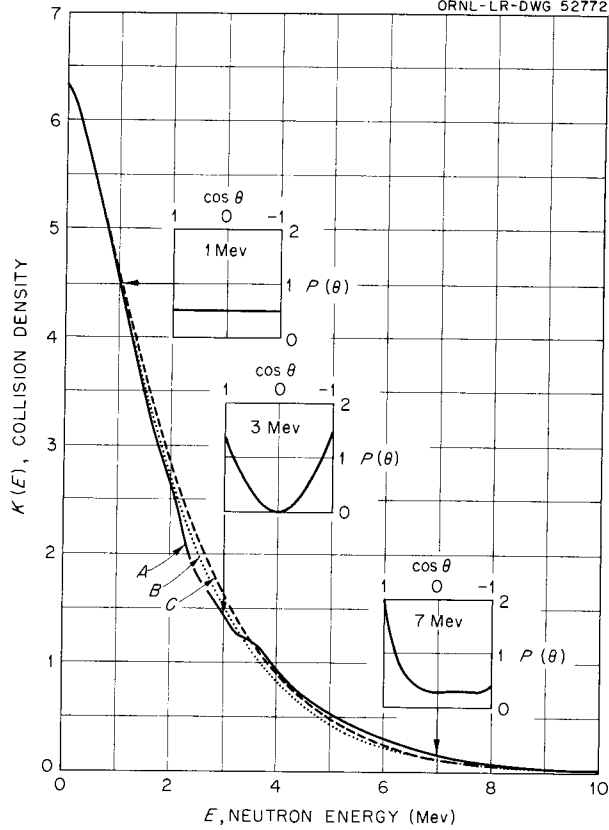


Fig. 2.1. Neutron Collision Density in a Homogeneous Graphite Reactor. Curve A is based on the C^{12} differential scattering cross section, curve B assumes spherically symmetrical scattering, and curve C is an approximate evaluation. The insets show the scattering cross section used for curve A.

UNCLASSIFIED
ORNL - LR - DWG 52773

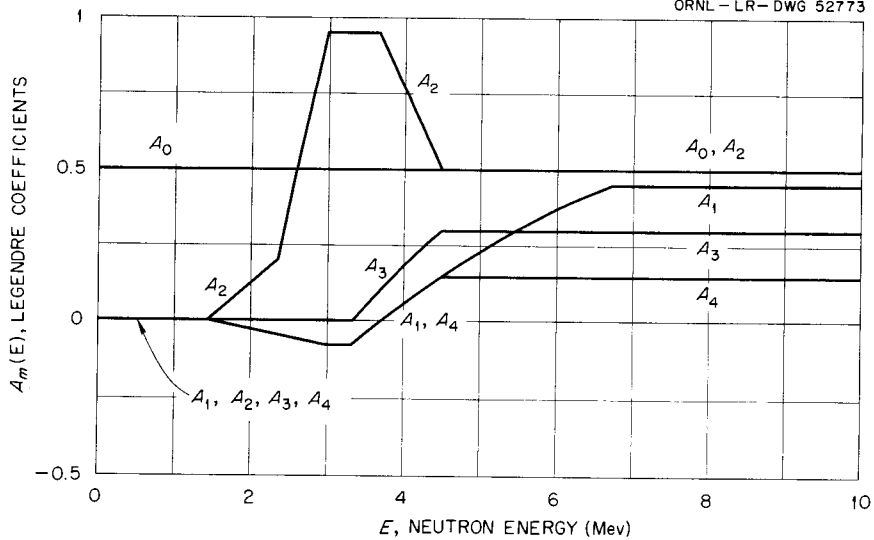


Fig. 2.2. Legendre Polynomial Coefficients for C^{12} Neutron Scattering.

From curve A of Fig. 2.1 and published total cross section data,⁸ the curves of Fig. 2.3 were constructed. The density of graphite assumed was 1.994 g/cc. [This choice allows one to set $\Sigma_s(\text{cm}^{-1}) = 0.1\sigma_s$ (barns), where σ_s is the microscopic scattering cross section.] The sharp irregularities in $E\phi(E)$ and in $\phi(E)$ for $E > 2$ Mev result from the strong resonances in the C^{12} scattering cross section, which also are responsible for the behavior of the differential cross section in this range.

The calculations of the spatial dependence of the fast-neutron collision density were made in terms of the ORNL Graphite Reactor. The unit cell of this reactor is shown in Fig. 2.4. The cell constant (unit translation) is b , and the radius of the fuel elements, including their jackets, is R_1 . The elements lie in the corner of a square cavity of side L . The rms distance from the center of the fuel element to the surface of the cavity is $R_2 = L/\pi^{1/2}$. The collision density in this model may be represented by

$$K(E, x, y) = \frac{1}{\xi} \sum_{\lambda=-\infty}^{+\infty} \sum_{\mu=-\infty}^{+\infty} \cos \frac{2\pi\lambda x}{b} \cos \frac{2\pi\mu y}{b} f \left[E; \frac{4\pi^2(\lambda^2 + \mu^2)}{b^2} \right], \quad (7)$$

where the space-independent coefficients are defined by

$$f(E; Q) = \int_E^{\infty} S(E') e^{-Q\Theta(E, E')} dE' . \quad (8)$$

In Fermi age theory, the quantity $\Theta(E, E')$ would be replaced by the age, defined according to

$$\tau(E, E') = \frac{1}{3\xi} \int_E^{E'} \frac{dE''}{[\Sigma_s(E'')]^2 [1 - \bar{\mu}(E'')]}, \quad (9)$$

where $\bar{\mu}(E)$ is the average cosine of the laboratory system scattering angle. It is sufficiently accurate in this calculation to assume spherically symmetrical scattering in the c.m. system, whence $\xi = \xi_s$ and

$$\bar{\mu}(E) = \frac{2}{3A} . \quad (10)$$

In the derivation of Eq. (7) it is assumed that the fuel rods are line sources of neutrons, which is rather inaccurate, as can be seen by reference to Fig. 2.4. If the vicinity of the fuel rod be "symmetrized" by replacing the square cavity of side L by the circular one of radius R_2 and if neutron interactions be ignored in the fuel rods themselves, the mean square distance, normal to a rod, traveled by a neutron before it makes a collision with a C^{12} atom is

$$\overline{\rho^2}(E) = R_2^2 + \frac{\pi R_2}{2\Sigma_s(E)} + \frac{4}{3[\Sigma_s(E)]^2} . \quad (11)$$

Part of this distance is due to the presence of the cavity and part to "first flight" of a neutron in the

⁸D. J. Hughes, B. A. Magurno, and M. K. Brussel, *Neutron Cross Sections*, BNL-325, 2nd ed., suppl. 1, p 55 (Jan. 1, 1960).

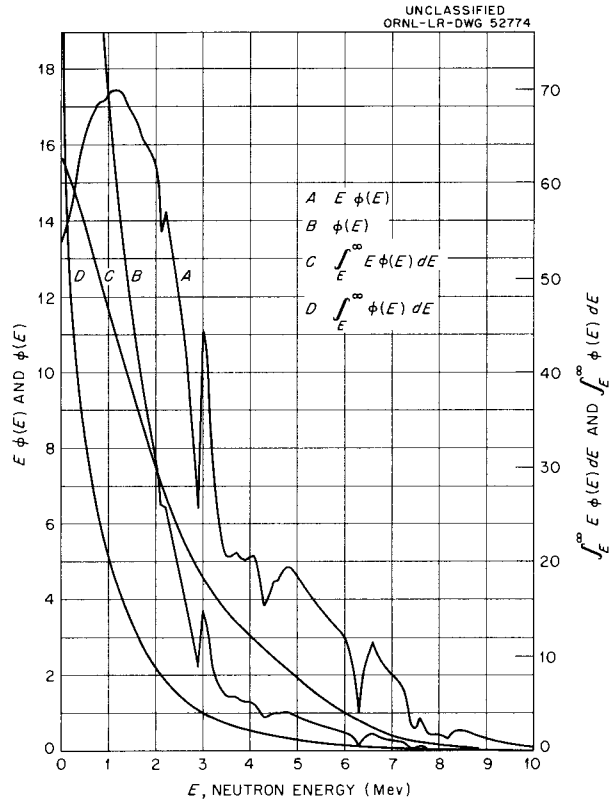


Fig. 2.3. The Fast-Neutron Flux and Related Functions in a Homogeneous Graphite Reactor.

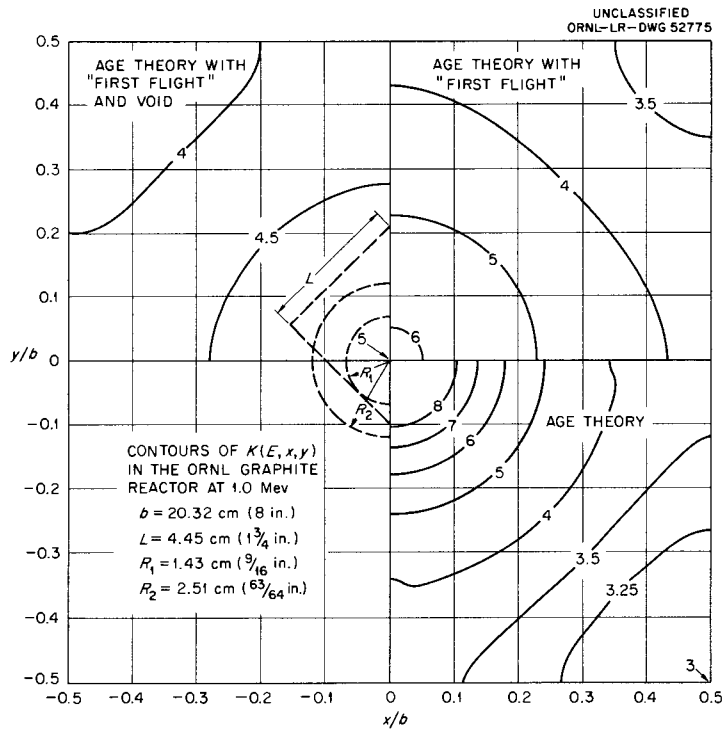


Fig. 2.4. Contours of $K(E, x, y)$ in the ORNL Graphite Reactor at 1.0 Mev.

moderator. As is well known, the mean square distance of travel in Fermi age theory is

$$\overline{\rho_{age}^2} = 4\tau \tag{12}$$

in cylindrical geometry. It is now assumed that neutrons born in a rod travel to the distance indicated by Eq. (11) before beginning to "age." After entering the aging process, however, the presence of the fuel rods and of the cavities is disregarded. With this model,

$$\Theta(E, E') = \tau(E, E') + \frac{1}{3[\Sigma_s(E')]^2} + \frac{\pi R_2}{8\Sigma_s(E')} + \frac{1}{4}R_2^2 \tag{13}$$

Equation (7) has been evaluated on an IBM 704 computer in three approximations: first, the age alone, Eq. (9), was used for $\Theta(E, E')$; next, the effect of "first flight" was introduced by using Eq. (13) with $R_2 = 0$; finally, the complete Eq. (13) was employed. Published cross section data⁸ were used to develop an approximation to the age, which allowed the integrals, Eq. (8), to be expressed in terms of tabulated functions. Contours of $K(E, x, y)$ are shown in Fig. 2.4 for $E = 1.0$ Mev, for each of the three models. The comparative flattening of the distribution using Eq. (13) with respect to that using Eq. (9) will be evident. In Fig. 2.5 is plotted the ratio of the collision density midway between rod centers to that at the center of the unit cell, $K(E, b/2, 0)/K(E, b/2, b/2)$, as a function of energy. The plot is based on the third approximation. This ratio is an approximate measure of the maximum spatial variation in the fast-neutron flux in a typical experimental facility in the Graphite Reactor. Its behavior above about 2 Mev is associated with the behavior of the C^{12} cross section in this region.

The results displayed above may be compared with experiments of two sorts. First, Blewitt *et al.*⁹ have reported that the ripple in the radiation damage rate in copper at 17°K, in Hole 12 of the Graphite

⁹T. H. Blewitt *et al.*, *Solid State Ann. Prog. Rep. Aug. 31, 1958*, ORNL-2614, p 67.

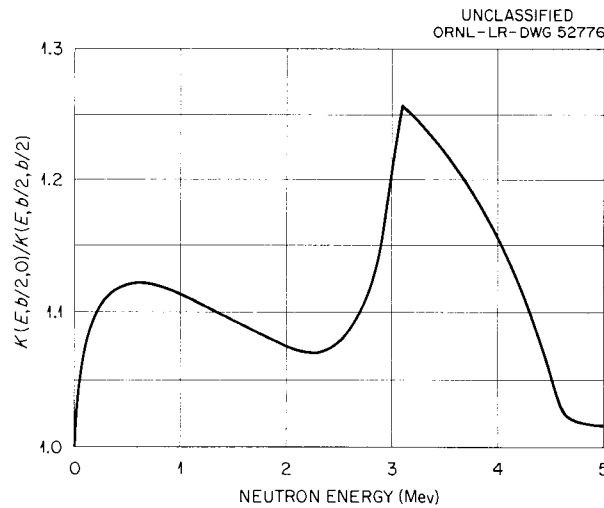


Fig. 2.5. Amplitude of Flux Ripple Along Center of a Unit Cell in the Graphite Reactor.

Reactor, is less than $\pm 4\%$ and probably less than $\pm 2\%$. To a first approximation, ignoring the energy dependence of the copper scattering cross section, the damage rate is proportional to $\int_0^\infty E \phi(E) dE$. Using the heterogeneous spectra calculated above, we compute

$$\frac{\int_0^\infty E \phi(E, b/2, 0) dE}{\int_0^\infty E \phi(E, b/2, b/2) dE} = 1.106 .$$

Thus, the maximum ripple in the damage rate should be about $\pm 5\%$. However, Hole 12 is sufficiently large (4×4 in.) that the amount of graphite between the experimental facility and the neighboring fuel rods is significantly less than assumed in the calculations. This may be regarded as adding to the moderated spectrum a nearly spatially independent component having the shape of the uncollided fission spectrum, thus reducing the ripple below that which would prevail in a fully moderated facility. Furthermore, the decrease in the copper scattering cross section with increasing energy and the effects of increased forwardness of scattering at higher energies will tend to reduce the calculated ripple. It is concluded that the calculations are consistent with the experiment cited.

Alternatively, the calculated spectra may be compared with the fast-flux measurements made in several facilities by Binder.¹⁰ For this purpose we employ the data which he reports for Hole A of the Graphite Reactor, choosing this because it approaches nearly the assumptions made in the heterogeneous calculations. Using published fission cross section data¹¹ for U^{238} (threshold about 1.4 Mev) and Np^{237} (threshold about 0.6 Mev) and the *homogeneous* flux spectrum of Fig. 2.3, we compute the results in Table 2.1. The accuracy of the calculated ratio of the response of the two detectors depends upon the accuracy of the two fission cross sections and upon the accuracy of the *shape* of the C^{12} scattering cross section. We do not believe the uncertainty from these sources to be less than about 10%, which amount has been indicated in the table. Corresponding results calculated for the fission spectrum,

¹⁰D. Binder, private communication.

¹¹H. W. Schmitt and R. B. Murray, *Phys. Rev.* **116**, 1575 (1959); W. D. Allen and R. L. Henkel, *Progr. in Nuclear Energy*, Ser. 1, vol 2, Pergamon Press, New York, 1958.

Table 2.1. Comparison of Calculated Fast-Neutron Spectrum with Experiments (Hole A)

Detector	$\int_0^\infty \sigma(E) \phi(E) dE$ (arbitrary units)		
	Calculated	Observed*	Fission Spectrum
Np^{237} (<i>n, f</i>)	49.74	0.94 ± 0.07	1.38
U^{238} (<i>n, f</i>)	7.67	0.13 ± 0.01	0.285
Ratio Np^{237}/U^{238}	6.48 ± 0.65	7.22 ± 0.80	4.83 ± 0.48

*D. Binder, private communication.

Eq. (2), are shown for comparison. The agreement between calculated and observed results is believed to be satisfactory.

Table 2.2 summarizes the data which Binder obtained in several holes in the Graphite Reactor. It will be seen that Hole 51 follows the fission spectrum very closely, a result to be anticipated from the presence of a converter in this facility. In order to estimate the flux spectrum in facilities intermediate between the virgin and moderated spectra, it is assumed that the spectrum may be represented by

$$\phi(E) = A[B \phi_H(E) + (1 - B) \phi_F(E)] \quad , \quad (14)$$

where A is an arbitrary scale factor and B is determined from

$$B = 0.0386 \frac{R - 4.832}{6.549 - R} \quad , \quad 4.832 \leq R \leq 6.485 \quad , \quad (15)$$

where R is the ratio of the activities induced in Np^{237} and U^{238} detectors. In Eq. (14), $\phi_H(E)$ is to be taken from Fig. 2.3 and $\phi_F(E)$ from Eq. (2). Values of B are recorded in Table 2.2.

Table 2.2. Summary of Binder's Fast-Neutron Flux Data in the ORNL Graphite Reactor*

Hole	Detector Response (arbitrary units)		Ratio	B
	Np^{237}	U^{238}		
51 (center)	4.64	0.96	4.83 ± 0.48	0
51 (12 in. out)	1.56	0.28	5.57 ± 0.56	0.02
1768	3.42	0.52	6.58 ± 0.66	1
A	0.94 ± 0.07	0.13 ± 0.01	7.22 ± 0.80	1
19 (can 18)	1.43	0.15 ± 0.02	9.53 ± 1.36	1

*D. Binder, private communication.

Part II
METALS AND ALLOYS



3. LOW-TEMPERATURE IRRADIATION STUDIES

RADIATION EFFECTS IN COPPER AND ALUMINUM ARISING FROM FISSILE IMPURITIES

T. H. Blewitt C. E. Klabunde
R. R. Coltman J. K. Redman

The isochronal annealing curve obtained from resistivity measurements on copper bombarded at temperatures below 10°K by reactor neutrons differs in some important aspects from that observed when the bombardment is performed by electrons whose energy is slightly in excess of the displacement threshold. Since the majority of the neutron damage arises from primary displacements whose energy is several orders of magnitude greater than the displacement threshold, these differences in recovery can be attributed to the energy of the primary displacement. Experimental evidence to support this concept cannot be obtained from neutron elastic interactions as it is difficult to change the neutron spectrum; however, by the utilization of fission reactions introduced by inelastic neutron interactions, particles of widely different energy can be introduced into a metal. In the experiments described here approximately 0.1 at. % of U²³⁵, U²³⁸, B¹⁰, and B¹¹ were added to aluminum and copper. In the cases of U²³⁵ and B¹⁰ it is well known that slow-neutron capture results in fission, with the U²³⁵ yielding two fragments (masses about 90 and 140) and about 150 Mev of energy. The B¹⁰ yields Li⁷ and an alpha particle with a combined energy of about 2.7 Mev. The isotopes U²³⁸ and B¹¹ are nonfissile and were added for control experiments.

The results obtained are as follows:

1. The initial rate of increase of resistivity with dose in U²³⁵-doped copper and aluminum is 150 times the rate for the pure metals. When the cross sections of the processes are considered, it can be concluded that initially each fission of U²³⁵ produces 900 times as many defects as a primary displacement arising from a reactor neutron.

2. In U²³⁵-doped copper and aluminum the resistivity increases in accordance with the following equation: $\rho = A[1 - \exp(-\alpha\phi)] + B\phi$. The saturation value, A, of the exponential term is in good agreement with that found by Cooper, Koehler, and Marx.¹ The experimental data can be seen in Figs. 3.1 and 3.2.

3. The isochronal annealing curves of U²³⁵-doped copper² and aluminum are similar to those of the pure metals when small fission doses are considered ($\Delta\rho < 5 \times 10^{-8}$ ohm-cm). At higher doses the annealing peak in the region from 35 to 45°K is diminished from that observed in the pure metals. This can be seen in Figs. 3.3 and 3.4.

4. In the case of B¹⁰-doped copper³ the resistivity increases at ten times the rate of pure copper. When scattering and absorption cross sections are considered, it can be concluded that each fission produces eight times as many defects as are produced from a primary displacement by a reactor neutron.

5. The resistivity-dose curve of B¹⁰-doped copper is linear (to a first approximation). This is shown in Fig. 3.5.

6. The isochronal annealing curve of copper irradiated by B¹⁰ fragments differs in some aspects from that observed from fast-neutron-irradiated copper. A higher percentage of the induced resistivity is observed to anneal in the temperature

¹G. Cooper, J. Koehler, and J. Marx, *Phys. Rev.* 97, 599 (1955).

²A difficulty in dissolving uranium in copper results in local segregation which is dependent upon the thermal history. This segregation results in an apparent decrease of the 35 to 45°K annealing peak.

³Boron is immiscible with aluminum.

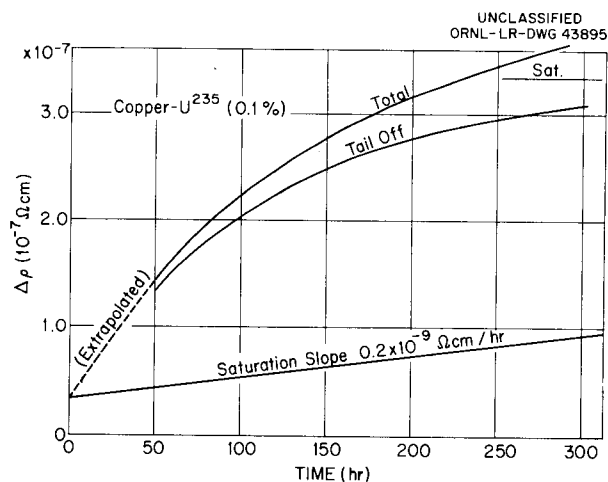


Fig. 3.1. Damage Rate of U²³⁵-Doped Copper. Bombardment temperature, 4.5°K. Flux, 6×10^{11} *nv*.

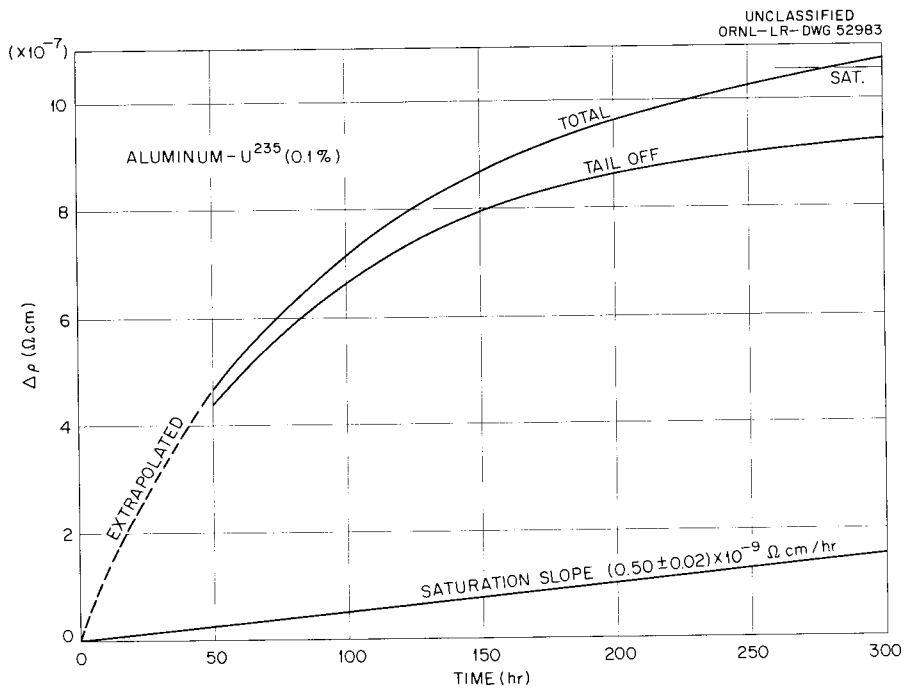


Fig. 3.2. Damage Rate of U²³⁵-Doped Aluminum. Bombardment temperature, 4.5°K. Flux, 6×10^{11} *nv*.

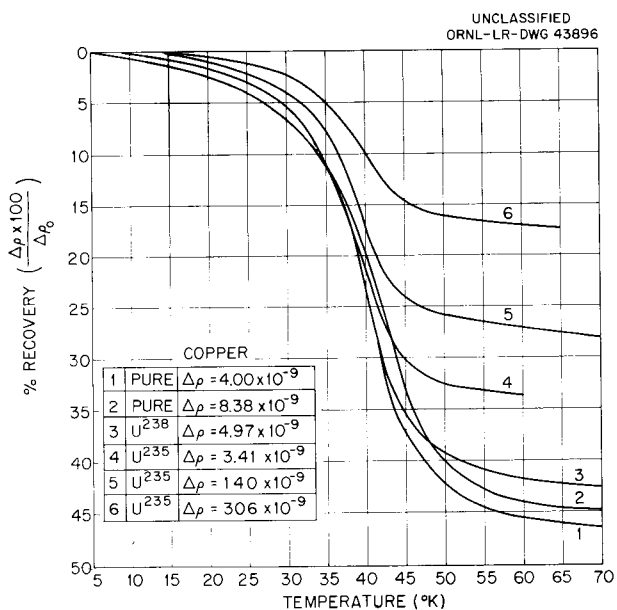


Fig. 3.3. Isochronal Annealing of Various Copper Specimens.

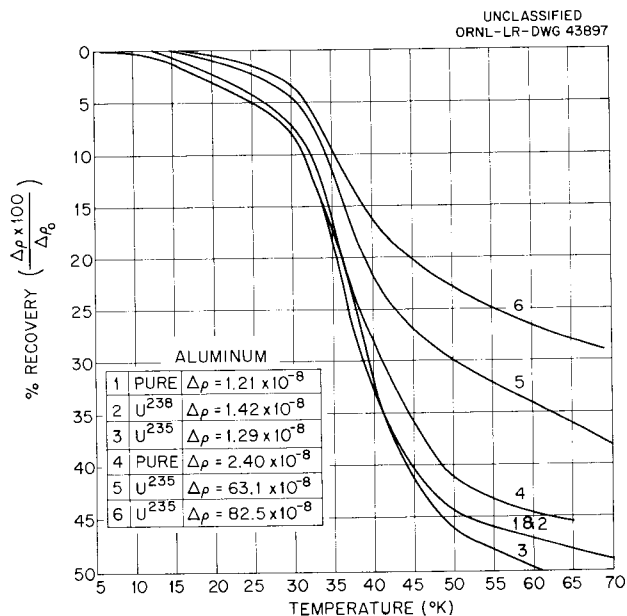


Fig. 3.4. Isochronal Annealing of Various Aluminum Specimens.

region below 60°K than is observed in the case of fast-neutron irradiation. This is illustrated in Fig. 3.6. Furthermore, when the details of the annealing curve are examined in the range from 7 to 35°K, three distinct annealing peaks are found

superimposed on the continuum found in neutron-irradiated copper. This is illustrated in the isochronal annealing curves shown in Fig. 3.7 and in the differential of the isochronal curve shown in Fig. 3.8.

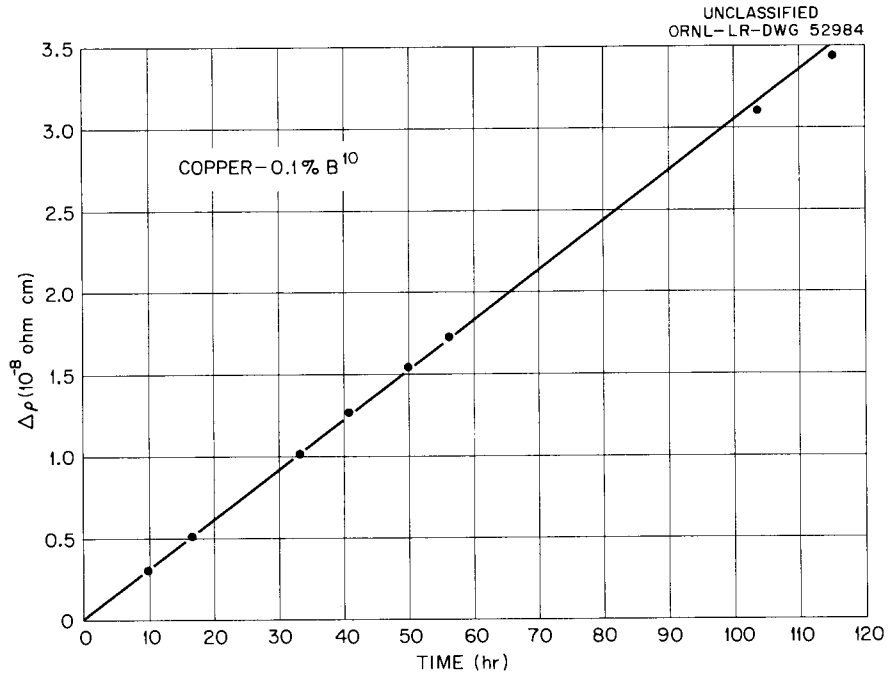


Fig. 3.5. Damage Rate of B¹⁰-Doped Copper. Bombardment temperature, 4.5°K. Flux, 6×10^{11} *nv*.

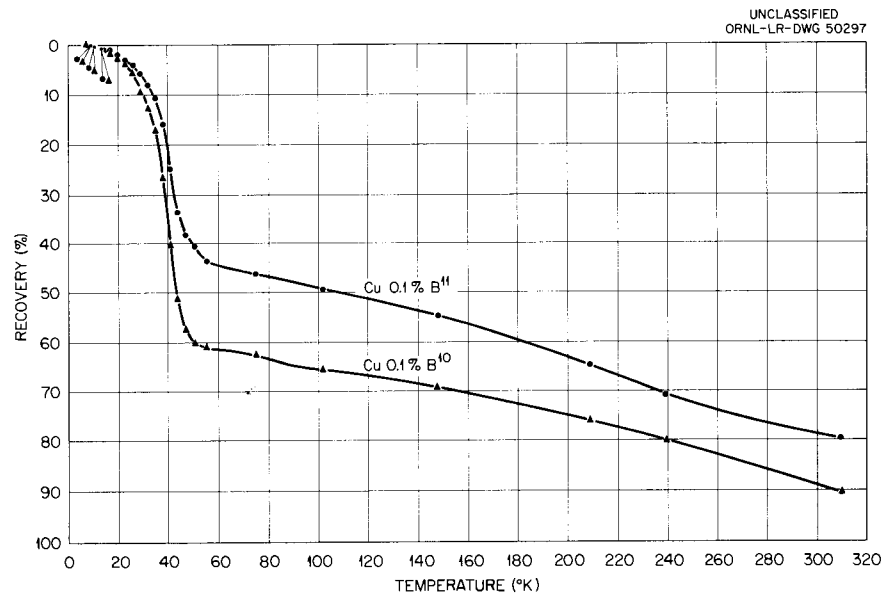


Fig. 3.6. Isochronal Annealing of Boron-Doped Copper. Bombardment temperature, 4.5°K. Flux, 4×10^{17} *nv*. 3-min pulses.

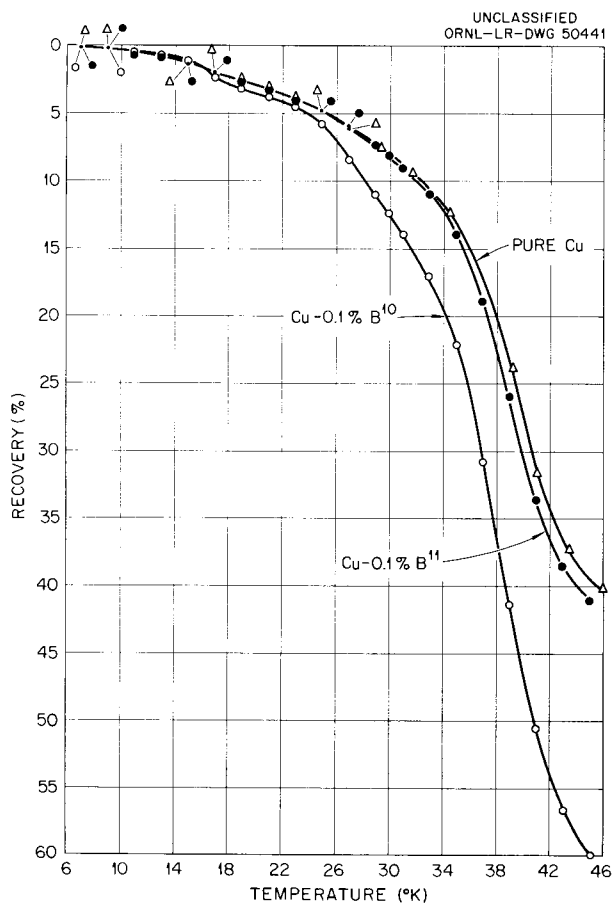


Fig. 3.7. Isochronal Annealing of Copper and B¹⁰-Doped Copper. Bombardment temperature, 4.5°K. Flux, 3×10^{17} nvt. 10-min pulses.

The appearance of discrete peaks in the low-temperature isochronal annealing of the boron-doped copper is highly significant as it establishes the differences and similarities of neutron- and

electron-irradiated copper. It can be readily seen from Fig. 3.7, where the differential isochronal annealing curves of electron, neutron, and B¹⁰ fission fragment (alpha particle) irradiated copper are shown, that the damage can be separated into a portion similar to neutron irradiation and a portion similar to electron irradiation. It can also be concluded that the main annealing peak in neutron-irradiated copper (35–45°K) and its satellite (50–60°K) coincide with those observed in electron irradiation. The main difference between the two types of damage, then, appears to be in the fact that the discrete peaks below 35°K are smeared into a continuum for neutron damage. On the other hand, it does appear that the main peaks in both electron and neutron damage (35–45°K) are probably the result of the same defect. These experiments, then, offer substantial evidence that the thermal spike does not play a serious role in neutron-irradiated copper.

The observed result that the resistivity-dose curve of U²³⁵-doped copper can be separated into two components, a linear term plus an exponential term, implies that two different kinds of lattice damage are occurring. Additional evidence to support this conclusion can be obtained by annealing a sample to room temperature after a high dose (e.g., $\Delta\rho \sim 3 \times 10^{-7}$ ohm-cm). A large fraction of the resistivity will remain, presumably associated with the linear terms; however, on rebombarding at 4°K the initial rate of resistivity increase is observed to be in agreement with that of a previously unbombarded sample. The deduction that at least two kinds of damage result from neutron bombardment is in agreement with that deduced from the earlier experiments on radiation hardening.

UNCLASSIFIED
ORNL-LR-DWG 50470

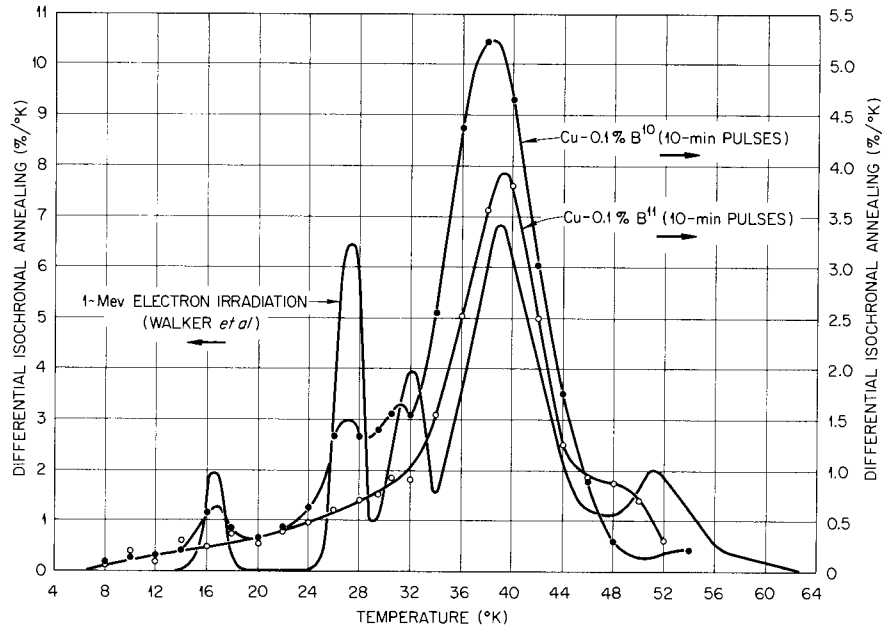


Fig. 3.8. Differential Isochronal Annealing of Copper. Bombardment temperature, 4.5°K. Flux, 3×10^{17} nvt.

LENGTH CHANGE MEASUREMENTS IN ALUMINUM AND COPPER

T. H. Blewitt C. E. Klabunde
R. R. Coltman J. K. Redman

The change in volume associated with neutron-irradiated metals is an interesting property to measure, as it depends primarily upon a homogeneous dilatation of the lattice spacing plus the movement of matter to a surface. On the other hand, the electrical resistivity depends primarily upon the scattering of electrons by the defect core. It would therefore appear unlikely that the contribution to the volume change from one of the radiation-induced defects (i.e., an interstitial) would give the same proportionate contribution to the electrical resistivity. In mathematical terms one would *not* expect

$$\frac{\Delta\rho_{\text{interstitial}}}{\Delta\rho_{\text{total}}} = \frac{\Delta V_{\text{interstitial}}}{\Delta V_{\text{total}}} \quad (1)$$

If, then, experimentally it were found during isochronal annealing that the percentage recovery of

resistance was identically equal to the percentage recovery of the volume (or length) change then, barring the very unlikely assumption that Eq. (1) held, it would have to be assumed that equal numbers of vacancies and interstitials were being removed.

An experiment of this type was then undertaken. Resistivity was measured in the usual way, and volume changes were measured by changes in length. This latter measurement was performed by making a bimetal strip. One half was a metal doped with 0.1 at. % U^{235} , the other half being the pure metal. Since the ratio of production of defects is 150 times greater in a U^{235} -doped specimen due to fission fragment damage, the dissimilar growth in the two metals will cause a bending and magnify the growth. The $\Delta l/l$ can easily be computed from the bending by elementary physics.

The results of this experiment for copper are shown in Figs. 3.9 and 3.10. In Fig. 3.9 the movement of the bimetal strip is plotted as a function of bombardment time at 4.5°K. In Fig. 3.10 the thermal recovery of the length change is shown.

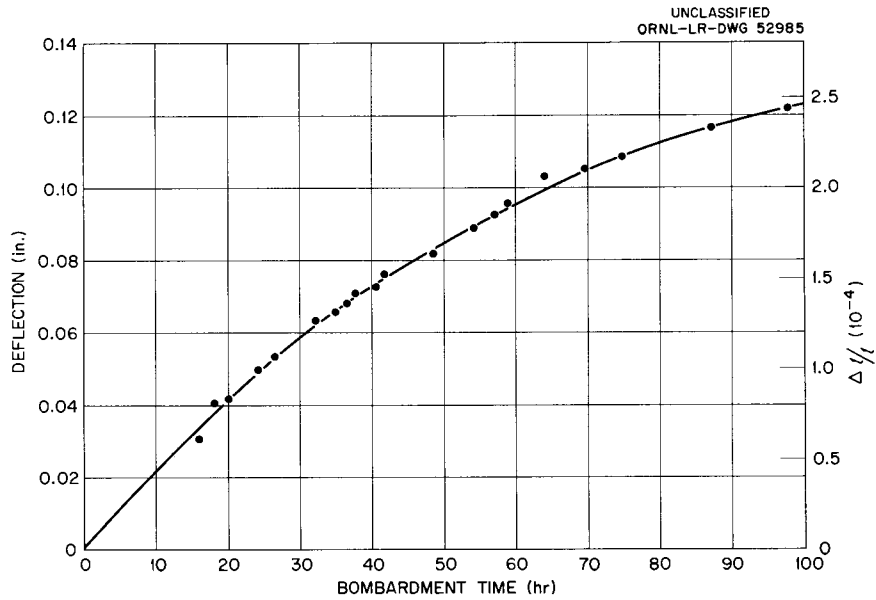


Fig. 3.9. Change in Length of U²³⁵-Doped Copper. Measured with bimetallic strip of Cu-0.1% U²³⁵ vs Cu-0.1% U²³⁸. Rig H.L. 10. Bombardment temperature, 4.5°K. Flux, 6×10^{11} *nv*.

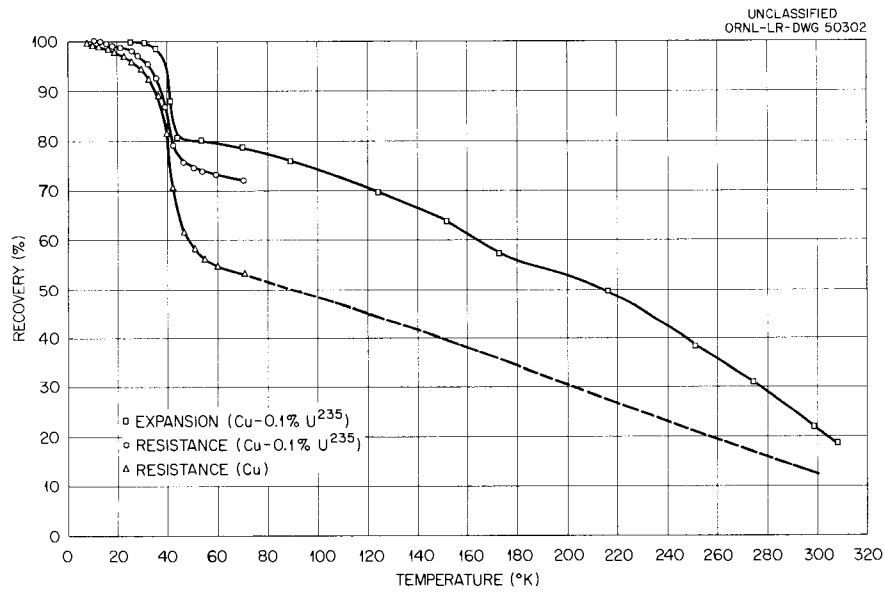


Fig. 3.10. Thermal Recovery of Length Change and Resistivity in Irradiated Copper. Bombardment temperature, 4.5°K.

While these results are not completely satisfactory due to the difficulty of obtaining a reproducible distribution of uranium in copper,⁴ an interesting deduction of the resistivity of Frenkel pairs can be made from the initial damage rate data of length change and resistivity. If it is assumed that one vacancy-interstitial pair expands the lattice 1.5 atomic volumes, then $\Delta l/l = 0.5$ for each pair. From the initial slope of Fig. 3.9 we have

$$\frac{d(\Delta l/l)}{dt} = 5 \times 10^{-6} \text{ per hour.}$$

Therefore, the production rate of pairs is 1×10^{-5} mole fraction per hour, or 1×10^{-3} at. %/hr. The initial rate of resistivity change for this material was measured as 4.25×10^{-9} ohm-cm/hr. The resistivity per atomic per cent of Frenkel pairs, then, is 4.25×10^{-6} ohm-cm. On the other hand, if it is assumed that 3 ev is the formation energy of an interstitial-vacancy pair, then in the low-temperature annealing peak the measured value of stored energy is 0.2 cal/mole (corresponding

to a resistivity recovery of 1.1×10^{-9} ohm-cm) which can be attributed to the annihilation of 2.8×10^{-9} at. % of pairs. The resistivity per atomic per cent of pairs then is 3.9×10^{-6} ohm-cm.

The results obtained from aluminum are similar to those of copper. The resistivity of 1 at. % of interstitial-vacancy pairs is 5×10^{-6} ohm-cm from the expansion measurements under the same assumptions and 9×10^{-6} ohm-cm from the stored-energy measurements. It would thus seem that the stored energy must be somewhat greater or the expansion somewhat less for a vacancy-interstitial pair in aluminum than in copper.

The isochronal annealing of the length change and of the resistivity in U^{235} -doped aluminum is shown in Fig. 3.11. Also plotted on this figure are the isochronal annealing curves of pure aluminum and B^{11} -doped aluminum. It can readily be seen that the recovery of fission damage is very similar to neutron damage. The most important feature of these data is that the annealing curve of the resistivity and that of the length change almost superimpose upon each other. It would thus seem that throughout the annealing spectrum of aluminum the vast majority of the interstitials and vacancies disappear by self-annihilation.

⁴A difficulty in dissolving uranium in copper results in local segregation which is dependent upon the thermal history. This segregation results in an apparent decrease of the 35 to 45°K annealing peak.

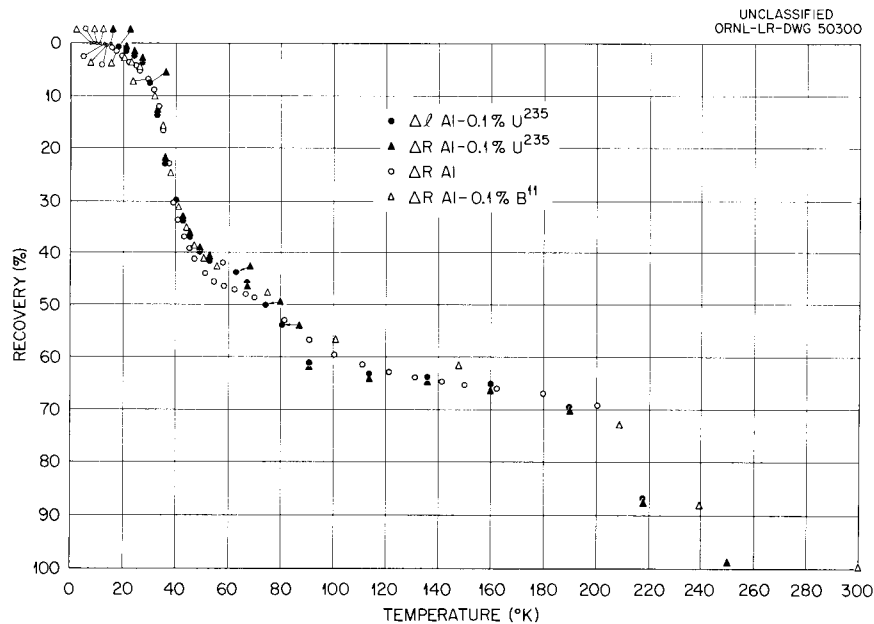


Fig. 3.11. Recovery of Irradiated Aluminum. Bombardment temperature, 4.5°K.

ISOCHRONAL ANNEALING OF NEUTRON-IRRADIATED METALS

T. H. Blewitt C. E. Klabunde
R. R. Coltman J. K. Redman

The annealing spectrum of neutron-irradiated metals has been studied by isochronal recovery of the radiation-induced resistivity. Seven face-centered cubic metals (Cu, Ag, Au, Ni, Pd, Pt, and Al) have been studied in great detail in the region from 7 to 300°K. The main purpose of these measurements was to search for annealing peaks in the region from 7 to 35°K and near 250°K. Such peaks have been found after bombardment with energetic electrons⁵ and deuterons⁶ but had not been found in earlier studies of neutron-irradiated metals.

All of the samples were bombarded in the ORNL Graphite Reactor near 4.5°K for 300 hr (8×10^{17} reactor neutrons/cm²). During the bombardment the resistivity was measured as a function of dose, and a linear relationship was observed. Isochronal annealing was done by a pulse technique; that is, all measurements of the resistivity were made at a constant temperature of 4.7°K following an annealing pulse of 3 min at the indicated temperature. This pulse technique is

⁵J. W. Corbett and R. M. Walker, *Phys. Rev.* 110, 767 (1958).

⁶G. D. Magnuson, W. Palmer, and J. S. Koehler, *Phys. Rev.* 109, 1990 (1958).

very important, as experiments show that the resistivity ρ at temperature T cannot be separated into a residual component ρ_0 and a temperature-dependent component ρ_T when ρ_0 and ρ_T are the same magnitude; that is, $\rho \neq \rho_0 + \rho_T$. With the pulse technique, however, all measurements are made near 4°K, where the term ρ_T approaches zero. The pulse temperature was measured by the use of a carbon resistor below 200°K and a copper-constantan thermocouple above this temperature.

The isochronal annealing curves for Cu, Ag, and Au are shown in Fig. 3.12, for Ni, Pd, and Pt in Fig. 3.13, and for Al in Fig. 3.14. The differentials for these isochronal annealing curves are plotted respectively in Figs. 3.15–3.17. The most important features evident from Figs. 3.12 and 3.15 are the absence of structure in the main annealing peak of Ag and Cu, the absence of a discrete annealing peak in Au, and the absence of a discrete annealing peak in the region just below room temperature in all three metals. In the Ni, Pd, and Pt series shown in Figs. 3.13 and 3.16, the outstanding features are the complicated annealing spectrum of Ni and Pd and the relative simplicity of the Pt annealing spectrum, which shows a major peak with two satellites.

It is also interesting to note that in both the Cu and Ag series and the Ni, Pd, and Pt series the temperature of the major annealing peak shifts to lower values as the mass increases (or as the Debye temperature θ_D decreases).

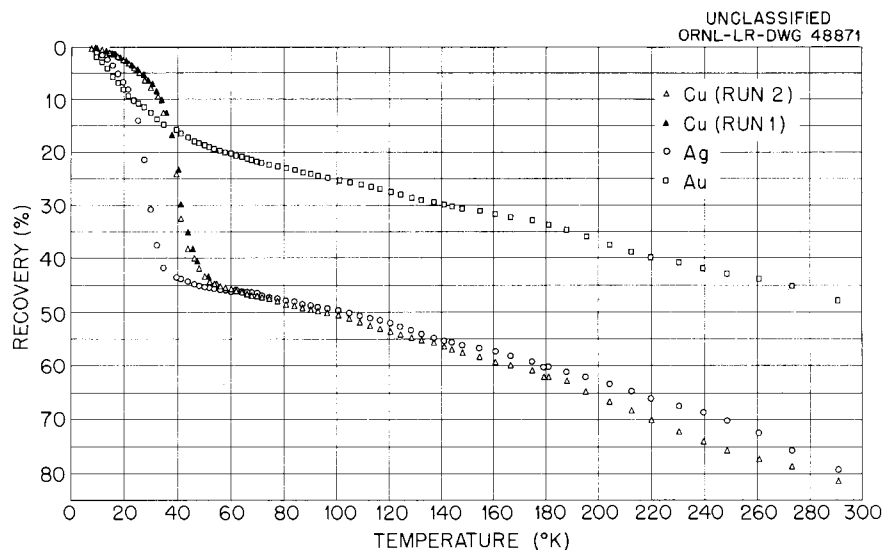


Fig. 3.12. Isochronal Annealing of Copper, Silver, and Gold.

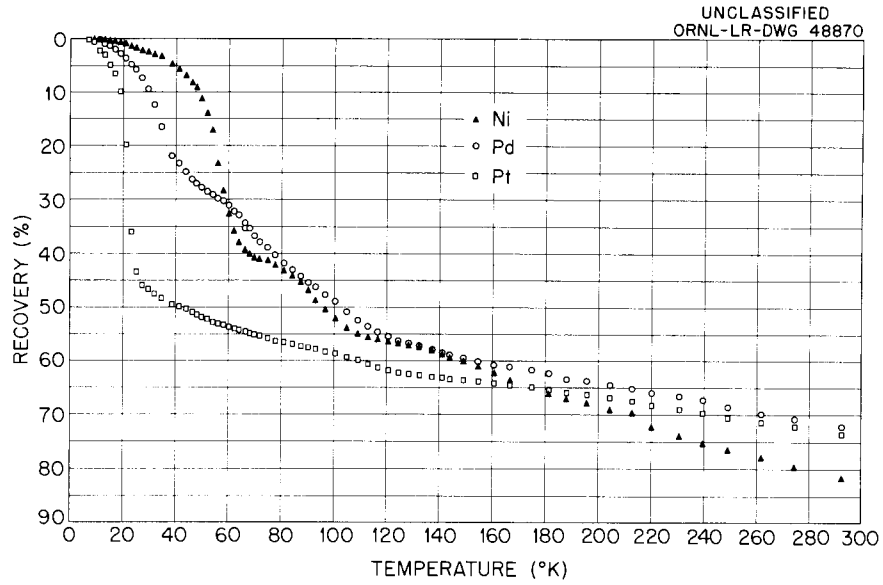


Fig. 3.13. Isochronal Annealing of Nickel, Palladium, and Platinum.

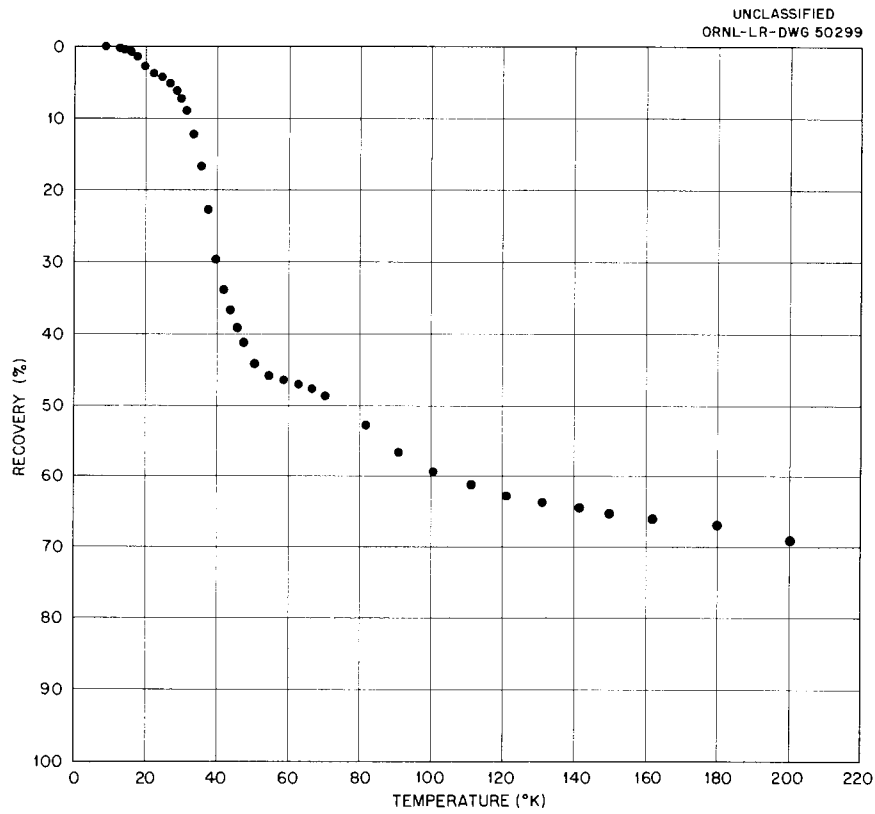


Fig. 3.14. Isochronal Annealing of Aluminum.

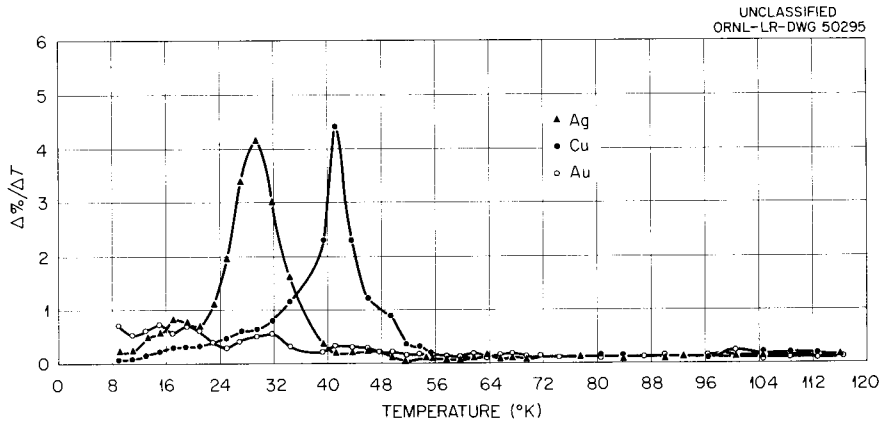


Fig. 3.15. Differential Isochronal Annealing of Copper, Silver, and Gold.

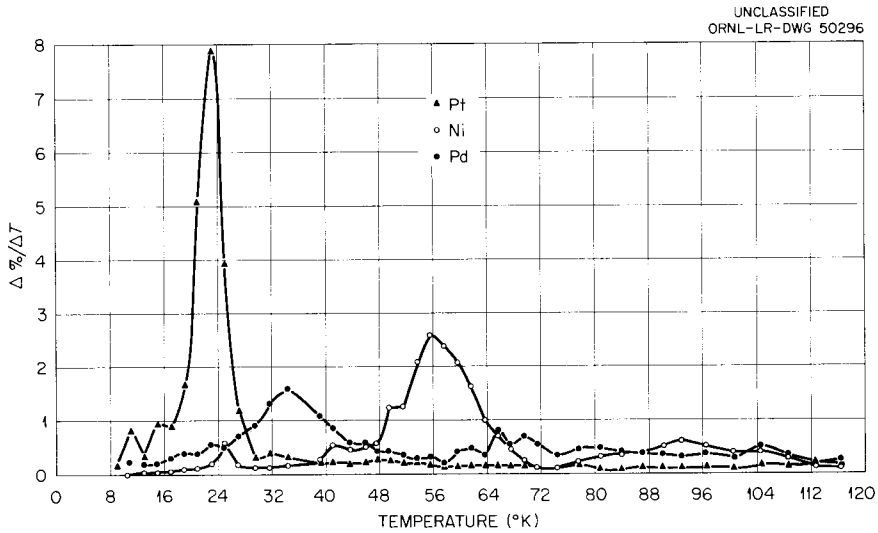


Fig. 3.16. Differential Isochronal Annealing of Nickel, Palladium, and Platinum.

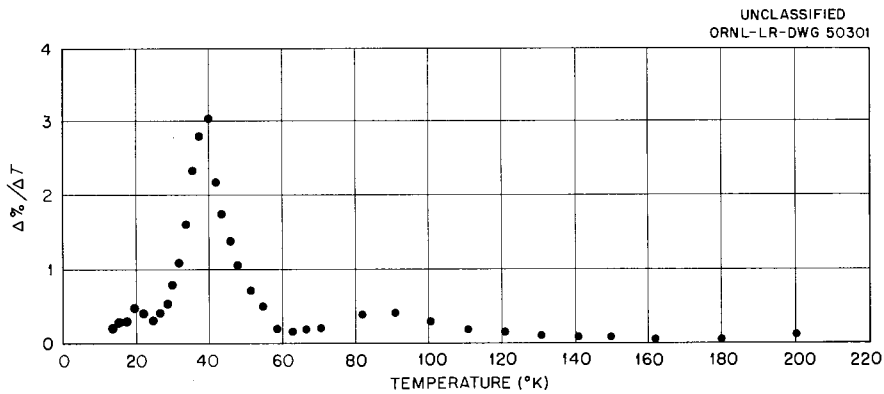


Fig. 3.17. Differential Isochronal Annealing of Aluminum.

HELIUM REFRIGERATOR MODIFICATION

T. H. Blewitt R. R. Coltman
C. E. Klabunde

The present low-temperature irradiation facility in which neutron bombardments can be made near 4°K has a usable sample chamber diameter of 1/2 in. (Construction and operating details of this facility have been described elsewhere.^{7,8}) There are a number of experiments which would be highly desirable to perform upon specimens bombarded at 4°K but which do not seem possible in the present facility because of the severe space limitations. Some of these experiments are stored energy, mechanical properties, and changes in length requiring greater sensitivity than those measurements described elsewhere in this report.

The present low-temperature facility uses a large-capacity helium refrigerator with adiabatic expansion engines to produce the refrigeration. This device then serves as a thermal shield and heat sink for a low mass flow, closed circuit Joule-Thomson expansion process by which liquid helium is produced at 4°K. From a study of the entropy diagram for helium and the present operating characteristics of the large helium refrigerator it appears that with appropriate modifications it might be possible to obtain engine discharge temperatures below the critical temperature of helium (5.2°K). If this result could be achieved, then the present Joule-Thomson expansion circuit could be eliminated and the original cryostat with a 1 1/4-in.-dia sample chamber could be used for bombardments near 5°K. This cryostat presently serves as a thermal shield for the liquefier circuit.

An attempt to reach such low engine-discharge temperatures requires the following modifications: (1) engine discharge pressures below the critical pressure of helium (18 psig); (2) over-all thermal heat load reduction; (3) increased heat exchanger efficiency. A new heat exchanger designed by the Low-Temperature Group and fabricated by the Joy Manufacturing Company has been assembled and insulated with a hard vacuum and multiple reflection shields. Operation of this heat exchanger indicates that substantial reductions in

thermal heat load and pressure drop have been achieved, and that the exchanger is capable of handling larger mass flows than those presently used. Installation of a new first-stage compressor is in progress. It is expected that this compressor will lower the engine discharge pressure to 9 to 10 psig and increase the mass flow by 30%.

The possible limiting factor in this approach could be the behavior of the expansion engines under these extreme conditions. If engine efficiency is found to decrease too much, then the modifications now in progress will permit the adaptation of a more simple Joule-Thomson expansion circuit that could handle considerable larger mass flow than the present circuit.

ENERGY RELEASE IN REACTOR-IRRADIATED
COPPER. PART II. THE 600 TO 700°K
RELEASE

T. H. Blewitt J. Diehl⁹ S. T. Sekula

The facility built in the pool of the Oak Ridge Research Reactor opposite fuel position A-4 previously described¹⁰ is currently being used for calorimetric studies as well as sample irradiations. Details of the calorimetric technique and stored energy measurements on neutron-irradiated copper are being prepared for publication¹¹ and the following is an abstract of the work:

The energy release associated with the recovery peak occurring between 600 and 700°K in neutron-irradiated copper was measured utilizing a new technique, that of nuclear heating. Following a bombardment at 40°C of 1.7×10^{20} fast neutrons of a 1/E distribution which raised the critical shear stress to 12.8 kg/mm² at 4.2°K (5.2 kg/mm² at 300°K), a release of 7.7 cal/mole was measured. By using this measured value of the energy release it is possible to estimate the number of defects annihilated if it is assumed that the annealing is the result of the migration and subsequent annihilation of a single defect. In this way the numbers of interstitials, vacancies, interstitial-vacancy pairs, and dislocation lines

⁷R. R. Coltman *et al.*, *Solid State Ann. Prog. Rep.* Aug. 31, 1958, ORNL-2614, p 69.

⁸J. T. Howe, R. R. Coltman, and T. H. Blewitt, "Liquid Helium Temperatures in an Atomic Reactor," *Proc. 1957 Cryogenic Eng. Conf.*

⁹Guest scientist from Max Planck Institut für Metallforschung, Stuttgart, Germany.

¹⁰T. H. Blewitt and J. Diehl, *Solid State Ann. Prog. Rep.* Aug. 31, 1959, ORNL-2829, p 78.

¹¹Submitted to the *Physical Review*.

required to account for the measured energy release were estimated. The values were respectively 5×10^{19} per mole, 2×10^{20} per mole, 4×10^{19} per mole, and 1×10^{12} cm/mole.

INTERNAL OXIDATION STUDIES OF DILUTE NOBLE METAL ALLOYS

S. T. Sekula

Introduction

Previous work^{12,13} has demonstrated that the heat treatment of 99.999% pure copper in oxygen at pressures as low as 10μ Hg results in a reduction of the residual resistivity, along with a disappearance of the resistance minimum. In an effort to understand this phenomenon more fully, several dilute alloys have been studied, and a portion of this work is reported here.

Before discussing the results obtained with specific alloys, it would be advantageous to consider in general terms the effect of an oxidation heat treatment on the residual resistivity of dilute alloys (0.1 at. % or less). In the case of copper-base alloys containing small amounts of Fe, Si, Al, and As, respectively, it has been found that annealing in oxygen at high temperatures results in a considerable decrease of the residual resistivity. An alloy of Ni in Cu, however, exhibits only a small decrease in the residual resistivity after such a heat treatment. These results can be qualitatively understood on the basis of the preferential oxidation of the impurities. During the heat treatment oxygen diffuses into the metal and may precipitate the impurities as oxides, thereby altering the electrical properties of the material and in some cases its magnetic properties. The factors which control the degree of internal oxidation of the impurities would then seem to be: (1) the free energy of formation of the oxides of copper and the impurity oxides, (2) the heat of solution of the alloying agent, and (3) the equilibrium oxygen concentration in the copper matrix at the annealing temperature. It should be pointed out that Cu_2O and impurity oxide inclusions are to be expected to increase the resistivity of the alloy, but this

effect is masked by the larger decrease in resistivity due to the removal of impurities from solid solution, even at low concentrations.¹³

Internal Oxidation in Copper-Iron Alloys

An alloy of 0.1 at. % iron in copper is characterized by a very large residual resistivity (1.0×10^{-6} ohm-cm) and a deep resistance minimum which is known to be due to the solution of iron in copper.¹⁴ Subsequent heat treatments in oxygen reduce the resistivity, make the minimum shallower, and decrease the temperature at minimum resistance. After a total time of 4 hr in 15μ of air at 750°C the minimum is not experimentally visible, and the residual resistivity is saturated at its low value of $\sim 5 \times 10^{-9}$ ohm-cm. This decrease in residual resistivity gives rise to a decrease of 35% in the room-temperature value. In this alloy it has been found that the oxidized iron impurities can be reduced with restoration of the original large residual resistivity. Magnetic measurements discussed elsewhere in this report support the view that the oxidized particles of iron aggregate into clusters of the order of 100 Å in diameter.

Internal Oxidation in Copper-Nickel Alloys

A 0.1 at. % nickel in copper alloy is among the alloys that are currently being studied, since nickel, a ferromagnetic metal, does not scatter electrons as strongly as iron in copper. Moreover, the free energy of formation of nickel oxide, in contrast to the iron oxides, does not differ appreciably from the free energy of formation of Cu_2O . Experimentally, it is found that the residual resistivity of this material is approximately 1.2×10^{-7} ohm-cm, in agreement with data of J. O. Linde.¹⁵ Annealing in oxygen at a pressure of 20μ Hg at 800°C causes the resistivity to decrease to a value of 1.1×10^{-7} ohm-cm. Further heat treatment at this temperature does not appreciably change this value. This is interpreted as an indication that only $\sim 10\%$ of the nickel is precipitated as an oxide. Thus the resistance minimum which is observed to disappear after the

¹⁴W. B. Pearson, *Phil. Mag.* 46, 920 (1955).

¹⁵J. O. Linde, *Elektrische Widerstandseigenschaften der verdünnten Legierungen des Kupfers, Silbers, und Goldes*, Gleerupska Univ.-Bokhandel, Lund, Sweden, 1939.

¹²J. K. Redman *et al.*, *Bull. Am. Phys. Soc.* 4, 150 (1959).

¹³S. T. Sekula, *Phys. Rev. Letters* 3, 416 (1959).

UNCLASSIFIED
ORNL - LR - DWG 52986

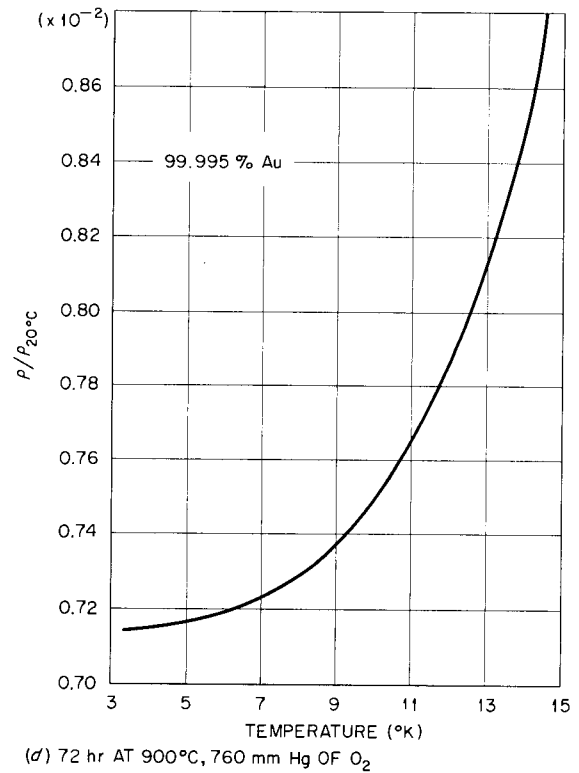
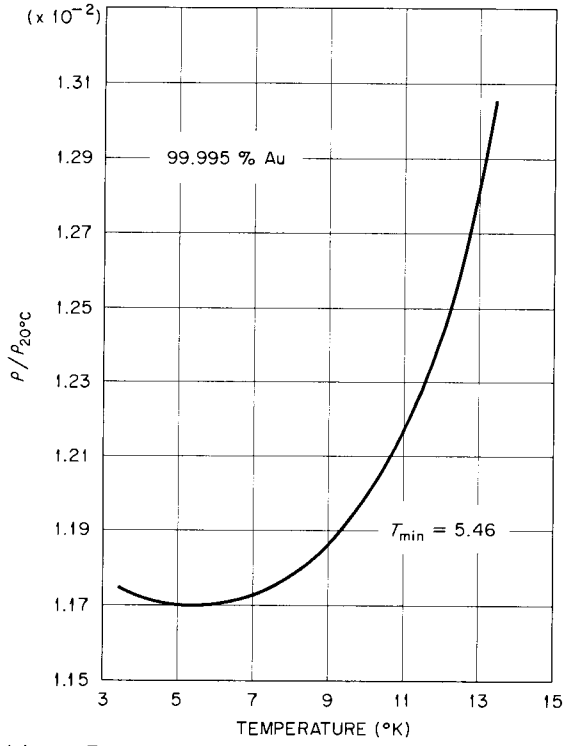
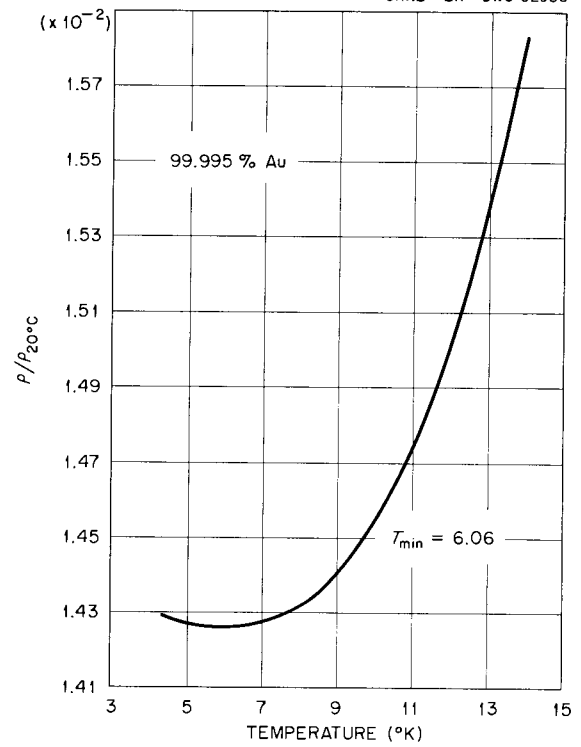
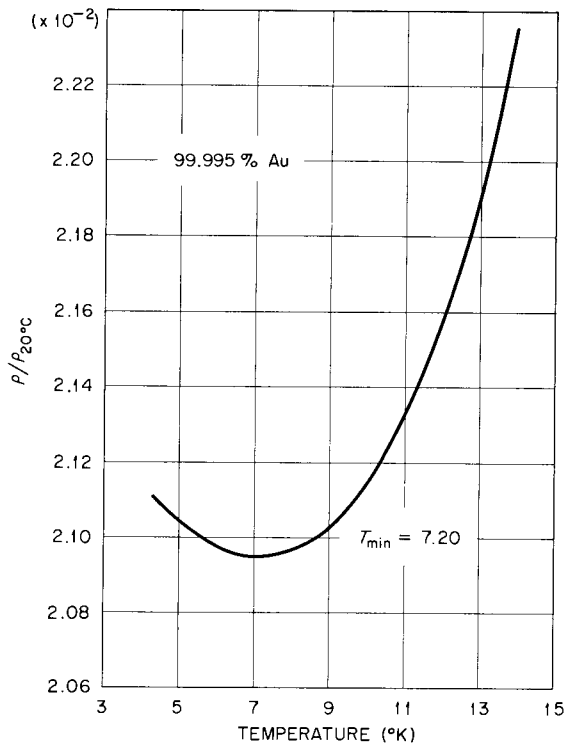


Fig. 3.18. Effect of Internal Oxidation on the Resistivity of Gold (99.995% pure); $\rho_{20^\circ\text{C}} = 2.20 \times 10^{-6}$ ohm-cm.

oxidation treatment is probably not due to the presence of nickel in solution. Subsequent activation analysis reveals trace amounts of cobalt ($\sim 4 \times 10^{-4}$ at. %), and it is believed that the minimum is due to this impurity.

Internal Oxidation in a Gold Alloy

Gold of 99.995% nominal purity has been analyzed by radioactivation and is found to contain silver as a major impurity in a relative concentration of 5.7×10^{-5} . The residual resistivity of this alloy is found to be approximately 4.1×10^{-8} ohm-cm, while the resistivity computed from the above-quoted concentration of silver and the resistivity contribution per atomic per cent of silver in gold given by Linde¹⁵ is approximately 2.0×10^{-9} ohm-cm. Since the radioactivation analysis has been carried out only for impurities having long-lived isotopes, it seems likely that other impurities are present in considerable concentrations.

The temperature dependence of the resistivity after a preliminary heat treatment in a reducing atmosphere is shown in Fig. 3.18a. The resistance minimum and residual resistivity are visibly affected by annealing in oxygen at high temperatures as shown in Fig. 3.18b and c. Figure 3.18d shows that, after a prolonged heat in oxygen at 1 atm, the minimum has vanished, and the residual resistivity has decreased to a value of $\sim 1.5 \times 10^{-8}$ ohm-cm. Subsequent heating in a reducing atmosphere (25 μ Hg of CO at 900°C) restores the minimum and the higher resistivity.

EFFECTS OF GASEOUS IMPURITIES ON THE MAGNETIC PROPERTIES OF COPPER

E. Sonder S. T. Sekula

Recent experiments on the influence of gaseous impurities on the resistance minimum and residual resistance of copper^{16,17} have shown that oxidation of 99.999% copper causes a reduction in residual resistance and the disappearance of the anomalous resistance minimum. Since small concentrations of iron are known to induce a resistance minimum in copper, it was felt worthwhile

¹⁶S. T. Sekula, *Phys. Rev. Letters* **3**, 416 (1959).

¹⁷J. K. Redman et al., *Solid State Ann. Prog. Rep.* Aug. 31, 1959, ORNL-2829, p 74; *Bull. Am. Phys. Soc.* **4**, 150 (1959).

to investigate the magnetic behavior of nominally pure copper upon annealing in reducing and oxidizing atmospheres.

In the Faraday method of measuring the magnetic susceptibility, a change in force due to a magnetic field gradient is measured with a sensitive balance. If the field strength and gradient are assumed constant along the length of the sample (i.e., if the sample is small), the susceptibility, κ_t , of a sample having a small amount of ferromagnetism is given by¹⁸ $\kappa_t = \kappa + c\sigma/H$, where κ is the field-independent paramagnetic or diamagnetic susceptibility per cubic centimeter, H is the magnetic field strength, and c and σ are the concentration and magnetic moment per gram of ferromagnetic material respectively. The intercept of a plot of κ_t vs $1/H$ will therefore yield the net diamagnetic susceptibility (this includes paramagnetic contributions of dissolved impurities) of the material; the slope of the plot will yield the amount of ferromagnetic constituent. In the case of the equipment used in these measurements the field variation along the full length of the specimen is appreciable, causing the plot of κ_t vs $1/H$ to deviate from a straight line. This, however, has no effect upon the accuracy of determining the susceptibility of purely diamagnetic or paramagnetic samples and only decreases the accuracy of determining κ and c in samples that contain a ferromagnetic constituent.

Figure 3.19 shows the behavior of a "reduced" (annealed for 2 hr at 900°C under 15 μ of CO) sample of 99.999% copper as a function of temperature. The increase of paramagnetism below $\sim 100^\circ\text{K}$ indicates the presence of a paramagnetic impurity. The data can be accounted for by assuming $\sim 5 \times 10^{17}$ magnetic centers per cubic

¹⁸L. F. Bates, *Modern Magnetism*, p 115, Cambridge Press, 1948.

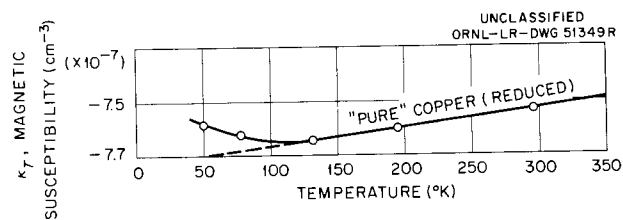


Fig. 3.19. Temperature Dependence of Magnetic Susceptibility of 99.999% Pure Copper.

centimeter, each having a magnetic moment of the order of 2 Bohr magnetons.

Figure 3.20 shows the field dependence of the susceptibility of the "reduced" and "oxidized" (annealed for 4 hr at 900°C under 20 μ of air) samples, the latter measured at 300 and 80°K. It is clear that there is no field dependence discernible for the case of the "reduced" sample. The curves for the "oxidized" sample, however, show a fairly steep slope. If $\sim 2 \times 10^{17}$ iron atoms were precipitated either as metallic iron or as a

ferrite, slopes of the magnitude observed would result.

The number, 2×10^{17} , that is consistent with the slopes of the κ_t vs $1/H$ plots is slightly less but is of the same order of magnitude as the number of dissolved impurity atoms deduced from Fig. 3.19.

In order to obtain further evidence that iron was the impurity that was causing the observed effects, a sample of copper containing $\sim 0.1\%$ iron was prepared. The temperature dependence of κ_t of this sample in the reduced state indicated that almost all (99.999%) of the iron was in a paramagnetic state. However, when the sample was oxidized, it was too strongly magnetic to permit measurement in the susceptibility balance. The sample, when hung on a string, was quite easily attracted by a small bar magnet.

It seems probable that the iron present in trace amounts in "pure" copper is removed from solution when oxygen is present. Such behavior would also explain the large decrease in the residual resistance of copper at low temperatures seen after oxidation treatment.^{16,17}

One further point of interest might be noted. In Fig. 3.20 the slope for the oxidized sample is greater at 80°K than it is at room temperature. This might indicate that some of the precipitate particles are small enough to be ferromagnetic at 80°K but paramagnetic (superparamagnetic¹⁹) at 300°K. Such particles would be roughly 100 to 300 Å in diameter.

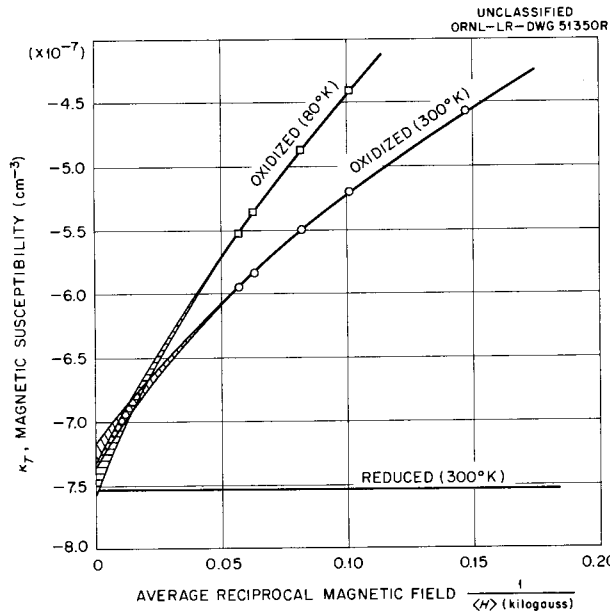


Fig. 3.20. Magnetic Field Dependence of the Susceptibility of Pure Copper After Reduction and Oxidation Anneal.

¹⁹T. O. Paine, *Magnetic Properties of Metals and Alloys*, p 158, American Society for Metals, Cleveland, 1959.

4. DISLOCATION INTERACTIONS

TEMPERATURE DEPENDENCE OF THE EFFECT OF FAST-NEUTRON-INDUCED DEFECTS ON THE INTERNAL FRICTION AND YOUNG'S MODULUS OF COPPER

D. O. Thompson V. K. Paré

Experiments of this type in the range 100 to 300°K were reported in the previous progress report and are described in a published paper.¹ During the year further measurements were made, up to a maximum temperature of 355°K.

The basis of the experiments is that in pure single crystals of copper there exists a readily measurable modulus defect with associated internal friction, due to the bowing, under the applied stress, of sections of dislocation line lying between fixed pinning points. The effect of irradiation is to introduce defects which, after diffusing to the dislocations, act as additional pinning points. The average dislocation line length between pinning points, \bar{l} , is thus reduced by irradiation according to the law

$$\bar{l} = \frac{l_0}{1 + \gamma t}, \quad (1)$$

where t is the irradiation time, l_0 is the initial average loop length, and

$$\gamma = \frac{n}{L} \sum_s \phi l_0, \quad (2)$$

in which $\sum_s \phi$ is the volume rate of production of primary knock-ons, n is the number of pinning points per primary knock-on, and L is the dislocation density. By applying these relations to the measurements it has been shown² that the modulus defect and internal friction vary, respectively, as \bar{l}^{-2} and \bar{l}^{-4} , in agreement with theories of Koehler³ and of Granato and Lücke.⁴

¹D. O. Thompson and V. K. Paré, *J. Appl. Phys.* **31**, 528 (1960).

²D. O. Thompson and D. K. Holmes, *J. Appl. Phys.* **27**, 713 (1956).

³J. S. Koehler, *Imperfections in Nearly Perfect Crystals*, p 197, Wiley, New York, 1952.

⁴A. Granato and K. Lücke, *J. Appl. Phys.* **27**, 583, 789 (1956).

In the present experiments, the internal friction and resonant frequency (about 10 kc) are measured continuously while the sample is being irradiated at various constant temperatures by a beam of fast neutrons from the ORNL Graphite Reactor. The pinning rate constant, γ , is obtained by fitting the theoretical expression to the data and is used as a relative measure of the number of radiation defects which are sufficiently mobile at the temperature of irradiation to diffuse to the dislocation lines.

It has been found that the theory outlined above requires some modification in that the samples normally contain two types of dislocations, one of which is pinned more rapidly than the other. The measurements of modulus defect are thus fitted by the equation

$$\frac{\Delta E}{E} = \frac{(\Delta E)_0}{E_0} \left[\frac{\alpha_1}{(1 + \gamma_1 t)^2} + \frac{\alpha_2}{(1 + \gamma_2 t)^2} \right], \quad (3)$$

while the logarithmic decrement is fitted by

$$\Delta = \Delta_0 \left[\frac{\beta_1}{(1 + \gamma_1 t)^4} + \frac{\beta_2}{(1 + \gamma_2 t)^4} \right]. \quad (4)$$

This analysis is justified by the fact that both decrement and modulus data can be fitted accurately, using the same values of γ_1 and γ_2 .

The pinning rates obtained thus far are plotted as a function of temperature in Fig. 4.1. Both γ_1 and γ_2 are given when available, but at low temperatures the pinning process proceeds very slowly and the experiment cannot be continued long enough to obtain all the parameters in Eqs. (3) and (4). In such cases the weighted average $\alpha_1 \gamma_1 + \alpha_2 \gamma_2$ is plotted.

When data have been taken over the whole temperature range, the plot in Fig. 4.1 is expected to consist of a series of steps, each corresponding to the attainment of mobility, with increasing temperature, by an additional type of defect (or freeing of an already mobile type of defect from a trap). Information on the location of these steps is also provided by experiments in which the sample is

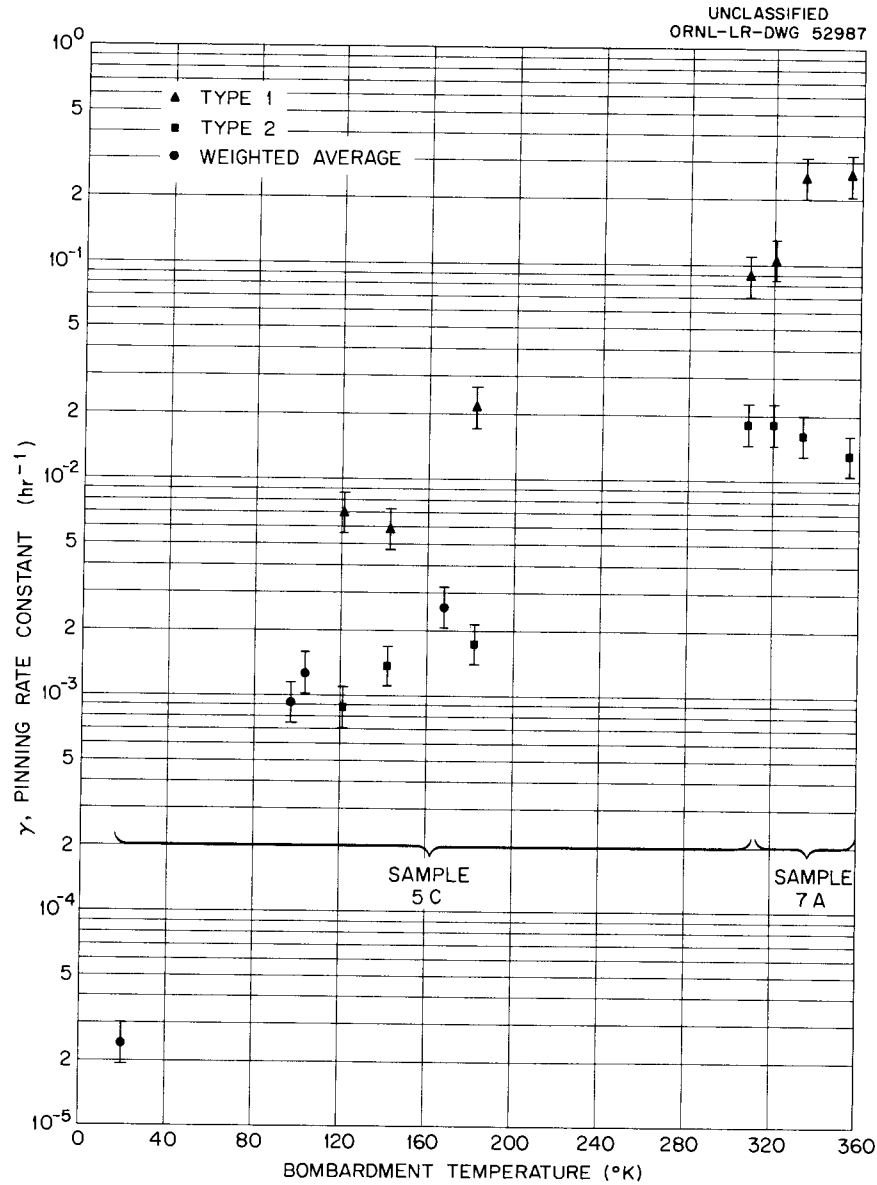


Fig. 4.1. Pinning Rate Constant γ as a Function of Temperature.

warmed after having been irradiated at a low temperature.^{1,5} Combining these results with the data of Fig. 4.1 shows that pinning defects become mobile in temperature ranges centered at 45, 160, 275, and 330°K. The last two of these stages account for over 90% of the total number of defects mobile at the highest temperature.

It is interesting to note that the increase in pinning rate at 330°K occurs only for the type 1

dislocations. Apparently the type 2 dislocations begin to lose their ability to trap defects in this temperature range. It is assumed that the type 2 dislocations are screws, while the type 1 dislocations are more nearly of edge orientation.

These experiments were halted early in the year in order to make additions to the electronic equipment and construct a liquid-helium cryostat and shielding assembly for use at beam hole HB-2 of the Oak Ridge Research Reactor. This work is now nearly complete.

⁵D. O. Thompson, T. H. Blewitt, and D. K. Holmes, *J. Appl. Phys.* 28, 742 (1957).

TEMPERATURE DEPENDENCE OF INTERNAL FRICTION FOLLOWING DEFORMATION AT 78°K

D. O. Thompson V. K. Paré

It was felt that an investigation of the effect on internal friction of point defects produced during plastic deformation would be a valuable supplement to the existing program of studying radiation defects. Since in copper some of the defects of interest are known to diffuse below room temperature, techniques were developed which allow the sample to be deformed and mounted in the apparatus, and measurements begun, while holding the sample continuously at the boiling point of nitrogen.

The samples are single-crystal rods of 99.999% copper, 0.25 in. in diameter and 4 in. long, similar to those used in other measurements. Torsional deformation, mounting, and partial assembly of the sample holder are done while the sample is being sprayed with liquid nitrogen and surrounded by a hollow liquid-nitrogen-filled clamshell jacket. Assembly of the sample holder is completed in a Dewar of liquid nitrogen and the unit is then quickly transferred to a precooled cryostat.

Measurements of the logarithmic decrement are made while warming the sample to successively higher temperatures. The first set of measurements, shown in Fig. 4.2, was made on sample 6A, whose specimen axis was approximately 10° from a cube direction. The maximum torsional strain produced in the deformation was 20%. The data show a number of peaks superimposed on a steeply rising "background." As higher temperatures are reached, the background is reduced; the peak at 192°K disappears completely, but the higher-temperature peaks appear to be more persistent. The shapes of the peaks are approximately what one would expect from thermally activated relaxation processes having activation energies of 0.3 to 0.5 ev.

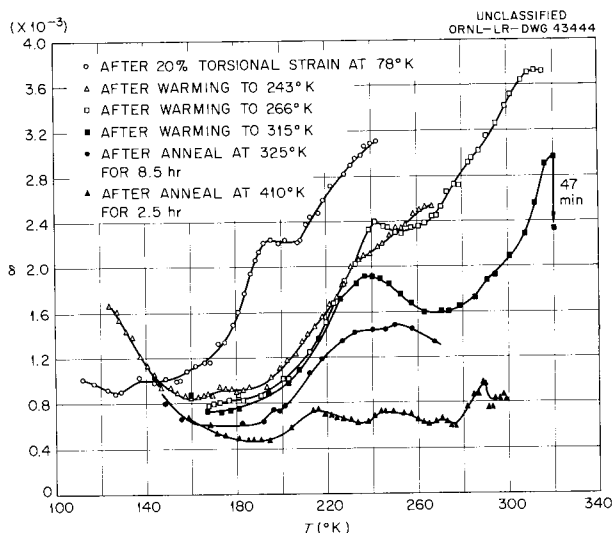


Fig. 4.2. Internal Friction of Sample 6A After Deformation at 78°K and Various Annealing Treatments.

The second set of measurements, shown in Fig. 4.3, was made on sample 7A, deformed to 11% maximum torsional strain. The axis of this sample was much farther from a cube direction than was that of 6A. The same background behavior is present but has about half the magnitude obtained in sample 6A. The peak structure is much less marked. In the first warmup there are a clearly evident increase in modulus and decrease in internal friction centered at 160°K. Presumably these result from pinning of dislocations by the same defects which cause the rise in pinning rate shown in Fig. 4.1 in the same temperature range.

Now that these preliminary runs have demonstrated the feasibility of the method, further measurements will be made in which the internal friction and modulus will also be measured below 78°K and irradiation will be used to pin down the dislocations so as to allow quantitative study of any point defect relaxations.

UNCLASSIFIED
ORNL - LR - DWG 52988

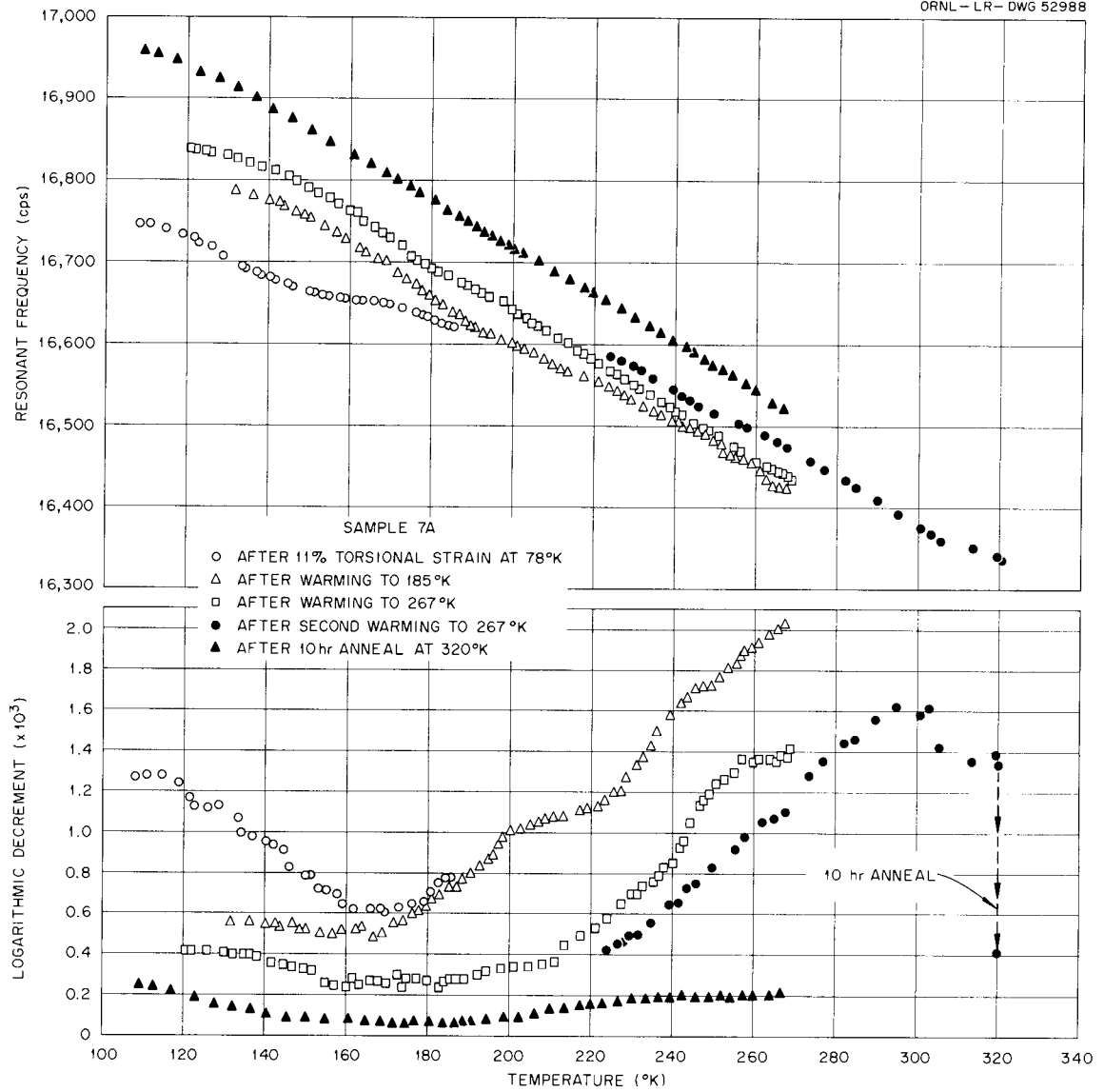


Fig. 4.3. Internal Friction of Sample 7A After Deformation at 78°K and Various Annealing Treatments.

EFFECT OF FAST-NEUTRON IRRADIATION ON INTERNAL FRICTION IN COPPER SINGLE CRYSTALS AT MEGACYCLE FREQUENCIES

D. O. Thompson V. K. Paré
F. W. Young, Jr.

These experiments were undertaken to supplement the data existing in the range 10 to 15 kc, to provide a test of the theory of dislocation internal friction, and to measure the dislocation parameters appearing in the theory. Measurements were made in the range 10 to 110 Mc by means of the pulse echo method, using a Sperry ultrasonic attenuation comparator. A 10-Mc X-cut quartz crystal was used to excite and detect longitudinal waves in the [110] direction of the sample. Sample preparation consisted of (a) cutting a slab, at the desired orientation, from a single-crystal ingot grown from Asarco 99.999% pure copper; (b) etching to remove the cold-worked layer; (c) lapping to parallelism; (d) etching; (e) annealing in vacuum at 1050°C for 24 hr. Irradiations and measurements were all made at room temperature.

In the first experiment,⁶ the internal friction was measured as a function of frequency before and after an irradiation known to be sufficient to pin down the dislocations fully. The dislocation internal friction (assumed to be the difference between the two measurements) was found to be accurately proportional to the reciprocal of the frequency.

Reference to the theory of Granato and Lücke⁴ shows that such behavior is predicted, provided that the damping force is strong enough to limit the dislocation motion at or below the frequency of measurement. In this case the inertia of the dislocation line will be important only at extremely high frequencies and can be neglected. Oen, Holmes, and Robinson⁷ have made a calculation of the resulting frequency dependence of the internal friction and modulus defect, avoiding an approximation used by Granato and Lücke. Analysis of the present measurements was made before the more accurate calculation was completed; however, the discrepancy in the internal friction caused by Granato and Lücke's approximation is too small to be detected by the available measuring equipment.

The predicted variation of decrement with frequency is shown in Fig. 4.4 in terms of the dimensionless variables

$$\frac{\Delta}{2R\lambda L\bar{l}^2} \text{ vs } \frac{4B\bar{l}^2}{\pi C}$$

⁶G. A. Alers and D. O. Thompson, to be published.

⁷O. S. Oen, D. K. Holmes, and M. T. Robinson, "Inertia-Free Model of Dislocation Line Motion," this report.

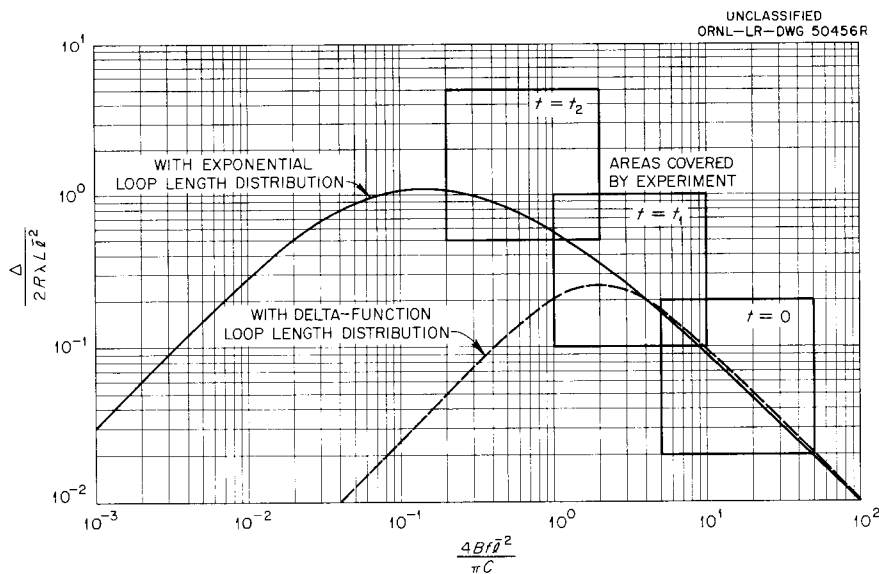


Fig. 4.4. Theoretical Variation of Internal Friction with Frequency, in Terms of Dimensionless Variables.

where

- Δ = logarithmic decrement,
- R = orientation factor,
- $\lambda = 8Gb^2/\pi^3C$,
- G = shear modulus on slip plane,
- b = magnitude of Burgers vector,
- C = dislocation line tension,
- B = dislocation damping constant,
- L = dislocation density,
- \bar{l} = average dislocation loop length,
- f = frequency of vibration.

As the average loop length \bar{l} is shortened by irradiation, the region of decrement and frequency covered by the experimental apparatus will move as shown in Fig. 4.4. It can be seen that the decrement will decrease first at the lowest frequencies and that the steepness of the decrease will depend on how widely the dislocation loop lengths are distributed.

To test this theory, the internal friction was measured at 10, 30, 50, 70, 90, and 110 Mc while the sample was being irradiated by fast neutrons at beam hole HB-2 of the ORR. Typical data, for 110 Mc, are shown in Fig. 4.5. Comparison with the solid curve shows that the theory can be fitted to the data quite well. This means that the calculated curve shown in Fig. 4.4 is (for the exponential loop length distribution) also confirmed.

An unexpected feature of the data is also illustrated in Fig. 4.5. The dashed line labeled $E_R = 1$

is the theoretical curve, applicable to 110 Mc, which is obtained by fitting the theory to the data at 10 Mc. The notation $E_R = 0.280$ for the solid line indicates that the irradiation produces only 28 pinning points effective at 110 Mc for every 100 pinning points effective at 10 Mc. It is felt that this is not a direct frequency effect but rather an amplitude effect. Under the damping-limited condition existing at the start of the experiment, the maximum amplitude of dislocation motion was estimated to be (in terms of the Burgers vector b) $20b$ at 10 Mc but only $2 \times 10^{-3}b$ at 110 Mc. It appears quite possible that such small motion is not very effectively restrained by pinning points.

From fitting the theory to the data one can obtain the quantities γ , B/L , and Ll_0^2 [for definitions of γ and l_0 , see Eqs. (1) and (2) above]. An additional advantage of the technique is that the sample surface is oriented so that etch-pit determinations of dislocation density are possible. The result was $L = 1.0 \times 10^7 \text{ cm}^{-2}$ averaged over the volume of the sample. This leads to $B = 1.5 \times 10^{-4} \text{ dyne sec cm}^{-2}$, in close agreement with the value of 1.6×10^{-4} calculated by G. Leibfried (quoted by Granato and Lücke⁴). It should be noted, however, that the experimental result is probably uncertain within a factor of the order of 2. Using line tension values calculated by deWit and Koehler,⁸ the initial average loop length was found to be $5 \times 10^{-4} \text{ cm}$ if the dislocations are pure edge and $1.4 \times 10^{-3} \text{ cm}$ if they are pure screw.

⁸G. deWit and J. S. Koehler, *Phys. Rev.* 116, 1113, 1121 (1959).

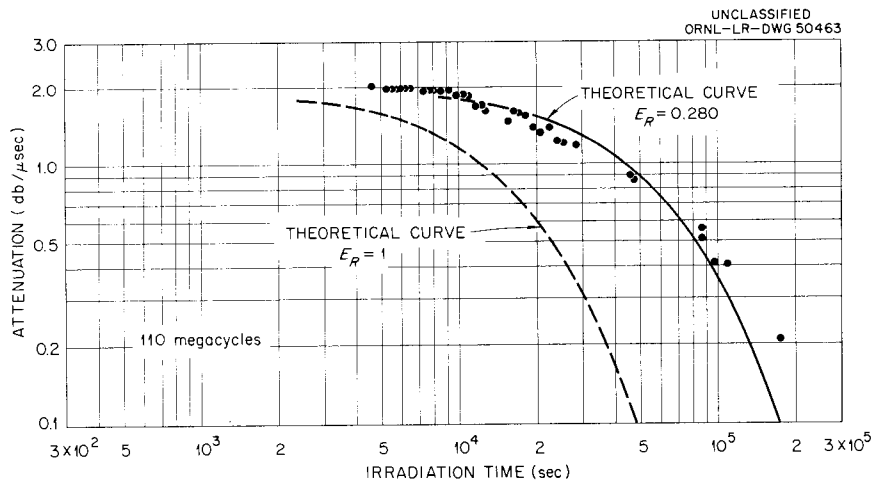


Fig. 4.5. Decrease of Internal Friction at 110 Mc During Irradiation, Compared with Theoretical Curves.

5. INVESTIGATIONS OF METAL SURFACES

F. W. Young, Jr.

L. D. Hulett

L. H. Jenkins

T. R. Wilson

ELECTROCHEMICAL DISSOLUTION OF COPPER SINGLE CRYSTALS

It is generally believed that areas of the surfaces of metallic single crystals which contain disordered regions, such as emergent dislocations, are more favorable energetically as reaction sites when material is removed from the crystal into a surrounding medium. To test this hypothesis, the electrochemical dissolution of single-crystalline copper in aqueous solutions is being studied.

Galvanostatic potential-current relationships have been measured for copper crystals of various surface orientations in acidic CuSO_4 solutions which were free of dissolved oxygen and which had been pre-equilibrated with metallic copper to prevent any side reactions. At the end of the reaction,

replicas of the metal surface were examined with the electron microscope so that any relationship between the defect structure of the metal and the current-potential data might be established.

Promising preliminary results have been obtained on surfaces of (100), (110), and (111) orientations. The following results obtained on crystals of (100) orientation in 0.2 M CuSO_4 (pH adjusted to 1.0 with H_2SO_4) are typical observations:

At current densities ranging from 5 to 15 $\mu\text{a}/\text{cm}^2$, pits which are thought to be related to the defect structure of the metal were observed on (100) surfaces. An electron micrograph of a replica of a surface of this type is shown in Fig. 5.1. Pitting is observed on a surface of this orientation neither at lower current densities nor at current densities



Fig. 5.1. Electron Micrograph of a Carbon Replica of (100) Surface Showing Pits Developed After 5½ hr at a Current Density of 10 $\mu\text{a}/\text{cm}^2$. 3600X.

between 15 and 40 $\mu\text{a}/\text{cm}^2$. For the higher current density region, facets, probably of (110) orientation, developed rapidly on the surface. It was established that the facets did not result from the growth of pits by surface observations made during the early stages of facet formation. Figure 5.2 illustrates the type of well-developed facets obtained.

Experiments currently in progress and planned for the future are designed to establish the exact

degree of correspondence between the pits produced and the dislocation structure in the surfaces as well as the different requirements of current density and/or potential to produce pitting on surfaces of different orientations. Concurrently, the deposition process will also be investigated. The electrochemical data should contribute to the understanding of electrode kinetics generally, and it is anticipated that the effects of surface orientation, defect structures, etc., on electrode processes will be established.

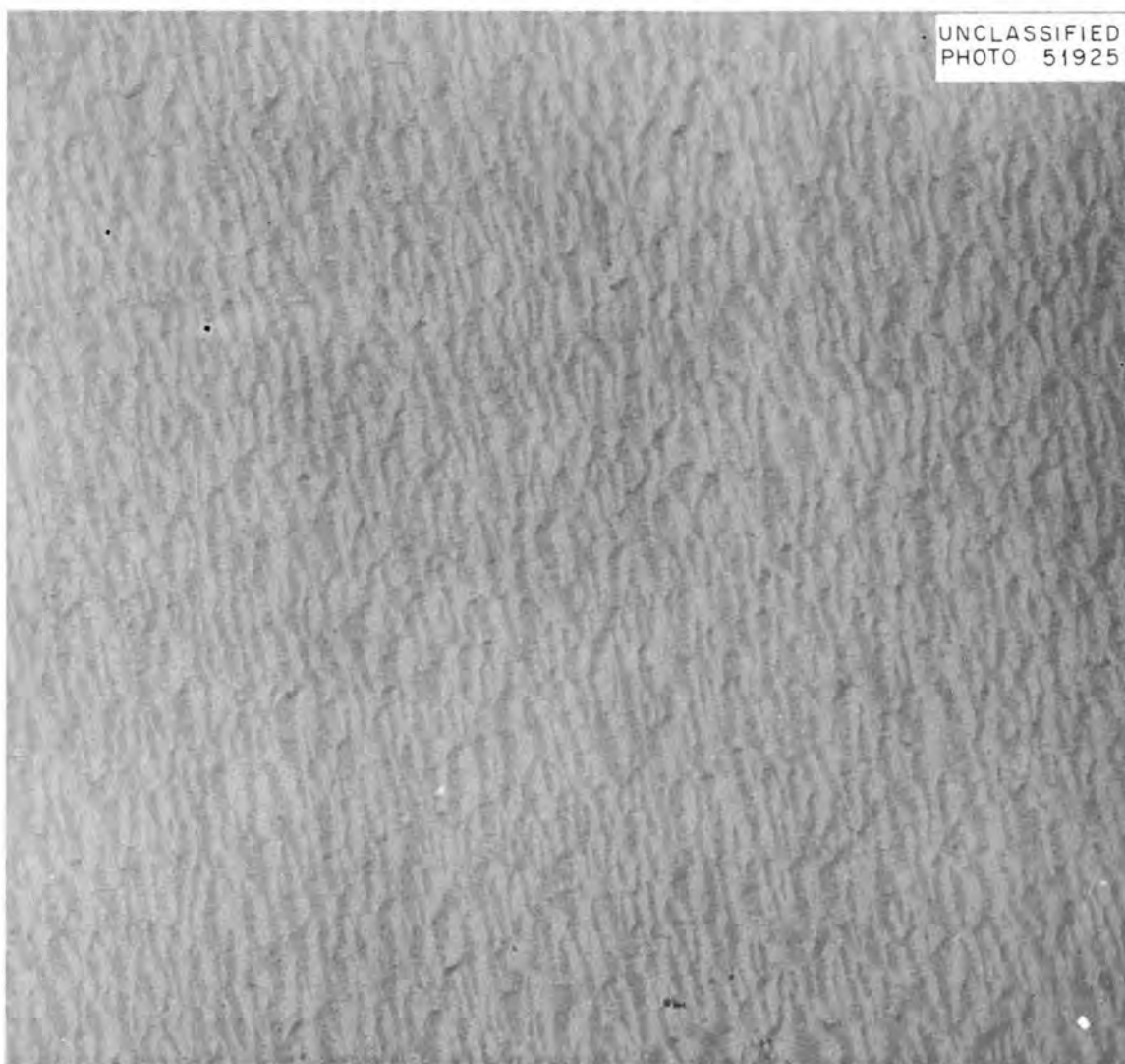


Fig. 5.2. Electron Micrograph of a Carbon Replica of (100) Surface Showing Early Stages of Facet Development After 2 hr at a Current Density of 20 $\mu\text{a}/\text{cm}^2$. Note that the total amount of copper removed is less than on the surface illustrated in Fig. 5.1. 11,000X.

DISSOLUTION OF COPPER IN AQUEOUS HYDROCHLORIC ACID

As a continuation of the studies of the effects of crystal plane and crystal imperfection on the dissolution kinetics of copper in aqueous solutions, the copper-dilute hydrochloric acid system is being investigated. Copper is dissolved by exposure to air-saturated solutions of hydrochloric acid, the mechanism probably involving, first, attack by the dissolved oxygen, followed by dissolution of the oxide by the acid.

The kinetics of this reaction are being studied by measuring the change in conductivity of the solution as a function of time. Preliminary results indicate that in $\sim 10^{-2}$ M HCl the dissolution rate is independent of the concentration of both hydrogen ion and dissolved oxygen. This fact suggests that the rate of dissolution is not controlled by mass transfer of reactants to, or products from, the surface. Observations of metal surfaces at the completion of the reaction reveal a faceted structure. Typical facets developed on the (110) face are shown in Fig. 5.3. Whether the facets develop from pits associated with surface imperfections has not yet been established.

The HCl-copper system is interesting for two reasons: (1) The indication that diffusion of reactants to and from the reaction interface is not the rate-controlling step suggests that reactivities

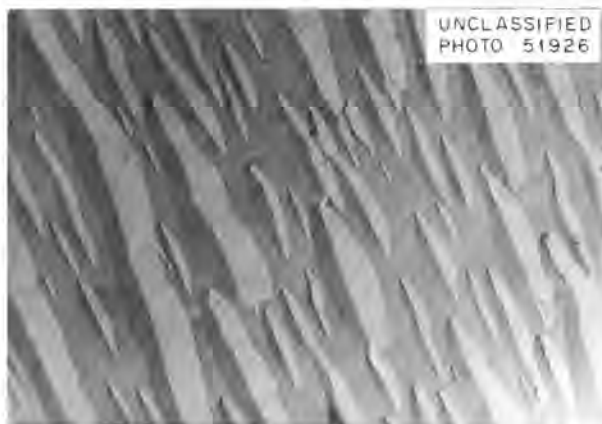


Fig. 5.3. Electron Micrograph of a Carbon Replica of (110) Surface Showing Well-Developed Facets After Removal of an Average of 5000 Atom Layers of Copper. 3000X. Reduced 17%.

of the various crystal faces can be studied profitably. (2) Perhaps this reaction, whose rate is controlled by a process on the metal surface, will yield useful information about the role of surface defects in such reactions.

THE ROLE OF CRYSTAL IMPERFECTIONS IN THE CHEMICAL REACTIVITY OF METAL SURFACES¹

Because the irradiation of solids introduces defects into crystals, it is necessary that the role of crystal imperfections in surface reactions be understood in order to solve the problems of the effect of irradiation on reactions occurring at metal surfaces. In this paper considerations are given to the role in surface reactions of two types of imperfections: point imperfections (vacancies, interstitials, and impurity atoms) and line imperfections (dislocations).

The development of etch pits at dislocations is considered. Some examples of such etch pits are shown, and experiments designed to determine the conditions for pit formation at dislocations are described.

Dislocations in general act as traps for the impurity atoms in crystals. Therefore, if the impurity atoms affect the chemical reactivity, the dislocations may act as line sources of impurity atoms and be points of high chemical reactivity. The enhancement of chemical activity at dislocations with impurities has been demonstrated by etch pit formation in aqueous solutions, and also by the increased rate of oxidation at points where dislocations meet the surface of slightly impure metals.

The role of nucleation in the growth of oxide films on metals is considered, and experiments on the effect of neutron irradiation on nucleation in oxide films are described.

It has long been known that the rate of oxidation of a metal is increased by increasing the number of imperfections which are the diffusing species. It is well known that a primary result of nuclear irradiation is to increase the vacancy and interstitial concentration. Therefore, the possibilities of surface reactions being affected by such an increase in point imperfections are discussed.

¹Abstract of a paper presented at a "Conference on Corrosion in Nuclear Reactors" in Brussels, Belgium, printed as a part of the report of the conference.

ETCH PITS AT DISLOCATIONS IN COPPER²

A possible mechanism for the development of etch pits at dislocations in copper by etching in solution is presented, and experiments are described which may substantiate this mechanism. Etchants which will develop pits at clean dislocations on the (111), (100), and (110) faces of copper are described. These etchants are capable of distinguishing between clean dislocations and dislocations with a "Cottrell atmosphere" in 99.999% copper. Clean edge and screw dislocations can also be differentiated with these etchants. Some observations concerning the relation of facet structure, developed by etching, to the dislocation structure of the crystal are reported.

GROWTH OF CRYSTALS AND PREPARATION OF SURFACES

In order to study the role of crystal imperfections in the chemical reactivity of metal surfaces, it is necessary that crystals with as few imperfections as possible be available for study. To this end programs are in progress on the growth of more perfect crystals of copper, and on methods of preparation of surfaces of desired orientation with the introduction of as few imperfections as possible.

The crystals of desired orientation which are being used in these studies are grown as flat plates in graphite crucibles, from seeds. A modified Bridgman technique is used, and the crystals are grown in vacuum ($\sim 10^{-5}$ mm Hg) at a rate of 1 in./hr. These crystals have a density of dislocations of 2 to 5×10^6 cm⁻² in the as-grown condition. In attempts to decrease the number of grown-in

dislocations a horizontal crystal-growing apparatus was constructed with a furnace so wound that it had gradients in both the horizontal and vertical directions. The hot zone of the furnace could be moved in the horizontal direction by lowering the power to the furnace in a controlled way. Thus a crystal could be grown without any movement or vibration. The furnace was also arranged so that the crystal was in a constant-temperature zone (1000°C) after it was grown, and it then could be cooled to room temperature very slowly. Thus the crystal could be grown with temperature gradients such that the direction of the solid-liquid interface could be controlled with respect to the growth direction, and it could be cooled after growth in a manner which minimized the possibility of vacancy introduction and subsequent formation of dislocations. Crystals grown in this apparatus also had a dislocation density of 1 to 5×10^6 cm⁻². In an attempt to determine if dislocations are introduced by the graphite mold, crystals are now being grown in a horizontal furnace in a graphite crucible which is open on one side.

An acid cutting saw which uses a stainless steel wire and concentrated nitric acid has been constructed. This saw gives a relatively smooth cut — about equivalent to that obtainable with a jeweler's saw — and will cut through a $\frac{3}{4}$ -in.-dia copper crystal in 8 hr. This instrument is being fitted with a goniometer so as to be able to cut along desired crystal directions.

An acid polishing wheel has been designed and constructed. From preliminary experiments with the polishing wheel it appears that it may be possible to polish crystals as rough as those obtained from the acid saw to a smoothness comparable to that obtainable with a conventional polishing wheel, without introducing an appreciable number of dislocations.

²Abstract of a paper submitted for publication to the *Journal of Applied Physics*.

6. ALLOY STUDIES

M. S. Wechsler

W. L. Harman¹

R. H. Kernohan

J. M. Williams

IRRADIATION EFFECTS ON COPPER-ALUMINUM
(15 at. % Al) ALLOYS

Electron Irradiation

It has been found that electron irradiation produces a decrease in the electrical resistivity of copper-aluminum (15 at. % Al) alloys. A similar decrease in resistivity has been observed upon neutron and gamma irradiation.²⁻⁴ However, the electron-irradiation experiments have the advantage that the electron energies and fluxes may be varied conveniently. A study of the effect of varying the energy of the bombarding electrons yields information concerning the energy dependence of the displacement cross section. Also, the flux dependence is of interest in view of recent theories⁵ of the mechanism of radiation-enhanced diffusion in alloys.

The effect on the rate of decrease of resistivity of varying the electron energy is shown in Fig. 6.1 for wires of 0.015-in. diameter irradiated at 100°C. It is seen that the resistivity decreases more rapidly as the electron energy is increased. The values of the electron energies shown in Fig. 6.1 are nominal; the actual incident energies are less than the nominal ones due to the decrease in energy in passing through the aluminum window of the Van de Graaff accelerator (about 0.05 Mev). It is to be noted that a perceptible decrease in resistivity was observed for the 0.3-Mev run. This indicates the importance of the displacement of aluminum atoms, since theoretical calculations⁶ specify that the displacement cross section of copper falls to zero at about 0.5 Mev, whereas the corresponding energy for aluminum is about 0.25 Mev.

The flux dependence of the reaction is illustrated in Fig. 6.2, where curves of resistivity vs irradiation time at 100°C are shown for a range of fluxes from about 2×10^{10} to 1.4×10^{13} electrons $\text{cm}^{-2} \text{sec}^{-1}$. Because of experimental difficulties in the measurement of the flux for the lowest-flux run, there is considerable uncertainty in the value 2×10^{10} electrons $\text{cm}^{-2} \text{sec}^{-1}$.

¹Co-op student from Virginia Polytechnic Institute.

²M. S. Wechsler and R. H. Kernohan, *Phys. and Chem. Solids* **7**, 307 (1958).

³R. H. Kernohan and M. S. Wechsler, "Neutron Irradiation of Cu-Al at Elevated Temperatures," to be published in *The Physics and Chemistry of Solids*.

⁴M. S. Wechsler et al., *Solid State Ann. Prog. Rep.* Aug. 31, 1959, ORNL-2829, p 110.

⁵G. J. Dienes and A. C. Damask, *J. Appl. Phys.* **29**, 1713 (1958).

⁶R. Fuchs, unpublished.

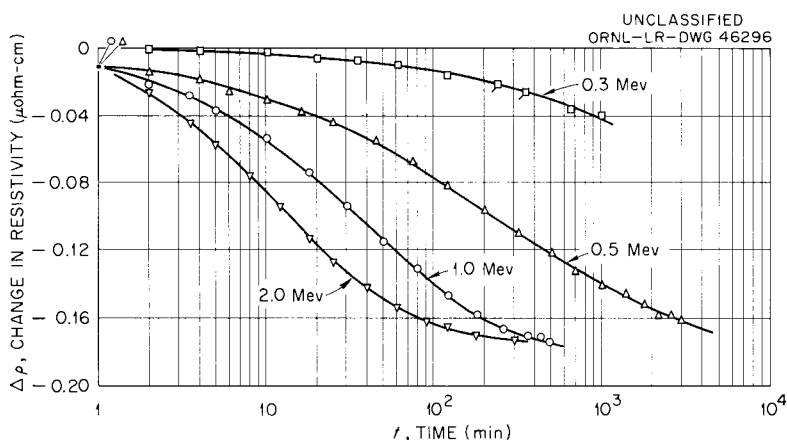


Fig. 6.1. Electron Irradiation of Copper-Aluminum Alloy (15 at. % Al) at Various Electron Energies. Change in resistivity vs time of irradiation. Irradiation temperature, 100°C. Electron flux, 1.4×10^{13} electrons $\text{cm}^{-2} \text{sec}^{-1}$. Temperature of measurement, -196°C.

The electron energy was held constant at 1 Mev for this series of runs. An analysis of these curves leads to the conclusion that a lattice displacement produced at lower fluxes is more effective in giving rise to the decrease in resistivity than one produced at higher fluxes. This point is discussed further in the section below ("Theoretical Analysis").

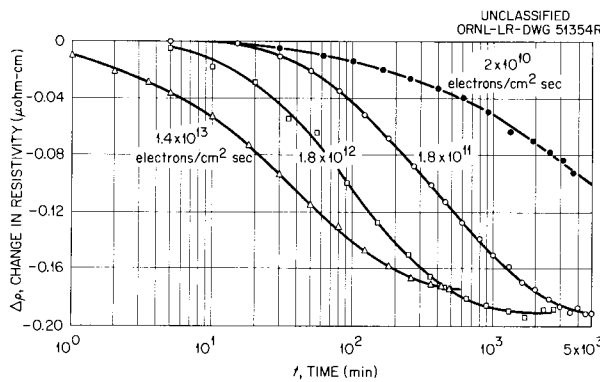


Fig. 6.2. Electron Irradiation of Copper-Aluminum Alloy (15 at. % Al) at Various Instantaneous Fluxes. Change in resistivity vs time of irradiation. Irradiation temperature, 100°C. Electron energy, 1 Mev. Temperature of measurement, -196°C.

Figure 6.3 shows the effect on resistivity of isochronal annealing following electron irradiation at -196°C. As can be seen by the points shown on the left side of the figure, the resistivity is increased only slightly (about 0.002 microhm-cm) as a result of the cold irradiation. Irradiation at 100°C under otherwise identical conditions of irradiation produces a decrease in resistivity of about 0.16 microhm-cm (Fig. 6.2). However, as is seen in Fig. 6.3, an isochronal annealing treatment subsequent to the irradiation at -196°C causes the decrease in resistivity to set in. This behavior is quite similar to that observed upon neutron bombardment (Fig. 6.3) and indicates that the defects produced upon irradiation must be mobile if the atomic rearrangement responsible for the decrease in resistivity is to take place.

Gamma Irradiation

The gamma-ray intensities available from Co⁶⁰ sources are also sufficient to stimulate the decrease in resistivity. Figure 6.4 shows the results of irradiations at 100°C in two gamma facilities. A comparison with the data obtained upon neutron and electron irradiation is made in the next section.

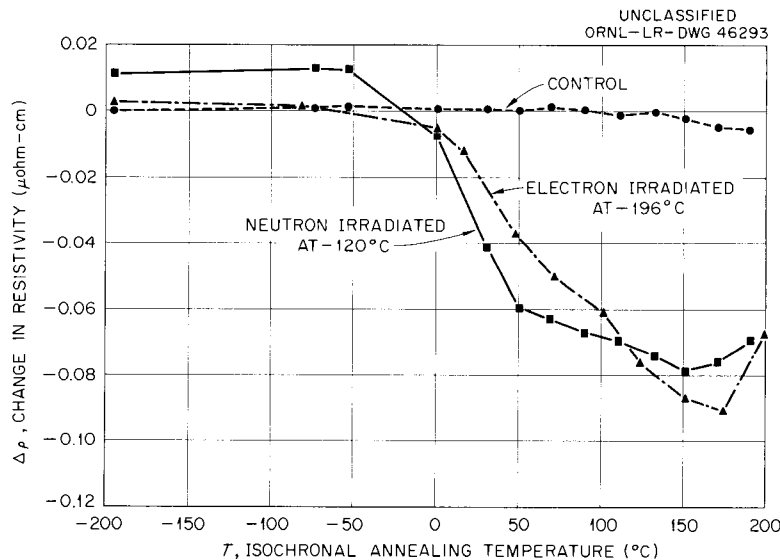


Fig. 6.3. Isochronal Annealing ($t = 30$ min) of Copper-Aluminum Alloy (15 at. % Al) Following Electron Irradiation at -196°C (Integrated Flux, 2×10^{17} Electrons/cm²; Electron Energy, 1 Mev) and Neutron Irradiation at -120°C (Integrated Flux, 2×10^{17} Neutrons/cm²). For comparison, the effect of the isochronal treatment on an unirradiated (control) sample is also shown. Temperature of measurement, -196°C.

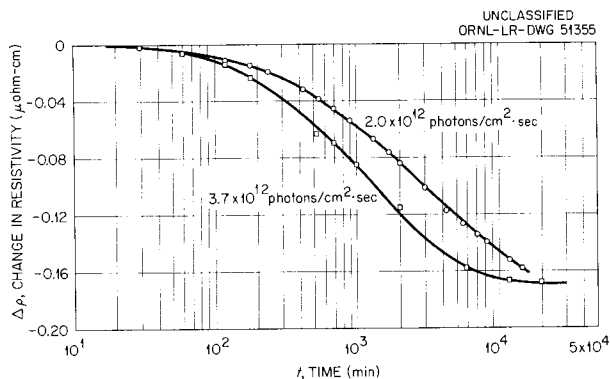


Fig. 6.4. Gamma Irradiation of Copper-Aluminum Alloy (15 at. % Al) at Two Instantaneous Fluxes. Change in resistivity vs time of irradiation. Co^{60} gamma source. Irradiation temperature, 100°C . Temperature of measurement, -196°C .

Theoretical Analysis

(in collaboration with J. H. Barrett)

Dienes and Damask⁵ have given a theory of radiation-enhanced diffusion in alloys such as copper-aluminum. They conclude that the buildup time of the defect concentrations is sufficiently short so that only the equilibrium concentrations of defects need to be considered. In this case the time necessary to reach half annealing, $\tau_{1/2}$, will be inversely proportional to the equilibrium concentration. Their basic equations for the fractional vacancy concentration v and interstitial concentration i are

$$\frac{dv}{dt} = K - K_v v - \nu_i v i$$

$$\frac{di}{dt} = K - K_i i - \nu_i v i$$

In these equations K is the number of interstitial-vacancy pairs created per atomic site per second; K_v and K_i are rate constants for the diffusion of vacancies and interstitials to fixed sinks; and ν_i is the jump frequency of interstitials. The last term in each equation represents the annealing of the defects by direct pair recombination. Dienes and Damask consider three cases: (1) diffusion to fixed sinks is dominant; (2) pair recombination is dominant; (3) both processes are of the same order of magnitude. In the first case, they find the equilibrium concentration of defects

is proportional to K . In the last two cases, the equilibrium concentration is proportional to $K^{1/2}$. The square-root dependence in the last two cases reflects the fact that the lifetime of a defect decreases with increasing flux; therefore, a defect produced at high flux will produce less annealing than one produced at low flux. In case (1) $\tau_{1/2}$ will be proportional to K^{-1} . In cases (2) and (3) $\tau_{1/2}$ will be proportional to $K^{-1/2}$.

In order to compare the results produced by different types of bombardments, the rate of production of defects needs to be calculated for each experiment. The work of Fuchs⁶ may be used to calculate K for the electron bombardments. The work of Oen and Holmes⁷ may be used to calculate K for the gamma-ray bombardments. The value of K for the neutron bombardment may be calculated from the cross section for fast-neutron scattering, the measured flux, and an estimate of the number of defects created per primary collision.

The value of $\tau_{1/2}$ for irradiation at 100°C is plotted as a function of K in Fig. 6.5. Because of difficulty in measuring small currents, the lowest-flux electron-irradiation point is questionable. The other electron-irradiation points indicate that $\tau_{1/2}$ is proportional to $K^{-1/2}$; the gamma- and neutron-irradiation points agree with this proportionality. It is of interest to compare these results with the theory of Dienes and Damask. Their theory and the results of Fig. 6.5 indicate that the annealing of the defects is either by pair recombination or by a mixture of pair recombination and diffusion to fixed sinks.

ANNEALING EFFECTS ON DEFORMED COPPER-SILICON ALLOYS

(in collaboration with H. M. Otte⁸)

The irradiation effects on copper-aluminum alloys described above demonstrate that the lattice defects introduced by irradiation are capable of stimulating a rearrangement in the relative positions of the different types of atoms present in the alloy. Since defects are also produced upon plastic deformation, the question arises as to

⁷O. S. Oen and D. K. Holmes, *J. Appl. Phys.* 30, 1289 (1959).

⁸Research Institute for Advanced Study, Baltimore, Md.

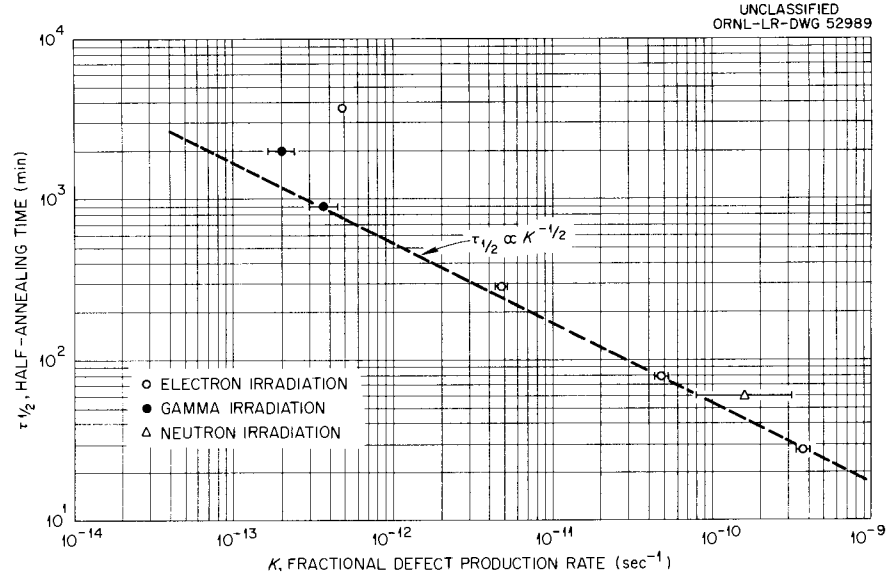


Fig. 6.5. Time Necessary to Reach Half Annealing as a Function of the Damage Rate in Copper-Aluminum Alloy (15 at. % Al). All irradiations were performed at 100°C.

whether similar effects may be realized in deformed alloys. To explore this possibility, an investigation of annealing effects on deformed copper-silicon alloys has been undertaken.

Figure 6.6 shows that large changes in the electrical resistivity of a commercial silicon-bronze alloy take place upon isochronal annealing following cold-working to a 45% reduction in area.

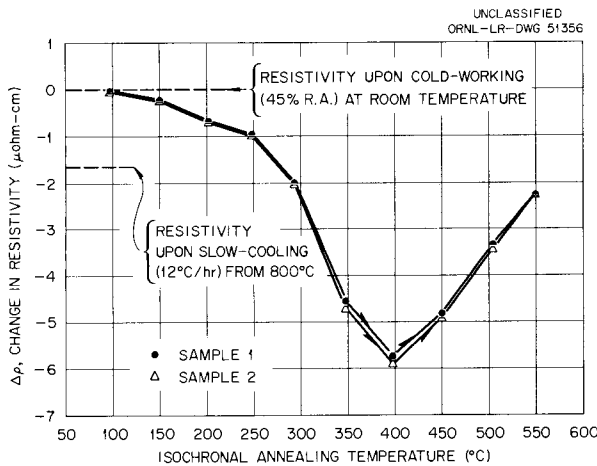


Fig. 6.6. Isochronal Annealing ($t = 2$ hr) of Two Samples of Copper-Silicon-Manganese Alloy (6.7 at. % Si, 1.3 at. % Mn) Previously Cold-Worked to 45% Reduction in Area. The two samples received identical treatments. All resistivity measurements were made at -196°C.

The cold-working introduces a resistivity of about 1.5 microhm-cm, whereas the total decrease in resistivity upon annealing is about 6 microhm-cm, or about 20% of the original value. Thus, these results suggest that the decrease in resistivity upon annealing is not due solely to the removal of the cold-worked condition. There appears to be an additional decrease in resistivity due, possibly, to an atomic rearrangement such as ordering or Guinier-Preston zone formation that is stimulated by the motion of defects introduced by the cold-working.

THE GENERALIZED THEORY OF THE MARTENSITIC CUBIC TO ORTHORHOMBIC PHASE TRANSFORMATION⁹

M. S. Wechsler H. M. Otte⁸

The crystallographic theory of the martensitic cubic-orthorhombic phase transformation is described in terms of a generalized lattice-invariant shear. For certain of the more symmetrical choices of the lattice-invariant shear, solutions for the undistorted plane are given as explicit functions of the lattice parameters of the two phases and a possible isotropic dilatation. The conditions for the existence of a solution and the criteria for the degeneracy of solutions are also discussed.

⁹Abstract of an article accepted for publication in *Acta Metallurgica*.

7. ELECTRON MICROSCOPE STUDIES

T. S. Noggle

J. O. Stiegler

FISSION FRAGMENT TRACKS IN UO_2 FILMS

Electron microscope studies of the tracks produced by fission fragments in thin films have been reported in the literature,¹ and the results to date may be summarized as follows:

1. The detection efficiency of the electron microscope observations in the UO_2 films 100 Å or less in thickness is 100% with an estimated experimental error of less than $\pm 25\%$. For films thicker than 100 Å the detection efficiency falls off due to the background texture of the films.
2. The tracks register in the films primarily as a result of a redistribution of material at the surface as a consequence of the continuous energy loss by the fragments in the form of electron excitation and ionization.
3. The minimum rate of energy loss which leads to registration of a track is on the order of 1000 eV/Å.
4. Track length distributions obtained on a variety of specimen preparations have yielded results which at present cannot be accounted for in terms of known physical phenomena applicable to the system under study. These results have indicated that for track lengths less than about 1μ the frequency of occurrence of all but the shortest tracks is significantly greater than is to be expected from the geometry of the system.
5. The track length distributions for tracks more than 1μ in length fall below the geometrically expected frequencies and have an effective cutoff at about 4μ . This rapid decrease in the experimental distribution can be accounted for qualitatively by consideration of Rutherford scattering. Uncertainty as to the cross sections for scattering at angles less than about 2° and the cumulative effect of small-angle scatterings inhibits a more quantitative treatment of this problem.

¹T. S. Noggle and J. O. Stiegler, *J. Appl. Phys.*, to be published in December 1960.

6. A small number of forked tracks have been observed which satisfy the conditions for two-body events involving collision of fission fragments with lattice atoms. In addition to being the first known "direct" observations of nuclear encounters in a solid, these events promise to give additional information with respect to energy dissipation rates necessary for track registration.

These observations are being continued with the goal of obtaining a better understanding of the factors which determine the registration of the tracks in the films and relating the track length distributions to physical processes involving the mutual interactions between the film material and the fission fragments.

The very high energy input needed for registration of the tracks raises questions as to the relative importance of various processes in the redistribution of material along the fission fragment path. One possible process, which can occur only at the free surface, involving evaporation or vapor transport of matter, cannot be readily detected by microscope methods; yet it may be an important process in these experiments. In view of experimental evidence that detectable evaporation of material from the surface of fissionable material does occur,² experiments have been devised and are in progress in which some of the thin-film techniques are being employed to measure the evaporation.

REPLICA STUDIES

The ethylenediamine replica stripping technique^{3,4} reported last year has been employed extensively in replica studies of copper surfaces for the Surface Studies Group. This experience has established the value and utility of this

²B. V. Ershler and F. S. Lapteva, *J. Nuclear Energy* 4, 471 (1957). This is a translation of an article which originally appeared in *Atomnaya Energ.* 1, 63 (1956).

³T. S. Noggle and J. O. Stiegler, *Solid State Ann. Prog. Rep.* Aug. 31, 1959, ORNL-2829, p 86.

⁴J. O. Stiegler and T. S. Noggle, *J. Appl. Phys.*, to be published in October 1960.

method in the preparation of high-resolution, preshadowed carbon replicas of copper surfaces covering a wide range of surface conditions.

Investigation of a widely used technique employing the evaporated wetting agent Victawet as a water-soluble parting layer for evaporated replicas has established that the heretofore accepted model for the behavior of this material is incorrect. The generally accepted model for the behavior of Victawet in this use postulates that vacuum evaporation occurs at low temperatures ($\sim 300^{\circ}\text{C}$), giving rise to a thin layer (monomolecular in the limiting case) deposited on the specimen surface which must be "activated" by the radiant energy from an incandescent filament which is normally also the evaporation source. This "activation" is postulated to occur as a result of the orientation

of the polar metal-organic molecules of the Victawet, giving rise to a hydrophilic surface. After subsequent evaporation of the replica material, the replica film may be readily stripped by immersion into water. It has been found that the apparent evaporation at low temperatures is actually the decomposition of the complex metal-organic material with loss of the organic components, leaving an inorganic residue identified as sodium metaphosphate (NaPO_3) to which the parting layer attributes are associated. The NaPO_3 does not evaporate at appreciable rates until temperatures approaching incandescence ($900\text{--}1000^{\circ}\text{C}$) are reached. In view of the organic material driven off prior to the evaporation of the active material, it is concluded that the NaPO_3 is preferable to Victawet in this application.

8. SURFACE BOMBARDMENT OF SOLIDS

A. L. Southern
D. R. Burrowbridge¹

M. T. Robinson
W. R. Willis²

Bombarding the surface of a solid with ionic beams leads to the loss of material from the solid by "physical sputtering." The obtaining of reliable experimental data, mainly due to G. K. Wehner,³ has led to the view that sputtering is a form of radiation damage. In the process, momentum is transferred from an incident ion to the solid lattice and eventually to an ejected atom.

When the bombarded solid is a single crystal, atoms are ejected in preferential directions near the close-packed directions of the lattice. This has been shown to occur when the energy of the impinging ion varies from less than 1 kev to 50 kev.⁴ Thompson⁵ bombarded a gold foil with high-energy protons and obtained patterns of ejected ions from the back side of the foil. Again, these were near the close-packed directions. Such experimental results indicate a focusing mechanism⁶ in momentum transfer and have led to attempts to develop a theory of sputtering.

Other studies of sputtering have been concerned with the ejected material and the surface of the solid. It has been shown that sputtered atoms are mostly (98%) uncharged⁷ and leave the surface of the solid with energy (~ 10 ev) considerably less than that of the impinging ion but greater than thermal.⁸ Low-energy sputtering is a very sensitive probe for studying the nature of surface contaminants, the molecular state of sputtered particles, and the course of heterogeneous chemical reactions.⁹ In these techniques, after the sputtered material is ionized, it is analyzed in a

mass spectrometer, which must be very sensitive. Such a spectrometer has been designed and purchase is now being arranged.

SPUTTERING RATIO OF TYPE 304 STAINLESS STEEL

As a first problem in sputtering, the work of Fairbrother and Foster¹⁰ on the sputtering of type 304 stainless steel by H^+ has been extended to Ar^+ in the energy range 1-5 kev.

Targets used in the experiments were cut from a single sheet of type 304 stainless steel, treated with dilute nitric acid, then degreased in perchloroethylene and hydrogen-fired. Following this they were placed in a vacuum desiccator, evacuated, then stored at 1 atm. Later tests showed no change in mass from further cycling from vacuum to atmospheric pressure.

The sputtering ratio S was computed from loss of mass of the targets and the measured current. Mass losses were converted to particles ejected using an average particle atomic weight computed from the chemical composition of the alloy. This number was taken to be 54.02. The total number of incident ions was computed from an integrated current, assuming singly charged ions. In terms of these quantities

$$S = \frac{N_{SA}}{N_{Ar^+}},$$

where

N_{SA} = number of ejected particles,
 N_{Ar^+} = number of incident ions.

Figure 8.1 shows the experimental arrangement. Argon ions formed in the ion source were accelerated and then focused in a zero-energy electrostatic lens on a defining iris. The collimated beam entered a Faraday cage, of which the target was an integral part, and struck at normal incidence (except for space charge effects).

¹⁰F. Fairbrother and J. S. Foster, *Sputtering of Stainless Steel by Protons in the 30-80 kev Range*, UCRL-4169 (Aug. 11, 1953).

¹Co-op student from Virginia Polytechnic Institute.

²Consultant, Department of Physics, West Virginia Wesleyan College, Buckhannon.

³N. Laegreid, G. Wehner, and B. Meckel, *J. Appl. Phys.* 30, 374 (1959).

⁴G. K. Wehner, *Phys. Rev.* 102, 690 (1956); V. E. Yurasova, N. V. Pleshivtsev, and I. V. Orfanov, *J. Exptl. Theoret. Phys. (U.S.S.R.)* 37, 996 (1959).

⁵M. W. Thompson, *Phil Mag.* 4, 139 (1959).

⁶R. H. Silsbee, *J. Appl. Phys.* 28, 1246 (1957); G. Leibfried, *J. Appl. Phys.* 31, 117 (1960).

⁷R. E. Honig, *J. Appl. Phys.* 29, 549 (1958).

⁸H. E. Stanton, *J. Appl. Phys.* 31, 678 (1960).

⁹R. C. Bradley and A. Arking, *Tech. Rep. No. 11 - A Study of a Platinum Surface Using a Mass Spectrometer*, AFOSR-TN-59-271 (Cornell Univ., 1959).

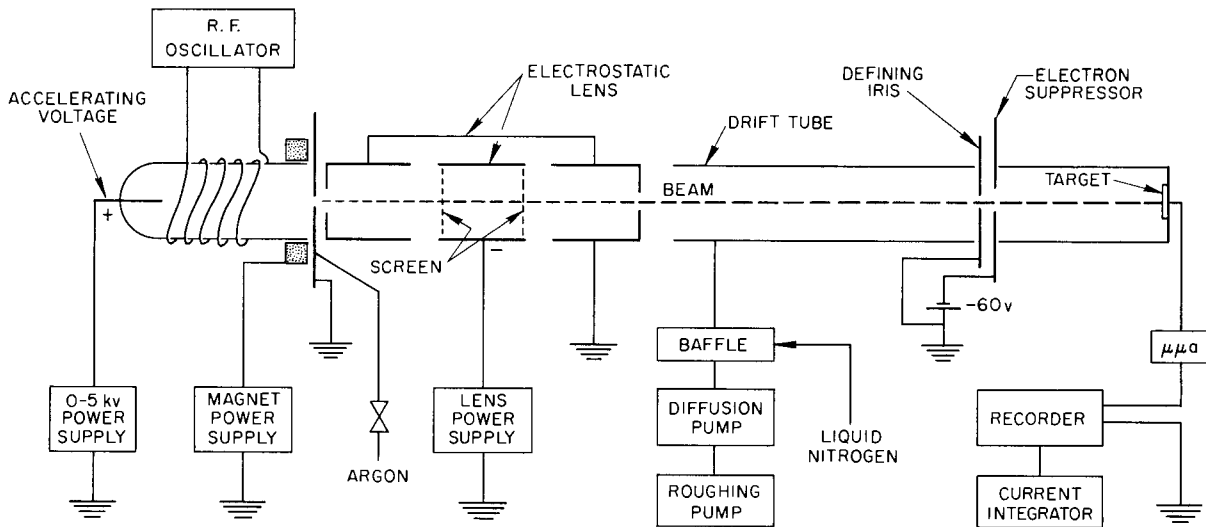


Fig. 8.1. Block Diagram of Experimental Setup for Sputtering Experiment.

Since the target was mounted in a Faraday cage, any secondary electrons escaping from the cage would be counted as beam current. However, for this to happen, the electrons must stream back up the beam and be shielded from the electron suppressor.

The ion source was of the type designed by Moak, Reese, and Good.¹¹ It was mounted in the tank coil of a self-exciting oscillator operated at 38 Mc. Radio-frequency power was smoothly variable from 0 to 150 w. Argon gas used in the source was found to be 99.97% argon by mass spectrometric analysis.

An analysis of the beam energy was made by inserting a counter field lens¹² between the electron suppressor and the Faraday cage. The construction of this apparatus is shown in Fig. 8.2. It was found that the energy distribution of the beam depended on the size of the defining iris. Figures 8.3-8.5 give ion current vs counter field lens potential for $\frac{1}{8}$ -, $\frac{1}{4}$ -, and $\frac{3}{8}$ -in.-dia irises. It should be noted that these measurements do not differentiate between singly and doubly charged ions.

Pressure in the system with the beam off was 2×10^{-7} mm Hg. With normal operating conditions, pressure in the target chamber was 10^{-5} mm Hg or less with the increase being due to argon gas. If one computes the arrival rate of background impurity molecules compared with beam ions, one finds that in the target area the ratio is about 1:5. There was no evidence of pressure dependence of the sputtering ratio.

Determination of the mass of targets was done using an Ainsworth microchemical balance. Mass variation was from 200 to 800 mg, which could be measured within 4% for the lower values. Most values were known within 2% or better.

For stainless steel

$$S = \frac{N_{SA}}{N_{Ar^+}} = 1.79 \frac{\Delta m}{Q},$$

where Δm is the mass loss in milligrams and Q is the total charge collected. Total charge was found from the integrator by the relationship

$$Q = 1.2 \times 10^{-5} \times \text{number of counts};$$

therefore,

$$S = 1.45 \times 10^5 \frac{\Delta m}{\text{number of counts}}.$$

¹¹C. D. Moak, H. Reese, Jr., and W. M. Good, *Nucleonics* 9(3), 18 (1951).

¹²G. Forst, *Z. angew. Phys.* 10, 546 (1958).

UNCLASSIFIED
ORNL-LR-DWG 52991

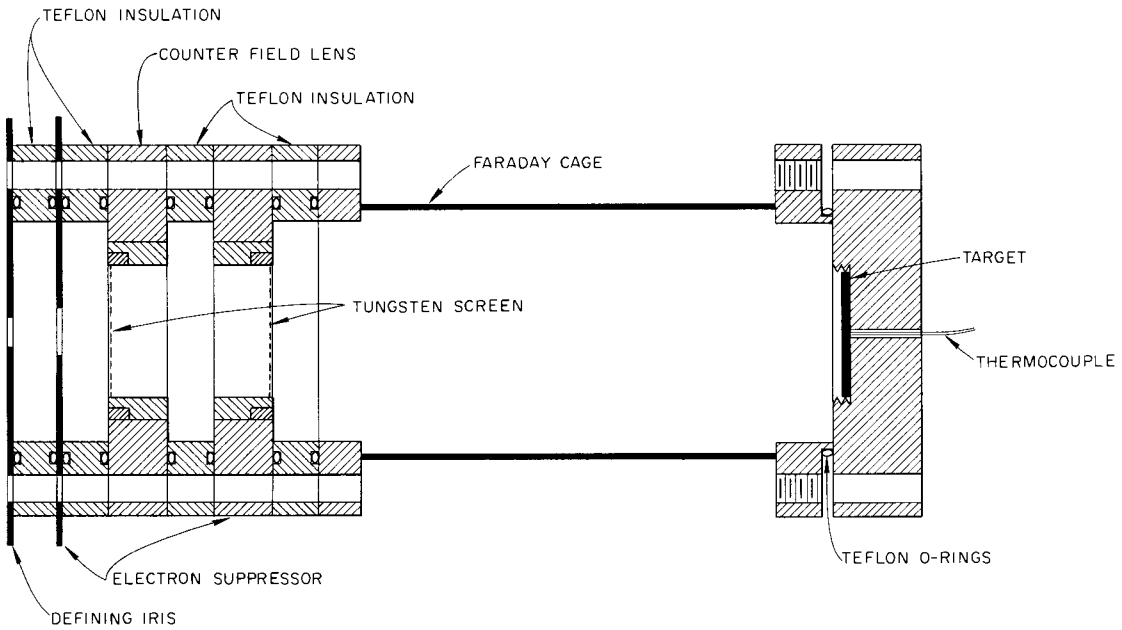


Fig. 8.2. Counter Field Lens and Faraday Cage Used in the Energy Analysis of the Ion Beam.

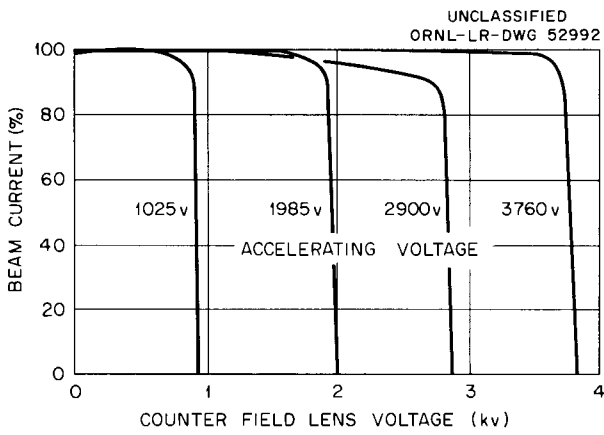


Fig. 8.3. Energy Analysis for $\frac{1}{8}$ -in. Defining Irls.

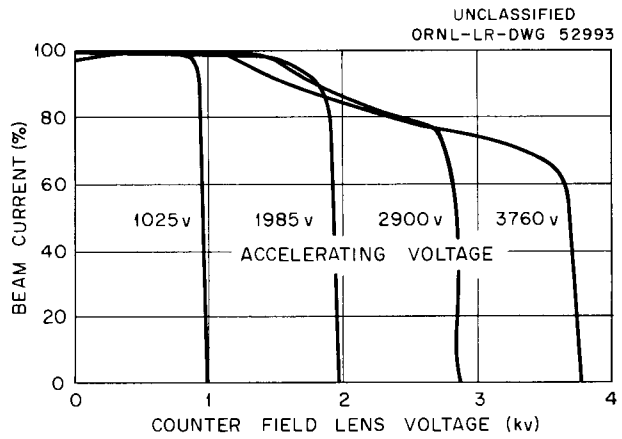


Fig. 8.4. Energy Analysis for $\frac{1}{4}$ -in. Defining Irls.

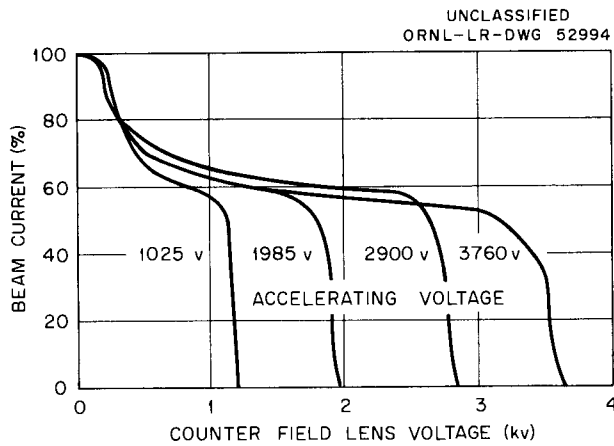


Fig. 8.5. Energy Analysis for $\frac{3}{8}$ -in. Defining Iris.

The error in measurement of Q is about 2%, so that the sputtering ratio should have a maximum instrument error of $\pm 6\%$.

The radio-frequency ion source has 95% of the ions within 100 ev of the desired energy when only $\frac{1}{8}$ in. diameter in the center of the beam is used.

When a $\frac{3}{8}$ -in. defining iris was used, only 40% of the beam was in the desired range.

The sputtering ratio increased with the energy of the ion beam; at 1 kev the sputtering ratio is 1.15 atoms/ion and at 5 kev the ratio is 2.6 atoms/ion. Figure 8.6 shows the sputtering coefficient vs energy.

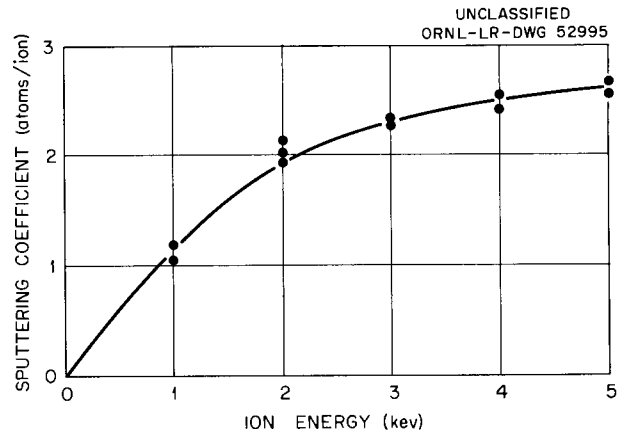


Fig. 8.6. Sputtering Coefficient vs Ion Energy for Type 304 Stainless Steel Bombarded with Ar^+ Ions.

9. BRITTLE FRACTURE OF METALS

J. C. Wilson

The purpose of this program is to obtain a more fundamental understanding of the processes responsible for irradiation-induced embrittlement of metals than has been possible in various project-oriented programs. Iron and its alloys are being studied first for two reasons: First, radiation embrittlement of steels is of great technological importance. Second, it is already known that the severity of radiation effects in high-purity iron-carbon alloys is substantially less than in steels of similar properties; so it is known that composition effects do exist.

The literature on iron and its alloys, described as "pure" or "high-purity," was surveyed. From the survey it was concluded that any worthwhile program would require much purer metal, better and more complete analyses, and more care in working and heat-treating than had been used heretofore.

Therefore, most of the effort of the first year has been spent in exploring purification methods, analytical means, and experimental methods for forming and heat-treating without contaminating the specimens. Limited experience (deduced from mechanical property measurements) has indicated that the reduction, cleaning, and heat-treating methods are adequate down to 0.05-in. wires.

The metals presently used for reference materials include four iron and iron-carbon alloys that were crucible-melted in vacuum from electrolytic iron by commercial suppliers. Oxygen is the most troublesome impurity (about 0.01%), but no supplier was willing to effect oxygen removal by exposing the melt to dry hydrogen.

A 1-lb piece of zone-refined iron, prepared for the American Iron and Steel Institute by Battelle, was compared with the above irons and found much better in all respects. An 8-lb ingot of zone-refined iron was subsequently ordered from Battelle; reduction and heat-treating schedules for this iron are now being developed. The tensile results (yield stress and temperature dependence of yield stress) from the 1-lb piece of zone-refined iron indicate its purity to be approximately that of the purer irons reported in the literature. Strain-aging and quench-aging experiments are under way.

Further purification of the vacuum-melted and zone-refined irons has been attempted by several methods. Chemical analyses are not yet complete, so the efficacy of the methods cannot be compared for specific elements. Measurements of yield strength and metallographic observations have shown that the methods tried have some effect. In the zone-refined iron, measurement of improved purification may require development of new analytical methods because the impurity contents already approach the lower limit of detection.

Solid-state electrolysis of several irons in vacuum at 800°C with a current density of 10 amp/mm² for times to 100 hr has been carried out. Differences in microstructure at cathode and anode are probably due to carbon transport. Larger specimens are being electrolyzed to provide enough material for complete chemical analysis of the ends and center and to determine the extent to which elements other than carbon are transported.

Solid-state zone refining by passing a short gamma-range zone slowly down an alpha specimen has been attempted, but a more reliable apparatus is needed.

Long-time, high-temperature vacuum heat treatments have been carried out to determine if purification takes place. Metallographic observations of 100-hr exposures to 750 to 850°C in a vacuum of 10⁻⁶ mm Hg show micron-sized particles of oxide on the thin, uniform oxide layer. The density of oxide particles seems to be some rough function of purity and is apparently sensitive to the material in the experimental apparatus. (Austenitic stainless steel and silica furnace tubes have both been used.) The effect of foreign atoms in the apparatus, gettering or shielding foils of tantalum, and the effects of vapor-deposited calcium getters are being explored.

Electron-beam melts of iron on a cold hearth have been made by T. Hikido, of the Metallurgy Division. One iron, containing 0.01% each of oxygen and carbon, showed marked grain-boundary brittleness after melting although metallography indicates a reduced oxygen content. Another high-purity iron with a higher carbon was also

melted with the intent of using the carbon to speed deoxidation. Double melting of 300-g buttons results in 10% loss of metal.

A large (75-lb) consumable-electrode, cold-crucible melt of steel, made in the Metallurgy Division at a pressure of about 15 μ , is being analyzed and its mechanical properties measured to determine the extent of impurity elimination after this treatment. Available high-purity iron stock will also be melted in this furnace.

A vacuum or inert-atmosphere apparatus for floating-zone refining of bars up to $\frac{3}{4}$ in. is under construction. Provision has been made for

a 300-amp "pinch" current to stabilize the molten zone. The apparatus and induction heater are adaptable to crucible melting also.

The purification work, chemical analyses, and physical measurements to indicate purity (low-temperature resistivity ratio, yield strength and its temperature dependence, and transformation temperatures) will go on until a reasonably high degree of purity is obtainable in a practical time in quantities sufficient for property measurements. At this point studies of precipitation of carbon and nitrogen, effect of quenched-in vacancies, and irradiation can be profitable.



Part III
NONMETALS



10. SEMICONDUCTOR STUDIES

RADIATION-INDUCED DISORDER IN SEMICONDUCTORS¹

J. W. Cleland J. H. Crawford, Jr.

Inhomogeneities in the distribution of lattice defects may have important consequences for the electrical behavior of neutron-bombarded semiconductors. Investigations of the range of energetic primary recoils have shown that these have appreciable ranges in close-packed solids,² for example, 160 Å for 25-keV copper recoils. Ranges of germanium recoils may be appreciably larger.³ Since the primary recoil loses energy primarily by elastic collisions within its range, most of the lattice damage from a 25-keV recoil in germanium must occur within a region 100 to 150 Å in radius. Theoretical considerations⁴ suggest that, in the absence of extensive relaxation, the defect concentration in such regions may be as great as 5 at. %. Since defects introduced into germanium by bombardment act as net acceptors, these regions are *p*-type islands in an *n*-type matrix and will be insulated from the *n*-type matrix by an electrical double layer. Such disordered regions and their surrounding zone of space charge will act as an insulating void which will block current flow. According to Juretschke *et al.*⁵ the measured conductivity of a solid containing small spherical voids is

$$\sigma_M = \frac{\sigma(1-f)}{1+f/2}, \quad (1)$$

where σ is the conductivity of the matrix and f is the fraction of the volume occupied by insulator.

Gossick, Crawford, and Cleland⁶⁻⁸ have described the structure of the double layer associated with the disordered regions (assumed spherical) in terms of a simplified model. For an

acceptor density N_1 within the region very much greater than the donor density N_2 in the matrix,

$$v_{sc} = \frac{4\pi r_2^3}{3} = \frac{\psi_p \epsilon r_1}{qN_2}, \quad (2)$$

where

- v_{sc} = total volume affected by the space charge,
- r_2 = radius of the insulating sphere,
- r_1 = radius of the disordered region,
- ψ_p = potential difference from the center of the disordered region to the matrix,
- ϵ = dielectric constant,
- q = electronic charge.

For reasonably high-purity germanium ($10^{13} < N_2 < 10^{15}$) and for $N_1 \geq 10^{19}$ nearly all the potential drop occurs outside of the disordered region and r_2 is one to two orders of magnitude greater than r_1 . For small concentrations of such regions, $f \approx \bar{v}_{sc} \Sigma_v \phi_d t$, where Σ_v is the probability that a fast neutron create a primary recoil sufficiently energetic to produce a disordered region and $\phi_d t$ is the integrated fast-neutron flux. As the concentration of regions increases, overlap of space charge is expected and the relation between f and ϕ_d becomes more complex. Therefore, in its present form the model is best applied to short neutron exposures ($f < 0.25$).

In this paper the results of neutron bombardment of germanium will be re-examined on the basis of the disordered-region model. As was pointed out previously,⁷ the relative contributions of isolated defect states and disordered regions are highly sensitive to the energy spectrum of the bombarding neutrons. Recently, the spectrum of the exposure facility in the Oak Ridge Graphite Reactor used in these studies has been explored in the fission energy range.⁹ It was found that $\phi(E_n > 0.7$

¹Accepted for publication in the Proceedings of the International Conference on Semiconductor Physics, Prague, Czechoslovakia, 1960.

²R. A. Schmitt and R. A. Sharp, *Phys. Rev. Letters* 1, 445 (1958).

³V. A. J. van Lint and R. A. Schmitt, unpublished results.

⁴D. K. Holmes and G. Leibfried, *J. Appl. Phys.* 31, 1046 (1960).

⁵H. J. Juretschke, R. Landauer, and J. A. Swanson, *J. Appl. Phys.* 27, 838 (1956).

⁶B. R. Gossick and J. H. Crawford, *Bull. Am. Phys. Soc.* 3, 400 (1958).

⁷J. H. Crawford and J. W. Cleland, *J. Appl. Phys.* 30, 1204 (1959).

⁸B. R. Gossick, *J. Appl. Phys.* 30, 1214 (1959).

⁹D. Binder, unpublished results.

Mev) = $2.7 \times 10^{11} \text{ cm}^{-2} \text{ sec}^{-1}$. The average energy of a primary recoil in germanium is $E_p = 19$ kev for $E_n = 0.7$ Mev. Theoretical considerations⁴ of the path length of primaries indicate that ~ 20 kev is the minimum E_p capable of producing an insulated disordered region.

Previously,¹⁰ the initial conductivity decrease of *n*-type germanium during neutron bombardment was attributed entirely to a decrease in electron concentration to the extent of -3.2 per incident or -18 per scattered fast neutron, based on an estimated total damaging flux $\phi_d = 8 \times 10^{11} \text{ cm}^{-2} \text{ sec}^{-1}$. By using the previously derived relation⁷ for the initial rate of conductivity change, namely

$$\left(\frac{d\sigma_M}{d\phi_d}\right)_{\phi_d=0} = q\mu_n \left(\frac{dn_M}{d\phi_d}\right)_{\phi_d=0} = -q\mu_n \left(A\Sigma_d + \frac{3\psi_p \bar{\tau}_1 \epsilon \Sigma_v}{2q} \right), \quad (3)$$

where A is the number of electrons removed per isolated defect and Σ_d is the probability per centimeter of defect production by a neutron of the spectrum employed, one may estimate the relative contributions of the two types of lattice disorder from the initial change in σ_M . Σ_d and Σ_v may be placed on a relative basis by employing $\Sigma_s = \sigma_s N_A$, the macroscopic scattering cross section. Strictly, σ_s is dependent on neutron energy, but the variation over the range of interest is not great; therefore, we assume it constant at 4 barns, giving $\Sigma_s = 0.18 \text{ cm}^{-1}$. We may now define $W_d = \Sigma_d/\Sigma_s$ and $W_v = \Sigma_v/\Sigma_s$. W_d , which includes the average number of defects produced by low-energy primaries, is not known. However, since it is assumed that every collision of neutrons with $E_n > 0.7$ Mev produces a disordered region of mean radius $\bar{\tau}_1$, $W_v = \phi(E_n > 0.7 \text{ Mev})/\phi_d$. Therefore, AW_d may be estimated from the space-charge model.

The value of ψ_p is given by the difference in Fermi levels ζ in the matrix and disordered regions. The defect energy-level structure may be taken into account by employing the limiting position of ζ (ref 11): $\zeta_1 - E_v = 0.125$ ev. For

n-type germanium with $N_2 = 10^{14} \text{ cm}^{-3}$, $E_c - \zeta_2 = 0.30$ ev and $\psi_p = 0.24$ v. We take $\bar{\tau}_1 = 100$ A. From Eq. (3) it is found that $AW_d = 4.5$ compared to $\bar{v}_{sc} W_v N_2 = 13.5$. Therefore, for this choice of $\bar{\tau}_1$ and partitioning of the neutron spectrum, the contribution to the decrease of σ_M due to defects is one-third that of the disordered regions.

The model may also be applied to the results of Ruby *et al.*¹² who found apparent electron removal rates in high-purity *n*-type germanium at 77°K to be 21, 12, and 12 for incident monoenergetic neutrons of 1.8, 3.2, and 4.8 Mev respectively. We assume that all collisions in this high-energy range lead to disordered regions. It should be noted that ψ_p is somewhat greater for a given N_2 at 77°K; for example, for $N_2 = 10^{14} \text{ cm}^{-3}$, $\psi_p(77^\circ\text{K}) = 0.58$ v. Hence, the calculated value of the apparent initial removal rate is 17 per incident neutron, which is in excellent agreement with experiment. The apparent removal rates for 100°K reactor bombardments,¹⁰ which are ~ 1.5 times the room temperature value, are also consistent with the model as expressed in Eq. (3), the partition between disordered regions and isolated defects being about the same as found for room temperature.

We yet need justification of the choice of $\bar{\tau}_1 = 100$ A. The variation of mobility is expected to give an even better test of the model. For short exposures ($f < 0.2$), $\bar{\tau}_1$ may be estimated from⁷

$$\left(\frac{dM}{d\phi_d}\right)_{\phi_d=0} = \frac{3\psi_p \bar{\tau}_1 \epsilon \Sigma_v}{4qN_2}, \quad (4)$$

where $M = \mu_H^M/\mu_H^0$, the assumption being made that μ_H is not changed appreciably by the bombardment. A previous evaluation⁷ employing Eq. (4) suffered from a lack of knowledge of neutron energy spectrum. By using the values of the flux quoted above to obtain W_v and the refinement in evaluating ψ_p which takes the defect energy-level structure into account, one obtains for the high-purity specimen $N_2 = 1.3 \times 10^{14} \text{ cm}^{-3}$, $\bar{\tau}_1 = 120$ A, which is in excellent agreement with the assumed value of 100 A used above.

An alternative test of the model employs the temperature dependence of M . It can be shown

¹⁰J. W. Cleland, J. H. Crawford, Jr., and J. C. Pigg, *Phys. Rev.* 98, 1742 (1955).

¹¹J. W. Cleland, J. H. Crawford, Jr., and J. C. Pigg, *Phys. Rev.* 99, 1170 (1955).

¹²S. L. Ruby, F. D. Schupp, and E. D. Wolley, *Phys. Rev.* 111, 1493 (1958).

that for small f

$$\frac{dM}{dT} \approx \frac{3\epsilon\bar{\tau}_1 \sum_v \phi_d t}{qN_2} \frac{d\psi_p}{dT}, \quad (5)$$

with $d\psi_p/dT$ containing not only the temperature dependence of ζ_2 but that of the band gap as well. Because of experimental inaccuracies and the restricted range of validity of (5), good M vs T data are difficult to obtain. One series of irradiations on a specimen with $n_0 = 1.6 \times 10^{15} \text{ cm}^{-3}$ has been analyzed and $\bar{\tau}_1$ evaluated. For exposures of 1.4×10^{14} and 2.8×10^{14} neutrons/cm², the values of $\bar{\tau}_1$ were found to be 170 and 140 Å respectively. In view of the contribution of carrier scattering from isolated defects at lower temperature, which tends to increase dM/dT , this is considered good agreement with the analyses given above.

Since the three correlations considered above depend on the presence of insulating regions in different ways, the space-charge model of disordered regions seems highly plausible.

Helpful discussions with B. R. Gossick, D. K. Holmes, and H. C. Schweinler are gratefully acknowledged.

TRANSMUTATION DOPING AND RECOIL EFFECTS IN SEMICONDUCTORS EXPOSED TO THERMAL NEUTRONS¹³

J. H. Crawford, Jr. J. W. Cleland

Nuclear reactions accompanying thermal-neutron capture provide an effective means of introducing acceptor or donor impurity into certain semiconductors. Moreover, the fixed rate of radioactive decay permits time-dependent observations of electronic properties; for example, the rate of shift of chemical potential with impurity introduction may be used to determine ionization energies of defects or impurities in much the same way as potentiometric titrations. Also, nuclear doping permits compensation of existing acceptors or donors, thereby altering the concentration of charge carriers, and provides a means of investigating the effect of impurity compensation on carrier mobility and impurity-banding phenomena. Besides chemical impurity, lattice defects may

¹³Abstract of a talk presented at the IAEA Conference on Radioisotopes in Research and Industry, Copenhagen, Denmark, 1960. The Proceedings of this conference will be published.

be created via recoil of nuclei on emission of radiation: capture gamma rays or decaying radiation.

Extensive studies of thermal-neutron exposure of germanium have been made. Of the five isotopes, three transmute to chemical impurity whose yields in atoms per 100 neutron captures and half lives are: Ga⁷¹ - 30.4, 11.4 days; As⁷⁵ - 9.8, 82 min; Se⁷⁷ - 1.2, 39 hr. Therefore, approximately three acceptors (Ga⁷¹) are introduced for each donor (As⁷⁵ and Se⁷⁷), and through choice of exposure one may decrease the electron concentration of n -type germanium to very low values or convert n -type germanium to p -type. The half life leading to Ga⁷¹ is conveniently long so that details of the "radioactive titration" may be followed by Hall coefficient and conductivity. Experiments also show that approximately one electron per neutron capture is removed by lattice defects created by the recoil of nuclei from capture gamma-ray emission. These displaced atoms may be restored to normal lattice sites by annealing at $\sim 450^\circ\text{C}$.

Recoil effects in silicon have also been observed, approximately two charge carriers being removed per capture. Implications of these results and those on germanium will be discussed in terms of the capture gamma-ray spectra. In indium antimonide the capture gamma rays from In¹¹⁵ are not sufficient to displace a large number of nuclei and the major effect is production of Sn¹¹⁶, a donor when substituted in an indium lattice position. Nuclear doping holds promise for investigating numerous compound semiconductors in which introduction of impurity by chemical means is difficult.

TRANSMUTATION DOPING AND RECOIL EFFECTS IN ISOTOPIC ENRICHED Ge⁷⁴ EXPOSED TO THERMAL NEUTRONS

J. W. Cleland R. F. Bass
J. H. Crawford, Jr.

It has previously been suggested¹⁴ that the average recoil energy expected from thermal-neutron capture in germanium and silicon is ~ 182

¹⁴H. C. Schweinler, *J. Appl. Phys.* 30, 1125-26 (1959); J. W. Cleland and J. H. Crawford, Jr., *Solid State Ann. Prog. Rep. Aug. 31, 1959*, ORNL-2829, p 125-27; see also "Transmutation Doping and Recoil Effects in Semiconductors Exposed to Thermal Neutrons," this report.

and 780 ev respectively; hence, each thermal-neutron absorption probably results in the formation of an interstitial atom, prior to any transmutation results.

Figure 10.1 is a plot of the log Hall coefficient and log resistivity vs inverse temperature for *n*-type germanium irradiated with a total integrated thermal-neutron flux of 4.0×10^{13} thermal neutrons/cm². Approximately 4×10^{12} electrons/cm³

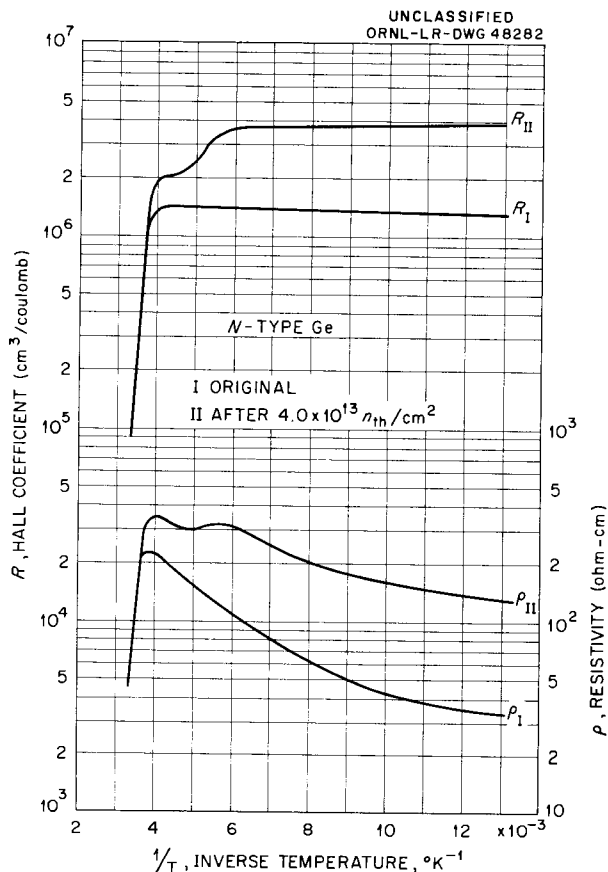


Fig. 10.1. Effect of Thermal-Neutron Irradiation on the Hall Coefficient *R* and Resistivity ρ Curves of *n*-Type Germanium. Log *R* and log ρ vs $1/T$ curves after exposure to 4×10^{13} thermal neutrons/cm² are compared with those obtained before exposure.

have been removed from conduction, and the pronounced step in the Hall coefficient and resistivity curves would indicate the formation of two defect states. Continued irradiation and an analysis of the slope places the shallow state at 0.20 ev below the conduction band, and continued irradiation converts the material to *p*-type. Similar data

have been obtained for germanium that was irradiated with Co⁶⁰ photons,^{14,15} where the formation of isolated interstitials and vacancies is expected.

Extensive experiments of this type have indicated that approximately one electron per neutron capture is removed by lattice defects created by the recoil of nuclei from capture gamma-ray emission in germanium, and approximately two electrons per each similar event in silicon. No evidence of any form of multiple defect production from the energetic recoil in germanium or silicon has been observed.

Table 10.1 shows the isotopic content, absorption cross section, fraction of thermal neutrons absorbed, and transmutation end product of isotopically enriched Ge⁷⁴. The total absorption

Table 10.1. The Isotopic Content, Absorption Cross Section, Fraction of Thermal Neutrons Absorbed, and Transmutation End Product of Isotopically Enriched Ge⁷⁴

Total neutron absorption cross section,
 $\sigma_a = 0.85 \times 10^{-24} \text{ cm}^2$

Isotope	Fraction, <i>f</i>	Cross Section, σ_a (cm ²)	Fraction of Neutrons Absorbed	End Product
$\times 10^{-24}$				
70	0.007	3.4	0.028	Ga ⁷¹
72	0.011	0.98	0.013	Ge ⁷³
73	0.156	14.0	0.256	Ge ⁷⁴
74	0.958	0.62	0.699	As ⁷⁵
76	0.008	0.36	0.004	Se ⁷⁷

cross section of this material is $\sim 0.85 \times 10^{-24} \text{ cm}^2$, and one would expect ~ 0.699 displaced As⁷⁵ atoms for each 0.256 displaced Ge⁷⁴ atom. Multiple defect creation by energetic recoils would produce Frenkel-type interstitials and vacancies that would serve as acceptor states in this material.

Figure 10.2 is a plot of the log Hall coefficient and log resistivity vs inverse temperature of a

¹⁵J. H. Crawford, Jr., and J. W. Cleland, *J. Appl. Phys.* 30, 1204-13 (1959).

high-purity, single-crystal *n*-type sample of 95.8%-enriched Ge⁷⁴ with an excess donor concentration¹⁶ of 1.2×10^{13} electrons/cm³. Note that thermal-neutron irradiation actually increases the *n*-type donor concentration in this sample. Note also that evidence for two defect states is observed, and that the net donor concentration is greatly enhanced by vacuum anneal at 450°C.

Table 10.2 summarizes the experimental data obtained from Fig. 10.2. The actual increase in donor concentration that was observed as a result of two successive irradiations is only about 9% of the expected increase in donor concentration due to the addition of As⁷⁵ before anneal; however, the total change in carrier concentration after the irradiations and a vacuum anneal at 450°C is almost identical with the expected total increase in donor concentration from the As⁷⁵. This result would indicate that the published values of absorption cross sections are correct (Table 10.1) and that our experimental determination of thermal-neutron flux values by CuAl foils is also quite valid.

¹⁶It should be mentioned that experimenters at the Bell Telephone Laboratories obtained 17 g of GeO₂ from the Stable Isotopes Division of the Oak Ridge National Laboratory and succeeded in the purification, zone refining, and growth of a single-crystal germanium ingot. We are deeply indebted to W. Brown, T. Geballe, and their associates of the Bell Telephone Laboratories for the use of 1.65 g of the original ingot.

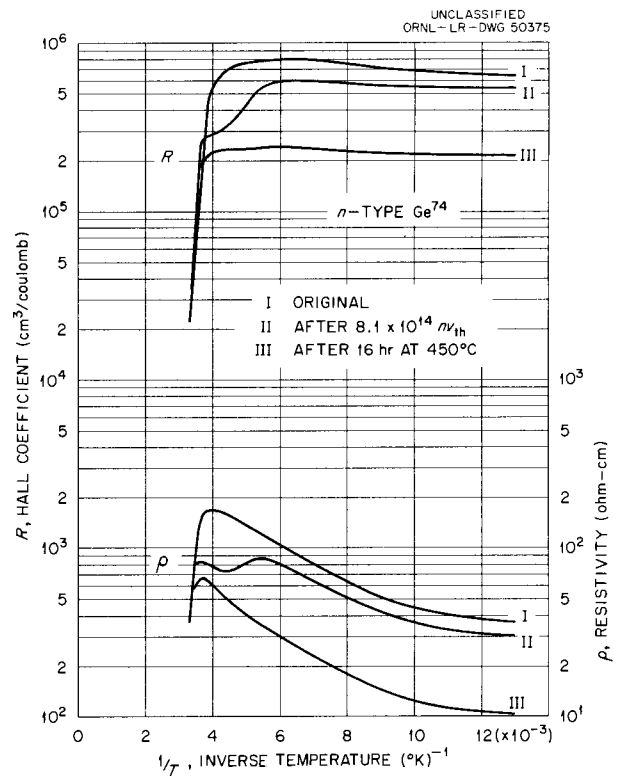


Fig. 10.2. Effect of Thermal-Neutron Irradiation and Vacuum Heat Treatment at 450°C on the Hall Coefficient *R* and Resistivity ρ Curves of Isotopically Enriched *n*-Type Ge⁷⁴. Log *R* and log ρ vs 1/*T* curves after exposure to 8.1×10^{14} thermal neutrons/cm² and after 16 hr at 450°C are compared with those obtained before exposure.

Table 10.2. The Carrier Concentration, Thermal-Neutron Flux, Change in Carrier Concentration, and Expected Increase in Carrier Concentration for *n*-Type Ge⁷⁴ as Affected by Thermal-Neutron Irradiations and a Vacuum Heat Treatment at 450°C

<i>n</i> , Carrier Concentration at 77°K (cm ⁻³)	Thermal Flux (neutrons/cm ²)	Δn , Change in Carrier Concentration at 77°K (cm ⁻³)	Expected Donor Increase, Ge ⁷⁴ -As ⁷⁵
1.148×10^{13}			
1.279×10^{13}	3.98×10^{14}	1.31×10^{12}	1.15×10^{13}
1.375×10^{13}	4.06×10^{14}	0.92×10^{12}	1.14×10^{13}
3.444×10^{13}	0.00	2.30×10^{13} *	2.29×10^{13} *

*After 16 hr vacuum anneal at 450°C.

The very evident absence of those Frenkel-type defects that removed conduction electrons in normal isotopic germanium is perhaps the most important problem in this experiment. In the previous work¹⁴ we observed the removal of two electrons for each actual thermal-neutron absorption and recoil. Under the same assumptions, and using the cross sections of Table 10.1, one would expect that an irradiation of 8.1×10^{14} thermal neutrons would produce 2.29×10^{13} displaced atoms/cm³ that have transmuted to As⁷⁵ by the time of measurement, and 8.4×10^{12} germanium atoms/cm³ that do not transmute. The other three isotopes can be neglected, since they absorb only ~4% of the thermal neutrons incident. These values would indicate that 1.57×10^{13} Frenkel-type defects would be created, and these would remove about 3.13×10^{13} electrons/cm³ from conduction, if the removal process was comparable to that observed for normal isotopic germanium (one electron removed per actual neutron absorption). Instead, one observes the addition of 2.23×10^{12} more donors after the irradiation, and about ten times that number after anneal.

It has been suggested that the initial recoil upon thermal-neutron absorption may result in a series of replacement-type collisions, or lattice displacements that effectively absorb the recoil energy without the creation of additional Frenkel-type defects. Such a mechanism would suggest that the original recoiling atom, which absorbed the thermal-energy neutron, is almost always left in a substitutional position, while some other normal lattice atom is placed in an interstitial position. This process would not be expected to operate with 100% efficiency, which might explain why only about one electron is removed from conduction for each actual thermal-neutron absorption and recoil, even though the Frenkel-type defect thus formed evidently has two electron-acceptor-type states.

The mechanism of replacement-type collisions is attractive, in that the original atom is often left in a substitutional position, and can later transmute as a substitutional impurity. This might be employed to explain the normal isotopic results, wherein irradiated and irradiated-annealed material changed identically as the Ga⁷¹ chemical impurity was introduced.

Under the above assumptions, the addition of As⁷⁵ as a substitutional atom might essentially

balance the removal of conduction electrons that resulted from the Frenkel-type defect that was created when some other lattice atom was placed in an interstitial position. One might even expect a net increase in donor concentration, since the substitutional process might be more effective than the replacement technique as a generator of a Frenkel-type defect. It should be mentioned, however, that one-third of the recoils in this material are those of Ge⁷³ that would not balance out the resulting defects. The fact that the sample is still more *n*-type after the irradiation would seem to indicate that this model of replacement collisions is not very adequate to explain these experimental results. It is therefore quite evident that additional experiments are necessary, before the phenomena of recoil defect introduction and transmutation doping experiments are well understood. Low-temperature thermal-neutron irradiation experiments would seem to be of paramount importance, since such a technique would freeze the displacements and defect states in until such a time that annealing-type studies could be made.

ANNEALING STUDIES OF IRRADIATED GERMANIUM

J. C. Pigg

The annealing studies reported previously have been continued.¹⁷ The irradiations have been conducted using Co⁶⁰ gamma irradiation and a constant sample temperature. The isochronal pulse anneals reported in ref 17 have been repeated using larger relative induced carrier changes than those reported previously. Consequently, better resolution of the effect has been obtained.

All the measurements have been made using samples cut from the same ingot, EP8. It is single-crystal, *n*-type, antimony-doped to a carrier concentration of $\sim 1.5 \times 10^{14}$ cm⁻³, obtained from Eagle-Picher.

Sample EP8-A was irradiated at liquid-nitrogen temperature until a change in carrier concentration of 1.26×10^{14} cm⁻³ was obtained. The sample was then annealed in the manner used in ref 17. The behavior in the temperature range between 77 and 300°K followed the pattern of that reported previously. When the temperature of the

¹⁷J. C. Pigg, *Solid State Ann. Prog. Rep. Aug. 31, 1959*, ORNL-2829, p 131-35.

pulses was extended into the higher temperature range of room temperature to slightly above room temperature, the observed changes were large compared with those observed below 250°K.

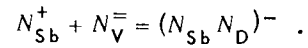
The results of anneals at temperatures in the range from 250 to 424°K of EP8-A are shown in Fig. 10.3. There are clearly at least two processes in operation. Approximately 90% of the mobility has recovered by the time that 5% recovery of the carrier concentration is obtained. One possible explanation of the results is in terms of a migration of charged defects (possibly vacancies) to charged impurity sites. Before irradiation the scattering is proportional to the antimony concentration:

$$N_{\text{scatter}} = N_{\text{Sb}}^+$$

After irradiation a doubly ionized defect contributes to the scattering:

$$N_S' = N_{\text{Sb}}^+ + N_V^=$$

On annealing, the defect migrates to an antimony site, forming a complex with a single excess charge:



Consequently, the concentration of charged scattering centers is restored to almost the initial value although the defect has not been removed. Although the total charge of the complex is that of a single charge center, there is still a dipole present which can scatter electrons, though much less efficiently than charged centers. Consequently, the mobility is not completely restored; and further recovery occurs as the defects are annealed.

The low rate of annealing of carrier concentration at temperatures below 400°K may be attributed to the inhibition of vacancy motion by this trapping at the antimony sites. If such is the case, the decomposition of Sb-V combination would be the controlling process in this range.

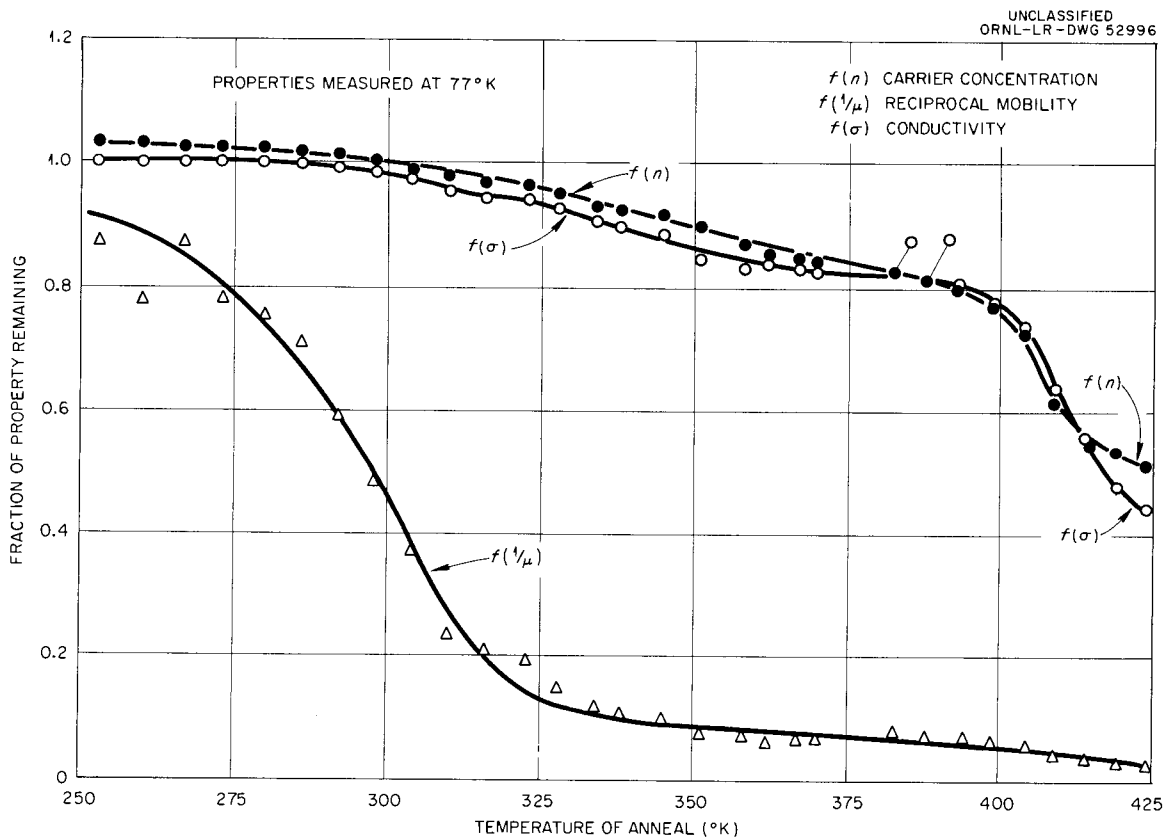


Fig. 10.3. Isochronal Anneal of Radiation-Induced Changes in Carrier Concentration and Mobility. Sample EP8-A.

SOLID STATE ANNUAL PROGRESS REPORT

In the rapid annealing above 400°K, it may be that the thermal energy is sufficient to decompose the SB-V compound and the controlling process is now vacancy diffusion.

The behavior in the temperature range above 400°K is currently being investigated by means of isothermal anneals. Sample EP8-B was irradiated at liquid-nitrogen temperature, brought to room temperature, and allowed to stand overnight. A Hall and resistivity vs temperature characteristic was then taken (see Fig. 10.4).

The temperature region of the 0.2-ev level reported by Cleland and Crawford¹⁸ was thus determined. The sample was then annealed at 407°K with measurements made at 77, 158, and 273°K, periodically (see Fig. 10.5). Cleland and Crawford found that 100°C annealing will remove the 0.2-ev level. When half the induced

¹⁸J. W. Cleland and J. H. Crawford, Jr., *J. Appl. Phys.* 30, 1204 (1959).

UNCLASSIFIED
ORNL-LR-DWG 52997

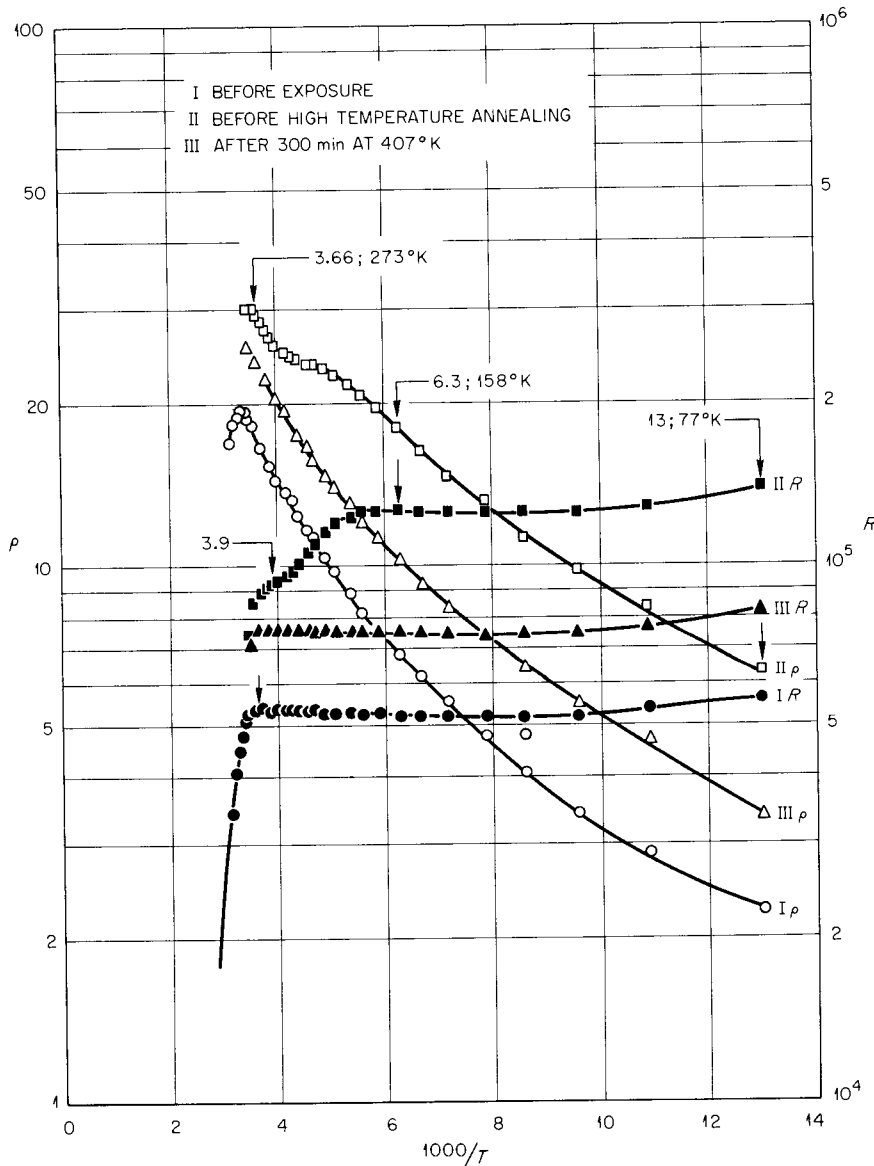


Fig. 10.4. Hall and Resistivity Characteristic Before and After Irradiation and Annealing. Sample EP8-B.

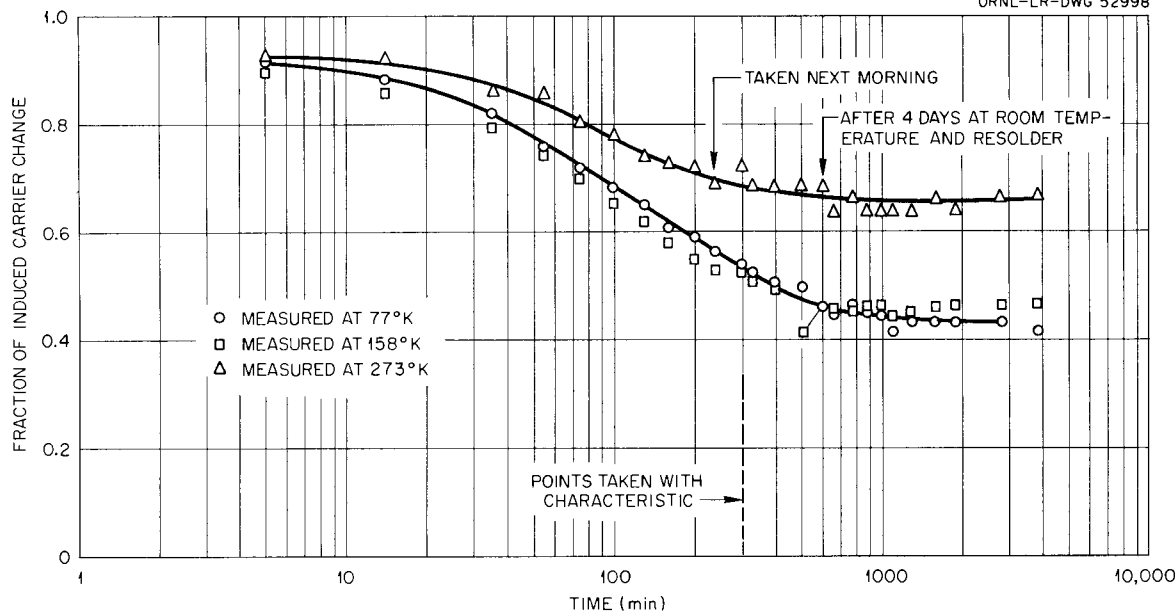
UNCLASSIFIED
ORNL-LR-DWG 52998

Fig. 10.5. Isochronal Anneal at 407°K of Induced Carrier Concentration in Co^{60} Gamma-Irradiated Germanium. Sample EP8-B.

carrier charge had been removed, a Hall characteristic showed that the 0.2-eV level had been removed (Fig. 10.4). The annealing curve flattened out at about 50% of the induced carrier concentration, measured at 77°K . The annealing at 273°K also flattened out about the same time but at a higher percentage of induced charge. Approximately 30% of the deep level has been annealed. This is in agreement with the results of Cleland and Crawford.¹⁸

Correlation of mobility and carrier concentration shown in Fig. 10.6 indicates the same general behavior as that observed in Fig. 10.3. The concentration of scattering centers, as indicated by $1/\mu$, has returned to the preirradiation value by the time that 50% of the induced carrier concentration has been removed. Brown *et al.*¹⁹ found that the change in $1/\mu$ as a function of carrier concentration is dependent upon the type of impurity. They found the $1/\mu_H$ vs n behavior to be the same during irradiation and anneal for antimony-doped material and the behavior to be quite different during irradiation and anneal for arsenic-doped material. The behavior reported here, in Fig. 10.6, is similar to the annealing

behavior of the arsenic-doped material of Brown *et al.* rather than to the antimony-doped material. The concentrations reported here, however, are of the order of 1.4×10^{14} , while those of Brown *et al.* were 2.0×10^{15} .

An irradiation was performed on EP8-D at dry-ice temperature and an isothermal anneal conducted at 410°K . The change in carrier concentration measured at 77°K is compared with similar measurements of EP8-B annealed at 407°K (see Fig. 10.7). Although the general behavior is similar for the two samples, there is a difference both in the annealing behavior and removal rate on irradiation. The removal rates at the two temperatures agree with those reported by Brown and Augustyniak.²⁰ On annealing, it is seen that the long linear section of EP8-B is not observed in EP8-D.

THERMOELECTRIC POWER IN GERMANIUM

O. E. Schow

As a result of previous efforts in the precise measurement of the thermoelectric power of germanium, control of ambient parameters was

¹⁹W. L. Brown *et al.*, *J. Appl. Phys.* 30, 1258 (1959).

²⁰W. L. Brown and W. M. Augustyniak, *J. Appl. Phys.* 30, 1300 (1959).

UNCLASSIFIED
ORNL-LR-DWG 52999

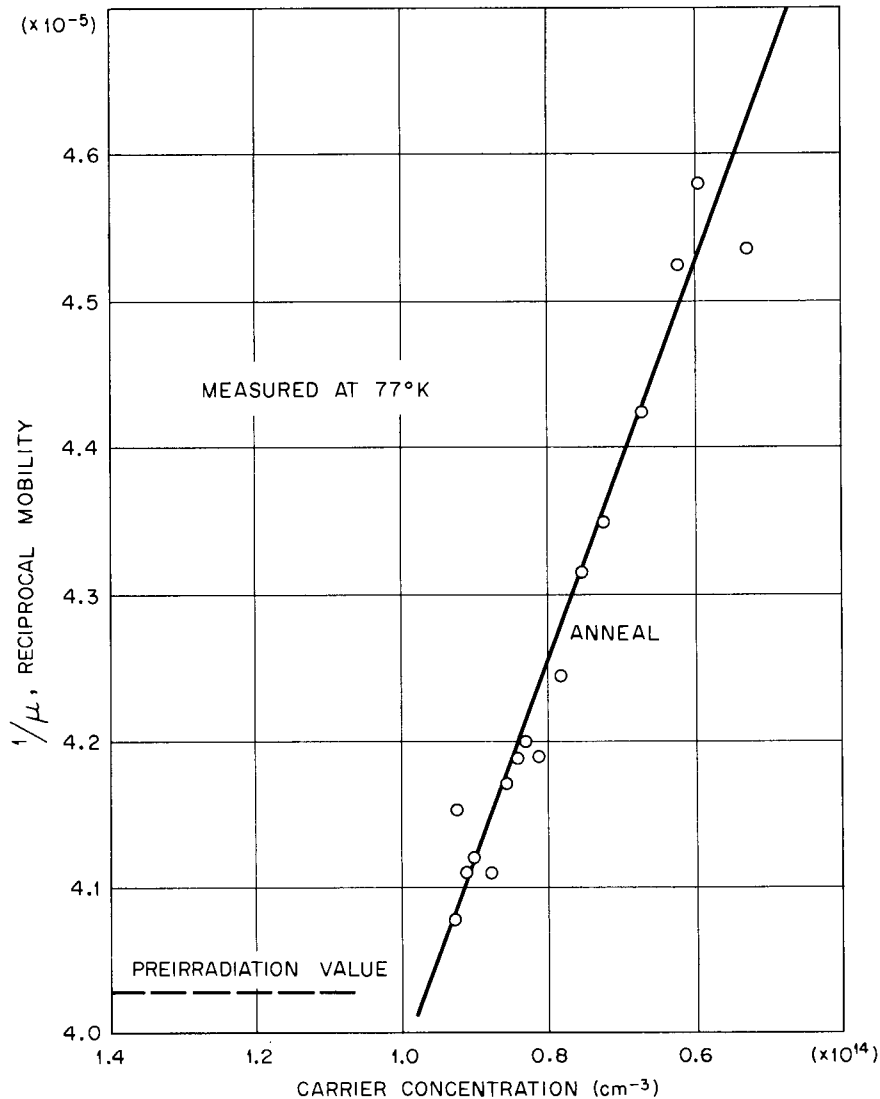


Fig. 10.6. Relation of Change in $\Delta(1/\mu)$ to Change in Carrier Concentration During Anneal. Sample EP8-B.

found to be of prime importance for accurate, reproducible results. Therefore, a well-designed air-conditioning system has been installed in the laboratory. The ambient room temperature is controlled to $\pm 0.05^\circ\text{F}$ so long as there are no drastic changes in the heat load of the laboratory, such as filling the cryostat with liquid nitrogen. In such a case, the temperature is held to $\pm 0.2^\circ\text{F}$, which is a short-time perturbation.

Line-voltage regulation is a critical factor because of the microvolt amplifiers and heater controllers which are powered from the a-c line

voltage. The critical instruments are powered from a line-voltage regulator which holds the voltage deviations to within ± 0.01 v at the power distribution panel.

The most difficult problem in measuring the thermoelectric power of germanium is the determination of the temperature difference between the hot and cold ends of the sample. An amplification of 5 is obtained in the ΔT measurement by use of a thermopile. The differential temperature is calculated from the slope of the ΔT vs thermal emf line. A typical plot

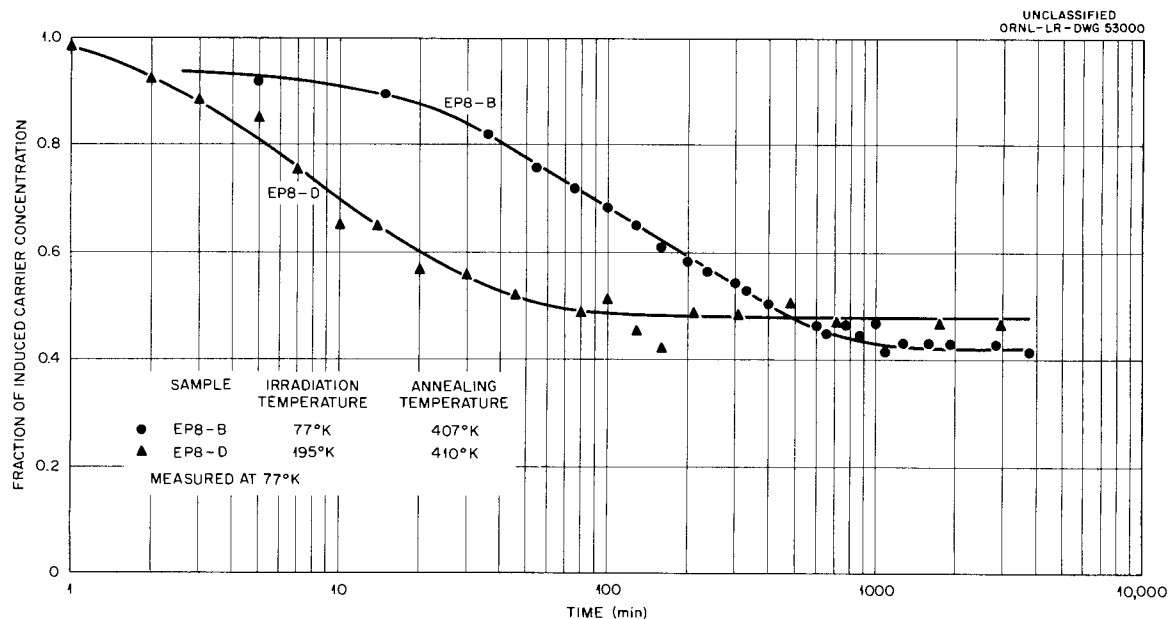


Fig. 10.7. Comparison of Annealing Behavior of Samples Irradiated at 77 and 195°K. Samples EP8-B and EP8-D.

is shown in Fig. 10.8. The slope calculation of the temperature difference completely eliminates all problems associated with the calibration of the thermopile. The only assumptions made are that the dE/dT for the copper-constantan thermocouples are the same as the NBS published values and that these values do not change during the 2 or 3 hr required for the measurements. The thermocouple wire has been calibrated in previous work, and it seems reasonable to expect similar results.

Several things are to be noted about Fig. 10.8. Even on the expanded scale, the precision is quite satisfactory. If the precision of the thermoelectric power measurement were expressed as an uncertainty in the differential temperature, it is expected that the values would be good to $\pm 1 \times 10^{-3}$ °C. These data, together with other experiments, suggest that any departure from a linear relation of the thermal emf vs ΔT is a contact phenomenon. The contact effect is troublesome and may have been regarded as instrumentation difficulties by others in the field.

The voltage and temperature measurements are made on a Rubicon six-dial Thermofree potentiometer. The residual thermal voltages of the

measuring system have been followed for over a year and are quite stable, varying slowly from -0.03 to -0.05 μV .

One feature of the control system is an electronic correction of the set point of the heat-sink controller such that, regardless of the ΔT value on the sample, the average temperature is held constant. This is very important when measurements are made in a region where the slope of the thermoelectric power curve is changing rapidly. The sample parameters are controlled to the extent that one can make measurements for increased statistical accuracy up to 8 hr without perturbations of the experimental conditions.

A result of our investigation is the use of a copper-germanium differential thermocouple for control purposes. It is very attractive at low temperatures, having a sensitivity gain of 50 times the thermoelectric power of the copper-constantan system. One use of the copper-germanium couple would be for controlling a zero temperature gradient between thermal shields in calorimetry experiments. By using existing commercial microvolt-level temperature controllers, one could approach 0°C ΔT to $\pm 0.0001^\circ\text{C}$ for a single differential thermocouple.

UNCLASSIFIED
ORNL-LR-DWG 53001

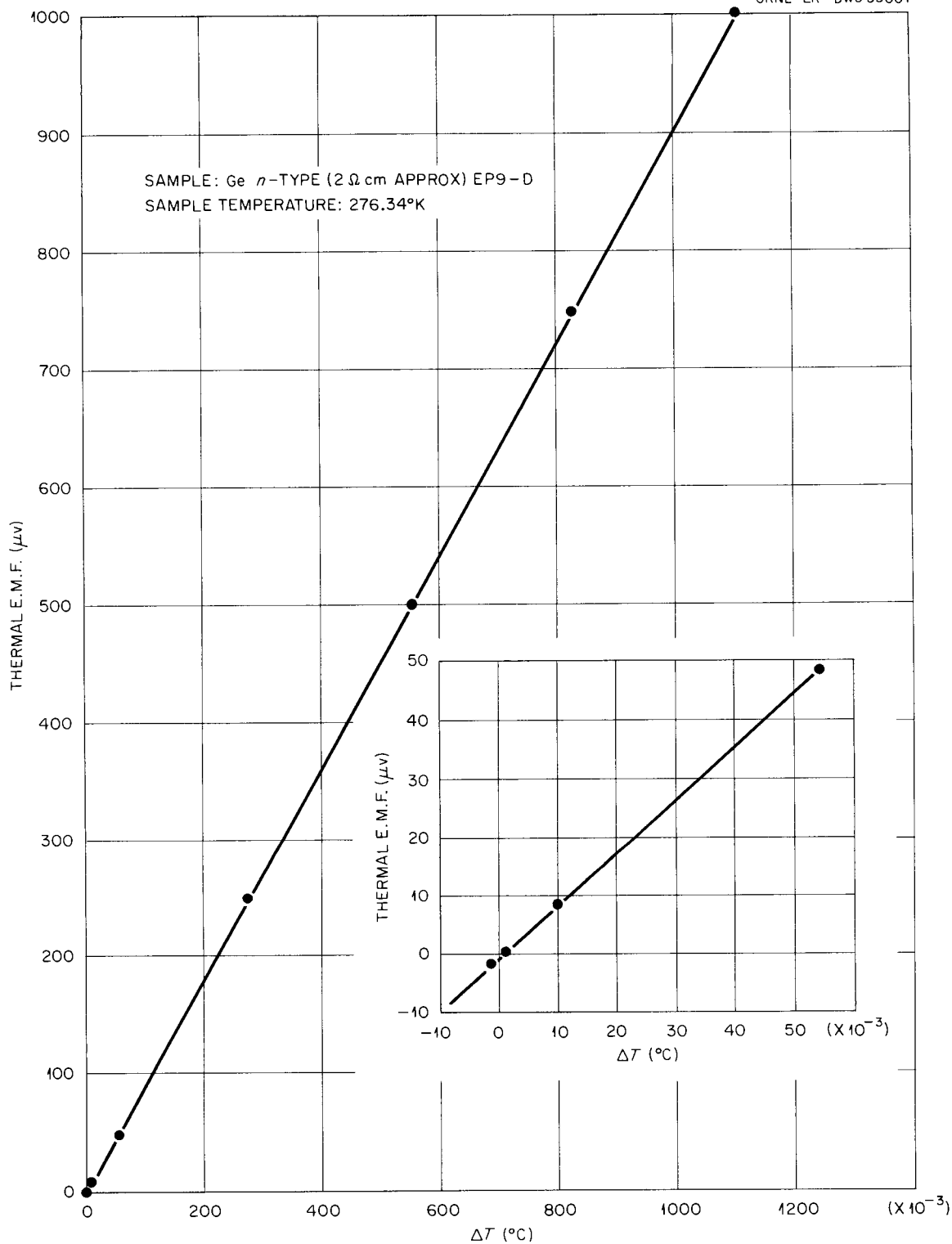


Fig. 10.8. Thermal EMF of Germanium as a Function of the Temperature Gradient at an Average Temperature of 276.34°K.

RADIATION EFFECTS IN *n*-TYPE TELLURIUM-DOPED GERMANIUM

J. W. Cleland R. F. Bass
J. H. Crawford, Jr.

The effect of radiation on the electrical properties of semiconductors has been extensively investigated in an attempt to better understand the nature of radiation-produced defects. The type and nature of the radiation-induced defect is known to depend critically on the type and nature of the incident bombarding particle. The change in electronic properties as a result of irradiation, however, also depends critically on the initial type and carrier concentration of the particular semiconductor, as influenced by the initial defect concentration of dislocations and vacancies and the amount and type of chemical impurity already present. The subsequent annealing of radiation-induced defects is also dependent on the initial concentration of other defects and is structure sensitive²¹ to the original chemical impurity in the material.

Transmutation doping effects in semiconductors exposed to thermal neutrons²² have recently been employed in attempts to sweep the Fermi level across the forbidden energy gap of initially *n*-type germanium. It was believed that inflections in the time rate of change of the charge carrier concentration during radioactive decay would permit a determination of the ionization energies (location in the energy gap) of deep-level defects introduced by dislocations, radiation, or by certain chemical impurities purposely introduced in the material. This method has not proved to be successful in most of the experiments to date; however, certain valuable information has been obtained on *n*-type tellurium-doped germanium material.

Tellurium is known to exist as a double donor²³ in *n*-type germanium, with energy levels at 0.11 and 0.30 eV below the conduction band. These

levels are apparently present in about equal concentration. Tellurium is difficult to introduce, because of a high vapor pressure in the melt; however, both melt-doped and diffused material have been made, and the following values have been determined:²³ maximum solubility, 2×10^{15} cm⁻³; distribution coefficient, 10^{-6} ; diffusivity (920°C), 10^{-11} .

High-purity *n*-type tellurium-doped single-crystal germanium was obtained²⁴ from the National Carbon Company. Curves I of Fig. 10.9, which is a plot of log Hall coefficient and resistivity vs reciprocal temperature, are typical for the original material. The initial carrier concentration at

²⁴We are indebted to R. D. Westbrook of the National Carbon Company for the careful preparation of this material.

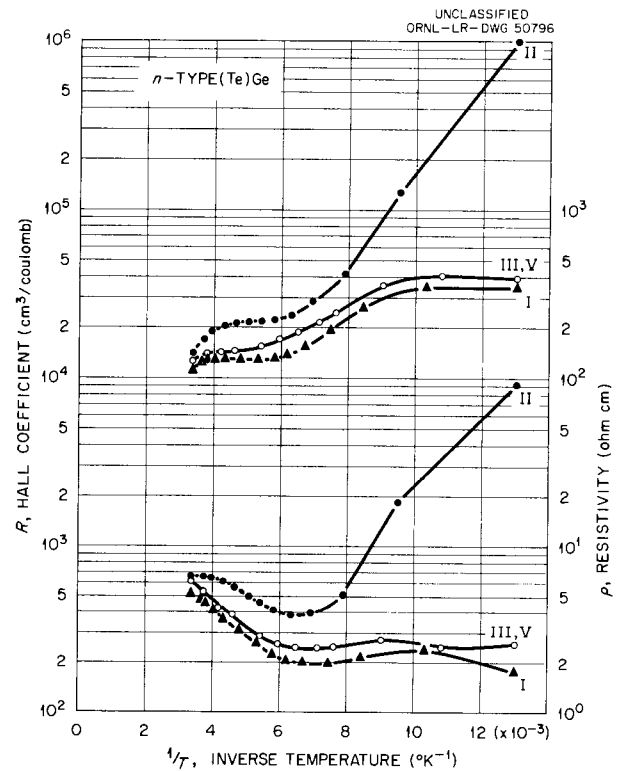


Fig. 10.9. The Effect of Co⁶⁰ Photon Irradiation and Vacuum Heat Treatment at 450°C on the Hall Coefficient *R* and Resistivity Curves of *n*-Type Tellurium-Doped Germanium. Log *R* and log ρ vs $1/T$ curves after exposure to 4×10^{17} photons/cm² (curves II) and after exposure to 8×10^{17} photons/cm² and 16 hr at 450°C (curves V) are compared with those obtained before exposure (curves I).

²¹W. L. Brown, W. M. Augustyniak, and T. R. Waite, *J. Appl. Phys.* 30, 1258 (1959).

²²H. C. Schweinler, *J. Appl. Phys.* 30, 1125-26 (1959); J. W. Cleland and J. H. Crawford, Jr., *Solid State Ann. Prog. Rep. Aug. 31, 1959*, ORNL-2829, p. 125-27; see also "Transmutation Doping and Recoil Effects in Semiconductors Exposed to Thermal Neutrons," this report.

²³W. W. Tyler, *Advances in Semiconductor Science*, Pergamon Press, New York, 1959.

77°K was 2.10×10^{14} electrons/cm³, and the difference in carrier concentration between 250 and 77°K would indicate the presence of 3.65×10^{14} donor atoms/cm³. The actual tellurium concentration evidently varied from 2.2 to 3.65×10^{14} atoms/cm³ in the various samples that were investigated.

Vacuum anneal at 450°C for 16 to 20 hr increased the total donor concentration of several control specimens by 15 to 20% but did not alter the apparent tellurium concentration by more than 10%. Vacuum anneal at 500°C for 20 hr did not further alter the total donor concentration appreciably; however, ~20% of the initial tellurium concentration was removed by this higher-temperature anneal. These values are affected by the presence of a gradient of tellurium concentration in the original ingot and the necessity of removing soldered leads and etching the sample between anneals.

The sample of Fig. 10.9 was irradiated with 4×10^{17} photons from a Co⁶⁰ gamma source. This irradiation removed 2×10^{14} conduction electrons/cm³ as determined at both 77 and 250°K (curves II). Note that no evidence of multiple trapping (two defect states) of the type observed in normal germanium irradiated with photons,²⁵ fast neutrons,²⁶ or thermal neutrons²² is evident. This behavior must reflect a sensitive balance between the 0.11-eV donor state of tellurium, the 0.20-eV acceptor state of radiation-induced defects, and those deep-lying states that have been predicted as a result of multiple ionization of radiation-induced defects. Critical examination of removal rates of conduction electrons and 100°C annealing experiments on tellurium-doped specimens might permit an evaluation of the validity of the energy-level position, acceptor or donor action, and possible coupling of such states; however, this has not yet been done.

The effect of vacuum anneal at 450°C (curves III), reirradiation with 4×10^{17} photons (not shown), and a second anneal (curves V), indicates that the total carrier concentration and the tellurium donor atom concentration were not grossly

altered by the formation of radiation-induced interstitials and vacancies, or by the subsequent removal of the radiation-induced disorder by vacuum anneal. The removal rate of conduction electrons in normal germanium by Co⁶⁰ photons is about 1.4×10^{-3} , where each interstitial-vacancy pair is assumed to remove two conduction electrons. These two irradiations would produce about 5.6×10^{14} Frenkel pairs/cm³; however, the carrier concentration was only reduced by about 6×10^{13} donors/cm³ by the anneal, and a large portion of this change may have been due to removal of the tellurium by the anneal itself.

Curves I of Fig. 10.10, which is a graph of the log Hall coefficient and resistivity vs reciprocal temperature, are also typical of the original material and represent the initial conditions, after 16 hr at 450°C, for two specimens that each contained about 3.7×10^{14} tellurium donor atoms/cm³.

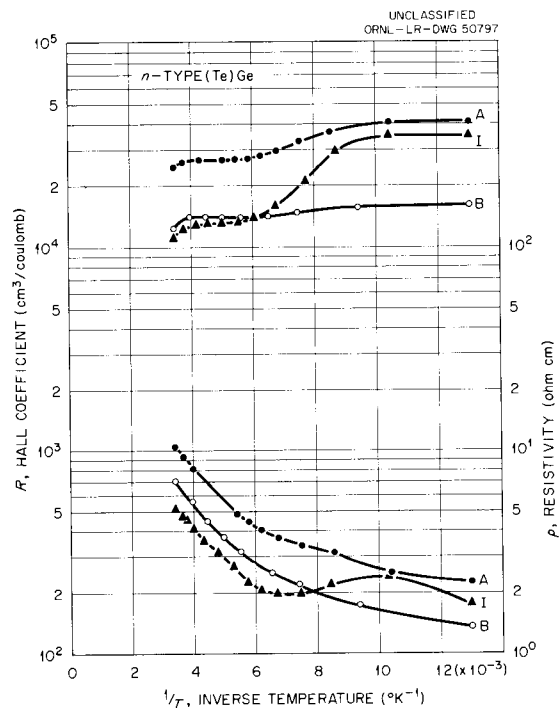


Fig. 10.10. The Effect of Fast- and Thermal-Neutron Irradiation and Vacuum Heat Treatment at 450°C on the Hall Coefficient R and Resistivity of Two Samples of n -Type Tellurium-Doped Germanium. Log R and log ρ vs $1/T$ curves after exposure to 4.7×10^{15} nvt (curves A) and 2.8×10^{16} nvt (curves B) and after 16 hr at 450°C are compared with a typical sample before exposure (curves I).

²⁵J. W. Cleland, J. H. Crawford, Jr., and D. K. Holmes, *Phys. Rev.* **102**, 722 (1956).

²⁶J. H. Crawford, Jr., and J. W. Cleland, *J. Appl. Phys.* **30**, 1204-13 (1959).

Both samples were irradiated in the pneumatic rabbit facility of the Oak Ridge National Laboratory Low Intensity Test Reactor, were vacuum annealed for 16 hr at 450°C to remove fast-neutron-induced defects, and were remeasured approximately 40 hr after the irradiation.

Sample A received $\sim 4.7 \times 10^{15} nvt_f$ (fast neutrons) and $\sim 4.7 \times 10^{15} nvt_{th}$, which would produce $\sim 6 \times 10^{13}$ arsenic atoms/cm³ by transmutation at the time of measurement. Approximately 2.7×10^{14} tellurium donor atoms/cm³ were removed, or compensated in some manner. Sample B received $\sim 2.8 \times 10^{16} nvt_f$ (fast neutrons) and $\sim 2.8 \times 10^{16} nvt_{th}$, which would produce $\sim 3.6 \times 10^{14}$ arsenic atoms/cm³ by transmutation at the time of measurement. Approximately 3.0×10^{14} tellurium donor atoms/cm³ were removed, or compensated in some manner. The total difference in carrier concentration between samples A and B is $\sim 3 \times 10^{14}$ electrons/cm³, which can be almost entirely attributed to the expected difference in donor-type arsenic concentration.

It is evident from these data that the removal or compensation of donor-type tellurium is not due to the introduction of arsenic; and it is also apparent that the removal or compensation process is not a single or linear function of the number of isolated interstitial-vacancy pairs created by photon irradiation, or the number of disordered regions created by fast-neutron-induced defects.

EXPLORATORY MEASUREMENTS TO
DETERMINE THE ANNEALING BEHAVIOR
OF RADIATION-INDUCED RECOMBINATION
CENTERS IN GERMANIUM

O. L. Curtis, Jr. J. H. Crawford, Jr.

Preliminary to making a detailed study of the annealing behavior of radiation-induced recombination centers in germanium, we have made a survey-type experiment in order to provide a general view of the behavior one might expect.²⁷ Three types of irradiating particles were used: 14-Mev monoenergetic neutrons, fission neutrons, and Co⁶⁰ gamma rays. In each case three specimens were used: 2-ohm-cm *p*-type, 2-ohm-cm *n*-type, and 15-ohm-cm *n*-type germanium.

²⁷O. L. Curtis, Jr., and J. H. Crawford, Jr., *Bull. Am. Phys. Soc.* 5, 196 (1960).

Figure 10.11 summarizes the results of these measurements. In this figure the fraction of damage remaining, as determined from the room-temperature lifetime values, is plotted as a function of the annealing temperature. Three temperatures were used: 104, 143, and 201°C. We have indicated the type and resistivity of the material by the symbols used for the points, and the type of irradiation by solid, dashed, and dotted lines.

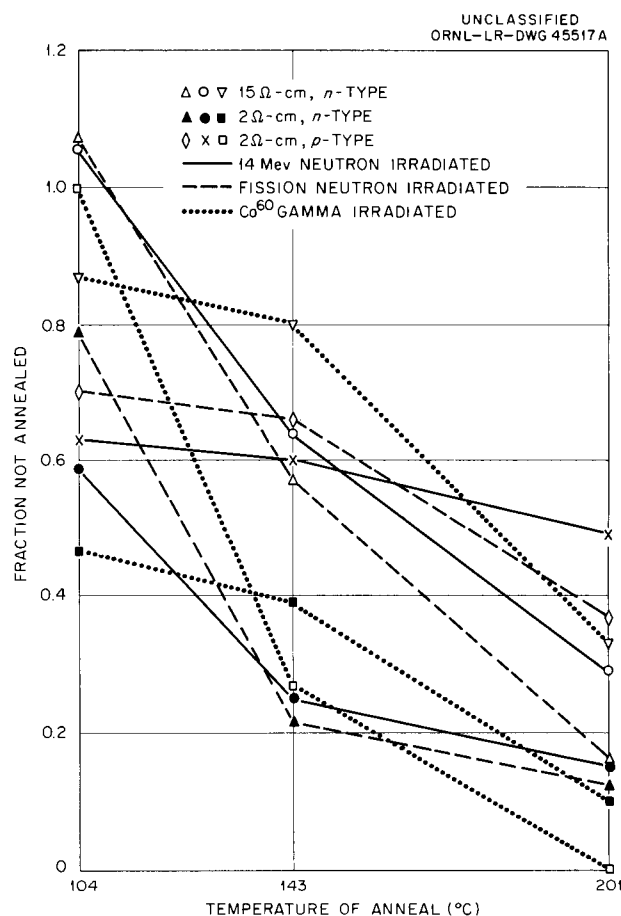


Fig. 10.11. The Fraction of Radiation-Induced Lifetime Changes Remaining After Successive 4-hr Anneals.

Several conclusions can be drawn immediately from this plot. The annealing behavior depends markedly both on the type of irradiation and the properties of the material. Two-ohm-centimeter *n*-type material anneals more readily than 15-ohm-cm *n*-type material regardless of the irradiation used. (The 15-ohm-cm value is nominal. Although the three specimens were from the same ingot, the values ranged from 11 to 15 ohm-cm.)

The most striking difference between types of irradiation is demonstrated by the *p*-type material. Here the annealing behavior for material irradiated by Co^{60} gamma rays is much different from the two specimens irradiated by neutrons throughout the annealing range.

One must be cautious with a plot such as this since the annealing may produce a change in the recombination process and thus render a number for the fraction of damage remaining not very meaningful. In fact, a change in process was indicated in some cases. To determine any such change, lifetime measurements were made as a function of temperature at each of the points indicated on the graph. There was no appreciable change in process indicated for *p*-type material or for 14-Mev-neutron-irradiated *n*-type material. However, for the fast-neutron- and gamma-irradiated specimens, there was a change.

Figure 10.12 shows the data for the 2-ohm-cm *n*-type specimen irradiated with fast neutrons. The 0.35-eV slope indicated immediately following

irradiation was reported earlier for this sample.²⁸ However, it should be noted that for all those samples previously measured having resistivities in the range above 5 ohm-cm a slope of ~ 0.24 eV is observed.²⁸ This steeper slope for this lower-resistivity specimen shows up very conclusively after the 104° anneal since it is now possible to extend the measurements upward in temperature without the danger of annealing at the temperature of measurement. This slope corresponds to that observed in *n*-type germanium irradiated with 14-Mev neutrons.²⁹ Evidently, for this latter specimen, there was no change in process due to the annealing.

In contrast, the 2-ohm-cm *n*-type sample irradiated with Co^{60} gamma rays displayed a very definite change in the recombination process. Figure 10.13 demonstrates a very striking early annealing accompanied by a definite change in

²⁸O. L. Curtis, Jr., *J. Appl. Phys.* 30, 1174 (1960).

²⁹O. L. Curtis, Jr., and J. W. Cleland, *J. Appl. Phys.* 31, 423 (1960).

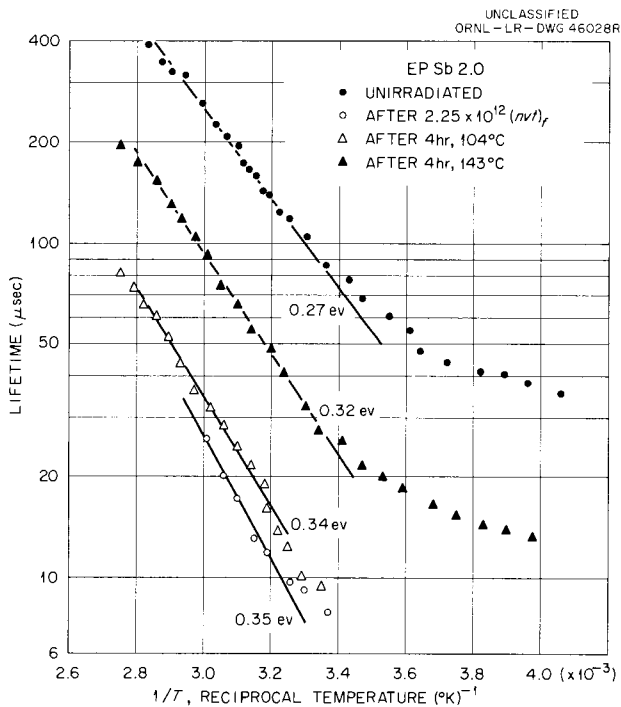


Fig. 10.12. Minority-Carrier Lifetime vs Reciprocal Temperature for a 2.0-ohm-cm *n*-Type Sample, Showing the Effect of Fast-Neutron Irradiation and Subsequent Annealing.

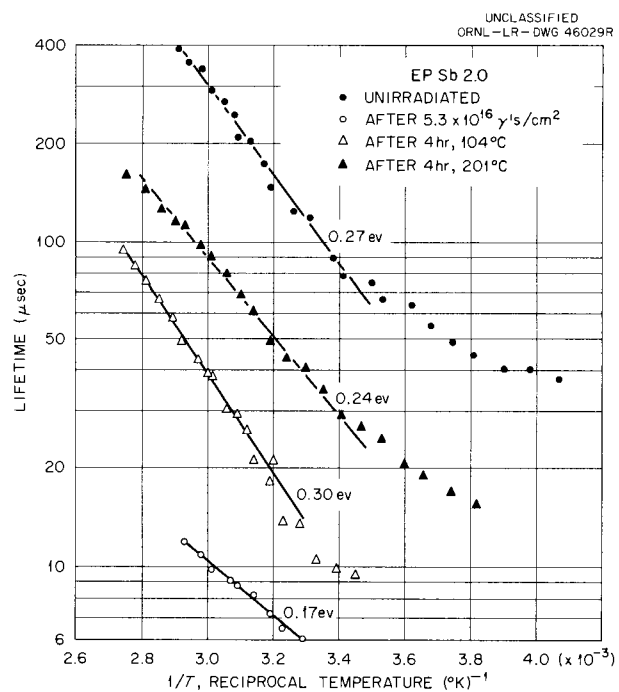


Fig. 10.13. Minority-Carrier Lifetime vs Reciprocal Temperature for a 2.0-ohm-cm *n*-Type Sample, Showing the Effect of Co^{60} Gamma Irradiation and Subsequent Annealing.

slope. Similar behavior is indicated in Fig. 10.14, which is a plot for a 15-ohm-cm specimen irradiated with fission neutrons.

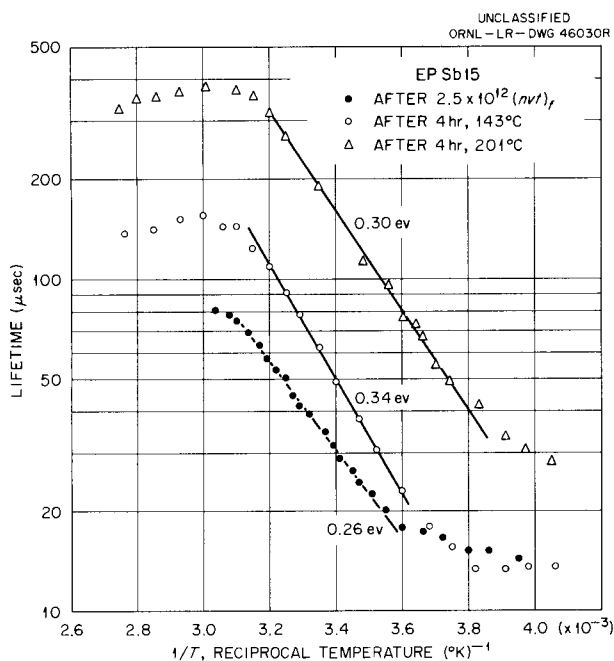


Fig. 10.14. Minority-Carrier Lifetime vs Reciprocal Temperature for a 15-ohm-cm *n*-Type Sample, Showing the Effect of Fast-Neutron Irradiation and Subsequent Annealing.

The fact that the presence of a deeper-lying level (indicated by the steeper slope) can be enhanced by increasing the impurity concentration of the specimen, or the energy of the irradiating particle, or by annealing leads to the possibility that these deep-lying levels are associated with antimony impurities (antimony being the doping agent), presumably combined with a vacancy or interstitial. Annealing or energetic bombardment would give the interstitial the opportunity to come into the region of the impurity atom. One complicating factor is that, while these deep-lying levels occur more readily in low-resistivity material, the over-all annealing also proceeds more rapidly, in spite of the fact that these levels are very effective for recombination (as indicated by the results of irradiation with 14-Mev neutrons). This work is being extended to a detailed annealing study, with special emphasis being placed on Co^{60} gamma-irradiated *n*-type material, both antimony- and arsenic-doped.

SOME FAST-NEUTRON EFFECTS IN GERMANIUM

M. C. Wittels

Germanium, as a zinc blende lattice, may be considered as two interpenetrating face-centered cubic lattices, one passing into the other by the translation

$$\frac{a_1 + a_2 + a_3}{4}$$

The atoms of the two face-centered lattices are not equivalent, however, and the eight atoms of the two face-centered units comprise the atoms in the germanium unit cell. Lattice planes whose structure factor is zero for each of the two face-centered lattices (those having mixed indices) also have a zero structure factor in germanium. Since the four atoms of each face-centered lattice scatter waves in phase, the unit cell behaves as though four atoms were placed at 0,0,0 and four atoms at $\frac{1}{4}, \frac{1}{4}, \frac{1}{4}$. For this reason, lattice planes whose $b + k + l$ is an odd multiple of two are forbidden in the germanium lattice by

$$|F|^2 = 16(f_a - f_b)^2 = 0,$$

where f_a and f_b are the atomic scattering factors for the atoms at 0,0,0 and $\frac{1}{4}, \frac{1}{4}, \frac{1}{4}$. In the perfect crystal $f_a = f_b$ and no forbidden reflections should appear. If this equality is upset by introducing impurities with different atomic scattering factors into the lattice, or by introducing other kinds of defects, the 1:1 ratio of atomic sites might become impaired and therefore result in the appearance of the so-called forbidden reflections. Some of these reflections have been observed in doped crystals, but they have also been observed in pure crystals irradiated with less than 5×10^{19} *nvt_f*. Investigations are continuing in the study of forbidden reflections in germanium, both pure and doped, together with the effects of fast-neutron irradiation.

Together with these studies, an effort is being made to determine the nature of fast-neutron-induced defects by x-ray lattice parameter and hydrostatic weighing measurements. A crystal of *p*-type germanium having a resistivity of 40 ohm-cm exposed at 85°C in the LITR to a total dosage of 3.98×10^{20} *nvt_f* showed a measured volume expansion of 0.77%. The volume expansion as calculated from the x-ray data was

only 0.46%. Since the effects produced are isotropic in a cubic crystal, it is apparent that the vacancies are the predominant defects stable at room temperature, because the greater actual volume expansions are associated with the creation of atomic sites. The spread between the two measurements is so very great, however, as to strongly suggest that forces about a vacancy site in germanium actually pull the atoms surrounding the vacancy outward from that site. This is not inconsistent with the rearrangement of the covalent bonds. Somewhat surprisingly, the hardness changes on (111) faces of this crystal increased from 708 to 870 KHN for a 50-g load. This is not to be expected in a covalent crystal with ruptured bonds. Further studies on the production of fast-neutron-induced defects in germanium are continuing.

GAMMA IRRADIATION OF SILICON

L. C. Templeton E. Sonder

Irradiation of *n*-type silicon has been continued on samples containing large amounts of oxygen impurity as a direct result of the normal growth process, as well as on silicon grown by special techniques (floating-zone melting) to keep the oxygen content below 10^{16} cm⁻³. Differences were found in the irradiation-induced electrical changes in the two types of material.

The results on silicon containing $\approx 5 \times 10^{17}$ oxygen atoms/cm³ have been published,³⁰ and the abstract follows:

The resistivity and Hall coefficient of *n*-type silicon containing oxygen have been measured as a function of temperature before and after a number of successive irradiations in a Co⁶⁰ gamma-ray source. A net acceptor level 0.17 ev below the conduction band was observed to result from the irradiation. Its rate of introduction was 7×10^{-4} traps/cm³ per photon/cm² in 50-ohm-cm material and was about twice that in more heavily doped material (~ 2 ohm-cm). Acceptor levels, lying deep within the forbidden gap, were also observed. Their total introduction rate was smaller than that of the 0.17-ev level by a factor of 50. A lowering of the mobility below $\sim 100^\circ\text{K}$ was also a result of the irradiations. In heavily irradiated samples this lowering of the mobility was much greater than could be explained on the basis of point-charge scattering.

In material containing a minimum of oxygen a level located about 0.5 ev below the conduction band is introduced. It is probably the same level as the "deep" level observed in standard silicon. However, it is introduced more rapidly in "oxygen-free"³¹ silicon of comparable resistivity.

An attempt was made to decrease the oxygen content of both a standard silicon sample and an "oxygen-free" sample by annealing at 975°C for one week and then cooling slowly to room temperature during another week. (It is known³² that heating of oxygen-containing silicon will cause the former to coagulate.) An increase in the introduction rate of the 0.5-ev level was observed in the standard silicon (sample 1019-3). However, there was no change in the "oxygen-free" material (sample RO45-3).

The data are summarized in Table 10.3, where the first four samples shown are all between 2 and 2.5 ohm-cm. Samples RO45-1 and -2 are "oxygen free"; 1019-2 is standard silicon; RO45-3 and 1019-3 have been annealed as discussed above.

Sample RO16, which is "oxygen free" but has a higher resistivity, shows an appreciably smaller introduction rate for the 0.5-ev level. If this sample really contains only small amounts ($< 10^{16}$) of oxygen,³³ then this would indicate that the introduction of the deep level is dependent as strongly on the amount of doping agent as it is upon the oxygen. Such behavior is further evidenced by the two samples 1123-4 and -30, which contain roughly the same amount of oxygen as does sample 1019-2, but which have a much higher resistivity. The introduction rate of the deep level in the case of these two samples is

³⁰E. Sonder and L. C. Templeton, *J. Appl. Phys.* 31, 1279 (1960).

³¹We shall refer to silicon grown by the floating-zone technique as "oxygen free." By the most sensitive technique for determining oxygen content that is known, infrared absorption measurements, oxygen in quantities greater than 10^{16} can be detected [W. Kaiser *et al.*, *Phys. Rev.* 101, 1264 (1956)]. It is usually assumed that floating-zone silicon contains less oxygen than that figure, but the exact amount seems to be indeterminate.

³²H. J. Hrostowski and R. H. Kaiser, *Phys. Rev. Letters* 1, 199 (1958).

³³We have not checked the infrared absorption of these samples. It is assumed that the producer (E. I. du Pont de Nemours and Co.), by using a floating-zone growing method, has been able to keep oxygen contamination below 10^{16} .

Table 10.3. Introduction Rate of Acceptor Levels in n-Type Silicon Irradiated with Co⁶⁰ Gamma Rays

Sample	Resistivity at Room Temperature (ohm-cm)	Net Donor Density (cm ⁻³)	Oxygen Content (cm ⁻³)	Introduction Rate (traps/cm ³ per photon/cm ²)		Ratio of Introduction Rate for the 0.17- and 0.5-ev Level
				Deep Level	0.17-ev Level	
RO45-1 } RO45-2 }	2.5	1.5 × 10 ¹⁵	Oxygen free	1.06 × 10 ⁻³	8 × 10 ⁻⁴	0.8
RO45-3	2.4	1.5 × 10 ¹⁵	Oxygen free and heated to 975°C	1.05 × 10 ⁻³	8 × 10 ⁻⁴	0.8
1019-3	2.0	2.0 × 10 ¹⁵	Heated to 975°C	4.3 × 10 ⁻⁴	1.2 × 10 ⁻³	2.8
1019-2	2.1	2.0 × 10 ¹⁵	~5 × 10 ¹⁷	1.3 × 10 ⁻⁴	1.4 × 10 ⁻³	11
RO16	9.4	4.5 × 10 ¹⁴	Oxygen free	7.0 × 10 ⁻⁵	9 × 10 ⁻⁴	13
1123-4	30	1.2 × 10 ¹⁴	~5 × 10 ¹⁷	1.7 × 10 ⁻⁵	7 × 10 ⁻⁴	43
1123-30	56	7 × 10 ¹³	~5 × 10 ¹⁷	1.4 × 10 ⁻⁵	7 × 10 ⁻⁴	49

almost a factor of 10 smaller than in the case of sample 1019-2.

It has been suggested that introduction rates of these levels may be affected by annealing during irradiation. The samples reach a temperature of 38°C while in the source. In order to check for the presence of annealing, a number of the samples were raised to 50 and 80°C for approximately 1/2 hr or held at room temperature for as much as 36 days. Except for changes of a few per cent in the Hall coefficient after raising the samples to 80°C, no annealing of the deep level was observed. However, in the case of one of the samples, there was an indication of room-temperature annealing of the 0.17-ev level. In this case after about 1 × 10¹⁴ acceptor levels had been introduced by the irradiation, a 40% change in the Hall coefficient (corresponding to a disappearance of 10¹² acceptor levels) was detected after the sample had been at room temperature for 13 months.

ELECTRICAL CONDUCTIVITY AND THERMO-ELECTRIC VOLTAGE OF CUPROUS OXIDE

C. C. Robinson

Work has been undertaken to study the radiation effects on the electrical conductivity and thermo-electric voltage of cuprous oxide. Such effort not only provides a natural extension of present

work on copper and extends work on semiconductors to another material, but may well provide (due to the chemical similarity) information applicable to other oxide semiconductors of multiple valence such as UO₂.

Initial effort has been directed toward the development of satisfactory radiation-experiment techniques and resolution of some of the differences reported in much of the previous work on this material.

Radiation-experiment techniques necessitate the development of a reliable contact to the sample since it is experimentally difficult to bombard the sample along with numerous lead wires. Two types of contacts were investigated: one, a silver-plated contact on the sample, the other, a gold-leaf pressure contact. Silver was selected because of its ease of application, although it does have a considerable vapor pressure above 650°C. This vapor pressure is considered unimportant here since temperature limits were set no higher than 650°C.

The samples used were prepared by oxidation of Chilean copper at 1000°C for 16 hr, annealing at a lower temperature for 2 hr, then water quenching to 25°C.³⁴

Silver plating was accomplished by use of a commercial plating bath. It was facilitated by

³⁴S. J. Angello, *Phys. Rev.* 62, 371 (1942).

wrapping a turn of silver wire around the upper limit of the area to be immersed in the solution. This provided the low-resistance path necessary. As the plating "grew" down the sample, it was slowly pulled from the bath to limit the thickness of the plating.

In the case of the gold pressure contacts, no preparation was made other than removing the sprayed solder contacts already on the sample and lightly filing the area underneath.

Thermocouples were held onto the sample with wrappings of appropriate foil - silver or gold - and the contact areas were further wrapped in quartz tape to inhibit temperature differences between the sample and the thermocouples. Silver- or gold-wire pressure electrical contacts were used from the foil to terminals outside the high-temperature region.

The sample was next put into a quartz tube and heated by resistive heaters outside the tube. A source of trouble has been noted in this arrangement in that the wrappings of quartz tape nearly filled the diameter of the tube. Because of this it was difficult to tell when, if ever, the pressure at the sample was the same as that measured near the end of the tube. A new apparatus has been constructed which will eliminate this difficulty.

The basic measuring circuitry is shown in Fig. 10.15. Plots were made of thermoelectric voltage

against ΔT at different temperatures and of electrical conductivity against an averaged temperature from thermocouples on each end of the sample. The block titled "Isolator" serves to electrically isolate one end of the sample from the other.

Results of repeated temperature-vs-conductivity runs indicate the following: Above approximately 300°C there is little change in the sample regardless of the treatment. A slight increase in resistance has been noticed above about 600°C but is considered to be significant only to the extent that it warrants further investigation.

Below approximately 300°C the resistance of the sample is a function of (1) time at room temperature, (2) time at elevated temperatures, and (3) pressure.

It seems apparent that there is no difference between the plated silver and the gold pressure contacts. Of course, whether either is a valid contact is still a matter of conjecture.

Although sample characteristics may change as a function of the above parameters of time and pressure, a standard treatment is indicated, permitting studies of radiation effects only. Essentially, this consists in maintaining the sample in vacuum at some elevated temperature, in the region of 500 to 600°C, for about 24 hr. The result of this "standard treatment" is a sample in which the resistance measured as a function of temperature during heating does not differ from the same measurements taken while the sample is being cooled. The same measurement taken during heating and cooling either in air or prior to the 24-hr period in vacuum at 500°C consistently shows differences in resistance at temperatures less than approximately 300°C. Differences in resistance have also been observed where the sample remained overnight at room temperature between one day's cooling curve and the next day's heating.

Figure 10.16 is a composite curve of a number of runs of the resistance of both samples as a function of $10^3/T^{\circ}K$, illustrating the above differences. The resistance vs $10^3/T^{\circ}K$ curve for any run of a sample normally followed the general contour of the edges of the composite curve. There was, however, one exception. The dotted-line extension of the curve, noted as A, was obtained only from the first run of the gold pressure contact sample. Unfortunately, the first time the other sample was heated, no data were taken.

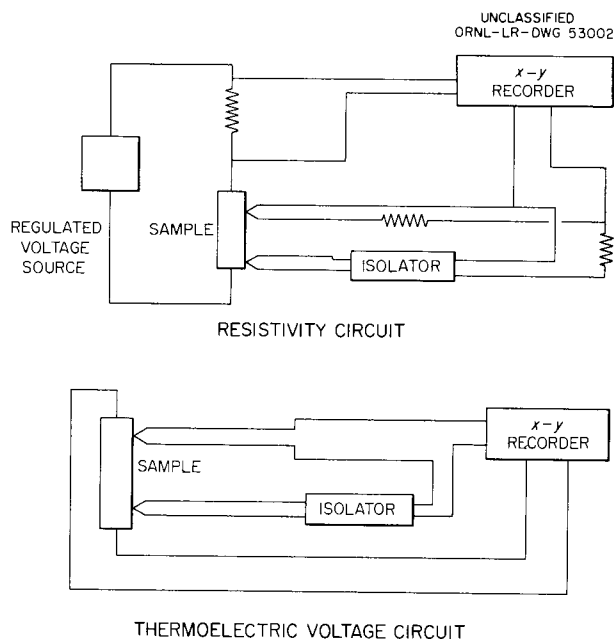


Fig. 10.15. Measuring Circuitry.

Therefore, whether this type of curve is found in all "long-aged" samples or is peculiar to this sample alone is not yet known. Differences in resistance above 300°C are attributed, primarily, to the difference in resistance of the two samples.

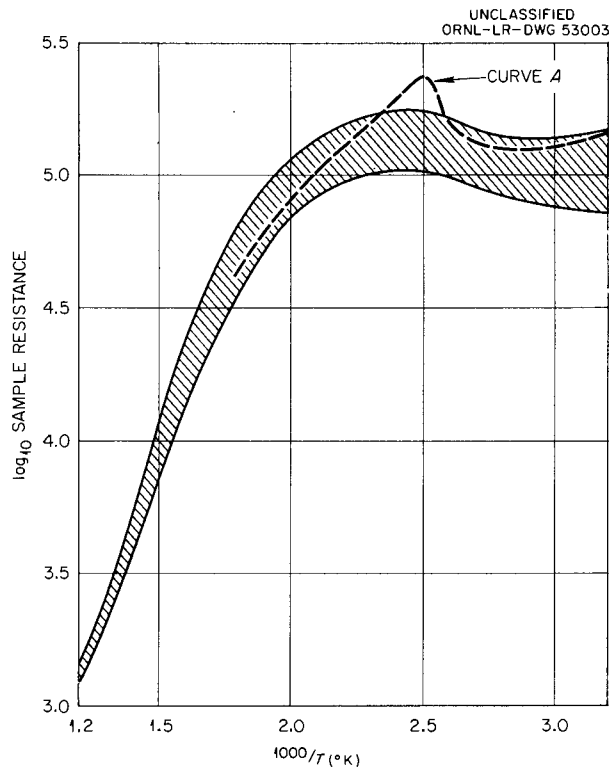


Fig. 10.16. Composite of Several Runs of Two Cuprous Oxide Samples.

Since major effort was placed on resistivity studies, only Fig. 10.17 is shown as an example of the thermoelectric voltage for the silver-plated sample. The upper edge of the shaded area represents room-temperature values, while the lower edge shows values at 500°C. The thermoelectric voltage as a function of temperature appears linear.

In addition to radiation studies, future work will be directed toward studies at lower temperatures - down to about -20°C - and refinement of vacuum studies. Contact problems will continue to be studied.

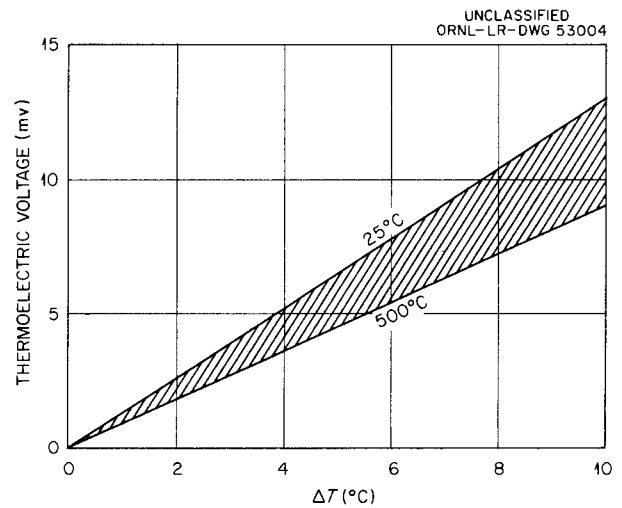


Fig. 10.17. Thermoelectric Voltage of Cuprous Oxide.

11. ALKALI HALIDES

ON THE MECHANISM FOR THE PRODUCTION OF F CENTERS IN NaCl BY IRRADIATION WITH GAMMA RAYS¹

F. W. Young J. H. Crawford, Jr.

Seitz² has suggested that excitons created during irradiation of ionic crystals recombine at crystalline imperfections such as dislocation jogs. Sufficient energy can thereby be deposited at the jogs to permit evaporation of vacancies from the dislocations, these evaporated vacancies becoming ionized subsequently to form F centers. Experiments by Nowick³ have indicated that the rate of production of F centers in NaCl is dependent on dislocation densities in the crystal, thereby apparently substantiating the suggestion of Seitz. However, if vacancies are evaporated from a dislocation, climb of the dislocation results. It can be shown that by gamma irradiation sufficient vacancies can be produced in NaCl which, if the Seitz mechanism is responsible, would cause the dislocations to climb distances which are observable with the optical microscope. By locating the positions of the dislocations in NaCl as etch pits before and after gamma-ray irradiation, and by determining the concentration of F centers introduced by irradiation, it has been shown that if any F centers were produced by evaporation of vacancies from the dislocations they were not a significant fraction of the total number.

DEFECT INTERACTIONS IN IRRADIATED CALCIUM-DOPED POTASSIUM CHLORIDE

J. H. Crawford, Jr. C. M. Nelson

The marked enhancement of the rate of formation of F centers in alkali halides containing alkaline-earth impurity has long been recognized.^{4,5} Recent studies of Etzel and Allard⁶ have shown that

the energy required for this structure-sensitive process is quite small in calcium-doped NaCl colored at room temperature. Rabin⁷ has observed little expansion in NaCl crystals containing Ca^{++} during x irradiation until the structure-sensitive stage is exhausted. In view of the law of mass action,

$$N_V^+ N_V^- = A e^{-E_s/kT}, \quad (1)$$

where N_V^+ and N_V^- are respectively the concentrations of cation and anion vacancies and E_s is the energy of formation of a pair of isolated vacancies, and the fact that Ca^{++} introduction enhances the concentration of cation vacancies, one would expect N_V^- to be drastically suppressed. Consequently, on this basis a decrease rather than an increase in the rate of F -center production would be expected in crystals doped with divalent cations. One must therefore conclude that the presence of divalent alkaline-earth impurity and the accompanying cation vacancies assist in some manner the creation of anion vacancies by the ionizing radiation.

Perhaps the simplest reasonable mechanism employs the isolated cation vacancy.⁸ One may visualize the capture of a hole by a halide neighbor of the cation vacancy, the resulting halogen atom relaxing into the cation vacancy and the energy released in the hole capture process assisting the anion vacancy so created to escape from the site of the event. This center can be described as a Cl_2^- molecule ion oriented in the $\langle 100 \rangle$ direction. Further ionization of the center by loss of an electron would lead to a Cl_2 molecule localized at the site of the original cation vacancy.⁹ The mechanism satisfies the experimental requirements

⁷H. Rabin, to be published.

⁸Evidence exists that Ca^{++} -vacancy complexes are appreciably ionized at room temperature. C. Bean [quoted by F. Seitz, *Revs. Modern Phys.* 26, 7 (1954)] finds that the association energy in NaCl is less than 0.08 ev. Hence the viewpoint that isolated vacancies are involved is not unreasonable.

⁹The term Cl_2 molecule is simply descriptive. The actual center may be the linear Cl_3^- molecule ion of the type described by Hersh [*Phys. Rev.* 105, 1410 (1957)]. Alternatively, it may be a true Cl_2 molecule with one component in the cation site and the other in a nearest-neighbor anion site.

¹Abstract of a paper presented at the Southeastern Section Meeting of the American Physical Society held in Gatlinburg, Tenn., Apr. 7-9, 1960.

²F. Seitz, *Revs. Modern Phys.* 26, 1 (1954).

³A. S. Nowick, *Phys. Rev.* 111, 16 (1958).

⁴H. Hummel, quoted by F. Seitz, *Revs. Modern Phys.* 26, 7 (1954).

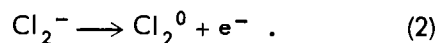
⁵H. W. Etzel, *Phys. Rev.* 87, 906 (1952).

⁶H. W. Etzel and J. G. Allard, *Phys. Rev. Letters* 2, 452 (1959).

of small energy absorption⁶ and small volume change⁷ per *F* center.

By ESR techniques, Hayes and Nichols¹⁰ have identified a center in Ca⁺⁺-doped KCl x-irradiated at 195°K which absorbs at 323 mμ with a Cl₂⁻ molecule ion oriented in the <100> direction. They attribute the center to hole capture at an associated Ca⁺⁺-vacancy complex. Very similar centers were also observed in Sr⁺⁺- and Ba⁺⁺-doped KCl, and their counterparts in KBr containing alkaline-earth impurity were observed as well. This type of center has the characteristics required by the mechanism described above, and, although Hayes and Nichols suggest that minor differences in peak position and thermal stability for the different alkaline-earth ions indicate an intimate connection with the impurity ion in question, we submit that, since these differences are near the limit of experimental precision, the peak near 325 mμ in KCl may equally well be ascribed to an isolated cation vacancy which has been converted to Cl₂⁻ and an anion vacancy by hole capture.¹¹

The 325-mμ band in KCl:Ca begins to disappear relatively rapidly on warming to the vicinity of -40°C. The purpose of this note is to describe the decomposition products of the center. As mentioned above, further decomposition of the Cl₂⁻ center may occur by the process



This reaction would not appreciably affect the *F* band, since it occurs above the temperature at which the *F'* band is stable (~200°K). Crystals of KCl containing 2.6 × 10⁻⁴ mole fraction of Ca⁺⁺ were x-irradiated (49 kv, 15 ma, 5 cm from target) at 195°K. The optical absorption in the near-ultraviolet region before (curve *a*) and after warming to ~-10°C (curve *b*) is shown in Fig. 11.1. The 325-mμ band markedly decreases in intensity and there is a marked growth in the V₂-V₃ region (2200 Å). The difference in absorption between curves *a* and *b* is plotted as curve *a* in Fig. 11.2. During this process the *F* band decreased only ~10% in intensity.

¹⁰W. Hayes and G. M. Nichols, *Phys. Rev.* 117, 993 (1960).

¹¹The Ba⁺⁺-doped crystals indeed seem to respond differently since x irradiation introduces two bands: one close to the position of the center considered here and one at longer wavelength. See ref 10.

If the process (2) is responsible for the variation in absorption, we must ascribe the 220-mμ band to Cl₂⁰ localized near the original vacant cation site. Since Cl₂⁻ is unstable above -40°C, the Cl₂⁰ center would be resistant to optical bleaching near room temperature, such as has been observed for the V₃ center. (This does not necessarily mean that the 220-mμ band is identical with the V₃ band.) However, at 195°K where the Cl₂⁻ center is stable, release of electrons in the crystal by *F*-band illumination should cause the reverse of process (2) to occur. The results of *F*-band illumination at ~195°K with light in the range 540 to 550 mμ are shown in Fig. 11.1, curve *c*, and the difference between curve *b* and curve *c* is plotted in Fig. 11.2 as curve *b*. The process is indeed reversed.

These results suggest that the mechanism proposed above for the enhancement of *F*-center production in alkali halides is indeed reasonable. The primary step is hole capture at a cation vacancy. The subsequent rearrangement creates an anion vacancy and a halogen atom in the cation

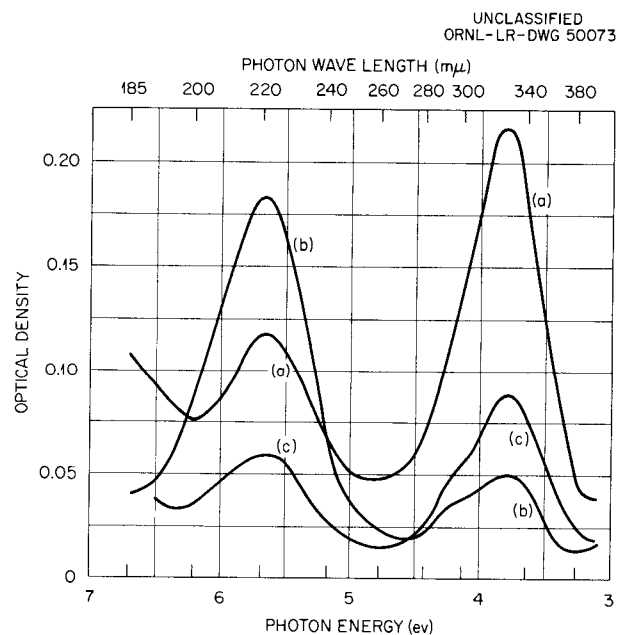


Fig. 11.1. Optical Density of X-Irradiated KCl:Ca Crystal After Various Treatments. Curve *a* after exposure to x rays at 195°K; curve *b* after warming to 263°K; curve *c* after 5 min illumination with *F* light at 195°K.

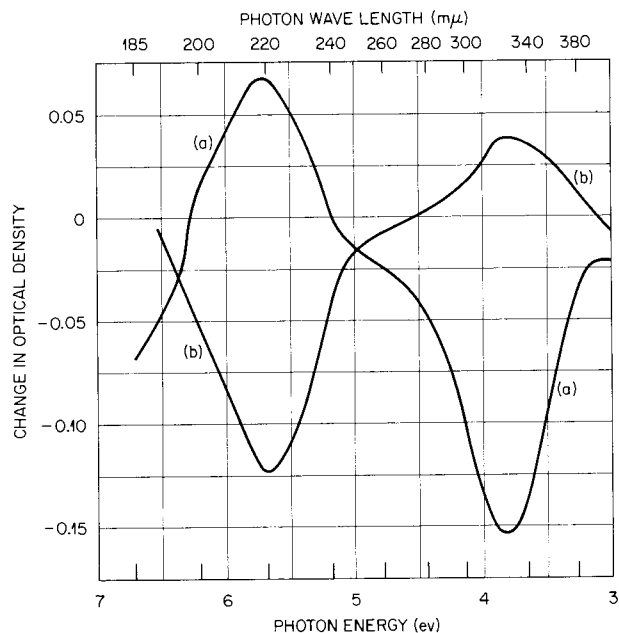
UNCLASSIFIED
ORNL-LR-DWG 50072

Fig. 11.2. Change in Optical Density After Various Treatments. Curve *a*, difference between curves *a* and *b* of Fig. 11.1; curve *b*, difference between curves *b* and *c* of Fig. 11.1.

site. Several questions remain, namely (1) What happens to the excess electrons released by the thermal ionization of the Cl_2^- center? and (2) Is the 220-m μ center to be identified with either the V_2 or the V_3 band? The first may find an explanation in the fact that an absorption below 190 m μ disappears with the thermal bleaching of the 325-m μ band.

We are indebted to H. C. Schweinler and J. H. Barrett for numerous helpful discussions.

MAGNETIC MEASUREMENTS OF ALKALI HALIDES

Since magnetic susceptibility measurements in some cases yield accurate numbers for the density of imperfections or impurities having unpaired electrons, such measurements, together with optical absorption determinations on alkali halide crystals, can elucidate some of the properties of color centers, namely, number of electrons (odd or even) attached to a center and oscillator strengths. Jensen¹² measured changes in the magnetic

¹²P. Jensen, *Ann. Physik* 34, 161 (1939).

susceptibility of potassium bromide at room temperature due to *F* centers. More recently, Rauch and Heer¹³ have measured the oscillator strength of *F* centers in a number of alkali halides. In addition, oscillator strengths have been determined using chemical means¹⁴ and electron spin resonance¹⁵ to estimate the number of *F* centers present.

As a preliminary to the investigation of more complex centers, it was felt worthwhile to measure the oscillator strength of the *F* center in KCl. With a balance of great sensitivity available here a somewhat larger range of *F* center concentrations could be investigated than had been investigated by the same experimental technique previously.¹³ Some preliminary measurements are described below.

The magnetic susceptibility of one sample each of pure, uncolored Isomet and Harshaw KCl was determined. A temperature-independent susceptibility of $-1.05 \times 10^{-6} \text{ cm}^{-3}$ was found for both samples between room temperature and 3°K. A number of additively colored samples were prepared by annealing KCl and potassium in a copper bomb for one to two weeks at 500–700°K. The colored samples exhibited a paramagnetic contribution to the susceptibility at low temperatures. The upper curve in Fig. 11.3 shows such a contribution to the susceptibility, plotted vs reciprocal temperature. The curve labeled "additively colored" in Fig. 11.4 is the absorption curve of a companion sample from the same crystal. It is evident from that curve that the predominant color center is the *F* center (at 2.2 eV) but that perhaps 8 to 10% as many *M* centers (absorbing at 1.5 eV) are also present.

The number of magnetic centers, obtained from the slope of the curve in Fig. 11.3 and the absorption data of Fig. 11.4, is given in Table 11.1 (data shown with an asterisk), together with results for other samples. Although only one susceptibility specimen was prepared and measured from each additively colored ingot, absorption measurements on a number of companion absorption plates were made. As can be seen from

¹³C. J. Rauch and C. V. Heer, *Phys. Rev.* 105, 914 (1957).

¹⁴F. G. Kleinschrod, *Ann. Physik* 27, 97 (1936).

¹⁵R. H. Silsbee, *Phys. Rev.* 103, 1675 (1956).

UNCLASSIFIED
ORNL-LR-DWG 53005

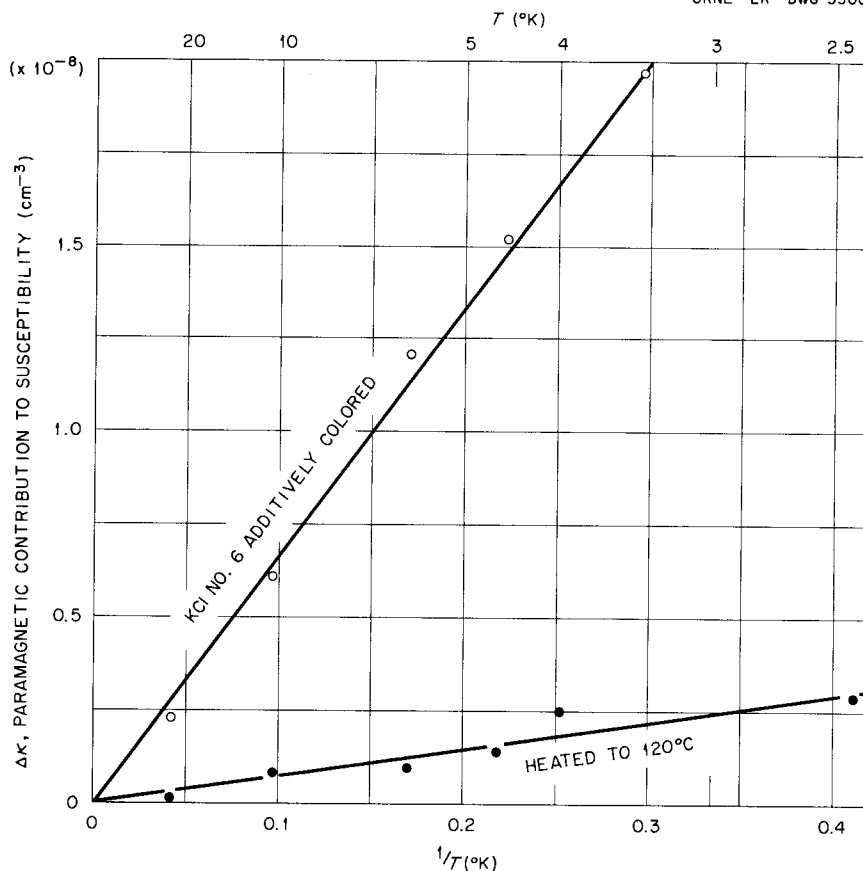


Fig. 11.3. The Paramagnetic Contribution to the Susceptibility of KCl at Low Temperature.

Table 11.1, there seemed to be considerable non-uniformity of coloration. This was especially true in the case of KCl No. 5, for which the coloration anneal had been somewhat shorter and at a lower temperature than in the case of other specimens.

In order to calculate oscillator strengths, the assumption was made that the average density of magnetic centers in the susceptibility sample was nearly the same as the average density in the optical plates. Also assumed, but not strictly true, is a Lorentzian line shape of the absorption curve, which makes possible the calculation of an oscillator strength using Smakula's equation.¹⁶ This permits comparison of our results with those of other investigators making that assumption.

¹⁶A. Smakula, *Z. Physik* 59, 603 (1930). A more convenient form of the equation is given by Kleinschrod, ref 14.

As seen from Table 11.1, the oscillator strengths in Harshaw and Isomet KCl fall between 0.9 and 0.7, with the smaller values seeming to occur in the more heavily colored samples. In view of the fairly large uncertainties inherent in obtaining oscillator strengths, our results are in surprisingly good agreement with Rauch and Heer's value¹³ of 0.66 in KCl containing $\sim 7 \times 10^{17}$ F centers, Silsbee's 0.85 in a 1×10^{17} sample,¹⁵ and Kleinschrod's 0.81 in a number of samples containing 10^{17} - 10^{18} F centers.¹⁴

Shown also in Table 11.1 are results on an electron-irradiated CsBr sample, prepared and irradiated by members of the Alkali Halide Group at the Naval Research Laboratory. The data indicate that coloration in this material introduces magnetic centers as it does in KCl.

One of the KCl samples (KCl No. 6) was annealed at 120°C in order to remove the F band

UNCLASSIFIED
ORNL-LR-DWG 53006

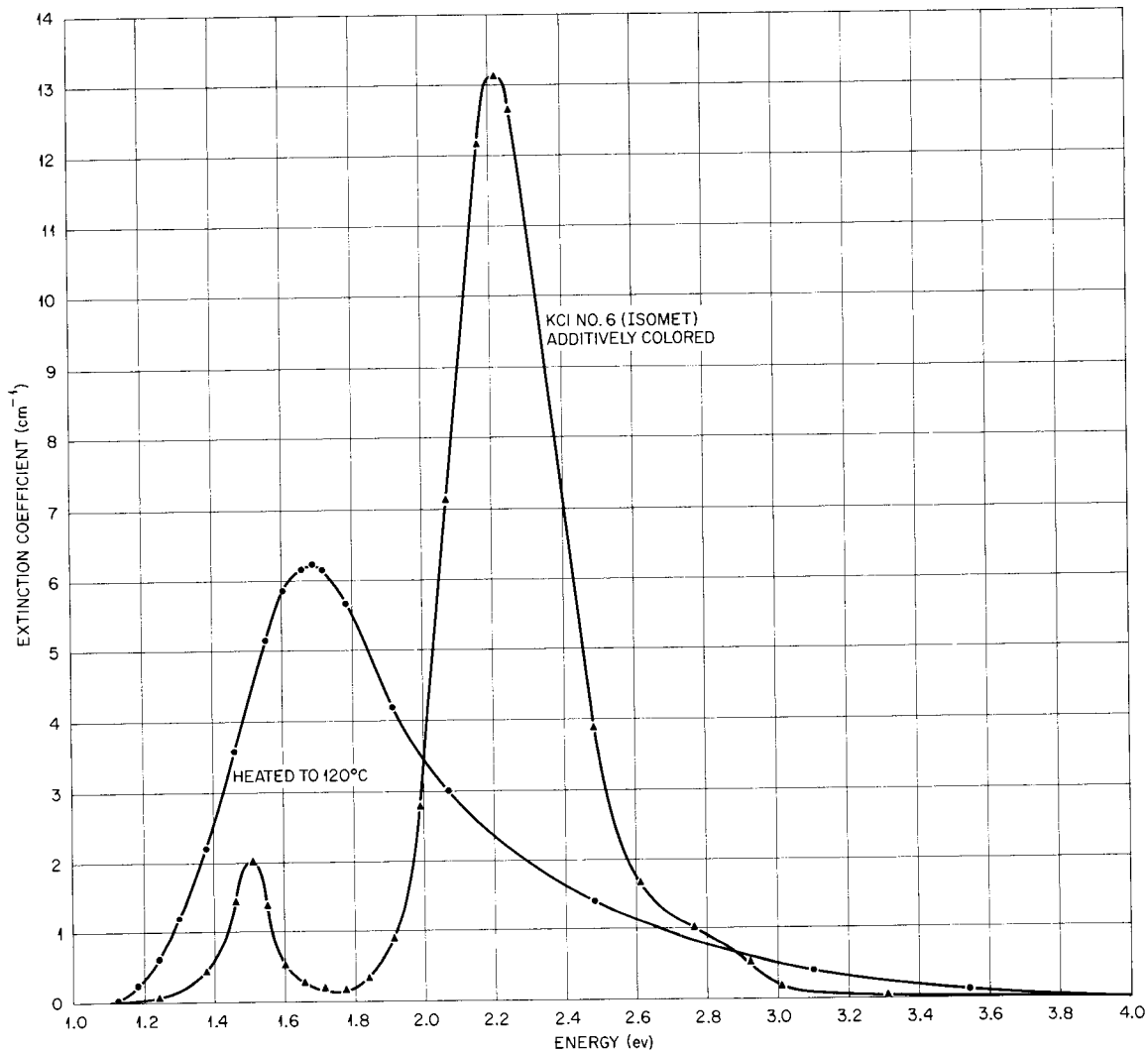


Fig. 11.4. Optical Absorption of One of the KCl Samples After Coloration and After Annealing to Produce the Colloid Band.

Table 11.1. Magnetic Centers in Alkali Halides

Ingot Designation and Source	Density of Magnetic Centers from Susceptibility Measurements, N_X (cm^{-3})	Extinction Coefficient (cm^{-1})	N_0 of Assuming Smakula's Equation (cm^{-3})	Average Oscillator Strength, $\langle f \rangle$
KCl No. 1 Isomet	$<4 \times 10^{15}$	Uncolored		
KCl No. 2, Harshaw	$<7 \times 10^{15}$	Uncolored		
KCl No. 5, Isomet	7.5×10^{16}	8.7	7.5×10^{16}	0.9 ($\pm 15\%$)
		6.9	5.9×10^{16}	
		9.3	7.9×10^{16}	
KCl No. 6, Isomet	$1.18 \times 10^{17*}$	11.5	9.8×10^{16}	0.81 ($\pm 10\%$)
		10.3	8.8×10^{16}	
		10.7	9.1×10^{16}	
		13.1*	$11.2 \times 10^{16*}$	
		10.8	9.2×10^{16}	
KCl No. 8, Harshaw	1.28×10^{17}	13.4	1.14×10^{17}	0.77 ($\pm 10\%$)
KCl No. 7, Harshaw	1.02×10^{18}	88.1	7.5×10^{17}	0.74 ($\pm 5\%$)
		88.1	7.5×10^{17}	
CsBr No. 1, NRL	4×10^{16}	Before coloration		
	1.1×10^{17}			

*Samples for which data are shown in Figs. 11.3 and 11.4.

and to introduce the so-called colloid band. The absorption spectrum is shown in Fig. 11.4. Measurements of the magnetic properties at low temperature are presented in Fig. 11.3 and indicate that most of the electrons which were unpaired when trapped by F centers are now in states that are no longer magnetic.

MAGNETIC SUSCEPTIBILITY OF POTASSIUM RHENIUM BROMIDE

E. Sonder

Magnetic susceptibility measurements on K_2ReCl_6 ¹⁷ had shown that a magnetic phase

change occurred between 10 and 20°K. Specific heat measurements between 14°K and room temperature had not shown a corresponding specific heat anomaly¹⁸ in that compound. However, in the bromide such a specific heat peak had been observed at 15°K, making it seem worthwhile to

¹⁷E. Sonder, *Solid State Ann. Prog. Rep. Aug. 31, 1959*, ORNL-2829, p 175.

¹⁸Recent specific heat measurements (R. H. Busey, private communication) have shown a specific heat peak at 12°K.

SOLID STATE ANNUAL PROGRESS REPORT

perform susceptibility measurements on the latter compound. The technique used was the same as that used in the case of the chloride.¹⁷ Figure 11.5 shows a comparison of the results of the measurements of the two compounds. The evidence for a magnetic phase change at 15.5°K in the K_2ReBr_6 is quite clear. Furthermore, as was the case in the chloride, there is no magnetic anomaly above about 50°K. The anomalous contribution to the specific heat that has been observed¹⁹ above that temperature must probably be attributed to structural rather than to magnetic changes.

¹⁹R. H. Busey *et al.*, *Chem. Ann. Prog. Rep.* June 20, 1960, ORNL-2983, p 71.

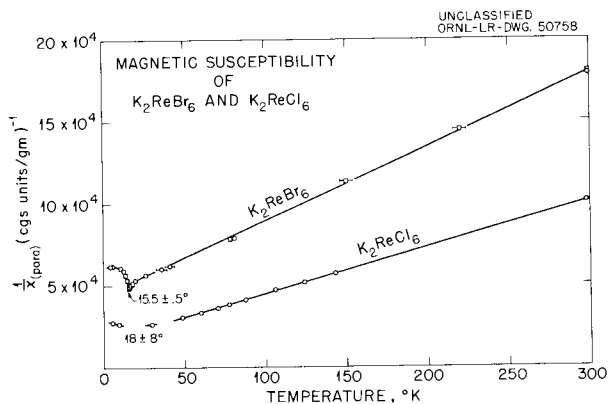


Fig. 11.5. Magnetic Susceptibility of K_2ReBr_6 and K_2ReCl_6 .

12. COVALENT CRYSTALS

HYPERFINE INTERACTIONS OF DEFECTS OF QUARTZ

R. A. Weeks

Hyperfine interactions of the E'_1 center with two nearby Si^{29} nuclei have been described.¹ This interaction was the basis for a model for the E'_1 center. However, additional observations have been made on a gamma-ray-irradiated synthetic crystal.² These measurements have shown the existence of additional hyperfine interactions with Si^{29} nuclei. These additional interactions have indicated that the model proposed for the E'_1 center is not correct. The additional data have not clearly defined a new model but are sufficient for a first approximation.

All the hyperfine lines arising from interactions of the E'_1 center with Si^{29} nuclei that have been observed are shown schematically in Fig. 12.1. There are three sets of lines, all of equal intensity and each $(3 \pm 1.0)\%$ of the central unperturbed line. For this orientation of the crystal with respect to H , the applied magnetic field, eight lines can be resolved and two more have been detected as a change of slope on the $d\chi''/dH$

curve of the central line. The lines have been labeled, and the observed separations are given in Table 12.1. The second-order interaction term used in the table does not take into consideration the anisotropy term. This term probably accounts for the discrepancy between the observed and calculated values.

Table 12.1. Hyperfine Lines of the E'_1 Center

Line	Splitting, A (oersteds)	$\frac{A^2}{2H_0} [I(I-1) - M_I^2]^*$ (oersteds)	
		Observed	Calculated
A	404	14.2	12.3
B_1	8.0	**	
B_2	6.8	**	
C_1	0.6	**	
C_2	~ 0.4	**	

* H_0 = field for unperturbed line $[00.1] \parallel H$;

$I = \frac{1}{2}$ (nuclear spin);

$M_I = \frac{1}{2}$ (nuclear magnetic quantum number).

** Less than experimental error.

¹R. A. Weeks and C. M. Nelson, *J. Am. Ceram. Soc.* 43, 399 (1960).

²Supplied by C. S. Brown, General Electric Co. Ltd., England.

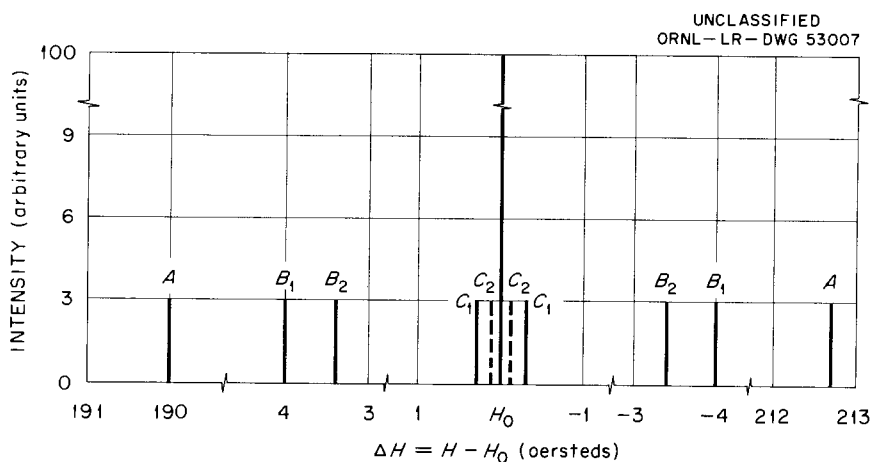


Fig. 12.1. The Hyperfine Lines of the E'_1 Center Observed in a Gamma-Ray-Irradiated Synthetic Single Crystal. The full values of the lines are given. Each pair of lines is identified by a common letter.

The relative intensities of these lines, their equivalence, their ratio to the central line, and their splitting suggest the preliminary model shown in Fig. 12.2. In Fig. 12.2 the separation of the atoms is indicated by the letters b and c . Then, from the reduced splitting of the C lines, $b < c$.

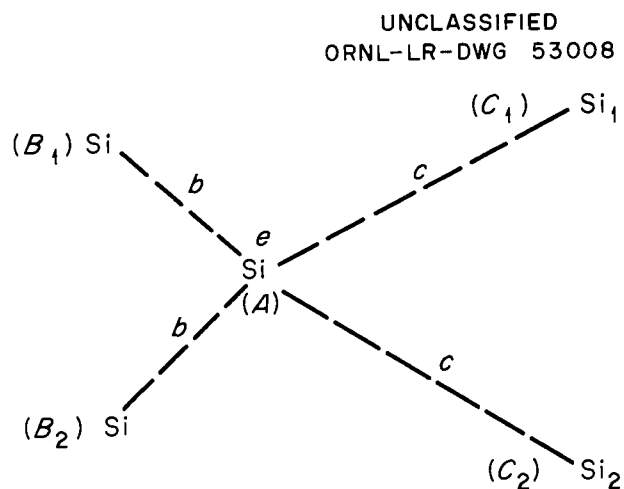


Fig. 12.2. A Model for the E_1' Center Based on the Hyperfine Lines Shown in Fig. 12.1. The letters b and c indicate relative distances of the B and C Si^{29} nuclei from the A nucleus. The dashed lines connecting the Si atoms emphasize the uncertainty of the connecting links between the Si atoms. The e on the A atom is the paramagnetic electron.

A DEFECT STRUCTURE OF SILICA

R. A. Weeks C. M. Nelson

A model for the structure of silica has been proposed in which the $Si-O$ tetrahedra are randomly oriented with respect to each other.³ Some recent experimental results⁴ have suggested that the orientation of one $Si-O$ tetrahedron with respect to the next may not be random. Such a correlation of the tetrahedra may give rise to short-range ordering.

Additional data on the rate of formation of a defect, the E_1' center,⁵ by irradiation with photons

³G. W. Morey, *The Properties of Glass*, p 564, Reinhold, New York, 1954.

⁴R. A. Weeks and C. M. Nelson, *J. Appl. Phys.* 31, 1555 (1960). Additional references are given in this paper.

have indicated that in the silica this defect is present in surprisingly high concentration if the irradiation and measurement are carried out at 78°K. The experimental results also suggest that the concentration observed in various silicas for the same irradiation conditions is approximately inversely proportional to the hydrogen content. These results have suggested that the E_1' center should not be considered as a defect but as a fundamental characteristic of the silica. The hydrogen in the silica forms $O-H$ bonds, which in some way suppress the E_1' center or the occupancy of the E_1' center by an electron.

In Fig. 12.3 the absorption band in the infrared region, which has been attributed to an $O-H$ stretching mode,⁶ is shown in several silicas and a single crystal. The maximum extinction coefficient, Emm^{-1} , observed in three silicas at 2.8μ shows that the absorption due to the $O-H$ bond is approximately 50 times less for the Corning 7943 than for the 7940 and at least an order of magnitude less than the Amersil O.G. 1.

In Table 12.2 a comparison is made between the reciprocal of Emm^{-1} of the $O-H$ band and the concentration of the E_1' center produced by an irradiation with Co^{60} gamma rays. A comparison of the data on the 7940 and 7943 indicates an inverse ratio of the $O-H$ band to the concentration of E_1' produced by gamma rays. The inverse ratio is also suggested by a comparison of the Amersil with the 7940 and 7943.

The Corning 7943 silica was irradiated with 50-kv (constant potential, 50 ma) x rays, and the absorption at $215 m\mu$ was measured without intervening warmup.⁷ The results are shown in Fig. 12.4. The maximum x-ray dose given is 1.28×10^9 rads absorbed in the silica, specimen No. 2, and is equivalent to the amount of energy absorbed from a 5.2×10^{16} -electron/cm² dose of 2-Mev electrons. There is no indication of saturation in the concentration of the E_1' center. The absorption coefficient is $405 cm^{-1}$ at the highest dose. If an oscillator strength of 0.08 and a width at half-maximum amplitude of 0.8 ev are

⁵R. A. Weeks and C. M. Nelson, *J. Am. Ceram. Soc.* 43, 399 (1960).

⁶D. L. Wood, *Phys. and Chem. Solids* 13, 326 (1960).

⁷Data for Fig. 12.4 were taken by G. Arnold and D. Compton, of the Naval Research Laboratory, and are used with their permission.

UNCLASSIFIED
ORNL-LR-DWG 53009

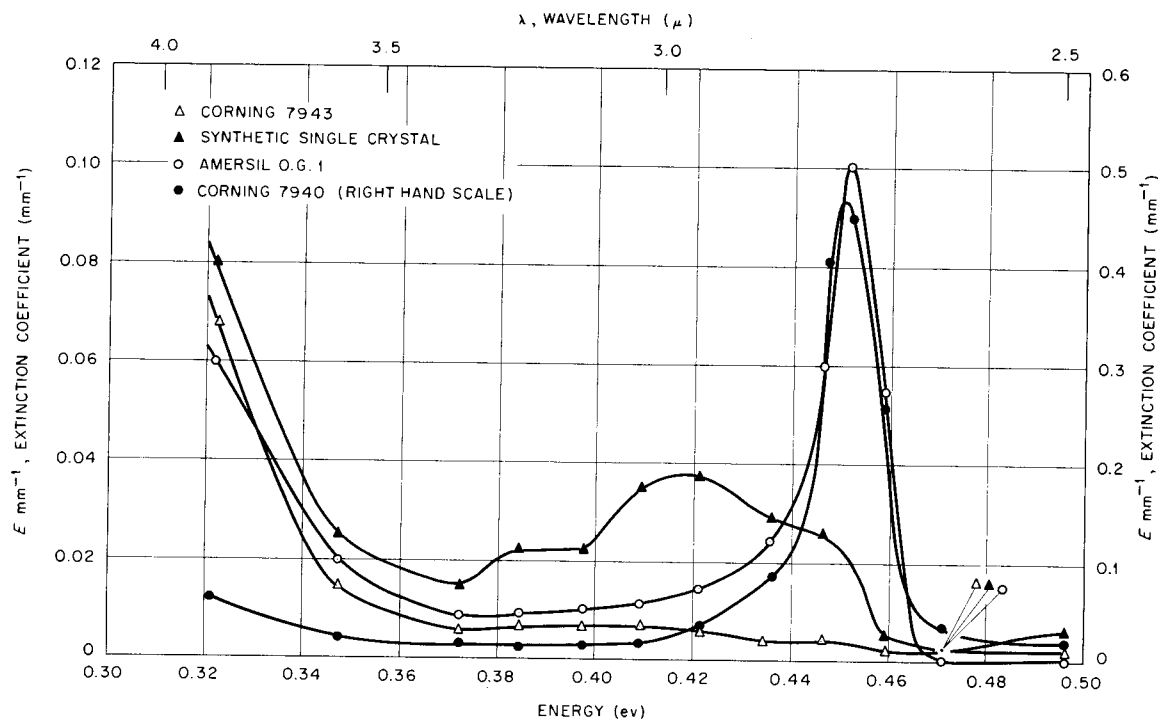


Fig. 12.3. The Intensity of the O-H Stretching Mode as Observed in Several Silicas and a Single Crystal.

Table 12.2. Intensity Comparisons of the 2.7- μ Band and the E_1' Center

Specimen ^a	$\frac{1}{E_{mm^{-1}}(2.7 \mu)}$ ^b	$E_{mm^{-1}}(215 m\mu)$ ^b	Intensity of ESR Line, $g \approx 2.0006^c$
Corning 7943	100	0.50	1.0
Corning 7940	2.2	0.01	0.02
Amersil O.G. 1	10	0.10	0.20

^aIrradiated with Co^{60} gamma rays to $\sim 10^6$ r.

^b $E_{mm^{-1}} \equiv$ extinction coefficient.

^cArbitrary units.

used in a Gaussian shape function,^{8,9} then the concentration of the E_1' center produced by the x rays is $\sim 1.7 \times 10^{19} \text{ cm}^{-3}$.

The specimen was annealed at 600°C for 24 hr and reirradiated and measured under the same

⁸R. A. Weeks and C. M. Nelson, *Bull. Am. Phys. Soc.* 5, 201 (1960).

⁹D. L. Dexter, *Solid State Physics*, vol 6, p 371, Academic Press, New York, 1958.

conditions. The concentration was decreased approximately 15% by this heat treatment (curve III, Fig. 12.4). The annealing apparently has produced an alteration in the structure to a small degree. The No. 1 specimen of 7943 (curve I) has approximately two-thirds the concentration of the No. 2 for the same dose. Upon warming the specimens to $\sim 23^\circ\text{C}$, the concentration of the E_1' center is observed to decrease by over an

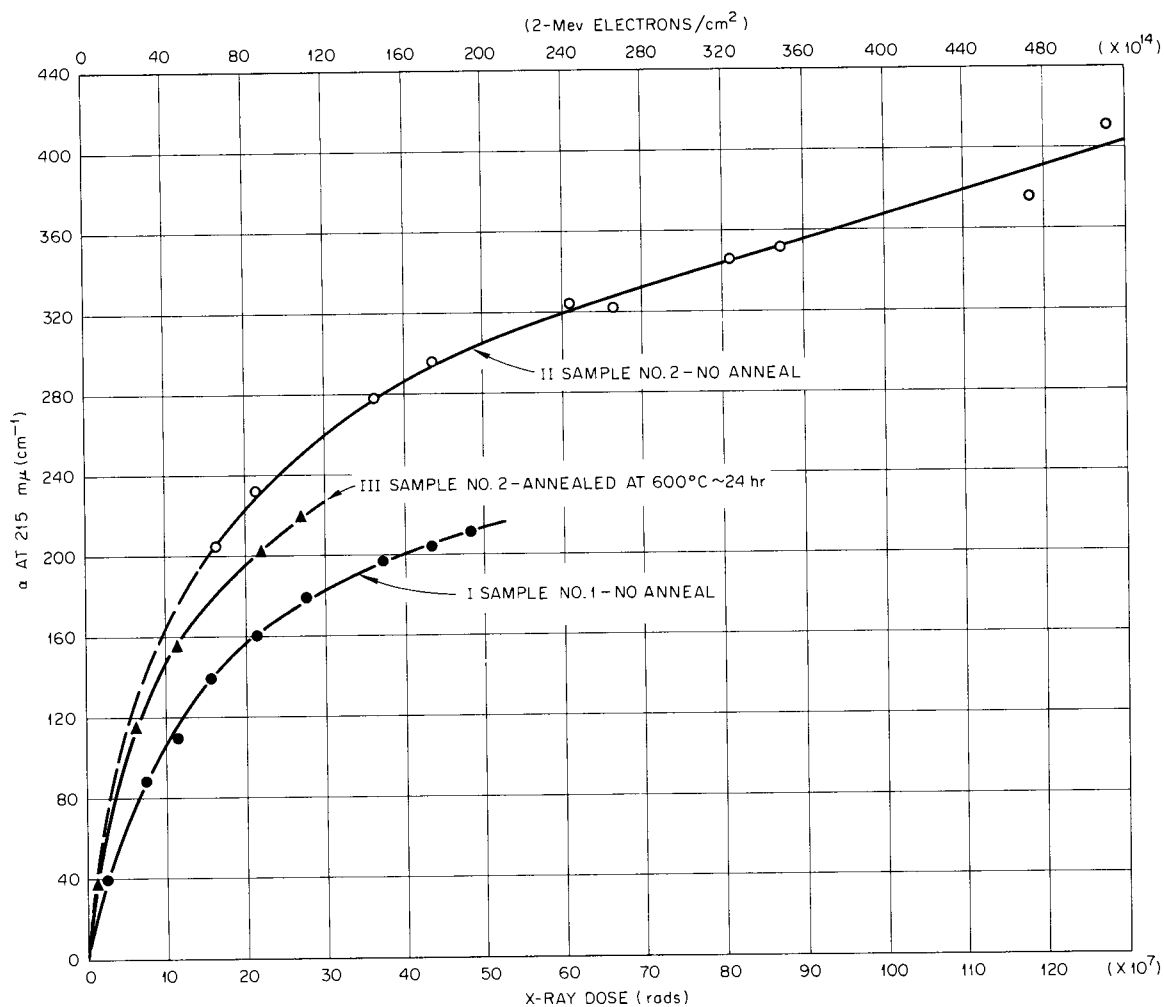


Fig. 12.4. The Intensity of Absorption at 215 mμ, Plotted as a Function of X-Ray Dose. The equivalent electron dose (equivalent in the sense of energy absorbed by the specimen) is shown at the top of the graph. The specimens were irradiated and measured at $\sim 78^\circ\text{K}$ without intervening warmup. The silica was Corning 7943 ("waterless") silica.

order of magnitude. Similar effects have been observed in the 7940 silica; but, of course, as indicated above, the concentration produced at 78°K is still in the same ratio to the 7943 as for the higher-temperature irradiations.

Electron spin resonance measurements on these three silicas have also shown that the envelope shape of the E_1' center is the same. Other features of the ESR spectrum do differ, particularly with respect to centers whose g values are greater than the free-electron g value of 2.0023. These differences are not directly related to the O-H band. However, there is one other difference

which seems to be related to the presence of the hydrogen. In either gamma-ray- or neutron-irradiated material, a pair of lines of equal intensity is observed with a separation of 74.5 oersteds. The intensity of these lines is approximately proportional to the intensity of the O-H band.

This pair of lines does have the appearance of hyperfine lines arising from an interaction of a paramagnetic center with a nuclear species whose nuclear spin I is $\frac{1}{2}$. Since the intensity of these lines is proportional to the intensity of the O-H band and thus inversely proportional to the intensity of the E_1' center, the lines cannot arise from

a hyperfine interaction of the E_1' center with Si^{29} , whose I is $\frac{1}{2}$. These data then suggest that the hyperfine interaction may be with the proton, whose I is $\frac{1}{2}$. The second-order hyperfine interaction is

$$\Delta H = \frac{A^2[I(I+1) - M_I^2]}{2H_0}$$

where A is the hyperfine interaction constant, I is the nuclear spin, M_I is the quantum number of the nuclear spin momentum in the direction of the applied field, and H_0 is the magnetic field at which the unperturbed line appears. The anisotropy term has been dropped.¹⁰ For $I = \frac{1}{2}$, $A = 74.5 \pm 0.1$ oersteds, and $H_0 = 3621.4 \pm 0.2$ oersteds (the position of the E_1' center), $\Delta H_{\text{calc}} = 0.4$ oersted. The observed difference is $\Delta H_{\text{obs}} = 2.8 \pm 0.1$ oersteds. Since the lines are quite narrow, ~ 5 oersteds at the inflection points, the anisotropy term can only make a contribution to ΔH that is small compared to ΔH . These results, therefore, suggest that the center which is interacting with the nuclear species $I = \frac{1}{2}$ is not the E_1' center.

One other indication of the nature of this center, from the above calculation, is the g value of the unperturbed line. The line falls at a value of H 2.4 oersteds less than the E_1' center; and, thus, for the frequency used in these measurements $g_{\text{obs}} > g_{\text{free electron}}$. This suggests that the center is a trapped hole.

Discussion

The inverse relationship between the intensity of the O-H band and the E_1' center suggests that the presence of the hydrogen must act in some way to suppress either the E_1 center or its occupancy by an electron (the E_1' center). The experiments described above do not clearly distinguish between these two possibilities.

The extremely high concentration of centers produced by irradiating with x rays at 78°K, coupled with the lack of any saturation, implies that any saturation probably falls above 10^{20} E_1' centers/cm³, between 1 and 10 at. %. Such a concentration suggests that in the silica the E_1 center is not a defect in the accepted meaning of the term. The production of such a high

concentration by a relatively small x-ray dose clearly indicates that this center is already present in concentrations of 10^{20} cm⁻³ or greater, and the x-ray irradiation only furnishes electrons which can occupy the center. The energy of the x rays would seem to eliminate atomic displacements as a source of these centers. This center should not, therefore, be regarded as a "defect" in the usual meaning of this term. It is probable that it is a fundamental property of the silica state.

ELECTRON SPIN RESONANCE IN NEUTRON-IRRADIATED TiO₂

R. A. Weeks R. D. Nelson¹¹

In reduced TiO₂ single crystals an ESR line has been observed at liquid-helium temperatures.¹² The properties of the line suggest that the resonance is due to a Ti⁺⁺⁺ ion. No ESR lines are observed at room temperature.

Observations have been made at room temperature on neutron-irradiated TiO₂ single crystals. The spectrum observed is shown in Fig. 12.5 for an orientation of the crystal such that the C axis is parallel to H , the applied magnetic field. Two lines are resolved, with g values of 1.986 ± 0.001 and 1.991 ± 0.001 . In Figs. 12.6 and 12.7 the orientation dependence of these lines is plotted as a function of rotation about two axes. For a rotation of H about the $[110]$ direction a line moves out from the $g = 1.986$ line, and as the rotation reaches 90° (Fig. 12.6), $[110]$ parallel to H , the line has split into three lines with an approximate intensity ratio of 1:2:1. The lines remaining in the region of $g = 1.986$ and 1.991 at 30° have an approximate intensity ratio of 1:3. At 90° these lines have split and there is an indication that there are four lines with intensity ratios of 1:2:2:1.

For a rotation axis along the $[001]$ direction a somewhat similar orientation dependence is observed. Since the 0° position corresponds to the 90° angle in Fig. 12.6, the spectrum is approximately the same. There are differences which may be due to a small misalignment of the crystal. Due to the very small signal-to-noise ratio, it was difficult to determine the line positions for some orientations. However, the best measurements

¹⁰D. J. E. Ingram, *Spectroscopy at Radio and Microwave Frequencies*, p 153, Butterworth, London, 1955.

¹¹Summer employee.

¹²P. F. Chester, *Bull. Am. Phys. Soc.* 5, 73 (1960).

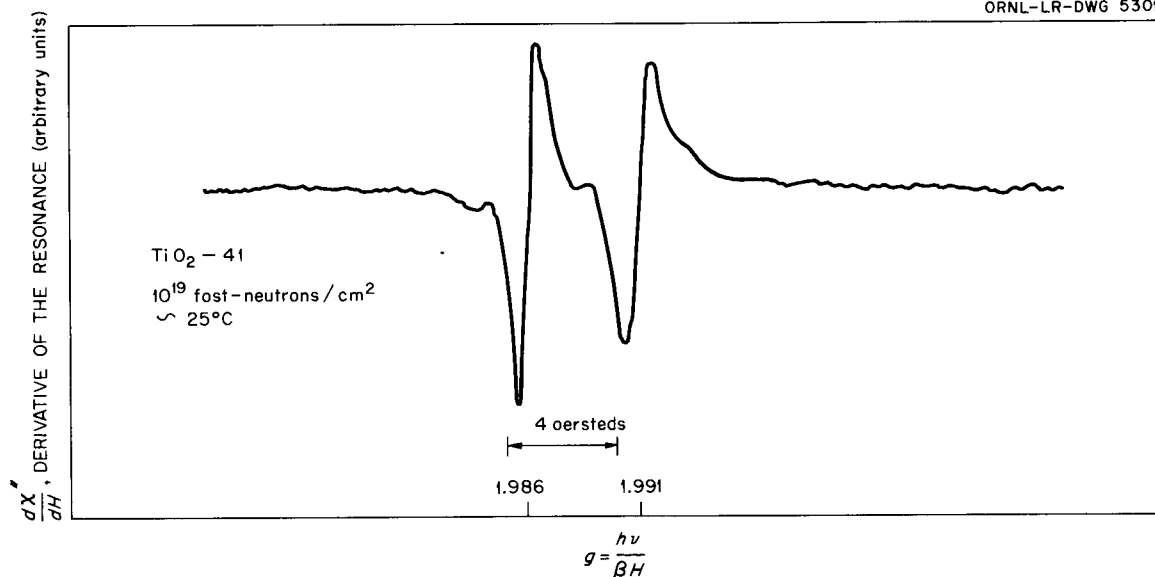


Fig. 12.5. A Portion of the ESR Spectrum Observed in Neutron-Irradiated TiO₂ Single Crystal at Room Temperature. The specimen was a bar, 0.1 × 0.1 × 0.6 cm. The [001] direction was parallel to *H*, and $\nu = 10,300$ Mc.

suggest that the ratio of the sum of intensities for lines in the region of $g = 1.938$ to the sum for those in the region of $g = 1.988$ is approximately 1:4.

The data in Figs. 12.6 and 12.7 could be explained by assuming a center whose effective spin $S = \frac{1}{2}$ and whose g values are $g_x \approx g_y \approx 1.988$ and $g_z = 1.938$. The 1:4 intensity ratio of the lines in the region $g = 1.938$ to those at $g = 1.988$ implies that there are four sites in the unit cell. The splitting of the line as the crystal is rotated to [110] || *H* suggests that $g_x \neq g_y$ for the one site in the unit cell which is being observed and that there is a small angle between g_x and g_y and the [110] direction.

A second possibility is that two distinct centers are observed, one which has only a very small anisotropy, such that $g_x = g_y = 1.991$ and $g_z = 1.986$; the second center would then have $g_x \approx g_y \approx 1.991$ and $g_z \approx 1.935$. In this case the intensity ratios are not particularly meaningful. The data in Fig.

12.7 then suggest that the first center may have a spin $S = 1$, whereas the second center should have a spin $S = \frac{1}{2}$. However, the probability of two centers having such similarities in g but differing in their spin states seems small. The possibility exists that this line is the same as that observed in reduced TiO₂ single crystals. The g values for this center¹² are $g_z = 1.940$, $g_x = 1.972$, and $g_y = 1.975$. The accuracy of the measurement is not given, and thus a positive identification is not possible. This identification is, however, contradicted by the splitting of the line (Figs. 12.6 and 12.7) at the $g = 1.938$ position. For the center observed by P. F. Chester, only a single line is found at the $g = 1.940$ position. A second difference between these observations and those of P. F. Chester is the orientation of the g tensor. He observes the g_z to be 25° from the [110] direction, whereas Figs. 12.6 and 12.7 show that the g_z of this center is approximately parallel to the [110] direction.

UNCLASSIFIED
ORNL-LR-DWG 53012

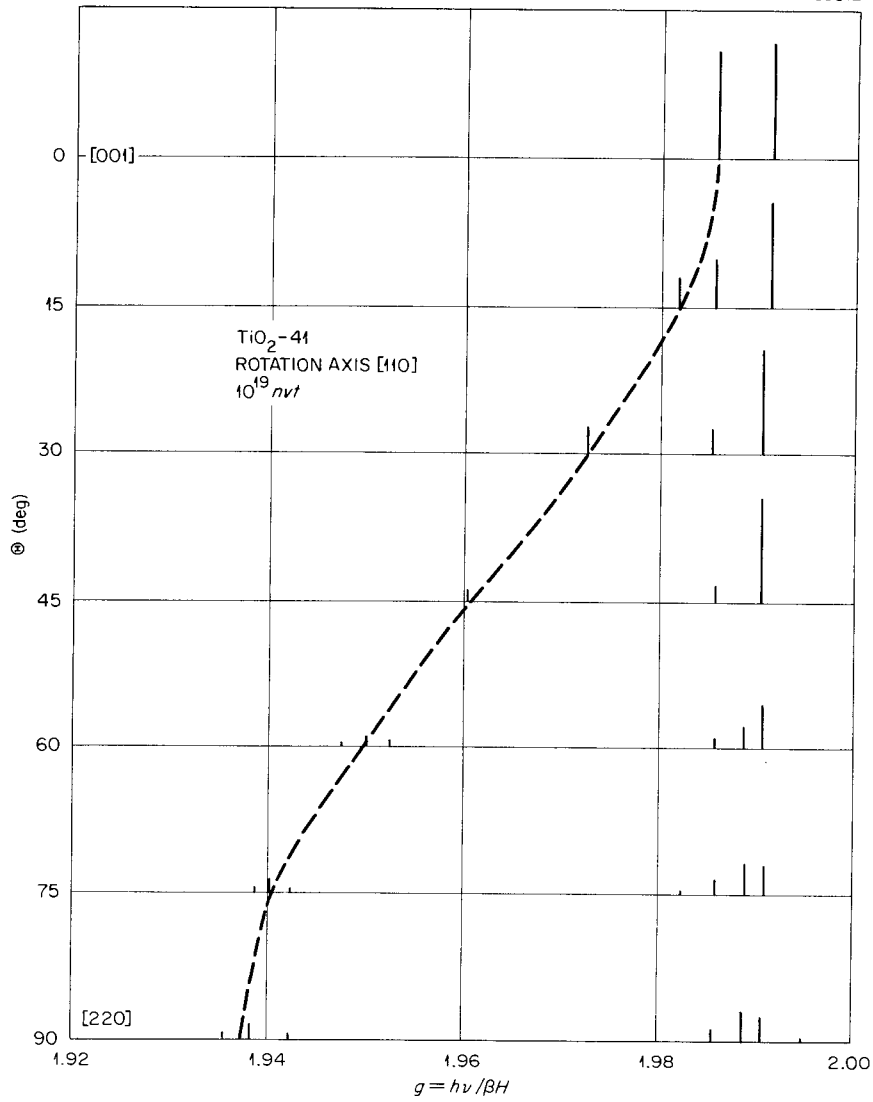


Fig. 12.6. The Orientation Dependence of the Lines Shown in Fig. 12.6 for a Rotation of H , the Applied Magnetic Field, About a $[110]$ Axis. The intensities shown by the heights of the lines are in arbitrary units and are $\pm 50\%$. The dashed curve connects the line positions for each angle.

UNCLASSIFIED
ORNL-LR-DWG 53013

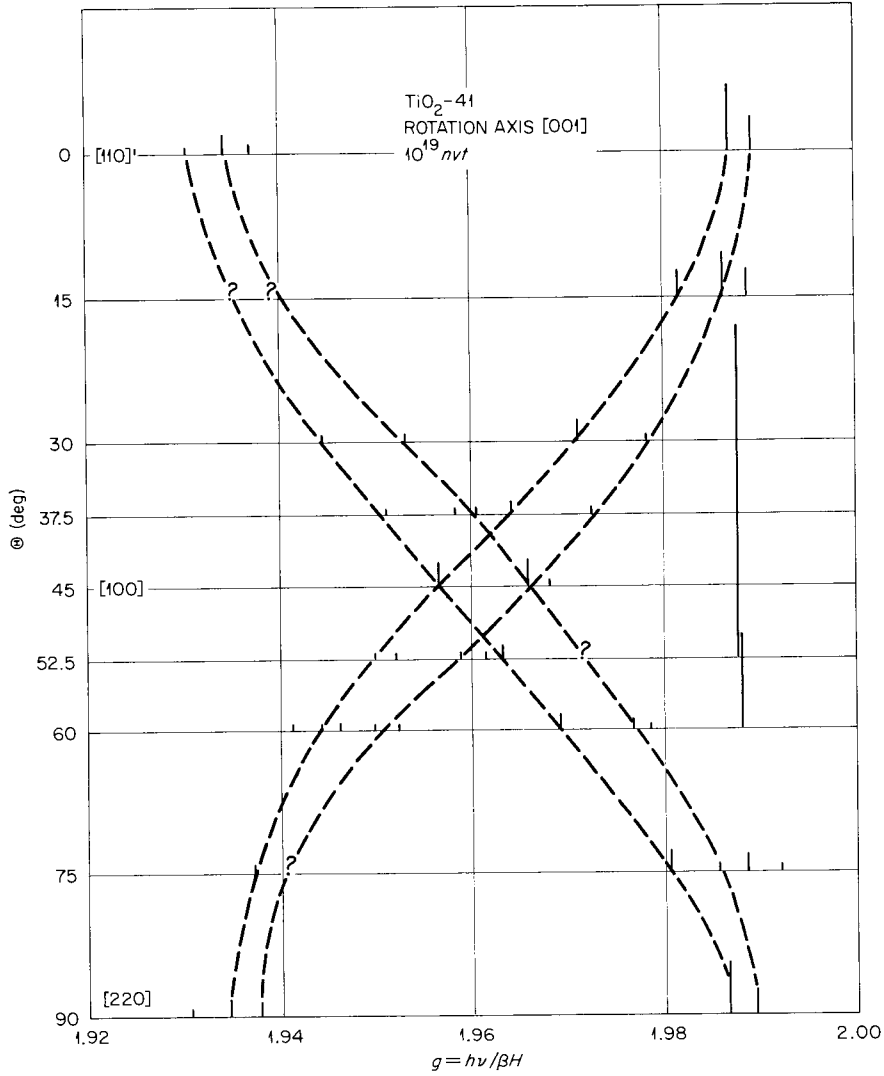


Fig. 12.7. The Orientation Dependence of the Lines Shown in Fig. 12.6 for a Rotation of H , the Applied Magnetic Field, About a $[001]$ Axis. The small question marks indicate that the line intensities are comparable with the noise level and, thus, their position is in doubt. No explanation for this rather odd variation of the signal-to-noise ratio with orientation has been found.

13. GRAPHITE AND CERAMICS

STORED ENERGY IN X-10 PILE GRAPHITE

M. C. Wittels F. A. Sherrill

A few weeks prior to the annealing of the ORNL Graphite Reactor several cores were taken from the most severely damaged region of the moderator for last-minute calorimetric studies to assist the annealing operation.

Some of the more important findings were: (1) a confirmation of the growth rate of stored energy up to 250°C ($2 \text{ cal g}^{-1} \text{ yr}^{-1}$), (2) the importance of low-temperature annealing to reduce possible large-scale temperature excursions, (3) lack of significant damage in the moderator 4 ft west of center, and (4) the slow buildup of damage slightly west of the present damaged region, near the reactor center.

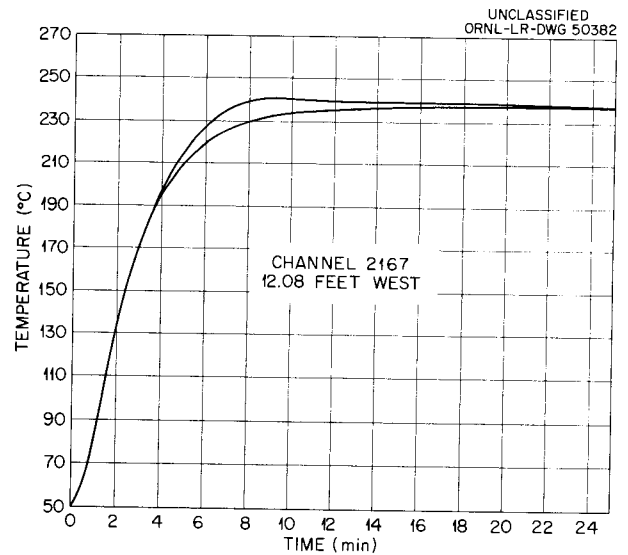
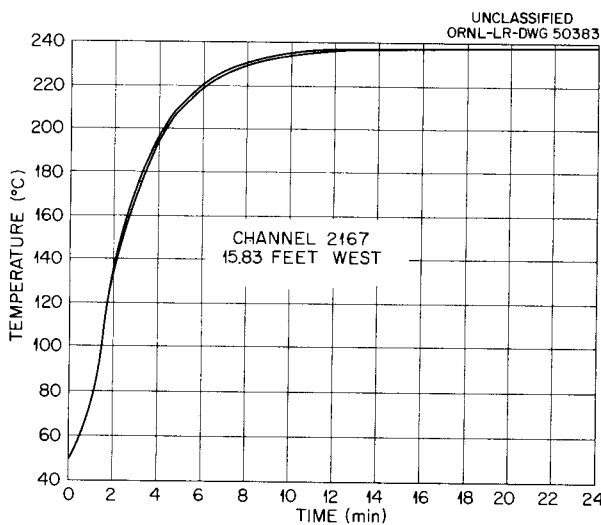
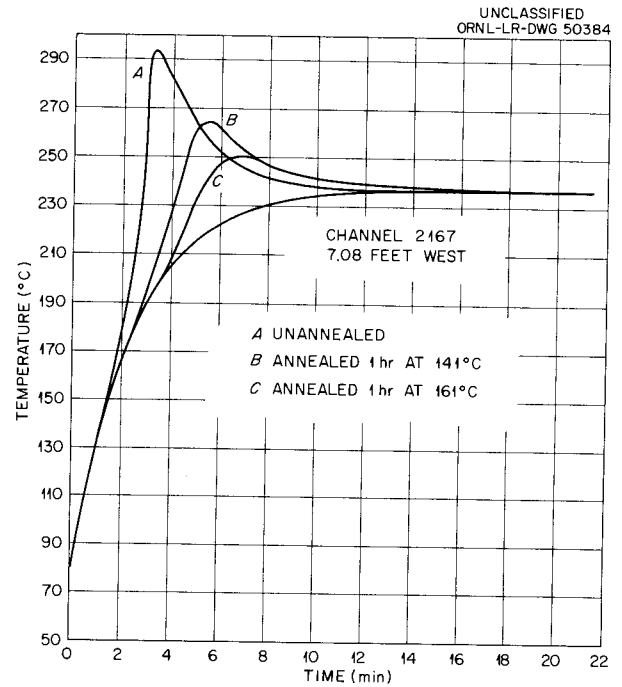
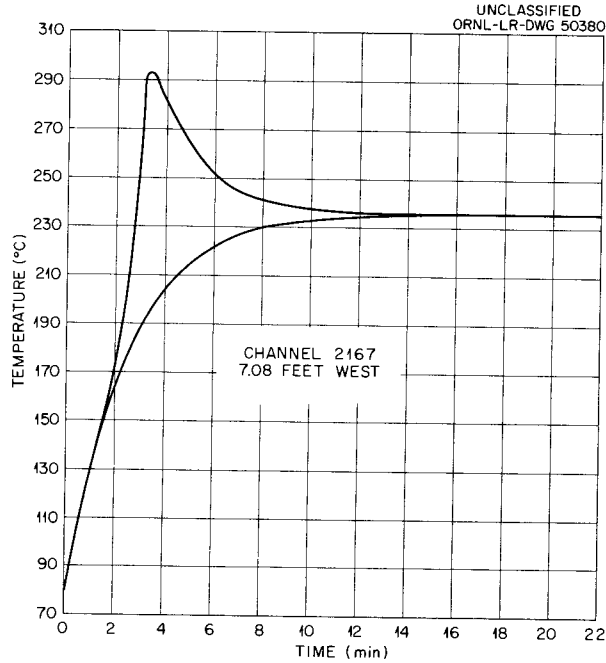


Fig. 13.1. Temperature Rise Curves Due to Stored Energy Release.

A typical stored-energy release curve from a sample showing the highest stored energy is given in Fig. 13.1a. For this sample the energy released up to 293°C was 51.3 cal/g. Portions of this same core were first annealed under controlled conditions (out-of-pile) in which no temperature excursions were permitted. The results of this low-temperature annealing are shown in Fig. 13.1b and confirmed previous analyses that dangerous temperature excursions could be avoided by a low-temperature soak. After annealing at 141°C for 1 hr, 31.7 cal/g remains up to 264°C, and after annealing at 161°C for 1 hr only 22.4 cal/g remains up to 250°C. Figure 13.1c shows the release curve for a sample 3.8 ft west of center that contains only 2.3 cal/g to 237°C. Figure 13.1d shows that the condition in the center of the reactor in channel 2167 is safe, containing only 13.3 cal/g to 237°C, but indicates that this region would contain spontaneously releasable stored energy in about 10 yr at the present rate of growth.

The Graphite Reactor was recently annealed by using fission heat and employing a reverse air flow technique in the reactor operation. The success of this operation is now being determined from postannealing cores taken from the reactor, and future operations will be guided by these results.

CERAMICS

C. D. Bopp O. Sisman R. L. Towns

The Effect of Irradiation on the Thermal Stability of Asbestos

Reactor irradiation lowers the temperature for the dehydration of four varieties of asbestos. Graphs of the rate of release of water on heating are plotted in Fig. 13.2. The irradiated material is more hygroscopic, as evidenced by the larger water content in the temperature range below about 350°C. The weight change was measured with a thermobalance on heating in a vacuum.

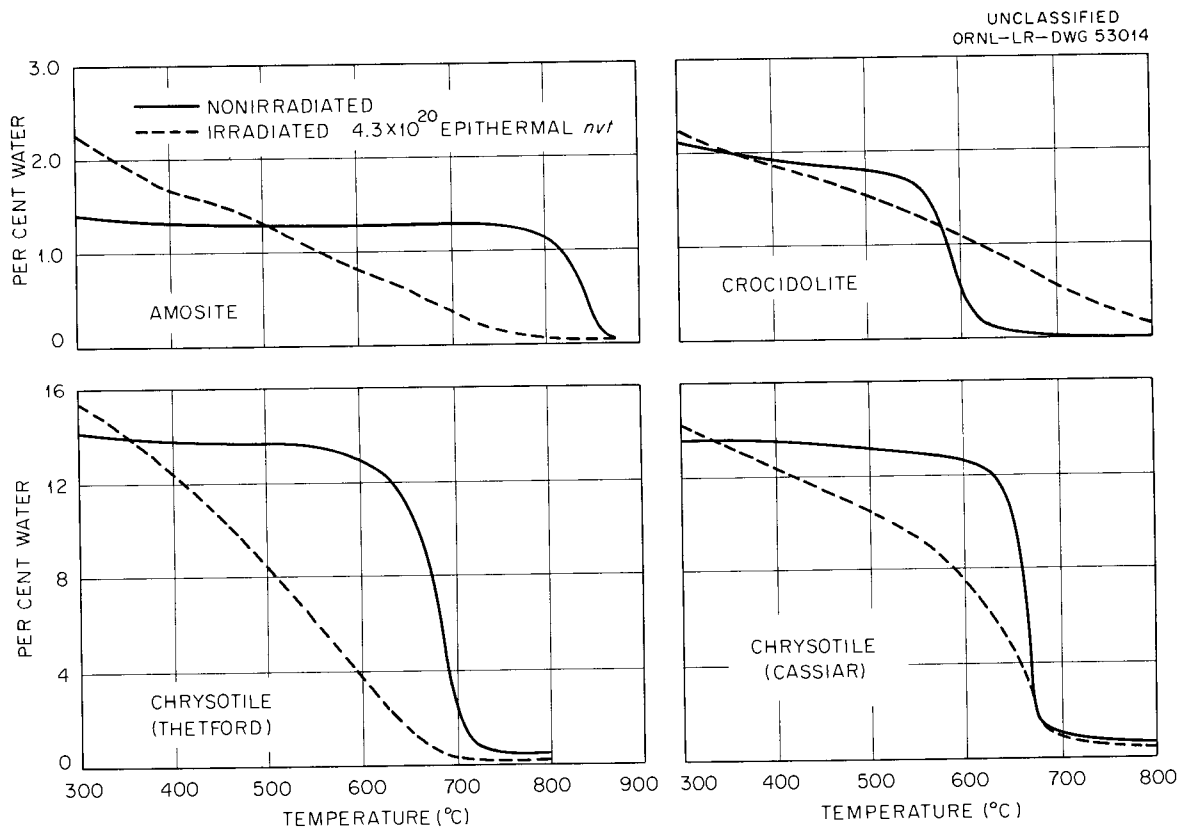


Fig. 13.2. Retention of Water on Heating of Asbestos.

The weight-loss-temperature relation was insensitive to the rate of heating in the range from about 50 to 500°C/hr. The irradiation exposure was conducted in the isotope stringer of the Oak Ridge Research Reactor. The specimens were contained in a helium-filled quartz capsule which was cooled through contact with the reactor cooling water. Since the specimens were small, their temperature was not much greater than that of the cooling water (less than 100°C). The integrated epithermal neutron flux listed in Fig. 13.2 was estimated from a spectrum measured in a similar (light-water-moderated) reactor¹ which was normalized to Al(*n,α*) monitors exposed along with the capsule.

The Effect of Irradiation on the Thermal Stability of Muscovite Mica

The effect of reactor irradiation on the kinetics of the dehydration of muscovite mica is shown in Table 13.1. The kinetics were second order in the temperature range indicated, and the data fitted the Arrhenius equation,²

$$k = A \exp\left(\frac{-E}{RT}\right),$$

where *k* is the rate of fractional decrease in

water content at the initial concentration of water in muscovite (about 0.045),³ *A* is the Arrhenius factor, and *E* is the activation energy. Table 13.1 shows that both the activation energy and the Arrhenius factor are decreased by irradiation. At lower temperatures than those indicated, the order of the reaction increased, but the reproducibility was poor. It is believed that this is associated with the formation of a glassy coating on the surface of the mica chips which impedes the evolution of water vapor.

The method of irradiation was described previously.⁴ Since the average kinetic energy of the epithermal neutrons is greater in a light-water than in a graphite-moderated reactor, the damage is greater for the former at a given integrated flux. This is the reason that the radiation-induced change in density listed in Table 13.1 is not in accord with the integrated epithermal flux. Exposures A and B were conducted in a vacant fuel channel in a graphite reactor; C, D, and E, adjacent to the lattice in the MTR light-water reactor.

The increase in the pressure of the water vapor evolved from the dehydration was measured

¹J. B. Trice *et al.*, *Solid State Ann. Prog. Rep.* Aug. 30, 1955, ORNL-1945, p 52.

²S. Glasstone, K. J. Laidler, and H. Eyring, *Rate Processes*, p 1, McGraw-Hill, New York, 1941.

³J. B. Holt, I. B. Cutler, and M. E. Wadsworth, *J. Am. Ceram. Soc.* 41, 242 (1958).

⁴O. Sisman, C. D. Bopp, and R. L. Towns, *Solid State Ann. Prog. Rep.* Aug. 31, 1957, ORNL-2413, p 80.

Table 13.1. The Effect of Reactor Irradiation on the Kinetics of the Dehydration of Muscovite Mica

Irradiation Treatment	Integrated Flux, Epithermal Neutrons (neutrons/cm ²)	Irradiation-Induced Density Change (%)	Temperature Range Studied (°C)	<i>E</i> (ev/molecule)	<i>A</i> (sec ⁻¹)
	× 10 ¹⁹				
Nonirradiated			740-800	4.0	1 × 10 ¹⁶
A*	8	-2.4	740-780	3.8	1.2 × 10 ¹⁵
B*	16	-2.8	740-780	3.5	6 × 10 ¹³
C**	4	-3.7	740-800	3.2	5 × 10 ¹²
E**	20	-13.8	490-540	2.5	10 ¹²
D**	20	-14.1	570-600	2.5	10 ¹²

*Graphite reactor, OGR.

**Light-water reactor, MTR.

SOLID STATE ANNUAL PROGRESS REPORT

manometrically, while the sample was held at constant temperature in an evacuated quartz glass tube. In order to avoid a back reaction, the water vapor was pumped out at intervals.

Prior to the dehydration run, water adsorbed on the surface of the specimen and of the quartz tube was removed by heating in vacuum at 250°C for about 15 min.

14. POLYMERS

W. W. Parkinson	W. K. Kirkland
D. Binder	O. Sisman
C. D. Bopp	J. E. White ¹

COMPARISON OF EFFECTS OF REACTOR
AND GAMMA IRRADIATION ON
POLYSTYRENE

In previous measurements of radiation effects on oriented polystyrene,² it was observed that the energy per cross link for gamma irradiation appeared to be about three times as great as that for reactor irradiation. Recently, it has been shown that, for a polymer which undergoes chain scission, the energy per scission is less for gamma than for neutron irradiation.³ The effect on polystyrene has been investigated further by irradiating two series of specimens for various times in a standard position of Hole 19 of the Graphite Reactor and in a 2.2×10^6 -r/hr Co⁶⁰ source.

Polystyrene molding pellets were sealed in quartz tubes after being evacuated to 2μ pressure for about 20 hr. After irradiation, the molecular weight of a specimen was determined by the well-established method of measuring the viscosities of dilute solutions of the polymer. The number of cross links per gram was calculated from the change in the number of molecules per gram.

The determination of the intensity of radiation of the gamma source was based on ceric sulfate dosimetry.⁴ Measurements were made five months apart with different ceric sulfate solutions, which were standardized separately in a known Co⁶⁰ source. The results were consistent with the calculated decay of Co⁶⁰. The radiation intensity of the reactor was determined by calorimetric measurements by Binder, Bopp, and Towns,^{5,6} using graphite and nylon. The reactor intensity during the irradiation of each sample was measured

by ceric sulfate solutions as a relative monitor. By comparing the ceric sulfate measurements at the time of the calorimetric determinations with the measurements during the irradiation of the polystyrene samples, the rate of energy deposition by the reactor was calculated to be $1.06 (\pm 0.08) \times 10^{18}$ ev/min per gram of polystyrene.

The results are shown in Fig. 14.1, where the number of cross links per gram is plotted vs the energy absorbed. The slopes of the lines are $2.5 (\pm 0.1) \times 10^{-3}$ and $0.76 (\pm 0.02) \times 10^{-3}$ cross links/ev for the reactor and the gamma source respectively. The reciprocals of these numbers are the energies required to produce one cross link: $4.0 (\pm 0.2) \times 10^2$ ev for the reactor and $1.32 (\pm 0.04) \times 10^3$ ev for the gamma source. Thus, irradiation by the reactor (neutrons plus gamma radiation) seems to be $3.3 (\pm 0.2)$ times as effective in producing cross links in polystyrene as irradiation by gamma rays alone. Added to the figure are data obtained for an oriented sheet of polystyrene.² These points were not considered in drawing the lines, but they do fit the lines quite well.

It must be pointed out that the different degree of cross-linking for reactor and gamma sources has been demonstrated only by viscosity measurements. It is possible that the effects caused by the two types of radiation differ in such a way as to produce very different molecular weight distributions although actually creating the same number of cross links. Viscosity measurements then would yield different average molecular weights, indicating an apparent difference in cross links. Measurements of a property not dependent on molecular weight distribution, such as solvent swelling, will be undertaken to differentiate between molecular weight distribution effects and true differences in cross-link yield.

¹Summer research participant, Southwestern Illinois Campus, Southern Illinois University, Alton.

²W. W. Parkinson *et al.*, *Solid State Ann. Prog. Rep. Aug. 31, 1958*, ORNL-2614, p 117.

³D. Binder, W. K. Kirkland, and R. L. Towns, *Solid State Ann. Prog. Rep. Aug. 31, 1959*, ORNL-2829, p 185.

⁴D. Binder, "Ceric Sulfate as a Pile Dosimeter," in sec 15, this report.

⁵C. D. Bopp, D. Binder, and R. L. Towns, *Solid State Ann. Prog. Rep. Aug. 31, 1959*, ORNL-2829, p 182.

⁶D. Binder, C. D. Bopp, and R. L. Towns, *Am. Soc. Testing Materials* 245, 26 (1960).

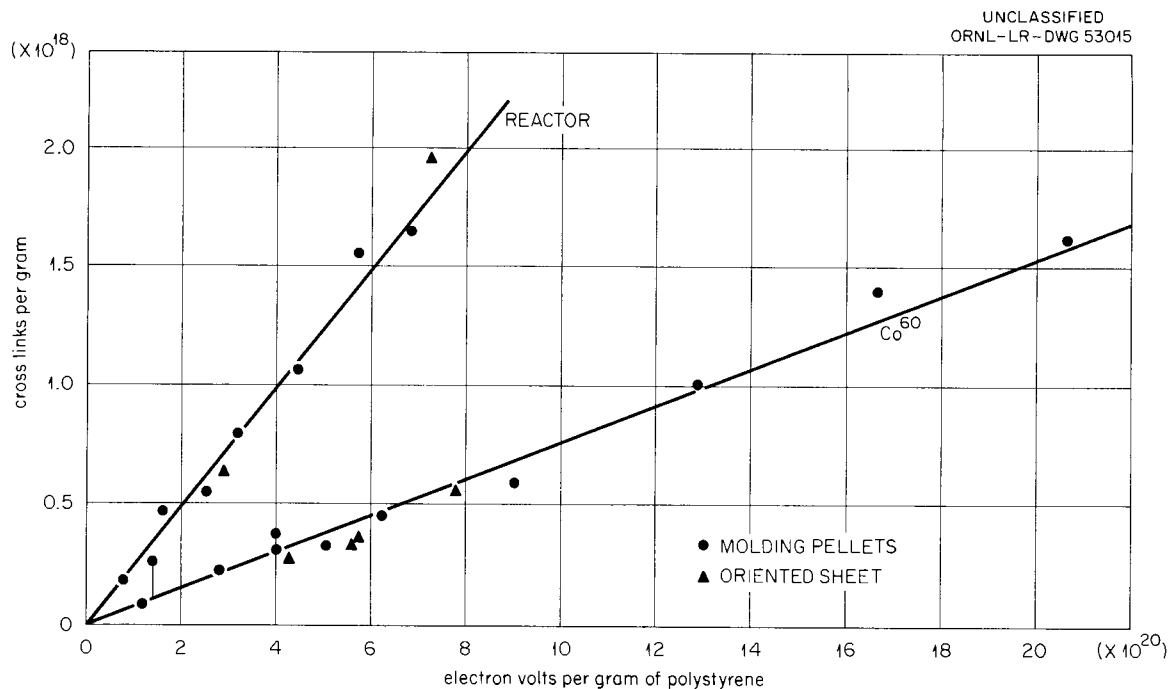


Fig. 14.1. Comparison of Reactor Radiation and Gamma Ray Effects on Polystyrene.

INFRARED STUDIES OF PLASTICS AND ELASTOMERS

Infrared absorption spectra of irradiated plastics and elastomers are being measured in an investigation of the changes in the molecular structure produced by radiation. Significant changes in the absorption peaks characteristic of the various isomeric configurations of the olefin groups ($-\text{CH}=\text{CH}-$) in synthetic and natural rubber have already been reported.⁷ To determine quantitative changes in the various olefinic groups, the infrared absorption coefficients of the characteristic peaks must be determined for the spectrophotometer used in the measurements, since the overlap of adjacent peaks is dependent on the optical characteristics of individual instruments. The earlier measurements of the absorption coefficients of olefinic hydrocarbon standards in carbon disulfide solution have been extended to the high concentrations in which the olefin groups occur in actual elastomers.

The contribution to the absorption peak characteristic of one olefin group by other isomeric

⁷W. W. Parkinson, W. C. Sears, and O. Sisman, *Solid State Ann. Prog. Rep.* Aug. 31, 1957, ORNL-2413, p 83.

groups, giving adjacent peaks in the spectrum, makes it necessary to solve equations for the concentrations of all groups simultaneously. To establish the equations for the absorption coefficients as a function of concentration the least-squares method of curve fitting has been employed. The equation calculated⁸ for *trans*-4-octene in carbon disulfide is

$$A = t(135.4c - 9.049c^2 + 0.4792c^3),$$

where A is infrared absorption [$\log(I_0/I)$] at 967 cm^{-1} , t is thickness in centimeters, and c is concentration in moles per liter. The measurements extended to a concentration of 6.3 moles/liter, that of the pure hydrocarbon. The calculated curve agreed with the experimental measurements within the limits of reproducibility of the spectrophotometer.

Absorption measurements have also been extended to the concentration of the pure hydrocarbon on solutions of three other standards: *cis*-4-octene, 1-octene, and 2,4,4-trimethyl-2-pentene. Equations for the absorption coefficients of these standards are also being calculated by

⁸Computed by the Mathematics Panel on the Oracle.

the Mathematics Panel. These equations will require the addition of terms containing the contribution to the absorption by the interfering olefin groups before formulation into a system of simultaneous equations applicable to an actual sample. Such simultaneous equations will be used for analysis of irradiated samples of natural rubber, polybutadiene, and styrene-butadiene rubber.

INFLUENCE OF THICKNESS AND ORIENTATION OF POLYMERS ON THE EFFECTS OF RADIATION

In earlier reports⁹ differences were described for radiation-induced cross-linking in specimens of polystyrene of different degrees of orientation and of different thicknesses. It was found that radiation produced cross-linking at a measurably faster rate in biaxially oriented specimens of 0.010-in. thickness than in random specimens of the same stock of 0.085-in. thickness. It was

also observed that random specimens of 0.010 in. thickness cross-linked more rapidly than specimens of the greater thickness.

Additional measurements have been made of cross-link yields in oriented and random specimens, and in randomized specimens of the thicknesses above. The difference in cross-linking rates of oriented and random specimens is the same as the difference in rates of random specimens of the two thicknesses, within the reproducibility of the measurements.

To find the cause of the higher cross-link yield in the thin specimens, measurements were made of weight losses and molecular weight changes as a result of pressing the 0.085-in. randomized specimens to 0.010-in. thickness. It was found that weight losses during pressing were only 0.03%. The molecular weight was reduced only slightly by the pressing operation. Therefore, the larger number of cross links measured after irradiation in the pressed specimens are produced during irradiation rather than by preirradiation pressing or heating. Experiments are continuing to determine if the thickness effect may be attributed to methods of preparing the specimens.

⁹W. W. Parkinson *et al.*, *Solid State Ann. Prog. Rep.*, Aug. 31, 1959, ORNL-2829, p 179.

15. DOSIMETRY STUDIES

NEUTRON FLUX MEASUREMENTS IN THE
ORNL GRAPHITE REACTOR

D. Binder

Measurements with threshold and resonance detectors over the period from April 1957 to April 1959 resulted in an accumulation of neutron flux values for the ORNL Graphite Reactor. The measurements are summarized in Table 15.1. The value ϕ_0 is the flux per $\ln E$ interval in an assumed $1/E$ spectrum above 0.4 ev. The other values are integral fluxes above the indicated thresholds, measured by the Np^{237} and U^{238} fission reactions and the $\text{S}^{32}(n,p)$ reaction. The thresholds were calculated for a fission spectrum and are somewhat insensitive to spectral shape. The threshold for the Np^{237} reaction is 0.7 Mev, with a cross section of 1.7 barns;¹ for the U^{238} reaction, 1.3 Mev and 0.54 barn; for S^{32} , 3.0 Mev and 0.30 barn. The relative accuracy is about 5% except where otherwise noted.

CERIC SULFATE AS A PILE DOSIMETER

D. Binder W. K. Kirkland

Ceric sulfate solutions were irradiated in reactor positions previously calibrated by calorimetry.² The yield for the ceric-to-cerous reduction re-

action per unit energy absorbed is known for gamma radiation,³ and the reactor measurements were used to determine the yield for reactor neutrons relative to gamma rays.

The irradiations were carried out in the ORNL Graphite Reactor in the center of Hole 51 and 5.5 ft from the center of Hole 19. The energy absorbed in water for the irradiations varied from 0.3 to 1.1×10^{17} ev/g. The ceric-to-cerous yield was determined by titration⁴ and normalized to a source calibrated by ferrous sulfate dosimetry. Initially assuming the same yield for neutrons as for gamma rays, we obtain the energy-absorbed values in column 1 of Table 15.2. Subtracting the energy absorbed from gamma rays as determined by calorimetry, the remainder is the energy absorbed from neutrons as shown in column 2. For comparison the corresponding values as determined by calorimetry are also shown.

The cerous yield for neutrons relative to gamma rays is determined by dividing the neutron values from the cerous measurements by the neutron values from the calorimetric measurements. The results are 1.0 ± 0.1 for Hole 51 and 1.4 ± 0.2 for Hole 19. The neutron yield is predominantly from recoil protons of energies in the 0.1 to 1 Mev range. The cerous yields for ionizing particles with the same energy loss per unit distance have

¹H. W. Schmitt and R. B. Murray, *Phys. Rev.* **16**, 1575 (1959).

²C. D. Bopp *et al.*, *Solid State Ann. Prog. Rep.* Aug. 31, 1959, ORNL-2829, p 182.

³C. J. Hochanadel and J. A. Ghormley, *J. Phys. Chem.* **21**, 880 (1953).

⁴Measurements by L. C. Bate.

Table 15.1. Neutron Flux in the ORNL Graphite Reactor at 3500 kw

Hole	Flux (neutrons $\text{cm}^{-2} \text{sec}^{-1}$)			
	ϕ_0	$\phi (>0.7 \text{ Mev})$	$\phi (>1.3 \text{ Mev})$	$\phi (>3.0 \text{ Mev})$
	$\times 10^{11}$	$\times 10^{11}$	$\times 10^{11}$	$\times 10^{11}$
51, center (converter)		2.73	1.78	
12 in. from center	0.30	0.92	0.52	
1768		2.01	0.97	
A	0.48 ± 0.03	0.55 ± 0.04	0.24 ± 0.02	
19, can 5		0.71		
can 9		0.87		
can 18		0.84	0.27 ± 0.04	0.08
52		0.65		

Table 15.2. Energy Absorbed in the ORNL Graphite Reactor at 3500 kw as Measured by Ceric Sulfate Dosimetry and Calorimetry

Position	Energy Absorbed (ev g ⁻¹ sec ⁻¹)			
	Ceric Sulfate		Calorimetry	
	Total	Neutrons	Total	Neutrons
	× 10 ¹⁷	× 10 ¹⁷	× 10 ¹⁷	× 10 ¹⁷
Hole 51	1.15 ± 0.04	0.76 ± 0.05	1.14 ± 0.04	0.75 ± 0.04
Hole 19	0.32 ± 0.02	0.26 ± 0.02	0.25 ± 0.02	0.18 ± 0.02

been compared with the yields for gamma rays,⁵ and the result is 1.2 ± 0.1, in agreement with the reactor measurements.

In view of the agreement, ceric sulfate can certainly be used as a relative monitor in a reactor hole previously calibrated by calorimetry. In addition, it is suitable as an approximate dosimeter for energy absorption in uncalibrated holes, providing the hydrogen content of the material to be irradiated is nearly that of water.

THE VARIATION OF ATOMIC DISPLACEMENTS WITH NEUTRON ENERGY

D. Binder

Monoenergetic-neutron irradiations of *n*-type germanium⁶ indicate that the number of atomic displacements does not increase with neutron energy in the range 2 to 5 Mev. Calculations were carried out to determine the effect of forward scattering of neutrons in this energy range. Forward scattering for medium-weight elements becomes more pronounced as the energy increases, which is equivalent to a smaller fraction of the neutron energy imparted to the recoil. This might account for a constancy or even a decrease in the number of displacements with energy.

The angular distributions of scattered neutrons are unknown for germanium, but it was assumed that qualitative results may be obtained by using the data for the neighboring elements copper and zinc.⁷⁻⁹ In Fig. 15.1 the computed values of the average recoil energy \bar{e} divided by the maximum recoil energy e_{max} are shown as a function of the neutron energy E_n . The average recoil energy is

proportional to the product $E_n(\bar{e}/e_{max})$ and this quantity was calculated for E_n equal to 1.8, 3.2, and 4.8 Mev, using the straight fit for \bar{e}/e_{max} in Fig. 15.1. The values are shown in Table 15.3, along with the experimental removal rates in *n*-type germanium.⁶ The average recoil energy is roughly constant, while the removal rates are either constant or show a decrease.

Table 15.3. Relative Values of Average Recoil Energies and Experimental Removal Rates for Three Neutron Energies

E_n (Mev)	$E_n(\bar{e}/e_{max})$ (Mev)	Removal Rate (cm ⁻¹)
1.8 ± 0.1	0.67	21 ± 6
3.2 ± 0.6	0.87	12 ± 3
4.8 ± 0.1	0.77	13 ± 4

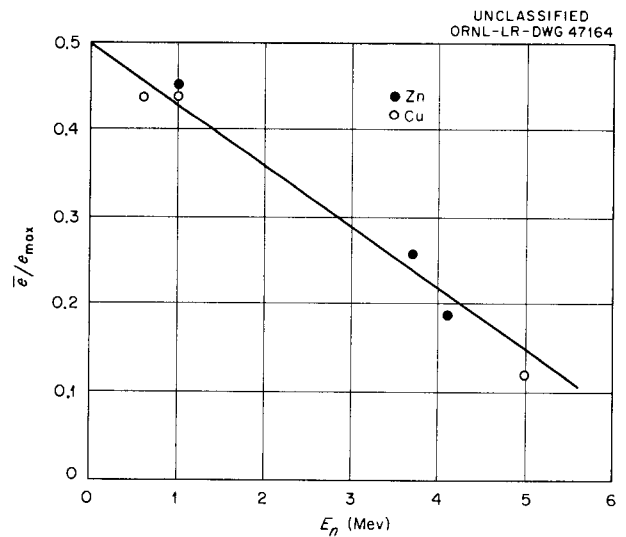


Fig. 15.1. Average Recoil Energy Divided by Maximum Recoil Energy, e/e_{max} , vs Neutron Energy, E_n .

⁵C. J. Hochandel (to be published).

⁶S. L. Ruby *et al.*, *Phys. Rev.* 111, 1493 (1958).

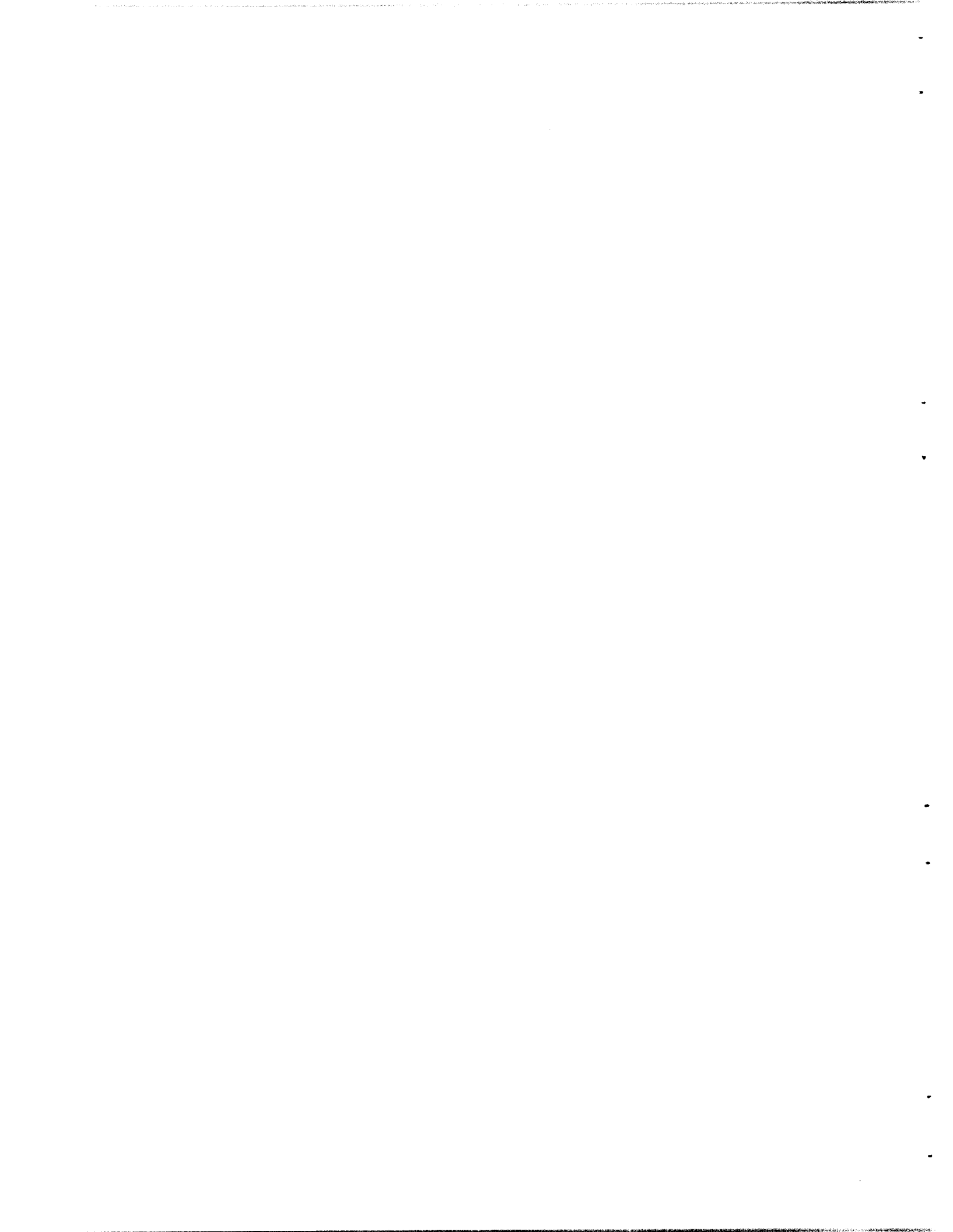
⁷D. J. Hughes and R. S. Carter, *Neutron Cross Sections, Angular Distributions*, BNL-400 (1956).

⁸M. K. Machwe *et al.*, *Phys. Rev.* 114, 1563 (1959).

⁹R. W. Hill, *Phys. Rev.* 109, 2105 (1958).



Part IV
REACTOR MATERIALS



16. HIGH-TEMPERATURE FUEL MATERIALS

O. Sisman

UO₂ IRRADIATION STUDIES - FISSION GAS RELEASE

J. G. Morgan M. T. Morgan
T. W. Fulton H. Robertson

The postirradiation studies of fission gas release from UO₂ have continued, with special emphasis on higher irradiation temperatures. The capsules irradiated in the LITR have provided data on gas release from UO₂ at operating temperatures up to 3150°F and at burnups of up to 22,000 Mwd/metric ton. The UO₂ samples varied in bulk density from 75 to 95% of theoretical. Both stoichiometric (O/U ratios less than 2.02) and nonstoichiometric (O/U ratios greater than 2.02) UO₂ were examined. Radioactive and stable fission gas release data were obtained both on the LITR and ORR irradiations. A total of 33 LITR capsules, 4 ORR capsules, and 1 ETR capsule have been examined.

The fission gas release appears to be quite dependent on density, stoichiometry, and temperature. The effect of burnup on gas release

was not marked over this range. When the O/U ratio was high (>2.1) the gas release was also high and masked out the effect of bulk density. Releases of 25 to 40% were obtained on nonstoichiometric UO₂ at operating temperatures above 2800°F for both the radioactive and stable gases.

The stoichiometric UO₂ was all above 92% of theoretical density and exhibited low gas release (1-2%) below 2800°F. Above 2800°F, however, the radioactive fission gas release increased, based on three capsules. More data are needed to define this trend, but up to 24% Kr⁸⁵ release was obtained on material irradiated at 3100°F. The fission gas release data are summarized in Tables 16.1 and 16.2 for the LITR capsules.¹

¹J. G. Morgan, M. T. Morgan, and M. F. Osborne, *Fission-Gas-Release from UO₂, Interim Report No. 1*, ORNL CF-60-7-11 (Aug. 16, 1960).

Table 16.1. Fission Gas Release from Nonstoichiometric UO₂ (O/U Ratios Greater than 2.02)

Capsule No.	Bulk Density (% of theoretical)	Oxygen to Uranium Ratio	Carbon Content (ppm)	Effective UO ₂ Temperature (°F)	Burnup Estimated from Co ⁶⁰ (Mwd/metric ton)	Immersion Density (g/cc)		Per Cent of Fission Gas Evolved (based on estimated burnup)				
						Preirradiation	Postirradiation	Kr ⁸⁵	Kr ^{85m}	Kr ⁸⁸	Xe ¹³³	Xe ¹³⁵
L-15a	91.43	2.0285	690	1700 ^a	5,900	10.05		0.059	0.019	0.004	0.010	0.004
L-14a	88.7	2.0285	690	1950 ^a	5,100	10.31	9.92	0.072	0.029	0.011	0.014	0.006
L-14b	90.26	2.0285	690	2100 ^b	5,100	10.46	10.04	0.13	0.057	0.019	0.029	0.017
L-2b	84.41	2.1299	2500	2200 ^b	3,600	10.06	10.29	13			9.0	
L-7b	95.15	2.0407		2200 ^b	6,100	10.54		0.075	0.019	0.033	0.066	0.035
L-7xa	94.99	2.0407		2200 ^b	16,000	10.51		0.074			0.16	
L-7xb	94.85	2.0407		2450 ^a	16,000	10.50		4.9			0.85	
L-6a	73.63	2.024		2100 ^b	14,000	10.48	10.47	1.9	0.091		0.293	0.049
L-6b	74.18	2.024		2500 ^b	14,000	10.52	10.53	2.1	0.035		0.132	0.026
L-8a	84.58	2.1326	3000	2300 ^a	7,100	10.19	10.13	4.6			0.007	
L-8b	85.01	2.1326	3000	2500 ^b	7,100	10.18	10.33	18			4.0	
L-11b	85.23	2.1401	630	2400 ^a	22,000	10.46		40			5.3	2.1
L-10b	95.19	2.0407		2800 ^a	1,600	10.48	10.26	16			30	27
L-3a	75.01	2.1178	2400	2800 ^b	4,600	10.66	10.61	1.5			0.42	
L-3b	74.87	2.1178	2400	3000 ^b	4,600	10.66	10.40	24			19	
L-18b	85.19	2.082	3100	3150 ^b	6,400 ^c	10.40	10.47	38			16	

^aEstimated from temperature plots, with emphasis on last month of operation.

^bEstimated temperature, from calculations and comparisons with other capsules.

^cCalculated from estimated neutron flux.

Table 16.2. Fission Gas Release from Stoichiometric UO₂ (O/U Ratios Less than 2.02)

Capsule No.	Bulk Density (% of theoretical)	Oxygen to Uranium Ratio	Carbon Content (ppm)	Effective UO ₂ Temperature (°F)	Burnup Estimated from Co ⁶⁰ (Mwd/metric ton)	Immersion Density (g/cc)		Per Cent of Fission Gas Evolved (based on estimated burnup)				
						Preirradiation	Postirradiation	Kr ⁸⁵	Kr ^{85m}	Kr ⁸⁸	Xe ¹³³	Xe ¹³⁵
UO ₂ -1-1	96	2.008		1750 ^a	4,000	10.57	10.76		0.026		0.0091	0.0024
UO ₂ -1-2a	96	2.008		1750 ^a	11,000	10.58	10.49			0.01	0.028	0.008
UO ₂ -1-2b	97	2.008		2000 ^b	11,000	10.63	10.62			0.025	0.033	0.012
L-17a	93.69	2.002		1800 ^a	10,600	10.43	10.52	0.94	0.04	0.04	0.20	0.05
L-17b	93.80	2.002		2000 ^b	10,600	10.38	10.46	3.1	0.13	0.24	1.3	0.32
L-16a	94.35	2.0052	70	1900 ^a	2,900	10.48	10.66	0.20			0.078	0.021
L-16b	94.38	2.0052	70	2050 ^b	2,900	10.47	10.58	0.033 ^c		<0.075 ^c	0.033 ^c	0.027 ^c
L-13a	93.68	2.0158	6500	1900 ^a	~ 11,000 ^d	10.60	10.67	0.21			0.034	
L-13b	92.07	2.0158	6500	2200 ^b	~ 11,000 ^d	10.60	10.68	2.0			0.057	
L-4a	92.07	2.0158	6500	2300 ^b	14,000	10.33	10.49	0.22	0.011	0.021	0.028	0.0085
L-4b	93.35	2.0158	6500	2500 ^b	14,000	10.56	10.41	0.54	0.012	0.020	0.04	0.0075
L-25a	95.17	2.020	200	2150 ^a	5,100	10.69		0.15			0.039	0.019
L-25b	94.90	2.020	200	2500 ^b	5,100	10.73		0.15			0.22	2.0
L-16xa	93.98	2.0052	70	2700 ^b	3,200	10.46		1.9				
L-16xb	94.35	2.0052	70	3000 ^a	3,200	10.48		6.4				
L-17xa	94.62	2.0052	70	2800 ^b	3,100	10.48	10.57				30	4.5
L-17xb	94.83	2.0052	70	3100 ^a	3,100	10.45	10.54	24			61	20

^a Estimated from temperature plots, with emphasis on last month of operation.

^b Estimated temperature, from calculations and comparisons with other capsules.

^c Probably low, since postirradiation examination indicated a small leak in the capsule during operation.

^d Calculated from estimated neutron flux.

The microstructure changes of UO_2 as the result of these irradiations have been of two types: (1) The low-density (75% of theoretical) material sintered during irradiation, and the structure be-

came better defined. (2) The higher-temperature irradiations of the dense material showed some grain growth and preferred orientation at 2700°F (see Fig. 16.1).

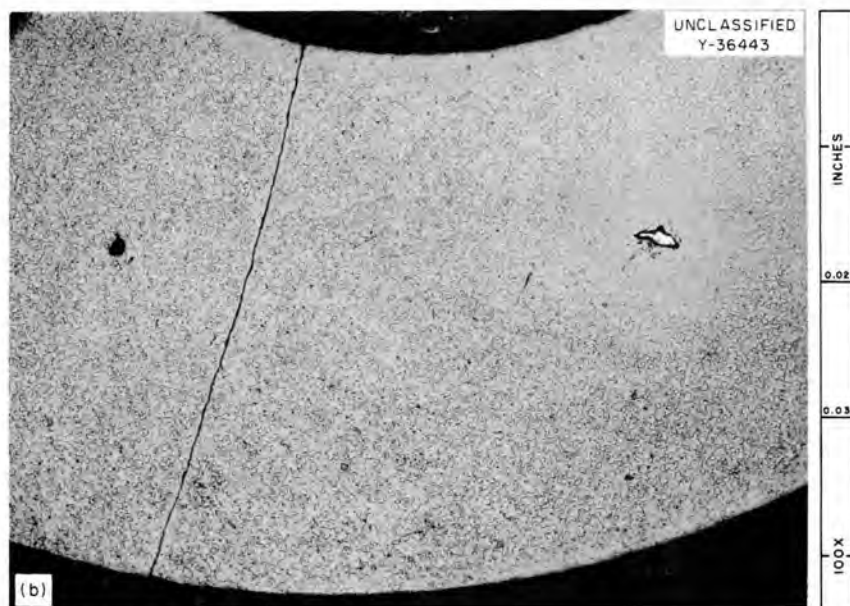
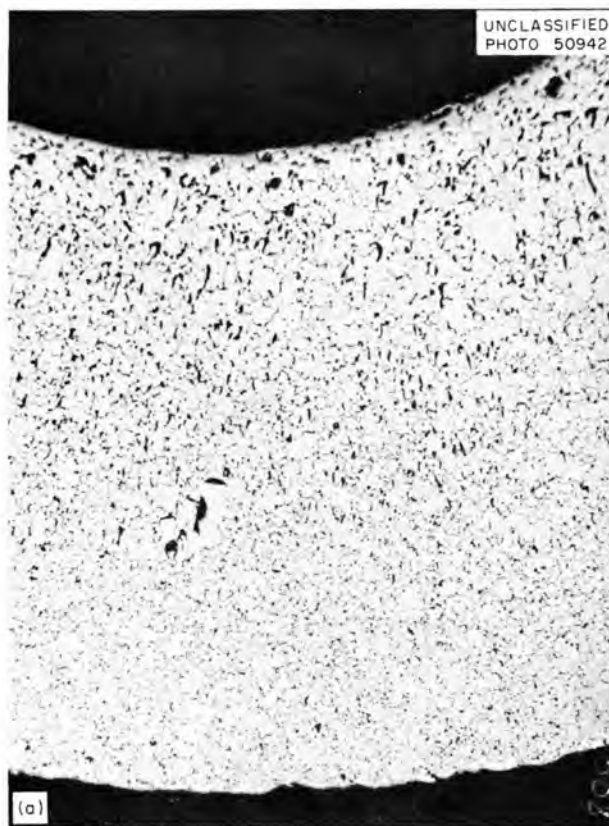


Fig. 16.1. Capsule 16Xa Containing 94% Theoretical Density UO_2 , Internal Irradiation Temperature 2700°F. (a) Before irradiation; (b) after irradiation. 100X. Reduced 30%.

**UO₂ IRRADIATION STUDIES - EGCR
PROTOTYPE FUEL**

J. G. Morgan J. W. Gooch
T. W. Fulton M. T. Morgan
M. F. Osborne

The first set of eight prototype fuel capsules, irradiated in the ORR, were examined. Both hollow and solid pellets of UO₂ were canned in 0.020-in.-wall stainless steel tubing and duplicated the diameter and operating temperature of the EGCR fuel element.

There was no evidence of significant distortion after operation at a cladding temperature of 1600°F and burnups of up to 3000 Mwd/metric ton. Post-irradiation diameter and profile measurements also showed little change. Gamma radioactivity scans of the capsules (Fig. 16.2) showed no evidence of nonuniform fuel distribution.

The possible pressure buildup in EGCR fuel elements from alkali metals having low boiling points has made it desirable to measure this pressure contribution in the prototype capsules. The pressure was measured in the hot cell as one of the prototype capsules was heated up to 1700°F. The results of the experiment indicated no significant contribution from high-temperature vaporization. The pressure measurement was carried to 1650°F during the first heat-up, then cooled and reheated to 1700°F. The deviation from a straight line on a plot of pressure vs temperature (Fig. 16.3) is about 4 psi at 1650°F (about 3% of the total pressure.) Since the cooling curve follows the second heat-up on a straight line, it may be assumed that the slight increase during the first heat-up was due to additional noble gas release from the UO₂.

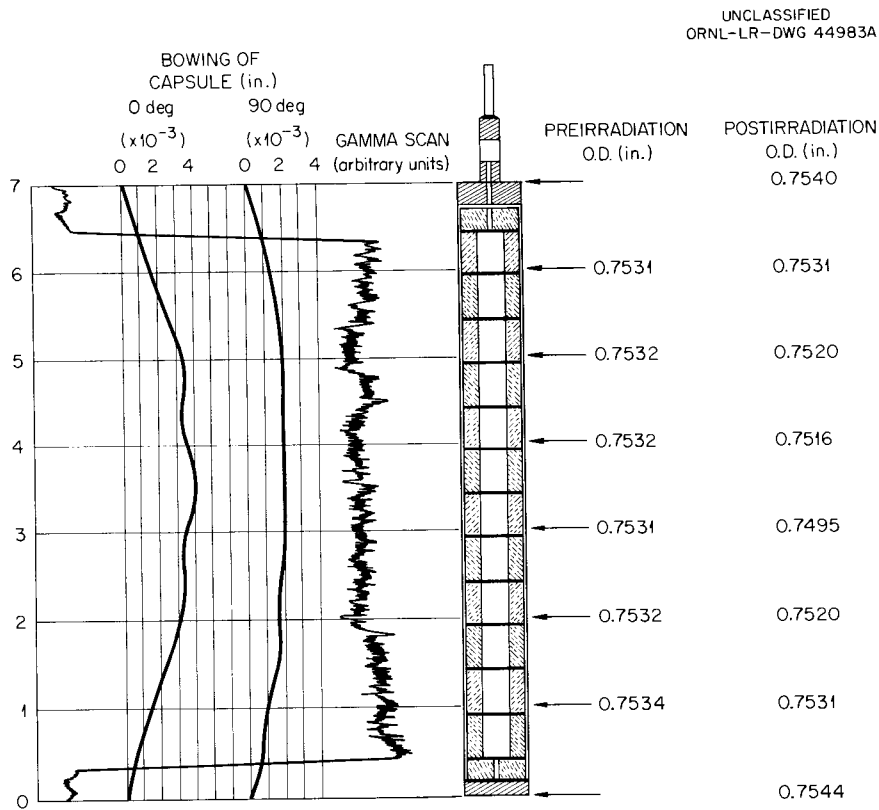


Fig. 16.2. Results of Dimensional Measurements and Gamma Activity Scan of ORR Capsule O-1.

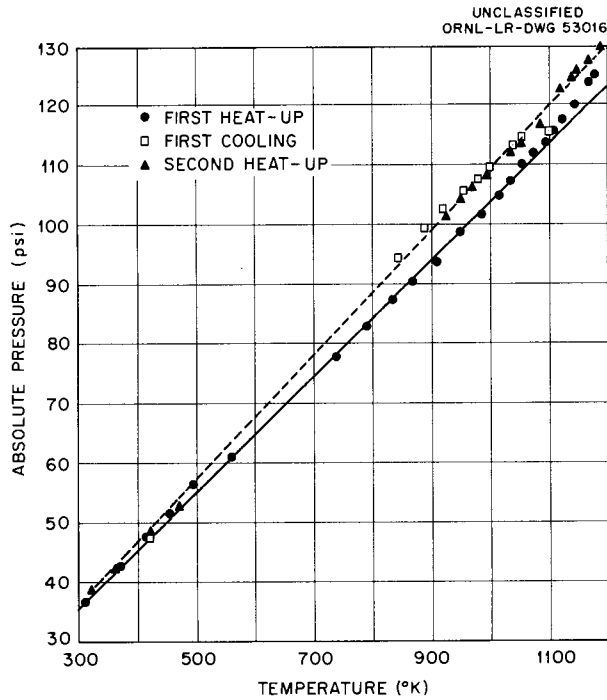


Fig. 16.3. High-Temperature Pressure Measurement, Capsule O-6.

ADVANCED FUEL MATERIALS STUDIES

P. E. Reagan C. D. Baumann
J. G. Morgan

The closed-cycle facility, ORR-B-9, has been placed in operation,² and testing of advanced fuel materials and coatings is scheduled in this facility in support of the Gas-Cooled Reactor Program. The first two experiments in the series contained two hollow pellets each of 95%-dense UO_2 canned in graphite and coated with Si-SiC. Previous tests in the laboratory have shown this coating to be oxidation resistant at 1800°F in air, and the coating-graphite-can combination had withstood internal pressures of 100 psi at those temperatures.

²P. E. Reagan, *Solid State Ann. Prog. Rep. Aug. 31, 1959*, ORNL-2829, p 198.

During irradiation the samples generate nearly 1000 w per cubic centimeter of fuel and are cooled by nitrogen passed directly over the sample. The coating temperature is maintained at 1500°F. Fission gas escape from the samples is detected by sampling the cooling gas stream.

The coating on one of the samples in the first experiment failed shortly after reactor startup, as evidenced by excessive fission gas activity in the coolant gas. The samples in the second experiment withstood 16 thermal cycles (caused by reactor shutdown) and a neutron exposure of 2.2×10^{20} nvt thermal. On the 17th thermal cycle one of the samples failed. Coatings of this type on previous tests at low temperature have remained intact after 5×10^{20} nvt. This failure is attributed to the unique thermal cycling (by fission heating from the inside) during these irradiations.

Postirradiation examinations were made on a ceramic fuel assembly irradiated in the MTR. The fuel body was a cylinder of UC_2 dispersed in graphite. Surrounding the fuel cylinder was a can of graphite (National Carbon type R-0020) with a permeability of about 10^{-4} cm²/sec (helium at room temperature). The threaded graphite end plug was sealed into the can with Si-SiC. The fuel, generating 300 w/cm³, was irradiated at a calculated center temperature of 3600°F. Thermocouples monitored the graphite can wall at 1300°F. Two such elements were tested together. Figure 16.4 shows the assembly after irradiation. One fuel cylinder was removed from its graphite can and examined for dimensional stability. The graphite can itself showed no external dimensional changes. After a burnup of 5.6% U^{235} atoms, the fueled graphite cylinder showed an average diameter decrease of 3.8%. The length increased by 3.5%. The cylinder appeared whole and uncracked.³ Fuel and fission product migration studies are planned for both the fuel matrix and the graphite can.

³J. G. Morgan and M. F. Osborne, *Irradiation Effects on UC_2 Dispersed in Graphite (ORNL-MTR-48-1), Interim Report No. 1*, ORNL CF-60-6-78 (Aug. 18, 1960).

UNCLASSIFIED
Y34652

Fig. 16.4. Irradiated Fuel Assembly, Exploded View.

INSTANTANEOUS FISSION GAS RELEASE EXPERIMENT

R. M. Carroll J. G. Morgan
C. D. Baumann G. S. Suessman⁴

A facility has been constructed in which fuel materials may be irradiated to determine their ability to retain gaseous fission products under a variety of operating conditions. The fuel is heated by its own fission power, which is regulated by moving the fuel into or out of the reactor neutron flux. The temperature of the fuel is regulated by air cooling. Fission gas from the fuel is entrained in an inert sweep gas and carried outside the reactor for analysis. The flux at the fuel may be determined by argon activation. To date, two samples of ceramic fuel, $\text{ThO}_2\text{-UO}_2$ and UO_2 , have been irradiated in the facility.

⁴On loan from Kernreaktor Co., Karlsruhe, Germany.

The facility and results of the $\text{ThO}_2\text{-UO}_2$ irradiation have been described in previous reports.⁵ The results of the UO_2 irradiation, summarized here, are given in detail in another report.⁶

Thermal Conductivity of UO_2

The UO_2 sample consisted of two high-density thin plates with thermocouples sandwiched between them and pressed against the outer surfaces. The plates were wide compared with their thickness, so edge losses could be neglected for heat and fission gas evolution. Because the plates were thin and the enrichment low, the flux depression through the plates was small and uniform power generation could be assumed. The thermal conductivity was determined by the temperature differential for uniform power generation in an infinite slab, which is

$$\Delta T = \frac{L^2 Q}{2K},$$

where Q is the power generated per unit volume, L the half thickness of the plate, K the thermal conductivity of the plate, and ΔT the temperature difference between the center and the surface of the plate.

The power generated in the fuel can be calculated if the neutron flux is known, since gamma heating is a small fraction of the total power. The flux is determined by substituting argon for helium as a sweep gas and measuring the argon activation. Because the volume of the fuel capsule is large compared with the positioning tube, the activation of the argon occurs primarily in the space surrounding the fuel. By varying the flow rate, the exposure time of the argon can be regulated, and several measurements of the same flux may be made. This type of measurement will give the instantaneous neutron flux to a precision of about 10%.

The flux measurements need be made only once for a particular fuel sample, since the power in the fuel is proportional to the flux, and the temperatures (for a given air cooling flow) are proportional to the power. By correlating the fuel

⁵R. M. Carroll and C. D. Baumann, *Solid State Ann. Prog. Rep.* Aug. 31, 1959, ORNL-2829, p 193-99.

⁶GCR Quar. Prog. Rep. June 30, 1960, ORNL-2964, p 167-74.

temperatures with the measured flux, the flux may be determined at any time by a temperature measurement.

The variation of thermal conductivity with temperature can be established by regulating the cooling air to change the temperature while the power is maintained constant. In the 550–1050°C range the variation in thermal conductivity with absolute temperature is

$$K = K_0 e^{-1.21T \times 10^{-3}}$$

No change in thermal conductivity of more than 15% (the instrument limit) was observed up to an exposure of 1.2×10^{20} nvt.

Fission Gas Release

The fractional release of krypton and xenon from the fuel increased by two orders of magnitude in six months. A release of stored energy was also observed at the end of this period. The energy release began at 500–600°F and amounted to 4–6 cal/g. This suggests that the increase in fission gas release was due to oxidation of the fuel rather than irradiation damage, since stored

energy has been reported only in UO_2 with an O/U ratio of 2.08 or more. The UO_2 used in this experiment originally had an O/U ratio of 2.01, but trace amounts of oxygen in the sweep gas could have increased the O/U ratio of the fuel. It is also known that an increase in O/U ratio results in an increased gas release.

The oxidation of the UO_2 was confirmed by substituting a sweep gas which was 3% H_2 –97% He, so that the UO_2 would tend to be reduced. The release of fission gas was reduced by a factor of 3 in one week with this treatment. At that time it was obvious, from temperature relations, that the thin plate sample had broken and perhaps crumbled, and the experiment was terminated.

The next experiments will be performed with thin plates of UO_2 assembled as before, with the object of determining the effect of grain size on the irradiation performance. Fission gas evolution, thermal conductivity, and electrical resistivity will be measured as a function of temperature and irradiation. A topical report is being issued for the first two samples.

17. RADIATION METALLURGY

O. Sisman

BRITTLE FRACTURE OF METALS - ANNEALING STUDIES

R. G. Berggren T. J. Humphries J. L. Snow¹

Isothermal annealing studies were conducted at several temperatures on tensile and impact specimens of an ASTM A-212 Grade B steel irradiated in the ORR pool-side facility to doses of 1 to 3×10^{19} nvt. The results of impact tests on these specimens are given in Fig. 17.1 as per

¹Co-op student, Auburn University.

cent recovery of transition temperature at each annealing temperature. Annealing times were $1\frac{1}{2}$ hr for all specimens. These results have been corrected for variations in fast-neutron exposure according to the curve shown in Fig. 17.2, data for which were obtained from LITR, ORR, and MTR irradiations. Some recovery was observed for annealing temperatures as low as 400°F, and 90% recovery was observed for annealing temperatures of 850°F. An interesting feature of this data is the anomaly between 550 and 600°F. This is the same temperature range in which a change of behavior is observed for the tensile specimens, to be discussed later.

The tensile test results are shown in Figs. 17.3 and 17.4. The load-elongation curves, Fig. 17.3, after irradiation to 1.5×10^{19} nvt for several annealing temperatures show a progression of effects. The large pre-yield-point plastic strain observed for irradiated but unannealed specimens decreased for increasing annealing temperatures. The large difference between upper and lower yield stresses dropped to zero at 400°F annealing temperature and approached unirradiated values for annealing temperatures above 600°F. Work hardening was small or nonexistent for lower annealing temperatures but was recovered for higher annealing temperatures. The uniform elongation (strain before necking) was very small for low annealing temperatures and was recovered

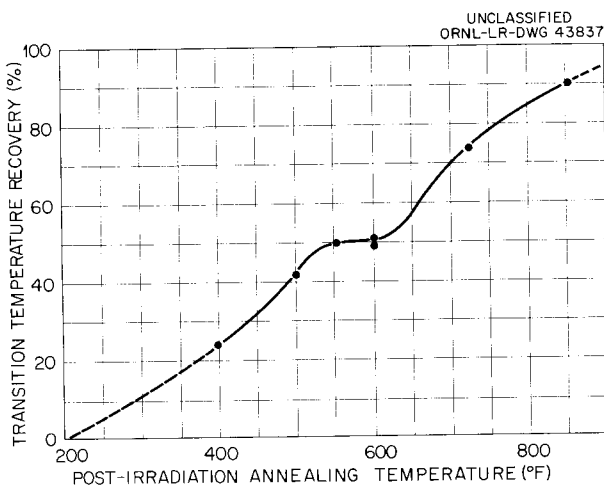


Fig. 17.1. Effect of Postirradiation Annealing on Transition Temperature Recovery of an ASTM A-212 Grade B Steel (Item 92).

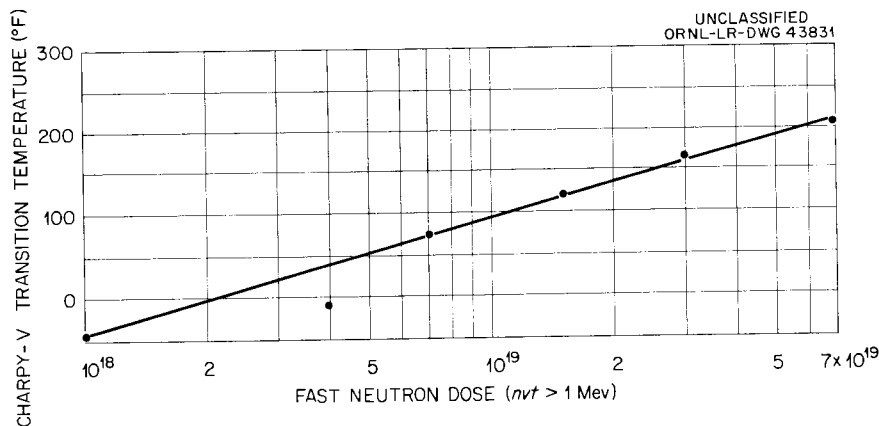


Fig. 17.2. Charpy-V Impact Transition Temperature of Irradiated Carbon-Silicon Steel ASTM A-212 Grade B (Item 92).

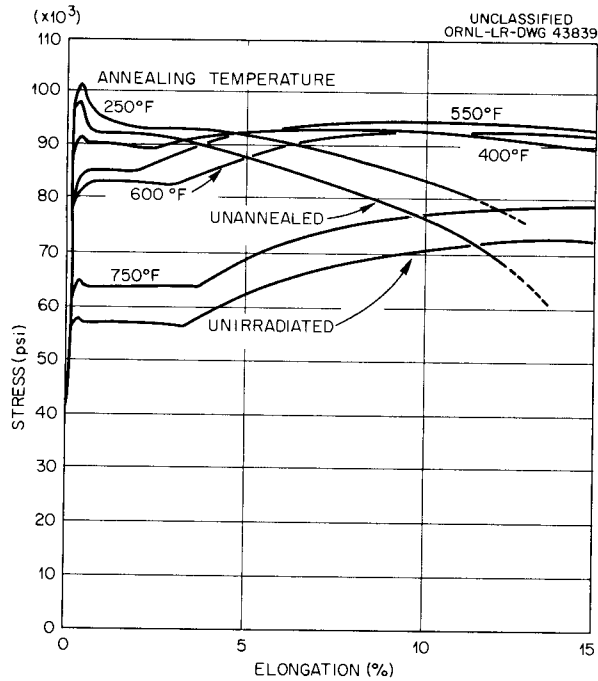


Fig. 17.3. Load-Elongation Curves for Postirradiation-Annealed ASTM A-212 Grade B Carbon Steel, Hot-Rolled (Item 92).

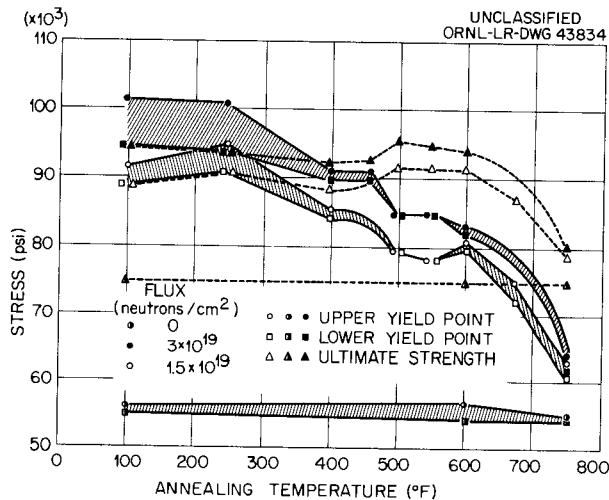


Fig. 17.4. Postirradiation Annealing of an ASTM A-212 Grade B Steel (Item 92).

at higher annealing temperatures. Annealing at 750°F resulted in about 80% recovery of the irradiation-induced property changes. This progression of behavior changes is depicted in Fig. 17.4. Data are also included for specimens irradiated to 3×10^{19} nvt, twice the exposure of

the specimens of Fig. 17.3. At 250°F recovery was very small and may even be negative. Between 250 and 400°F, slight recovery was observed. Increasing the annealing temperature to 465°F resulted in no further recovery. In the temperature interval between 465 and 500°F there was a decrease in yield stress but an increase in ultimate strength, and the "drop in load" at yielding became zero. There was little or no change in recovery between 500 and 550°F. At 600°F the final stages of recovery were observed. It is apparent that the recovery processes vary considerably with temperature and that several mechanisms of recovery are involved. There may be as many as five stages of recovery in this particular steel.

The annealing recovery of a Swedish steel, designated 21YY (ref 2), similar to ASTM A-212 Grade B but of higher manganese content, appeared to be much simpler than the above processes. The load-elongation curves for this steel are shown in Fig. 17.5. While recovery seems to occur at lower temperatures for this steel, it should be noted that the yielding behavior after

²Composition of Swedish 21YY steel, Degerfors Järnverks AB, heat No. M-6896: C, 0.13%; Si, 0.34%; Mn, 1.66%; P, 0.011%; S, 0.033%; Cr, 0.07%; Ni, 0.05%; Cu, 0.15%; Al (soluble), 0.027%.

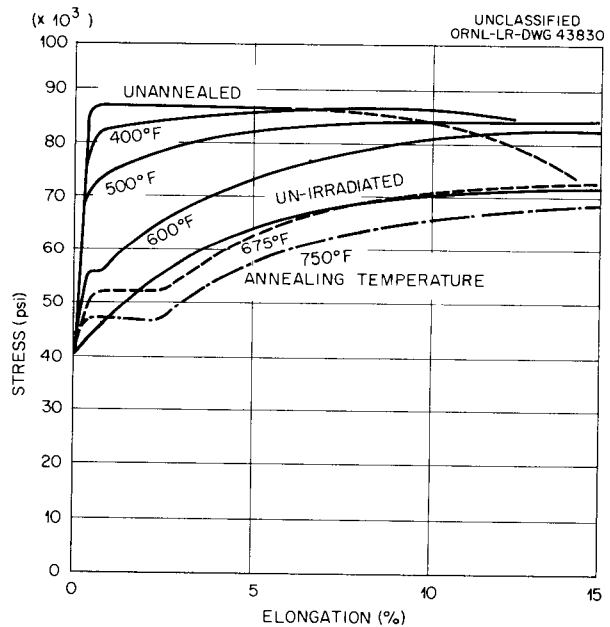


Fig. 17.5. Load-Elongation Curves for Postirradiation-Annealed Carbon Steel 21YY, Normalized (Item 132).

irradiation and annealing is not the same as it had been before irradiation. This steel has shown little or no region of low work-hardening rate before irradiation, but after irradiation and a 750°F anneal there was several per cent yield point strain before work hardening became apparent.

There is some evidence³ that the recovery behavior of a steel irradiated at an elevated temperature cannot be readily predicted from recovery data obtained on steels irradiated at lower temperatures. Annealing may not restore all the preirradiation properties; and although annealing at 900°F may be required to accomplish nearly complete recovery, adequate or even superior properties may be obtained by partial recovery at lower temperatures. It is recognized that the 1½-hr annealing periods used in this study are much shorter than would be practical for a reactor pressure vessel, and, therefore, longer annealing times should be studied.

BERYLLIUM IRRADIATION STUDIES

J. R. Weir⁴ W. W. Davis
 V. R. Bullington⁴ P. Dragoumis⁵
 D. Gates

Beryllium has for many years been attractive to reactor designers as a moderator for low-temperature reactors. Recent interest in gas-cooled reactors has resulted in the investigation of beryllium as a possible canning material for fuel

elements. This interest is warranted because of the potential economic advantage of using low-enrichment fuel clad with beryllium, which has a very low thermal-neutron cross section.

One of the potential problems involved with the use of beryllium in this high-temperature application is the effect of the (n,2n) and (n,α) reactions and the resulting internal gas generation on the physical and mechanical properties of beryllium metal. According to Ells and Perryman⁶ the nuclear reactions and related physical data pertinent to this investigation are as shown in Table 17.1. Earlier investigators reported somewhat different threshold energies and cross sections for these reactions. Calculations by Redding and Barnes⁷ indicated that the compositions of the gases formed at 10²⁰ nvt would be similar to those predicted by Ells and Perryman, but that the total gas produced per cubic centimeter of beryllium would be 0.146 cc instead of approximately 0.23 cc. The effects of the gases may

³R. G. Berggren *et al.*, *Solid State Ann. Prog. Rep.* Aug. 31, 1959, ORNL-2829, p 213.

⁴On loan from Metallurgy Division.

⁵On loan from General Nuclear Engineering Corp.

⁶C. E. Ells and E. C. W. Perryman, *J. Nuclear Materials* 1, 73 (1959).

⁷G. B. Redding and B. S. Barnes, *Neutron-Induced Nuclear Reactions in Solids Resulting in Gas Formation*, AERE-M/R-1750 (1955).

Table 17.1. Nuclear Reactions in Beryllium

Reaction	Threshold Energy (Mev)	Cross Section (mb)	Gas Produced* at 10 ²⁰ nvt (>1 Mev)
(n,2n) Be ⁹ + n → Be ⁸ + 2n, Be ⁸ → 2He ⁴	2.71	600	He ⁴ , 0.2
(n,α) Be ⁹ + n → He ⁴ + He ⁶ , He ⁶ $\xrightarrow{\beta^-}$ Li ⁶ , Li ⁶ + n → He ⁴ + H ³ , H ³ $\xrightarrow{\beta^-}$ He ³ , He ³ + n → H ¹ + H ³	0.71	80	He ⁴ , 0.03; H ₂ ³ + H ¹ H ³ , 0.006

*Cubic centimeters of gas per cubic centimeter of beryllium.

be to cause swelling by the precipitation and growth of bubbles. In addition, the mechanical properties may be deleteriously affected.

In order to investigate the effects the gas generation would have on beryllium irradiated while at an elevated temperature, an experiment was prepared and inserted in the ORR core position B-8. The constructional details of the experiment have been described previously.⁸ Briefly, the experiment consisted of an aluminum can sized to fit an ORR fuel element position with an access tube to the pool surface to accommodate furnace leads, thermocouples, etc. The aluminum can contained 21 beryllium sheet specimens clad in stainless steel jackets. Each specimen was contained in a small resistance furnace and was thermocoupled to allow temperature control.

Experimental difficulty with the furnace leads caused removal of the experiment before the desired exposure was reached; however, the specimens received sufficient neutron exposure to warrant detailed postirradiation examination. The temperature of the specimens was 500 to 600°C as measured by Chromel-Alumel thermocouples welded to the outside of the stainless steel jackets approximately 0.015 in. from the beryllium specimens. The neutron exposure was measured with neptunium and sulfur monitors and reached a level of approximately 1.5×10^{20} *nvt* (> 0.6 Mev) in 24 days, which should produce approximately 0.2 cc of gas (STP) per cubic centimeter of beryllium.

Postirradiation density, dimensions, hardness, and bend strength measurements have been completed. The density measurements indicate that swelling of 1.5 to 5% occurred during the exposure. The data of Ells and Perryman obtained by post-irradiation annealing of beryllium specimens irradiated at approximately 50°C indicate a density decrease of 1.5% on annealing at 595°C for a time period equivalent to the duration of the ORNL high-temperature irradiation. This beryllium had received a neutron dose of 10^{22} *nvt* (> 1 Mev) in the MTR. This is roughly a factor of 100 greater exposure than in the ORNL experiment. The reason for this great a difference between the results of the two types of experiment is not apparent at present, although a greater density

decrease would be expected for beryllium irradiated at high temperature than for postirradiation annealing of beryllium having the same exposure.

The hardness and bend strength measurements indicate that there was no significant hardening (or strengthening) produced by the irradiation. The ductility, as measured by the deflection at fracture during the bend test, was not changed.

A second high-temperature irradiation experiment has been performed in an attempt to reproduce the swelling results of the experiment described above. This experiment operated entirely satisfactorily during the exposure and has been removed from the ORR. Postirradiation examination of the 24 beryllium specimens from this experiment is under way.

ZIRCALOY-2 TEST PROGRAM

J. T. Stanley W. E. Brundage

An experiment is being constructed for determination of the stress-rupture strength of Zircaloy-2 during irradiation in the pool-side position P-6 of the ORR. This experiment is similar to the Inconel tube burst tests previously described.⁹ Three major changes in experimental conditions are necessary for the Zircaloy experiment, namely atmosphere, stress level, and temperature interval.

The temperature range of interest for Zircaloy-2 experiments is 500 to 700°F. These are much lower temperatures than have been used in the previous Inconel experiments. In order to maintain these low temperatures in the presence of the high gamma heating, it is necessary to place a water-cooled stainless steel tube inside the Zircaloy tube. A mockup of the proposed specimen has shown that an operating temperature at least as low as 700°F should be possible. Higher stress levels will be needed for this experiment, but this is not expected to produce any great experimental difficulties.

Atmosphere control is the major experimental problem of the Zircaloy experiment. At the temperature of these tests Zircaloy-2 only reacts very slowly with oxygen and nitrogen, but the reaction with hydrogen is rapid. Opinions vary on how much hydrogen is detrimental to the mechanical properties of Zircaloy, but it seems desirable to try to

⁸GCR *Quan. Prog. Rep. Dec. 31, 1959, ORNL-2888, p 133.*

⁹J. C. Wilson *et al., Solid State Ann. Prog. Rep. Aug. 31, 1958, ORNL-2614, p 106.*

SOLID STATE ANNUAL PROGRESS REPORT

keep total hydrogen pickup below 10 ppm during the course of the experiment.

The experiment can will be filled with helium gas and will remain sealed during the experiment. The impurities originally present in the helium are insignificant, but outgassing of materials in the experiment can may contribute appreciable contamination. The sources of outgassing will include adsorbed water vapor and hydrocarbons and possibly some hydrogen dissolved in various metals. The outgassing properties of the various components of the experiment are now being studied with the aim of discovering procedures to minimize this problem.

INCONEL TUBE BURST TESTS

N. E. Hinkle W. E. Brundage
 J. C. Zukas

Data previously reported^{10,11} indicate a reduction in the rupture life of Inconel at 1500°F in air

by a factor of 3 to 5 when subjected to neutron bombardment in either the MTR or the ORR. A hypothesis to explain these results was presented. This hypothesis suggests that the transmutation of the boron to produce helium during neutron bombardment gives rise to void formation which weakens the metal. The present testing program is aimed at determining whether the presence of boron is responsible for the observed decrease in rupture life.

Six special heats of Inconel, containing different concentrations of natural boron (or the B¹⁰ isotope) (see Table 17.2), have been fabricated into specimens for this investigation. Due to the limited

¹⁰J. C. Wilson *et al.*, *Solid State Ann. Prog. Rep.* Aug. 31, 1958, ORNL-2614, p 106.

¹¹N. E. Hinkle *et al.*, *Solid State Ann. Prog. Rep.* Aug. 31, 1959, ORNL-2829, p 214.

Table 17.2. Boron Concentration in Inconel and Other Tube Burst Material

Material	Manufacturer	Heat No.	Boron Concentration* (ppm)		
			Soluble	Insoluble	Total
MTR Inconel	International Nickel Co.	NX 8962	30	1	31
CX-900 Inconel	International Nickel Co.	NX 5757	41	1	42
Special Inconels					
No. 1	International Nickel Co.	0B			< 10
No. 2	International Nickel Co.	2B			20
No. 3	International Nickel Co.	10B			100
No. 4	International Nickel Co.	4B11		(B ¹¹ enriched)	40
No. 5	International Nickel Co.	6B11		(B ¹¹ enriched)	60
No. 6	International Nickel Co.	6B10		(B ¹⁰ enriched)	60
Type 304 ELC stainless steel	Manufacturer unknown		16	1	17
Type 304 stainless steel	Superior Tube Co.	23999X	10	6	16
INOR-8	Westinghouse	M-1664	8	6	14

*The soluble and insoluble analyses were supplied by Cyrus Feldman of ORNL. Where only total concentration is listed, the figure was supplied by the manufacturer and is nominal.

quantity of these materials (only five or six specimens per heat are available for in-pile experiments), testing has been delayed until installation of instrumentation for improved temperature control is complete. In the interim, testing of the original Inconel test material (INCO heat No. NX 8962) has continued. One of these specimens, No. 9-4 in Table 17.3, was stressed out-of-pile after an irradiation of approximately 19,000 Mwhr at 1500°F. The rupture life of 117 hr is reasonably close to the average in-pile rupture life of 95 hr, and to the rupture life of 110 hr observed when specimens are irradiated for periods up to 8000 Mwhr at 1500°F prior to in-pile stressing. This suggests the possibility that the reduced rupture life might be observed in Inconel and similar materials in post-irradiation testing programs.

A set of specimens from another heat of Inconel (INCO heat No. NX 5757) has been tested at 1500°F in air at stresses from 3000 to 5000 psi.

The in-pile rupture lives for this material, listed in Table 17.3, are a factor of nearly 2 lower than the out-of-pile rupture lives. The out-of-pile data¹² indicate that this heat is considerably weaker than the usual Inconel. The unusual scatter observed in the in-pile results at 4000 psi is unexplained.

It is planned to perform low-flux, short-time irradiation of metallographic specimens of Inconel coated with an alpha-sensitive emulsion. This technique¹³ may yield information concerning the distribution of boron (specifically the B¹⁰ isotope). Other nickel-base and ferrous alloys of interest will be inspected by this method if the tests on Inconel prove informative.

¹²Unpublished data received from C. R. Kennedy of the Metallurgy Division, ORNL.

¹³B. A. Thompson, *Trans. Met. Soc. AIME* 218, 228 (1960).

Table 17.3. Effect of Neutron Bombardment on the Rupture Life of Inconel at 1500°F in Air: ORR Experiments

Material	Specimen No.	Stress (psi)	Irradiation Dose at Rupture ^a (Mwhr)	Rupture Life (hr)
CX-900 Inconel	14-4	3000	8,860	443
	14-7	3000	8,620	431
	14-8	3000	6,000	299
	7-5	4000	1,800	113 ^b
	7-6	4000	990	62
	9-3	4000	300	18.5
	14-6	4000	3,620	181
	14-9	4000	2,160	108
	14-10	4000	700	35
	14-1	5000	1,320	66
MTR Inconel	14-5	5000	1,400	70
	9-4	5000	~ 19,000	117 ^c
	11-5	5000	2,500	173 ^d
	11-6	5000	1,460	73 ^e
	11-7	5000	1,860	141 ^d
	11-8	5000	1,820	91

^aThe thermal and fast (>1 Mev) integrated neutron doses may be estimated by multiplying the megawatt-hours by 4×10^{15} and 1.3×10^{15} , respectively.

^bFailed during a high-temperature excursion.

^cStressed out-of-pile after irradiation at 1500°F.

^dStress applied approximately 48 hr before neutron bombardment began.

^eHigh temperature suspected.

SOLID STATE ANNUAL PROGRESS REPORT

STAINLESS STEEL AND INOR-8
TUBE BURST TESTS

N. E. Hinkle J. W. Woods¹⁴
W. W. Davis J. C. Zukas

Type 304 stainless steel is being used for the fuel canning material in the EGCR. The stress-rupture life is being studied to see the effect of irradiation on the potential life expectancy of the fuel element. As shown in Table 17.2, the stainless steels contain less than half as much boron as does the Inconel. Tests at 1500°F in air were performed on a few specimens of type 304 ELC stainless steel and of type 304 stainless steel (Superior Tube Company heat No. 23999X). The

results on the type 304 ELC, shown in Table 17.4, when compared with the rupture results usually reported, indicate a factor of 2 decrease in the rupture life at stresses of 2500 and 3500 psi. Results on type 304, when compared with control tests on the same material,¹⁵ also indicate a factor of 2 decrease in the rupture life. Since these initial tests, the type 304 test program has received increased emphasis in order to provide design data for various reactor projects, including EGCR. As part of this program, one ORR experiment was devoted to testing type 304 stainless steel at 1300°F at stresses from 9000 to 13,000 psi. These results indicate no change in rupture

¹⁴On loan from Metallurgy Division.

¹⁵Unpublished data received from J. W. Woods and J. T. Venard of the Metallurgy Division.

Table 17.4. Effect of Neutron Bombardment on the Rupture Life of Stainless Steel at 1300 and 1500°F in Air: ORR Experiments

Material	Specimen No.	Temperature (°F)	Stress (psi)	Irradiation Dose at Rupture (Mwhr)	Rupture Life (hr)
304 ELC	9-1	1500	2,500	~ 11,000	786
	9-2	1500	2,500	7,300	456
	11-3	1500	2,500	~ 15,500	910
	11-4	1500	2,500	~ 11,500	700
	7-1	1500	3,500	4,860	304
	7-2	1500	3,500	4,000	250
	11-1	1500	3,500	8,980	449
	11-2	1500	3,500	6,160	308
	11-10	1500	3,500	5,440	272
	304	7-3	1500	4,000	~ 12,000
9-6		1500	4,000	~ 8,900	673
9-7		1500	5,000	5,400	337
9-8		1500	5,000	8,300	518
15-1		1300	9,000	~ 23,500	1680
15-5		1300	9,000	~ 26,000	> 1850*
15-9		1300	9,000	~ 26,000	> 1850*
15-4		1300	11,000	8,200	512
15-7		1300	11,000	7,700	480
15-10		1300	11,000	7,400	462
15-2		1300	13,000	2,100	130
15-6		1300	13,000	2,300	144
15-8		1300	13,000	1,950	122
15-3		1300	13,000	~ 11,900	197**

*Test terminated.

**Stressed after 8700 Mwhr of neutron bombardment at 1300°F.

life when compared with preliminary out-of-pile data on the same material.¹⁵ Testing of this material is presently in progress at temperatures of 1500 and 1600°F.

Five specimens of INOR-8 were tested along with some of the stainless steel specimens. This material contained about one-fourth as much boron as did the Inconel. As shown in Table 17.5, the in-pile results at 1500°F in air were almost identical to the out-of-pile data. It is of importance to note that the out-of-pile rupture life reported here is abnormally low and not representative of INOR-8.

NIOBIUM TUBE BURST TESTS

N. E. Hinkle J. W. Woods¹⁴
 W. E. Brundage J. C. Zukas

A test program, capable of in-pile stress-rupture testing in the temperature range of 1700 to 2100°F in a high-purity helium atmosphere, has been initiated for studies on refractory-metal-base alloys. For the first refractory metal experiments an alloy of niobium-1% zirconium was selected. Work on the refractory metal program has consisted of experiment design, development of machining, welding, and brazing techniques for the specimens, studies of atmosphere purity control, and development of experiment assembly techniques.

Table 17.5. Effect of Neutron Bombardment on the Rupture Life of INOR-8* at 1500°F in Air: ORR Experiments

Specimen No.	Stress (psi)	Irradiation Dose at Rupture (Mwhr)	Rupture Life (hr)
9-9	4000	8400	525
9-10	4000	8460	529
7-8	6000	8340	171**
7-9	6000	2710	170
7-10	6000	2740	171
B-22-Z	8000	0	70
B-23-Z	6000	0	180
B-24-Z	6000	0	177

*INOR-8 is a nickel-base alloy containing approximately 16% molybdenum and 7% chromium.

**Stress applied after 5600 Mwhr of neutron bombardment at 1500°F.

The design of the in-pile assembly and the out-of-pile auxiliary components is essentially complete, and fabrication of parts has begun. The experiment components are shown in Fig. 17.6.

UNCLASSIFIED
 PHOTO 51245

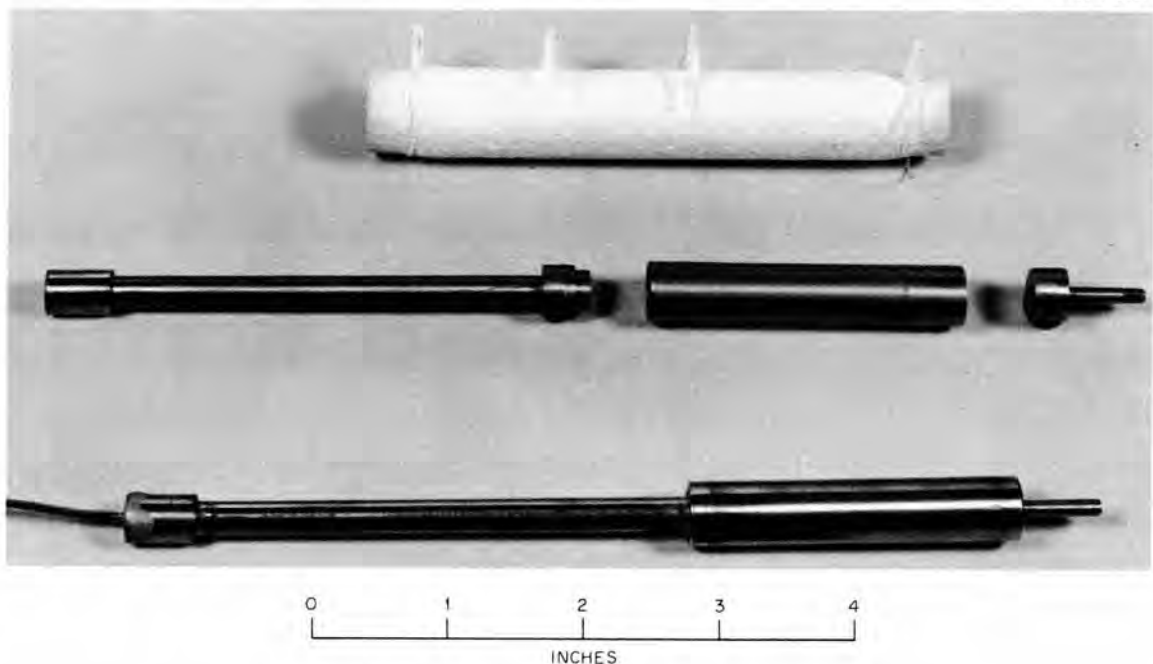


Fig. 17.6. Niobium Stress Rupture Specimen Assembly.

SOLID STATE ANNUAL PROGRESS REPORT

The furnace shown in Fig. 17.6 is one type under consideration for these tests. Since this furnace weighs 50 g, it may be too massive for low-temperature tests. (The gamma heat generation is about 7 w/g at 30-Mw reactor operation.) A second furnace (fabricated from mineral-insulated and swaged heater wire) is being developed, and is expected to weigh about 15 g. Preliminary bench testing of both furnace types indicates that type 2 furnaces will permit in-pile operating temperatures as low as 1700°F, while experiments using type 1 furnaces may be limited to operation above 1900°F.

The refractory metals generally react readily with oxygen, nitrogen, carbon, and hydrogen,

and the Nb-Zr alloy is no exception. In order to obtain accurate data from in-pile, as well as out-of-pile, tests, it is necessary to be very careful in design, assembly, and operation to eliminate materials which might contaminate the specimens. Techniques are being worked out to minimize contamination during assembly, and a purification system will be installed in the helium supply system to absorb the contaminants contained in the bottled helium. In addition, the experiment design includes zirconium and tantalum maintained at elevated temperature for the purpose of gettering impurities released by long-term out-gassing during the experiment.

PUBLICATIONS, PAPERS, AND SPEECHES

- R. G. Berggren
 "Radiation Effects in Ferritic Steels," paper presented at AEC Welding Forum, Chicago, Illinois, Oct. 15, 1959.
- R. G. Berggren, W. E. Brundage, W. W. Davis, N. E. Hinkle, and J. C. Zukas
 "Tensile and Stress-Rupture Properties of Irradiated Stainless Steels and Inconel," paper presented at AEC Welding Forum, Chicago, Illinois, Oct. 15, 1959.
- D. S. Billington
 "Nuclear Reactors as Tools for Metallurgical Research," talk presented to Oak Ridge Chapter, American Society for Metals, Oak Ridge, Tennessee, Jan. 20, 1960.
 "Radiation Effects in Crystalline Inorganic Solids," *Sci. American* **201**, 201 (1959).
- D. Binder
 "A Technique for Using the Np²³⁷ Fission Reaction as a Detector for Fast Neutrons in a Reactor," *Rev. Sci. Instr.* **31**, 902 (1960).
- D. Binder, C. D. Bopp, and R. L. Towns
 "Measurements of the Energy Absorbed from Pile Neutrons," *ASTM Bull.* No. 245, 26 (1960).
- T. H. Blewitt
 "Low Temperature Studies of Irradiation Effects," talk presented at meeting of Southeastern Section, American Physical Society, Gatlinburg, Tennessee, April 7-9, 1960.
- T. H. Blewitt, R. R. Coltman, and C. E. Klabunde
 "Annealing Kinetics of Neutron Irradiated Aluminum and Copper," *Australian J. Phys.* **13**, 347 (1960).
- T. H. Blewitt, D. K. Holmes, and R. R. Coltman
 "Low Temperature Radiation Damage Studies; the Oak Ridge Viewpoint on Basic Mechanisms," p 3-4 in *Proc. Lattice Defects in Noble Metals Conf., Canoga Park, California, Oct. 16-17, 1958*, NAA-SR-3250.
- R. M. Carroll
 "Instantaneous Fission-Gas-Release Experiment," paper presented at Eighth Meeting of High-Temperature Fuels Committee of the AEC, Oak Ridge, Tennessee, Dec. 2-3, 1959.
- J. W. Cleland and J. H. Crawford, Jr.
 "Radiation and Annealing Studies on Defect-Acceptor States in Germanium," talk presented at meeting of Southeastern Section, American Physical Society, Gatlinburg, Tennessee, Apr. 7-9, 1960.
 "Radiation-Induced Disorder in Semiconductors," paper presented at International Conference on Semiconductor Physics, Prague, Czechoslovakia, Aug. 29-Sept. 3, 1960.
 "Thermal Neutron Radiation Effects in Semiconductors," *Bull. Am. Phys. Soc.* **5**, 196 (1960).
- A. F. Cohen
 "Low Temperature Thermal Conductivity of Lithium Fluoride Crystal upon Irradiation by Thermal Neutrons and Co⁶⁰ Gamma Rays," p 173 in *Bull. inst. intern. froid, Annexe, 1958-1* (Conference on Refrigeration, Commission 1 of the International Institute, held June 17-21, 1958, Delft, Netherlands), 1959.
- R. R. Coltman, T. H. Blewitt, and C. E. Klabunde
 "Radiation Damage in Bismuth," *Bull. Am. Phys. Soc.* **5**, 147 (1960).

SOLID STATE ANNUAL PROGRESS REPORT

- R. R. Coltman, T. H. Blewitt, and S. T. Sekula
"The Effects of Annealing in Oxygen on the Resistivity of High Purity Copper," paper presented at International Conference on High Purity Metals, Paris, France, Oct. 12-14, 1959.
- J. H. Crawford, Jr.
"Creation of Defects in Alkali Halides by Ionizing Radiation," talk presented at Gordon Research Conference on Chemistry and Physics of Solids, Meriden, New Hampshire, Aug. 8-12, 1960.
"The Effects of Radiation on Diamond Lattice Semiconductors," talk presented at meeting of Southeastern Section, American Physical Society, Gatlinburg, Tennessee, Apr. 7-9, 1960; also presented at Joint Carolina-Duke Physics Colloquium, Chapel Hill, North Carolina, Apr. 19-22, 1960.
- J. H. Crawford, Jr., and A. F. Cohen
"The Effect of Fast Neutron Bombardment on the Thermal Conductivity of Silica Glass at Low Temperature," p 165 in *Bull. inst. intern. froid, Annexe, 1958-1* (Conference on Refrigeration, Commission 1 of the International Institute, held June 17-21, 1958, Delft, Netherlands), 1959.
- O. L. Curtis, Jr., and J. W. Cleland
"Monoenergetic Neutron Irradiation of Germanium," *J. Appl. Phys.* **31**, 423 (1960).
- O. L. Curtis, Jr., and J. H. Crawford, Jr.
"Annealing of Radiation-Induced Recombination Centers in Germanium," *Bull. Am. Phys. Soc.* **5**, 196 (1960).
- D. K. Holmes, J. W. Corbett, R. M. Walker, J. S. Koehler, and F. Seitz
"On the Interpretation of Radiation Effects in the Noble Metals," *Proc. U.N. Intern. Conf. Peaceful Uses Atomic Energy, 2nd, Geneva, 1958* **6**, 274 (1959).
- D. K. Holmes and G. Leibfried
"Range of Radiation Induced Primary Knock-Ons in the Hard Core Approximation," *J. Appl. Phys.* **31**, 1046 (1960).
- D. K. Holmes and D. O. Thompson
"The Investigation of Radiation Damage Using Acoustics," paper presented at ASM Seminar on Resonance and Relaxation in Metals, Chicago, Illinois, Nov. 1, 1959.
- L. H. Jenkins
"Dissolution of Single Crystals of Copper in Aqueous Ethylenediamine," *J. Electrochem. Soc.* **107**, 371 (1960).
"Observations on Surface Structures of Copper Single Crystals Undergoing Aqueous Dissolution," talk presented at Gordon Research Conference on Corrosion, New London, New Hampshire, July 18-22, 1960.
- C. E. Klabunde, T. H. Blewitt, and R. R. Coltman
"Fission Fragment Damage in Copper and Aluminum," *Bull. Am. Phys. Soc.* **5**, 147 (1960).
"Stored Energy and Specific Heat Measurements Using Nuclear Reactor Heating," paper presented at Fourteenth Calorimetry Conference, New Haven, Connecticut, Sept. 10-12, 1959.
- G. Leibfried
"Correlated Collisions in a Displacement Spike," *J. Appl. Phys.* **30**, 1388 (1959).
"Defects in Dislocations Produced by Focusing Collisions in f.c.c. Lattices," *J. Appl. Phys.* **31**, 117 (1960).

- C. F. Leitten, Jr., R. J. Beaver, and A. E. Richt
 "Stainless Steel Clad Dispersion of Boron in Iron for Pressurized Water Reactors," *J. Nuclear Materials* **2**, 136 (1959).
- E. J. Manthos
Disassembly and Metallographic Examination of In-Pile Loop ORNL MTR-44-1, ORNL CF-60-2-90 (Feb. 24, 1960).
Disassembly and Metallographic Examination of the Nose Coil from In-Pile Loop ORNL MTR-44-2, ORNL CF-60-9-19 (Sept. 1, 1960).
- R. V. Meghreblian and D. K. Holmes
Reactor Analysis, McGraw-Hill, New York, 1960.
- J. G. Morgan
 "ORNL-GCR Capsule Irradiations," paper presented at Eighth Meeting of High-Temperature Fuels Committee of the AEC, Oak Ridge, Tennessee, Dec. 2-3, 1959.
- J. G. Morgan, M. T. Morgan, and M. F. Osborne
Fission Gas Release from UO₂. Interim Report No. 1, ORNL CF-60-7-11 (Aug. 16, 1960).
- J. G. Morgan and M. F. Osborne
Irradiation Effects on UC₂ Dispersed in Graphite. Interim Report No. 1, ORNL CF-60-6-78 (Aug. 18, 1960).
- C. M. Nelson
 "Fast Neutron and Gamma Coloration in KCl," paper presented at 1959 International Symposium on Color Centers in Alkali Halides, Corvallis, Oregon, Sept. 9-11, 1959.
- C. M. Nelson and J. H. Crawford, Jr.
 "Optical Absorption in Irradiated Quartz and Fused Silica," *Phys. and Chem. Solids* **13**, 296 (1960).
- C. M. Nelson and R. A. Weeks
 "Trapped Electrons in Irradiated Quartz and Silica: I. Optical Absorption," *J. Am. Ceram. Soc.* **43**, 396 (1960).
- V. K. Paré and D. O. Thompson
 "Effect of Fast Neutron Induced Defects on the Internal Friction and Young's Modulus of Copper," *Bull. Am. Phys. Soc.* **5**, 147 (1960).
- W. W. Parkinson and D. Binder
 "Post-Irradiation Oxidation and Molecular Weight Changes in Polystyrene and Polymethyl Methacrylate," paper presented at meeting of American Society for Testing Materials, San Francisco, California, Oct. 11-16, 1959.
- M. T. Robinson, A. L. Southern, and W. R. Willis
 "Diffusion of Deuterium in Deuteron-Irradiated Copper," *J. Appl. Phys.* **31**, 1474 (1960).
- S. T. Sekula
 "Resistance Minimum and Resistivity of Copper at Low Temperatures," *Phys. Rev. Letters* **3**, 416 (1959).
- O. Sisman
 "High-Level Spill at the Hilac," *J. Nuclear Safety* **1**, 88 (1960).
 "The Properties and Behavior of Irradiated High Polymers," talk presented to Akron, Ohio, Polymer Lecture Group, Apr. 1, 1960.
- E. Sonder and H. C. Schweinler
 "Magnetism of Interacting Donors," *Phys. Rev.* **117**, 1216 (1960).

SOLID STATE ANNUAL PROGRESS REPORT

- E. Sonder and L. C. Templeton
"Effect of Dissolved Oxygen on Radiation Damage in *n*-Type Silicon," *Bull. Am. Phys. Soc.* **5**, 196 (1960).
"Gamma Irradiation of Silicon. I. Levels in *n*-Type Material Containing Oxygen," *J. Appl. Phys.* **31**, 1279 (1960).
- D. O. Thompson and V. K. Paré
"Effect of Fast Neutron Bombardment at Various Temperatures upon the Young's Modulus and Internal Friction of Copper," *J. Appl. Phys.* **31**, 528 (1960).
"Effects of Neutron Irradiation on the Internal Friction of Copper at Megacycle Frequencies," talk presented at Gordon Research Conference on Chemistry and Physics of Solids, Meriden, New Hampshire, Aug. 8-12, 1960.
"Internal Friction of Copper Following Deformation at 78°K," *Bull. Am. Phys. Soc.* **5**, 153 (1960).
- M. S. Wechsler
"Nuclear Reactors as Tools for Metallurgical Research," talk presented to Chattanooga Chapter, American Society for Metals, Chattanooga, Tennessee, Oct. 20, 1959.
"On the Theory of Martensitic Transformations. The Generalized Lattice Invariant Shear and the Degeneracy of Solutions for the Cubic to Tetragonal Transformation," *Acta Met.* **7**, 793 (1959).
- M. S. Wechsler and R. H. Kernohan
"Lattice Defects in a Copper-Aluminum Alloy," *Acta Met.* **7**, 599 (1959).
"Reply to the Letter of Damask and Dienes on 'Neutron-Irradiation Effect on Copper-Aluminum Alloys,'" *Phys. and Chem. Solids* **12**, 107 (1959).
"Resistivity Measurements on Cu-Al upon Electron and Gamma Irradiation," *Bull. Am. Phys. Soc.* **5**, 147 (1960).
- M. S. Wechsler and H. M. Otte
"The Generalized Theory of the Martensitic Cubic to Orthorhombic Phase Transformation," paper presented by H. M. Otte at Fifth General Assembly, International Congress and Symposia, International Union of Crystallography, Cambridge, England, Aug. 15-24, 1960.
- M. S. Wechsler, T. A. Read, and D. S. Lieberman
"The Crystallography of the Austenite-Martensite Transformation. The [111] Shear Solutions," *Trans. Am. Inst. Mining, Met., and Petrol. Engrs.* **218**, 202 (1960).
- R. A. Weeks
"Defects of the Quartz System Produced by Neutron Irradiation," p 37 in *Proc. 13th Ann. Symposium Frequency Control, Asbury Park, New Jersey, May 12-14, 1959*, U.S. Army Signal Research and Development Laboratory, Fort Monmouth, New Jersey, 1959.
- R. A. Weeks and C. M. Nelson
"Oscillator Strengths of Three Optical Absorption Bands in Quartz and Fused Silica," *Bull. Am. Phys. Soc.* **5**, 201 (1960).
"Trapped Electrons in Irradiated Quartz and Silica: II. Electron Spin Resonance," *J. Am. Ceram. Soc.* **43**, 399 (1960).
- M. C. Wittels
"Lattice Vacancies in Neutron-Irradiated Germanium," *Bull. Am. Phys. Soc.* **5**, 375 (1960).
"Release of Wigner Energy from Graphite," *J. Nuclear Safety* **1**, 22 (1959).

- M. C. Wittels and F. A. Sherrill
 "Some Irradiation Effects in Non-metallic Crystals," p 269 in *Advances in X-ray Analysis* (ed. by W. M. Mueller), vol 3, Plenum Press, New York, 1960.
- F. W. Young, Jr.
 "Crystal Imperfections and the Chemical Reactivity of Metal Surfaces," paper presented at Ninth Annual AEC Corrosion Symposium, Boston, Massachusetts, May 10-12, 1960.
 "Etch Pits and Dislocations in Pure Copper," *Bull. Am. Phys. Soc.* **5**, 190 (1960).
 "Mechanisms of Dislocation Etch Pitting," talk presented at Gordon Research Conference on Physical Metallurgy, Meriden, New Hampshire, June 27-July 1, 1960.
 "Nuclear Reactors in Metallurgical Research," talk presented to Richmond Chapter, American Society for Metals, Richmond, Virginia, Sept. 29, 1959.
 "Oxide Nuclei and Dislocations," *Acta Met.* **8**, 117 (1960).
- F. W. Young, Jr., J. V. Cathcart, and L. H. Jenkins
 "The Role of Crystal Imperfections in the Chemical Reactivity of Metal Surfaces," *AEC-Euratom Conference, Aqueous Corrosion of Reactor Materials*, TID-7587, p 30 (July 1960).
- F. W. Young, Jr., and J. H. Crawford, Jr.
 "On the Mechanism for the Production of F-Centers in NaCl by Irradiation with Gamma Rays," talk presented at meeting of Southeastern Section, American Physical Society, Gatlinburg, Tennessee, Apr. 7-9, 1960.
- F. W. Young, Jr., and A. T. Gwathmey
 "Development of Facets, Spirals, and Etchpits on Copper Crystals by Heating to High Temperatures in High Vacua," *J. Appl. Phys.* **31**, 225 (1960). This work was done at the University of Virginia.
- F. W. Young, Jr., and T. S. Noggle
 "Evidence for Dislocation Reactions in Copper," *J. Appl. Phys.* **31**, 604 (1960).
- J. C. Zukas and R. G. Berggren
 "Flux Measurements and Irradiation Assemblies Used in the LITR, MTR, and ORR Reactors," paper presented at AEC Welding Forum, Chicago, Illinois, Oct. 15, 1959.

PREVIOUS WORK WHICH HAS BEEN RECENTLY DECLASSIFIED

- Radiation Damage Conference, March 23-24, 1953. Parts I and II*, ORNL CF-53-3-276 (Dec. 20, 1954; declassified Aug. 10, 1959):
- C. D. Baumann
 "Radiation from an Irradiated Liquid Lithium Stream," p 468-70.
- R. G. Berggren
 "Effect of Radiation on Impact Strength of Metals," p 279-86.
- C. D. Bopp and O. Sisman
 "Radiation Stability of Elastomers and Plastics," p 370-74.
 "Relation of the Radiation Stability of Polymers to Chemical Structure," p 375-77.
- R. H. Kernohan
 "Fission Fragment Damage," p 98-112.
- J. G. Morgan and G. W. Keilholtz
 "Liquid Fuel Studies in the MTR and LITR," p 51-79.
- F. Muckenthaler, F. Smith, and J. B. Trice
 "Nuclear Heating in the LITR," p 444-57.

- W. W. Parkinson
"Design and Operation of High-Temperature In-Pile Liquid-Metal Experiments," p 458-67.
- A. E. Richt and J. G. Morgan
"Dynamic Radiation Testing Facility for Liquid Fuels," p 495-98.
- M. T. Robinson
"Xenon-135 in Fluoride Fuels," p 153-55.
- C. C. Webster
"Differential Thermal Analysis of Irradiated Salts," p 471-77.
- J. C. Wilson, J. C. Zukas, and W. W. Davis
"Creep of Inconel and Stainless Steel Under Irradiation," p 268-78.

INTERNAL DISTRIBUTION

1. J. H. Barrett
2. R. F. Bass
3. C. D. Baumann
4. P. R. Bell
5. W. T. Berg
6. R. G. Berggren
7. J. O. Betterton, Jr.
8. D. S. Billington
9. D. Binder
10. E. P. Blizard
11. T. H. Blewitt
12. A. L. Boch
13. E. G. Bohlmann
14. C. D. Bopp
15. C. J. Borkowski
16. G. E. Boyd
17. M. A. Bredig
18. R. B. Briggs
19. H. Brooks (consultant)
20. F. R. Bruce
21. W. E. Brundage
22. C. T. Butler
23. N. Cabrera (consultant)
24. R. M. Carroll
25. C. E. Center
26. R. A. Charpie
27. J. W. Cleland
28. R. G. Cleland (consultant)
29. A. F. Cohen (consultant)
30. R. R. Coltman
31. J. A. Cox
32. J. H. Crawford, Jr.
33. F. L. Culler
34. J. E. Cunningham
35. O. L. Curtis
36. W. W. Davis
37. S. E. Dismuke
38. L. B. Emler (K-25)
39. J. L. Fowler
40. J. H. Frye, Jr.
41. J. L. Gabbard
42. B. R. Gossick (consultant)
43. R. J. Gray
44. W. R. Grimes
45. D. E. Harrison (consultant)
46. N. E. Hinkle
47. A. Hollaender
48. D. K. Holmes
49. A. S. Householder
50. L. D. Hulett
51. T. J. Humphries
52. H. B. Huntington (consultant)
53. J. T. Howe
54. L. H. Jenkins
55. L. K. Jetter
56. R. W. Johnson
57. R. J. Jones
58. W. H. Jordan
59. C. E. Klabunde
60. G. W. Keilholtz
61. C. P. Keim
62. M. T. Kelley
63. R. H. Kernohan
64. E. M. King
65. J. A. Krumhansl (consultant)
66. G. Leibfried
67. A. B. Lewis (consultant)
68. T. A. Lincoln
69. S. C. Lind
70. R. S. Livingston
71. H. G. MacPherson
72. C. J. McHargue
73. W. D. Manly
74. E. J. Manthos
75. A. J. Miller
76. E. C. Miller
77. J. W. Mitchell (consultant)
78. J. G. Morgan
79. K. Z. Morgan
80. M. T. Morgan
81. J. P. Murray (Y-12)
82. C. M. Nelson (consultant)
83. M. L. Nelson
84. T. S. Noggle
85. O. S. Oen
86. M. F. Osborne
87. V. Paré
88. W. W. Parkinson
89. D. Phillips
90. J. C. Pigg
91. M. E. Ramsey
92. T. A. Read (consultant)

- | | |
|---------------------------------|---|
| 93. P. E. Reagan | 121. C. D. Susano |
| 94. J. K. Redman | 122. J. A. Swartout |
| 95. P. M. Reyling | 123. E. H. Taylor |
| 96. A. E. Richt | 124. L. C. Templeton |
| 97. H. E. Robertson | 125. D. O. Thompson |
| 98. C. C. Robinson | 126. David Turnbull (consultant) |
| 99. M. T. Robinson | 127. M. S. Wechsler |
| 100. A. F. Rupp | 128. R. A. Weeks |
| 101. O. E. Schow | 129. A. M. Weinberg |
| 102. H. C. Schweinler | 130. E. P. Wigner (consultant) |
| 103. H. E. Seagren | 131. M. K. Wilkinson |
| 104. W. C. Sears (consultant) | 132. G. C. Williams |
| 105. F. Seitz (consultant) | 133. J. M. Williams |
| 106. S. T. Sekula | 134. W. R. Willis (consultant) |
| 107. F. A. Sherrill | 135. J. C. Wilson |
| 108. E. D. Shipley | 136. C. E. Winters |
| 109. R. H. Silsbee (consultant) | 137. M. C. Wittels |
| 110. O. Sisman | 138. E. O. Wollan |
| 111. M. J. Skinner | 139. F. W. Young |
| 112. L. Slifkin (consultant) | 140. J. C. Zukas |
| 113. G. P. Smith | 141. Biology Library |
| 114. A. H. Snell | 142-144. Central Research Library |
| 115. E. Sonder | 145. Health Physics Library |
| 116. A. L. Southern | 146-195. Laboratory Records Department |
| 117. R. L. Sproull (consultant) | 196. Laboratory Records, ORNL R.C. |
| 118. J. T. Stanley | 197. ORNL - Y-12 Technical Library,
Document Reference Section |
| 119. E. E. Stansbury | 198. Reactor Experimental Engineering Library |
| 120. J. O. Stiegler | |

EXTERNAL DISTRIBUTION

199. W. W. Shaver, Corning Glass Works, Corning, New York
200. S. H. Liebson, Naval Research Laboratory, Washington, D.C.
201. Boeing Airplane Company
202. Division of Research and Development, AEC, ORO
203. J. R. Johnson, Minnesota Mining and Manufacturing Co., St. Paul
204. A. E. Ruark, AEC, Washington
205. G. L. Stiehl, Convair Division of General Dynamics Corp., San Diego
206. C. C. Webster, Engineering Center, Westinghouse Electric Corp., E. Pittsburgh
207. R. O. Bolt, California Research Corp., Richmond
208. Benjamin Lax, Lincoln Laboratory, Lexington, Massachusetts
209. George H. Wagner, Linde Air Products Company, Tonawanda Laboratory, East Park Drive and Woodward Avenue, Tonawanda, New York
210. D. K. Stevens, Materials and Metallurgy Branch, Division of Research, U.S. Atomic Energy Commission, Washington, D.C.
211. J. B. Trice, General Electric Company - ANPD, Applied Materials Research, Building D, Cincinnati 15, Ohio
212. R. I. Leininger, Battelle Memorial Institute, 505 King Avenue, Columbus, Ohio
213. Westinghouse Electric Corp., Research Laboratories, Pittsburgh, Pennsylvania
214. J. G. Castle, Jr., Physics Dept., Westinghouse Electric Corp., Research Laboratories, Pittsburgh, Pennsylvania

215. C. Kikuchi, University of Michigan, Willow Run Laboratory, Ann Arbor, Michigan
216. N. R. Beaudry, Office of Ordnance Research, Duke Station, Durham, North Carolina
217. J. Hitch, Office of Isotope Development, AEC, Washington
218. Ira Zartman, Division of Reactor Development, USAEC, Washington, D.C.
219. P. W. McDaniel, Division of Research, USAEC, Washington, D.C.
220. H. Y. Fan, Solid State Physics Dept., Purdue University, Lafayette, Indiana
221. T. J. Turner, Department of Physics, Wake Forest College, Winston-Salem, North Carolina
- 222-831. Given distribution as shown in TID-4500 (15th ed.) under Physics and Mathematics category
(75 copies - OTS)

Reports previously issued in this series are:

ORNL-1025*	Period Ending January 31, 1951
ORNL-1095	Period Ending April 30, 1951
ORNL-1128*	Period Ending July 31, 1951
ORNL-1214*	Period Ending October 31, 1951
ORNL-1261*	Period Ending January 31, 1952
ORNL-1301*	Period Ending May 10, 1952
ORNL-1359*	Period Ending August 10, 1952
ORNL-1429*	Period Ending November 10, 1952
ORNL-1506*	Period Ending February 10, 1953
ORNL-1606	Period Ending August 31, 1953
ORNL-1677	Period Ending February 28, 1954
ORNL-1762*	Period Ending August 30, 1954
ORNL-1851*	Period Ending February 28, 1955
ORNL-1852	Period Ending February 28, 1955
ORNL-1944	Period Ending August 30, 1955
ORNL-1945	Period Ending August 30, 1955
ORNL-2051	Period Ending February 29, 1956
ORNL-2052*	Period Ending February 29, 1956
ORNL-2188	Period Ending August 30, 1956
ORNL-2189*	Period Ending August 30, 1956
ORNL-2413	Period Ending August 31, 1957
ORNL-2614	Period Ending August 31, 1958
ORNL-2829	Period Ending August 31, 1959

*Classified.